



University  
of Glasgow

Kazemtabrizi, Behzad (2011) Mathematical modelling of multi-terminal VSC-HVDC links in power systems using optimal power flows. PhD thesis.

<http://theses.gla.ac.uk/2937/>

Copyright and moral rights for this thesis are retained by the author

A copy can be downloaded for personal non-commercial research or study, without prior permission or charge

This thesis cannot be reproduced or quoted extensively from without first obtaining permission in writing from the Author

The content must not be changed in any way or sold commercially in any format or medium without the formal permission of the Author

When referring to this work, full bibliographic details including the author, title, awarding institution and date of the thesis must be given.



University  
of Glasgow

**Mathematical Modelling of Multi-terminal  
VSC-HVDC Links in Power Systems using  
Optimal Power Flows**

A Thesis submitted to the  
Department of Electronics and Electrical Engineering of  
The University of Glasgow  
For the degree of Doctor of Philosophy

By  
**Behzad Kazemtabrizi**

July 2011

© Behzad Kazemtabrizi, 2011

*For my beloved family,*

*To my parents, Esmail and Fatemeh, and to my brother,  
Mehrdad, without whose love, constant encouragement and support  
this project would have been impossible.*

*To my beautiful friend, partner and soul mate  
Behnaz*

## Abstract

An advanced mathematical model of the Voltage Source Converters (VSC) suitable for optimal power flow (OPF) solutions using Newton's method for augmented Lagrangian functions has been developed in this research, using first principles – this model is far more flexible and realistic than the existing VSC models aimed at fundamental frequency power systems studies. The model is based on a new set of power injections, which take place at both the DC and the AC sides of the voltage source converter. Unlike existing models, which are based on the use of the controllable voltage source paradigm, the new VSC model takes into account, in an aggregated form, the phase shifting and scaling up/down nature of the Pulse Width Modulation (PWM) control. The physical attributes of the DC/AC converter relating to the amplitude modulation ratio is well encapsulated by a complex tap-changing ratio variable which enters the OPF formulation as two fully independent state variables. Furthermore, the new VSC model makes provisions for the independent representation of the ohmic and switching losses, together with a variable capacitive susceptance which represents the DC capacitor contribution corresponding to a given VSC's operating condition. This is a very powerful and flexible modelling resource, which is amenable to a more realistic representation of the operational characteristics of actual voltage source converters.

The nodal active and reactive powers of the VSC are suitably modified to accommodate more complex models corresponding to back-to-back, point-to-point and multi-terminal High Voltage Direct Current (HVDC) transmission links, within Newton's OPF algorithm – the various model representations of the HVDC links use two or more VSC models, resulting in a new and more powerful way of VSC-HVDC representation. These models are subsequently used to interconnect otherwise independent AC systems. Since the AC systems operate asynchronously, multiple Slack buses are required to carry out power flows and OPF solutions.

The new models are developed and presented in quite a comprehensive manner throughout the thesis. System simulations are carried out in order to illustrate the VSC-HVDC modelling flexibility in representing various modes of VSC-HVDC operation by selecting a range of control modes. It should be noticed that a straightforward extension of the VSC model yields a new STATCOM model of unrivalled modelling flexibility. It has been observed that the new models do not impair the strong convergence characteristics exhibited by Newton's iterative method.

As an integral part of this research, a computer program written in MATLAB has been developed to perform OPF system simulations. The program is capable of solving conventional power systems of an arbitrary complexity, multi-terminal VSC-HVDC transmission links and combined AC/DC transmission systems. It follows that less complex systems comprising one or more STATCOM, back-to-back and point-to-point VSC-HVDC can be solved with ease, using the Newton OPF computer program. It should be brought to attention that existing power systems commercial or distribution free packages with OPF facilities do not possess the advanced modelling capabilities exhibited by the new VSC model and its extensions, presented in this thesis.

## **Acknowledgements**

I wish to convey my deepest gratitude towards Prof. Enrique Acha, my PhD supervisor during this project, with whose invaluable technical support and constant mentorship I was able to fulfil the goals of my research seamlessly.

I would also like to thank my parents, Esmail, and Fatemeh, for providing the financial support for me to conduct my PhD project and for their continued encouragement during the past four years.

Finally I would like to thank the Department of Electronics and Electrical Engineering at The University of Glasgow for providing me the necessary facilities for conducting my research. Particularly, my thanks go to my colleagues, Carlos, Okara and Madjid with whom I shared office for the past four years.

## Abbreviations

**AVR:** Automatic Voltage Regulator

**CPF:** Conventional Power Flow

**CSC:** Current Source Converter

**ECP:** Equality Constrained Problem

**FACTS:** Flexible AC Transmission Systems

**GTO:** Gate Turn-Off Thyristor

**HVAC:** High Voltage Alternating Current

**HVDC:** High Voltage Direct Current

**ICP:** Inequality Constrained Problem

**IGBT:** Insulated Gate Bipolar Transistor

**KKT:** Karush-Kuhn-Tucker

**MVAR:** Mega Volt Ampere Reactives

**MW:** Megawatts

**NOC:** Necessary Optimality Condition

**OLTC:** On-Load Tap Changer

**OPF:** Optimal Power Flow

**PAR:** Phase Angle Regulator

**PIM:** Power Injection Model

**PST:** Phase Shifting Transformer

**p.u.:** per unit

**PWM:** Pulse Width Modulation

**SPWM:** Sinusoidal Pulse Width Modulation

**SSSC:** Static Series Synchronous Controller

**STATCOM:** Static Compensator

**SVC:** Static VSC Compensator

**SVS:** Synchronous Voltage Source

**TCR:** Thyristor Controlled Reactor

**TCSC:** Thyristor Controlled Series Capacitor

**TTC:** Total Transfer Capability

**UPFC:** Unified Power Flow Controller

**VSC:** Voltage Source Converter

## List of Variables

The following variables are used in the mathematical expressions throughout this thesis:

$x$ : Vector of system's state variables

$y$ : Objective function's variable(s)

$\theta$ : The complex nodal voltage phase angle (degrees)

$V$ : The complex nodal voltage magnitude

$Y = G + jB$ : Nodal admittance

$G$ : Electrical conductance

$B$ : Electrical susceptance

$Z = 1/Y = R + jX$ : System impedance

$R$ : Electrical resistance

$X$ : Electrical reactance

$S = P + jQ$ : The nodal complex apparent power

$P$ : Nodal active power

$Q$ : Nodal reactive power

$\lambda$ : Lagrangian multiplier for active equality constraints

$u$ : Lagrangian multiplier for active inequality constraints

$z = [x, y, \lambda, u]^T$ : Vector of all the system's variables and multipliers

$m_a = T e^{j\varphi_{ps}}$ : Compound transformer model's complex variable tap phasor

$T$ : Variable tap changer ratio

$\varphi_{ps}$ : Variable phase shifter angle

$\alpha$  or  $\varphi$ : Penalty parameter/factor

$j = \sqrt{-1}$ : The complex operator

## Partial Derivative Notation

For simplicity and in order to avoid making up too much space in writing the partial derivatives, a special notation is used in this thesis.

Notice that this is for notation purposes only.

If  $X$  is a function of vector  $z_i = [a, b]^T$  then its second order partial derivative (or the Hessian terms) with respect to  $z_i$  is written throughout this thesis as such:

$$\nabla_{ab}^2 X = \frac{\partial^2 X}{\partial a \partial b}$$

The first order partial derivative (or the Jacobian and Gradient terms) is written as below:

$$\nabla_a X = \frac{\partial X}{\partial a}$$

These terms have been used on numerous occasions throughout the chapters in this thesis.

## Table of Contents

<b>Abstract</b> .....	<b>iii</b>
<b>Acknowledgement</b> .....	<b>iv</b>
<b>Abbreviations</b> .....	<b>v</b>
<b>List of Variables</b> .....	<b>vi</b>
<b>Partial Derivatives Notation</b> .....	<b>vii</b>
<b>Table of Contents</b> .....	<b>viii</b>
<b>List of Figures</b> .....	<b>xi</b>
<b>List of Tables</b> .....	<b>xiii</b>
<b>List of Charts</b> .....	<b>xv</b>
<b>1 Introduction</b> .....	<b>1</b>
<b>1.1 Project Outline</b> .....	<b>1</b>
<b>1.2 Main Concepts</b> .....	<b>8</b>
1.2.1 Optimal Power Flow Algorithm .....	8
1.2.2 Flexible AC Transmission Systems (FACTS) and FACTS-based Power Systems	
8	
1.2.3 Voltage Source Converters (VSCs).....	8
1.2.4 VSC-HVDC Transmission Systems .....	9
<b>1.3 Aims and Objectives</b> .....	<b>9</b>
<b>1.4 Main Contributions to the Field of Power Systems Research</b> .....	<b>11</b>
<b>1.5 Publications</b> .....	<b>13</b>
<b>1.6 Thesis Outline</b> .....	<b>14</b>
<b>1.7 References</b> .....	<b>16</b>
<b>2 Optimal Power Flow</b> .....	<b>21</b>
<b>2.1 Introduction</b> .....	<b>21</b>
<b>2.2 An Overview of Power Flow Problem</b> .....	<b>23</b>
<b>2.3 Optimal Power Flow Algorithm</b> .....	<b>27</b>
2.3.1 An Overview of Optimal Power Flow Problem: Formulation and Solution	
Algorithms .....	27
2.3.2 Newton’s Method for Augmented Lagrangian Function in Optimal Power Flow:	
Mathematical Toolbox .....	31
2.3.3 Quadratic Penalty Function in Augmented Lagrangian Method (Exact Penalty	
Function) .....	42
2.3.4 Modelling Criterion of Power System components in OPF: A Parametric	
Example .....	44
2.3.5 Summary of Newton’s Method for an Augmented Lagrangian Function.....	51
<b>2.4 Optimal Power Flow Scenarios applied to Power Systems</b> .....	<b>53</b>
2.4.1 8-node System .....	54
2.4.2 9-node System .....	58
2.4.3 11-node System .....	66
2.4.4 IEEE 14-node System.....	69
2.4.5 IEEE 30-node System.....	71
<b>2.5 Optimal Power Flow Formulation: A Flow Chart</b> .....	<b>77</b>
<b>2.6 Alternative Solution Algorithms for OPF including Meta-Heuristics</b> .....	<b>78</b>
<b>2.7 Conclusion</b> .....	<b>79</b>

2.8	References.....	80
3	<b>Optimal Power Flow Modelling for Shunt FACTS Controllers .....</b>	<b>83</b>
3.1	Introduction .....	83
3.2	An Overview of FACTS Modelling for Power Flow Studies (Conventional and Optimal).....	86
3.3	<b>Shunt Compensator Modelling in OPF using Newton’s method for Augmented Lagrangian Function .....</b>	<b>88</b>
3.3.1	STATCOM OPF Formulation (Controllable Voltage Source Model) .....	90
3.3.2	SVC OPF Formulation (Variable Susceptance Model).....	95
3.4	<b>Optimal Reactive Power Control in Power Systems .....</b>	<b>97</b>
3.4.1	Compensated 8-node System.....	97
3.4.2	Compensated IEEE 30-node System.....	109
3.5	Conclusions.....	112
3.6	References.....	112
4	<b>Advanced Voltage Source Converter Model in Optimal Power Flow algorithm using the Compound Transformer Concept .....</b>	<b>115</b>
4.1	Introduction .....	116
4.2	Compound Transformer Concept.....	120
4.3	<b>VSC Compound Transformer Model for Optimal Power Flow Algorithm via Newton’s Method .....</b>	<b>122</b>
4.3.1	Derived Nodal Power Flows in Compound Transformer Model .....	125
4.3.2	Compound Transformer OPF Formulation .....	127
4.3.3	Compound Transformer Model Modes of Operation.....	132
4.4	<b>AC Stand-alone Operation Tests.....</b>	<b>135</b>
4.4.1	Control Mode: 1.0.0.....	136
4.4.2	Control Mode: 2.1.0.....	137
4.4.3	Control Mode: 2.2.0.....	137
4.4.4	Control Mode: 3.1.0.....	138
4.4.5	Control Mode: 3.2.0.....	138
4.4.6	Control Mode: 4.2.2.....	139
4.4.7	Control Mode: 4.2.1.....	139
4.4.8	Results Discussion.....	139
4.5	<b>DC Stand-alone Operation Tests.....</b>	<b>142</b>
4.5.1	Case One.....	144
4.5.2	Case Two .....	145
4.6	<b>5-node Benchmark System Test: Changes in System Conditions.....</b>	<b>147</b>
4.7	Conclusion .....	150
4.8	References.....	151
5	<b>Advanced Mathematical Modelling of Back-to-Back, Point-to-Point and Multi-terminal VSC-HVDC Transmission Systems in OPF using Newton’s Method.....</b>	<b>154</b>
5.1	Introduction .....	155
5.2	<b>Advanced Back-to-Back VSC-HVDC Mathematical Model in Optimal Power Flow Algorithm using Compound Transformer Model.....</b>	<b>160</b>
5.2.1	Back-to-Back VSC-HVDC Compound Model’s OPF Formulation .....	161
5.2.2	Reactive Power Constraint .....	168
5.2.3	Linear System of Equations.....	170
5.2.4	Back-to-Back VSC-HVDC Compound Model’s Modes of Operation .....	170
5.3	<b>Optimal Power Flow Control in Back-to-Back VSC-HVDC Transmission Systems.....</b>	<b>174</b>
5.3.1	Two-terminal Back-to-Back VSC-HVDC.....	175

5.3.2	Multi-terminal Back-to-Back VSC-HVDC .....	179
5.3.3	Multi-terminal Back-to-Back VSC-HVDC: Four Terminals Meshed .....	186
<b>5.4</b>	<b>Advanced Point-to-Point VSC-HVDC Compound Model's OPF Formulation using Expanded Compound Transformer Model.....</b>	<b>188</b>
5.4.1	Problem of Point to Point active power control in Compound Transformer Model 188	
5.4.2	Expanded Compound Transformer Model Reduced Admittance Matrix and Derived Nodal Powers .....	191
5.4.3	Equivalent Admittance Elements for the Expanded Compound Transformer in Rectangular and Polar Forms.....	194
5.4.4	The Expanded Compound Transformer Constraints Set within the OPF .....	198
5.4.5	The Expanded Compound Transformer Exclusive Lagrangian .....	199
5.4.6	Point-to-Point VSC-HVDC System OPF Formulation using Expanded Compound Transformer .....	200
<b>5.5</b>	<b>The Inequality Constraints .....</b>	<b>205</b>
<b>5.6</b>	<b>Optimal Power Flow Control in Point-to-Point VSC-HVDC System Configurations.....</b>	<b>206</b>
5.6.1	Two-terminal Point-to-Point VSC-HVDC .....	206
5.6.2	Multi-terminal VSC-HVDC .....	208
<b>5.7</b>	<b>Multi-terminal VSC-HVDC Interconnection System for a realistic AC Network 210</b>	
<b>5.8</b>	<b>Conclusion .....</b>	<b>213</b>
<b>5.9</b>	<b>References.....</b>	<b>214</b>
<b>6</b>	<b>Conclusion.....</b>	<b>217</b>
6.1	General .....	217
6.2	A Final Note Regarding Embedded HVDC into an AC System .....	222
6.3	Suggestions for Possible Future Work.....	223
<b>Appendix I.....</b>		<b>225</b>
<b>Appendix II.....</b>		<b>255</b>

## List of Figures

Figure 2.1 - 4-node Test System .....	44
Figure 2.2 – 8-node Test System .....	56
Figure 2.3 - 9-node Test System (Optimal Power Flow Solution) .....	60
Figure 2.4 - 9-node Compensated Test System (Optimal Power Flow Solution) .....	62
Figure 2.5 - 11-node Test System (Optimal Power Flow Solution) .....	67
Figure 2.6 - 14-node Test System (Optimal Power Flow Solution) .....	70
Figure 2.7 - 30-node Test System (Optimal Power Flow Solution) .....	74
Figure 3.1 - STATCOM Controllable Voltage Source Model .....	92
Figure 3.2 - SVC Variable Susceptance Model .....	95
Figure 3.3 - 8-node System OPF Solution (SVC Case One) .....	99
Figure 3.4 - 8-node System OPF Solution (SVC Case Two) .....	104
Figure 3.5 - 8-node System OPF Solution with STATCOM in place of SVC .....	108
Figure 4.1 - Voltage Source Converter - Fully Controlled Self Commutated Converter .....	117
Figure 4.2 - Current Source Converter - (a) Fully Controlled Line Commutated Converter (b) Fully Controlled Self Commutated Converter .....	117
Figure 4.3 - Compound Transformer - (a) The variable phase shifter ratio models both active power and nodal voltage magnitude controls (b) Phasor diagram for leading operation .....	121
Figure 4.4 - (a) VSC Compound Transformer Model (b) Phasor diagram for converter's lagging operation and control on primary .....	123
Figure 4.5 - Compound Transformer as a series compensator (No Control).....	136
Figure 4.6 - Compound Transformer as a series compensator (Voltage Control on primary) .....	137
Figure 4.7 - Compound Transformer as a series compensator (Voltage Control on secondary) .....	137
Figure 4.8 - Compound Transformer as a series compensator (Power Control on primary). 138	
Figure 4.9 - Compound Transformer as a series compensator (Power Control on secondary) .....	138
Figure 4.10 - Compound Transformer as a series compensator (Power on secondary; Voltage on secondary) .....	139
Figure 4.11 - Compound Transformer as a series compensator (Power on primary; Voltage on secondary) .....	139
Figure 4.12 – Compound Transformer feeding the DC Load.....	144
Figure 4.13 – VSC Compound Transformer feeding the DC Load .....	145
Figure 4.14 – VSC Compound Transformer feeding the DC Load (Generator 2 active power schedule limited to 0.3 per unit) .....	146
Figure 4.15 - Partial OPF Solution for the normal 5-node Benchmark system; Notice the active power flow between “Lake” and “Main” .....	148
Figure 4.16 - Partial OPF Solution for the 5-node Benchmark system with the compound transformer regulating power between "Lake" and "Main" .....	148
Figure 5.1 – Two-terminal Back-to-Back VSC-HVDC Compound Transformer Model (Notice that the common node is at the receiving ends).....	162
Figure 5.2 - Multi-terminal Back-to-Back VSC-HVDC Compound Transformer Model Configuration .....	166
Figure 5.3 - A two-station Back-to-Back VSC-HVDC System modelled with Compound Transformers (Notice the Active Power Control Constraints are on the receiving ends) .....	171
Figure 5.4 - Two-terminal Back-to-Back VSC-HVDC Compound Transformer Model OPF Solution (node “5” is the infinite bus) .....	175

Figure 5.5 - Two-terminal Back-to-Back VSC-HVDC Compound Transformer Model OPF Solution (node "1" is the infinite bus).....	178
Figure 5.6 - Multi-terminal Back-to-Back VSC-HVDC Compound Transformer Model OPF Solution (nodes "5" and "7" are infinite buses) (notice the variable shunt susceptance values in per unit).....	179
Figure 5.7 – Multi-terminal Back-to-Back VSC-HVDC Compound Transformer Model Test Case Two OPF Solution.....	184
Figure 5.8 – Multi-terminal Back-to-Back VSC-HVDC Compound Transformer Model Test Case Three OPF Solution.....	185
Figure 5.9 - Multi-terminal back-to-back VSC-HVDC Compound Transformer Model OPF Solution: Four-terminal Meshed.....	187
Figure 5.10 - Two-terminal Point-to-Point VSC-HVDC System (Notice the DC power losses in the DC transmission line) .....	189
Figure 5.11 - The Expanded (Augmented) Compound Transformer Model.....	191
Figure 5.12 - Expanded Compound Transformer Model Reconfiguration (Notice the shift in output power controls and the power balance at the common DC node) .....	192
Figure 5.13 - Two-terminal Point-to-Point VSC-HVDC Expanded Compound Transformer Model .....	200
Figure 5.14 - Multi-terminal VSC-HVDC Expanded Compound Transformer Model.....	201
Figure 5.15 - Two-terminal Point-to-Point VSC-HVDC Compound Transformer Model OPF Solution (node "5" is the infinite bus) .....	206
Figure 5.16 - Multi-terminal VSC-HVDC Compound Transformer Model OPF Solution...	209
Figure 5.17 – 46-node Test System (only the connecting bus in each 14-bus segment has been shown).....	210

## List of Tables

Table 2.1 – Generators Constraints Set.....	55
Table 2.2 - Fixed Tap Transformer Data .....	55
Table 2.3 - Generators' Optimal Power Flow Dispatch .....	56
Table 2.4 - System Optimal Power Flow.....	57
Table 2.5 - Calculated Transformers Powers (at optimum).....	57
Table 2.6 - Incremental Generation Costs (Multipliers).....	57
Table 2.7 - Generators Constraints Set .....	59
Table 2.8 - Fixed Tap Transformers Data.....	59
Table 2.9 - Fixed Tap Connecting Transformer Data.....	59
Table 2.10 - Generators Optimal Power Flow Dispatch.....	60
Table 2.11 - System Optimal Power Flow.....	61
Table 2.12 - Calculated Transformer Powers (at optimum) .....	61
Table 2.13 - Incremental Generation Costs (Multipliers).....	61
Table 2.14 - Generators Optimal Power Flow Dispatch.....	62
Table 2.15 - System Optimal Power Flow.....	63
Table 2.16 - Calculated Transformer Powers (at optimum) .....	63
Table 2.17 - Incremental Generation Costs (Multipliers).....	63
Table 2.18 - Generators Constraints Set .....	66
Table 2.19 - Fixed Tap Transformers Data and Shunt Compensators.....	66
Table 2.20 - Generators Optimal Power Flow Dispatch.....	67
Table 2.21 - Transformers Calculated Powers (at optimum).....	68
Table 2.22 - Incremental Generation Costs (Multipliers).....	68
Table 2.23 - Shunt Reactive Powers (Compensators) .....	68
Table 2.24 - Generators Optimal Power Flow Dispatch.....	70
Table 2.25 - Transformer Calculated Powers (at optimum) .....	71
Table 2.26 - Incremental Generation Cost (Multipliers) .....	71
Table 2.27 - Shunt Reactive Powers (Compensators) .....	71
Table 2.28 - Generators Optimal Power Flow Dispatch.....	73
Table 2.29 - Transformers Calculated Powers (at optimum).....	73
Table 2.30 - Incremental Generation Costs (Multipliers) - First 15 nodes.....	74
Table 2.31 - Incremental Generation Costs (Multipliers) - Second 15 nodes .....	74
Table 2.32 - Shunt Reactive Powers (Compensators) .....	74
Table 3.1 - Generator's Optimal Power Flow Dispatch (the amounts in parentheses belong to the uncompensated case).....	99
Table 3.2 - Calculated Transformer Powers (at optimum) .....	99
Table 3.3 - Incremental Generation Costs .....	100
Table 3.4 - SVC Operation (Case One) .....	100
Table 3.5 - SVC Model Reactive Compensation Capability in OPF.....	101
Table 3.6 - Voltage Magnitude Variations at the presence of no SVC.....	102
Table 3.7 - Generators Optimal Power Flow Dispatch (SVC Regulating Voltage) .....	104
Table 3.8 - Calculated Transformer Powers (at optimum) .....	104
Table 3.9 - Incremental Generation Costs .....	105
Table 3.10 - SVC Operation (Case Two).....	105
Table 3.11 - Generators Optimal Power Flow Dispatch.....	107
Table 3.12 - Calculated Transformers Powers (at optimum).....	107
Table 3.13 - Incremental Generation Costs .....	107
Table 3.14 - STATCOM Operation at optimum (Voltage Regulation Mode) .....	107
Table 3.15 - STATCOM and SVC Comparison in IEEE 30-node System (Compensation at node 24) .....	110
Table 3.16 - STATCOM controlling reactive power at node 24 .....	111

Table 4.1 - Compound Transformer Model Modes of Operation.....	133
Table 4.2 - Compound Transformer Model Control Modes.....	135
Table 4.3 – Compound Transformer Model’s Modes of Operation as a Series Compensator in the 4-node System Simulations.....	140
Table 4.4 - VSC Compound Model DC Load Test Results.....	147
Table 5.1 - Back-to-Back VSC-HVDC Compound Model's Plausible Modes of Operation	171
Table 5.2 - Back-to-Back VSC-HVDC Converter Station's Control Modes.....	173
Table 5.3 - Two-terminal Back-to-Back VSC-HVDC Compound Transformer Model Modes of Operation .....	176
Table 5.4 – System Optimum Cost (in \$/hr).....	177
Table 5.5 - System Optimum Cost (in \$/hr) .....	178
Table 5.6 - Multi-terminal Back-to-Back VSC-HVDC Compound Transformer Model Modes of Operation (notice that the rectifier station is tasked with maintaining the voltage at the AC side) .....	180
Table 5.7 - System Optimum Cost (in \$/hr) .....	181
Table 5.8 - The Multiple Test Case Scenarios Required Active Power Dispatch (at the DC node) .....	182
Table 5.9 - System Optimal Power Flow Dispatch (in per unit) .....	182
Table 5.10 - Operation of Complex Tap Ratio for the three Converter Stations.....	183
Table 5.11 - Multi-terminal Back-to-Back VSC-HVDC Compound Transformer Model Modes of Operation for the Four-terminal Meshed.....	186
Table 5.12 – Four-terminal Meshed System Optimum Cost (in \$/hr).....	187
Table 5.13 - Reactive Power Equality Constraint for Point-to-Point VSC-HVDC Model ...	201
Table 5.14 - Two-terminal Point-to-Point VSC-HVDC Compound Transformer Model Modes of Operation .....	207
Table 5.15 - System Optimum Cost (Point-to-Point) (in \$/hr) .....	207
Table 5.16 - Multi-terminal VSC-HVDC Compound Transformer Model Modes of Operation .....	208
Table 5.17 – Multi-terminal VSC-HVDC System Optimum Cost (in \$/hr).....	209
Table 5.18 – Multi-terminal VSC-HVDC Compound Transformer Model Modes of Operation for the 46-node System .....	211
Table 5.19 – 46-node System Final OPF Results .....	212
Table 5.20 – 46-node System Final VSC Results.....	213

## List of Charts

Chart 2.1 - Incremental Cost Price Comparison – Minimal Deviation from Optimum Operating Point .....	64
Chart 2.2 - Generators Reactive Power Dispatch .....	64
Chart 2.3 - 9-node System Voltage Profile (in per unit).....	65
Chart 3.1 - 8-node System Nodal Voltage Comparison (Uncompensated Case vs. SVC Case One).....	100
Chart 3.2 - 8-node System Voltage Comparison (SVC Case One vs. SVC Case Two).....	105
Chart 3.3 - STATCOM Model vs. SVC Model Voltage Regulation Modes produce the exact same results .....	109
Chart 4.1 - Compound Model's Phase Shifter Angle Variations in the 4-node System Simulations (within limits) .....	141
Chart 4.2 - Compound Model's Tap Changer Ratio Variations in the 4-node System Simulations (within limits) .....	142



# 1 Introduction

## 1.1 Project Outline

The management of the flow of electricity in an electrical power system has been an ongoing challenge for power engineers since the time of the early transmission systems – the names of Edison, Ferranti, Tesla, Steinmetz and more recently, Hingorani and Gyugyi are closely associated with this endeavour. It is yet not practical to store electrical power at the multi-MW-level in one storage device, hence, a balance between generation and load must be met at each point in time – allowances must be made for power system losses. Furthermore, the electrical power network is prone to undergoing various kinds of instabilities and it is highly vulnerable to experiencing short-circuit faults due to both external and internal phenomena which are random in nature. Notwithstanding such difficulties, a smooth management of the flow of electricity is of paramount importance to the reliable and uninterrupted operation of the electrical power network [1, 2]. From the early days of the electricity supply industry the power network has been equipped with various kinds of ancillary devices aimed at ensuring its continued and safe operation. This ancillary equipment has been designed to control specific variables of the power network at specific points, namely, voltage magnitude, line impedance and reactive power flow [3, 4]. From very early on, it was recognized that iron core inductors and bank of capacitors were very effective devices for counteracting the operational over-voltages and under-voltages that are quite natural phenomena in overhead transmission lines and cables. However, such devices were permanently connected or their connection/disconnection was carried out by mechanical means, which meant slow responses and not able to aid the power network during emergency conditions. More recently developments in the area of power electronics have given birth to a new set of controllers, which are both faster and far more reliable than their older counterparts, which were mechanically controlled. The large array of new devices are all electronically controlled and are said to belong to a family of power system controllers termed Flexible AC Transmission Systems (FACTS) [2-4]. The FACTS-based technology is living up to its promise to deliver power system's enhanced reliability and stability as well as power quality [2]. It is little wonder that the global

electricity supply industry, large manufacturers of electrical equipment and the research establishment all have thrown their weight behind the FACTS initiative, originally developed and nurtured in EPRI, Palo Alto, California two decades ago [2-24] This research project advances further the understanding and applicability of FACTS controllers from the vantage of network-wide modelling aimed at optimal power flow solutions.

A key aim of this research project is to develop advanced mathematical models of a particular kind of a FACTS component termed the Voltage Source Converter (VSC) which is made up of a pre-defined array of fully controlled power electronic switches, typically Insulated Gate Bipolar Transistors (IGBT) (or Gate Turn-Off Thyristors – GTO) [2-4, 25-27]. The Pulse Width Modulation (PWM) scheme is used to control the switching in the IGBT valves (on and off states) in such a way that the VSC is capable of either importing or exporting reactive power from the network to regulate voltage magnitude up to its rated capacitive value. If a suitable source of active power is available on the DC side of the VSC then the regulating capabilities extend to active power in addition to reactive power [2-4, 26, 28-38]. VSC's have proven to be extremely fast (with IGBT switching capacity standing at up to 10 kHz) in responding to network demands - voltage magnitude regulation, active power transfer capacity improvement, reactive power compensation, power quality disturbance amelioration and the damping of sustained power system oscillations [4].

The latest break-through in the applicability of the FACTS technology has been the use of two VSCs to transmit AC power using the rectification/inversion resource afforded by the VSC structure, having given rise to the new area of High Voltage Direct Current Transmission using Voltage Source Converters (VSC-HVDC) [2, 28, 32, 36, 39]. Two competing brand names are currently in the market: ABB's HVDC-Light and Siemens's HVDC Plus. Two distinct possibilities are well established, the zero distance or back-to-back scheme and the point-to-point scheme where underground cables or submarine cables of a considerable length link the two VSCs on their DC sides.

Bulk electrical power is transmitted mainly by using High Voltage Alternating Current (HVAC) transmission lines or cables, from source to demand. For distances

longer than 700 km it becomes economically justifiable to transmit the electricity using classical High Voltage Direct Current (HVDC) lines [5, 28, 32, 36, 40].

The classical (conventional) HVDC technology uses power thyristors, which are semi-controlled valves with line commutating capabilities. However, the six-pulse or higher-pulse thyristor-based converter is indeed a fully controlled bridge (i.e. Gratz Bridge) – they are termed Current Source Converters (CSC). Power thyristors switch on at only once per cycle. Notwithstanding this low-switching characteristic of the classical HVDC, this technology remains unassailable for bulk power, long-distance transmission applications but its Achilles heel has been the lack of progress in expanding the technology to cover the growing demand for truly multi-terminal HVDC transmission schemes - the current state of the technology is the Sardinia-Corsica-Italy (SACOI) HVDC scheme which is a three-terminal link where the three converters are connected in series. Owing to the need to balance the currents, it does not seem plausible to operate a meshed DC system using CSCs [32, 36].

However, the development of a new kind of power electronics equipment (IGBTs or GTOs) which are fully controlled and switch on and off at a rate considerably higher than the fundamental, has opened a new window of opportunity for the development of truly multi-terminal HVDC systems. This is possible because the converter structures arising from the combined use of fully controlled valves and PWM control are VSCs as opposed to CSCs [32, 36, 37]. Due to the characteristics of these converters and their ability for seamless control of all the fundamental components of the power system, namely voltage, active and reactive powers, they introduce better flexibility and controllability in the system than conventional line commutated thyristor-based HVDC transmission systems [3-5, 28, 29, 33, 35, 36, 38-42]. VSC-HVDC is better placed to play a full role in providing interconnections for the safe and efficient integration of renewable sources of energy - for instance, Wind Farms and PV installations into the AC grid [4, 28, 32, 33, 43, 44].

Furthermore, VSC-HVDC links may be used to interconnect two or more independent networks each with a multiple autonomous segments of generation and demand. In the case of a segmented power system the main advantage of such a configuration would be that the different areas would be completely isolated from one another and that re-synchronisation would no longer be required (as it is the case in

AC connections). Hence, the fault contribution of each area would be limited to that area and other sections of the system will be screened [4, 36, 41]. Furthermore independent active/reactive support of the VSC provides voltage regulation at the point of connection as well as power flow control from one area to the other improving the system's stability and overall power quality. For instance in the case of excessive reactive power demand due to the use of heavy loads, the converters will provide the amount of required reactive power, fixing the voltage at a pre-specified level which is well within the safe operational margins and in accordance to the grid requirements [41].

The VSC-HVDC interconnection systems are finding favour in the interconnection of renewable sources of energy, for example, offshore Wind Farms, to the utility grid via DC undersea cables [33, 43, 44]. The HVAC transmission technology is not considered the best option for interconnecting off-shore sources of energy to the utility grid, since the active power transfer capability becomes impaired due to the highly capacitive nature of the currents in submarine/underground AC cables after only a few tens of kilometres [33]. By contrast, VSC-HVDC systems do not suffer such shortcomings - the only limitations of DC submarine/underground cables will be their thermal and physical limits as opposed to operational limits.

VSCs do not require a source of reactive power to achieve commutation, they are able to control reactive power independently of the AC system and are a good choice for interconnecting a weak AC grid to a strong one where rotating sources of reactive power, namely generators or synchronous condensers, are limited; in some cases they may just not be available [4, 28, 32, 42]. Owing to their great many operational advantages, VSC-HVDC systems are in pole position to become the technology of choice in future power transmission design and development scenarios, once the electronic valve technology develops further – higher power ratings and smaller switching losses would need to be achieved.

The main drive of this project is to develop a flexible and robust mathematical model for assessing, at the system level, the operational characteristics of the VSC-HVDC systems, which are more likely to be the basis of future power grids.

In recent years much research has been put into the area of mathematical modelling of VSC-HVDC technology [2, 6, 11, 23, 26, 29, 31, 35, 37, 38, 45-48], but an advanced model for power flows and optimal power flow analyses, beyond the conventional models based on the controllable voltage source concept, is still lacking. Accordingly, this research project has been tasked with developing such an advanced model to ensure optimal power flow solutions of VSC-HVDC-based transmission systems, which are robust towards the convergence and where all the operational characteristics of actual VSCs are suitably encapsulated. This stands in contrast to previous VSC-HVDC models where the VSC is treated as a controllable voltage source where the converter's PWM control characteristics are not explicitly represented. Therefore, results generated using the equivalent voltage source concept may not necessarily be accurate since limits violations in, for instance, the PWM linear limits or the capacitor rating values may not be easily detected. Also, the switching losses accrued by the PWM control may not be easily accounted for even in an approximated manner.

Efforts have been made to overhaul the voltage source model with means of overcoming such shortcomings. For instance, the amplitude modulation index of the PWM control has been included as a separate state variable in the OPF formulation [26, 31]. However, this method of modelling still regards the VSC as a controllable voltage source with nodal active and reactive powers that are a function of the system voltage phasors but which do not link directly with the PWM control characteristic.

In contrast, the new VSC-OPF model introduced in this project produces a new set of active and reactive powers that explicitly incorporates the PWM amplitude modulation ratio. In this way, the VSC controls the output voltage phasor in both phase angle and magnitude directly to achieve active and reactive power control, closely following the control behaviour of the actual VSC. Meanwhile, it inherently accounts for the converter's switching losses in the form of a shunt resistor. The new VSC model possesses great many modelling advantages over previous models in terms of flexibility and accuracy of representation and, at the same time, maintains the strong numerical performance of the original Newton's method. A fact of paramount importance which has so far not been emphasized is that the nodal structure of the new model makes it straightforward to combine it with other elements of the power system either in its AC side or in its DC side. In its AC side it may

combine with a tap-changing transformer to make up a STATCOM. Connections in their DC sides open the door for VSC-HVDC modelling representation.

Indeed, the new VSC OPF model is easily extended to represent back-to-back and point-to-point VSC-HVDC links and, more importantly, multi-terminal VSC-HVDC configurations. The back-to-back configuration essentially comprises two VSC converters connected in series in their DC sides and the point-to-point system includes a DC cable between the two VSCs. The multi-terminal VSC-HVDC system practically poses no restriction in the form that the DC network may take; it can be multi-terminal radial or multi-terminal meshed. The converter is modelled in OPF in such a way that it reflects the independent active/reactive power control of the actual VSC. Moreover, it does include the DC transmission losses within the VSC power flow equations. No other OPF model developed for the VSC is known to possess such strong analytical capabilities.

An OPF with such well developed VSC-FACTS and HVDC modelling attributes is an essential platform to incorporate models of the various kinds of renewable energy sources, which more often than not are connected to the power grid through power electronic converters of the VSC type. This lay on the realm of future research but it is quite clear the modelling and software foundations presented in the thesis has opened the door for the optimal power flow solutions of electrical power systems where large blocks of renewable generation lies side-by-side with conventional generation leading up to the new power system paradigm, the so-called smart-grid technology.

The mathematical framework used to develop the OPF models of the VSC, STATCOM and the various VSC-HVDC schemes is the well-known power formulation that incorporates “cost” function that are minimized/maximized – the application is termed Optimal Power Flow (OPF) and the solution procedure is Newton’s method [1, 2, 49-61]. The OPF is essentially a constrained non-linear optimisation problem that is applied to electrical power grids to ascertain the system’s optimum operating point in steady state while adhering to a specified set of operating constraints.

Henceforth, the purpose of the OPF solution is to define the operating conditions within which an arbitrary power system, which may be under the influence of multiple power controllers, operates optimally. The OPF algorithm determines these conditions through fine-tuning system's state variables which are kept within safe operational margins. These limits are called constraints and are essential for the realistic representation of the system behaviour [2, 49, 54, 57, 59, 60].

Due to the complexity of modern power systems especially the great many non-linearity introduced by controllers of various kinds, among them the power electronics-based controllers, the OPF is solved by iteration. A large number of methods are available to solve the ensuing set of non-linear equations with Newton's iterative method having proven its worth in the application researched in this work and this has been chosen to be the main solution algorithm [4, 62-64]. Typically in an OPF problem formulation, the objective function to be minimized is taken to be the generator's fuel cost function, which is a quadratic function of the generator's active power [1, 2]. If the objective function is taken to be the generator's fuel cost function then, upon convergence, the OPF will yield the optimum results for the generators' active power generation and their load dispatch. The economic load dispatch of generators within a power system is arguably one of the most important aspects of steady state optimization analysis in power system studies. It should be noted that throughout this research project, for purposes of maintaining consistency, the objective function is always taken to be the generator's cost function. Other alternative objective functions can however be selected depending on the purposes of the problem. The generic OPF modelling criterion introduced in this thesis is designed to incorporate any types of objective functions as long as they can be represented by smooth convex analytical expressions.

In summary the main objective of this project is to develop a robust mathematical model for Voltage Source Converters and VSC-HVDC links used to design safe and reliable interconnections in power systems. Coupled with their strong controllability features, they contribute to developing fully flexible and controllable power systems, which are more immune to unforeseen disturbances. Such a power grid would be the foundation of future system design scenarios.

## 1.2 Main Concepts

The following concepts are the main topics featured in this research:

- Optimal Power Flow Algorithm
- Flexible AC Transmission Systems (FACTS) – Shunt Controllers
- Voltage Source Converters
- High Voltage Direct Current Transmission systems based on Voltage Source Converters (VSC-HVDC)

### 1.2.1 Optimal Power Flow Algorithm

The OPF algorithm using Newton's method is the main analytical toolbox of this project. All the mathematical models presented in this research thesis are designed for the OPF simulations and analysis. The models are tested in a variety of system configurations, both small and medium size test systems.

### 1.2.2 Flexible AC Transmission Systems (FACTS) and FACTS-based Power Systems

One of the main topics of concern in this research is the modelling of the latest generation of FACTS devices, which are based on the use of Voltage Source Converters. However, the thrust of the research has been in the incorporation of these models into the OPF algorithm using Newton's method to enable improved OPF analysis in electrical power networks to enable the global power industry to experiment realistic operating scenarios where the new FACTS technologies are incorporated.

### 1.2.3 Voltage Source Converters (VSCs)

The voltage source converter comprises the major body of this work. The VSC controls the network parameters using Pulse Width Modulation scheme, which gives rise to a controllable output voltage phasor. An advanced model for the voltage source converter has been developed in this project, which accounts for the converter's control characteristics as exclusive state variables in the OPF formulation. The model presented in this research is the first of its kind, which is considered a

complete paradigm shift in power injection modelling methods especially VSC-based systems including VSC-HVDC of various kinds.

#### **1.2.4 VSC-HVDC Transmission Systems**

The VSC-HVDC transmission is a relatively new technology, which has several promising features especially in modern power system design scenarios due to the robust capabilities of the self-commutated voltage source converter. The VSC-HVDC is gaining momentum particularly in recent years due to its robust operating features enabled by a relatively simple control method, namely the PWM. In this research, a robust mathematical model for VSC-HVDC transmission systems has been developed which is suitable for carrying out OPF analysis for a wide range of system configurations.

### **1.3 Aims and Objectives**

The main objectives behind the research reported within this thesis are listed as below.

- To incorporate VSC-FACTS and VSC-HVDC modelling capabilities in an existing Optimal Power Flow program written in MATLAB code. The program has the capability to carry out optimal power flow solutions for practically any type of electrical power network - small, medium and large scale - and exhibiting any configurations which is operational in practice. The network may include or may not include VSC-FACTS and VSC-HVDC. The OPF computer program written in MATLAB has been written to be solved using Newton's method and therefore all the models developed throughout this project are compatible with Newton's method.
- To develop a generic robust modelling criterion for the OPF algorithm using Newton's method for augmented Lagrangian functions suitable for modelling different kinds of power system components, including power flow controllers and VSC-HVDC transmission links.

- To develop a comprehensive and flexible model for the Voltage Source Converter within the OPF algorithm which must include the PWM switching control characteristic in an aggregated form as well as the switching losses that occur in any realistic converter. The new model is an essential improvement to the existing VSC controllable voltage models and therefore a new set of nodal power flows must be realized. The new VSC-OPF model must exert the realistic converter's four-quadrant power control operation.
- To develop a new OPF model for modern shunt reactive compensators, namely Static Compensator (STATCOM) based on the new VSC modelling paradigm; the interfacing tap-changing transformer ought to be incorporated. The new model must possess the control capabilities of a realistic STATCOM and must not add unduly to the complexity in the OPF simulation using Newton's method for augmented Lagrangian functions.
- To extend the newly developed VSC-OPF model into the realm of VSC-HVDC transmission links. The VSC-HVDC models must work seamlessly for both back-to-back, point-to-point power transfer applications and multi-terminal VSC-HVDC systems. It must also include the capabilities of realistic VSC-HVDC systems in controlling both active power and voltage magnitude in an arbitrary system.
- To carry out a series of OPF simulations for a variety of systems including shunt VSC-FACTS controllers for the purposes of optimal reactive power control and direct voltage regulation. Notice that neither series VSC-FACTS (SSSC) nor compound shunt-series VSC-FACTS controllers (UPFC) will be addressed in this research.
- To devise and perform OPF simulation scenarios for multi-terminal VSC-HVDC links to accommodating several realistic autonomous AC grids into one single interconnected system to prove further the notion that multi-terminal VSC-HVDC links are well suited to carrying out the integration, in an asynchronous manner, of otherwise independent system.

## 1.4 Main Contributions to the Field of Power Systems Research

As a result of this research project, the following contributions have been made to the field of power system analysis and modelling.

- A robust computer program for solving OPF problem using Newton's method for augmented Lagrangian function has been developed in MATLAB. Apart from carrying out OPF solutions for systems with conventional configurations, this program includes mathematical models developed throughout this research for advanced shunt controllers as well as multi-terminal VSC-HVDC systems. The program has been used for carrying out robust OPF simulations for a range of standard test systems such as the IEEE 14 and 30-bus systems, as well as for other contrived systems.
- A generic modelling criterion has been introduced which is suitable for developing mathematical models for OPF algorithm within the augmented Lagrangian function framework. The generalized OPF modelling approach is sufficiently flexible to accommodate any type of power system component since the Lagrangian functions associated with the models are developed from their nodal active and reactive powers. This particular modelling approach is developed in such a way that the component's steady state operational control abilities are featured as exclusive state variables within the OPF algorithm. Consequently, all the models for system controllers that are presented throughout this thesis have been based on this general modelling approach.
- An advanced mathematical model for the STATCOM within the OPF algorithm using Newton's method has been developed. For completeness, the controllable voltage source STATCOM model based on the augmented Lagrangian function framework has also been developed for comparative purposes with the advanced model of the STATCOM. It calls to attention that here-to-fore, no STATCOM-OPF models for Newton's method for augmented Lagrangian functions seem to have been reported in the open literature. The STATCOM models based on the equivalent voltage source

concept that have been reported are for positive-sequence power flows and three-phase power flows.

- A comprehensive OPF model for the Voltage Source Converter has been developed which is not based on a controllable voltage source behind the coupling impedance. The new VSC-OPF model accommodates realistic VSC control characteristics in the form of exclusive state variables in the OPF formulation. Furthermore, the model describes the performance of an actual VSC in AC/DC systems with a high degree of fidelity. The bi-directional active and reactive power flow control of a realistic VSC is modelled using the appropriate control constraints. To date, the VSC-OPF model developed as part of this research seems to be the most powerful analytical model developed for the purpose of OPF solutions – both in terms of the number of state variables that it encapsulates and in terms of the modularity which may grow incrementally to be a STATCOM or that may be expanded very dramatically to become a full multi-terminal VSC-HVDC system of an arbitrary configuration.
- Suitable connections of two or more VSC-OPF building blocks yield VSC-HVDC transmission link models, namely the back-to-back, the point-to-point and the multi-terminal schemes. The nodal active and reactive powers for the VSC-OPF model are modified to inherently include the DC link's transmission losses. The VSC-HVDC OPF model and its extensions, is the most comprehensive mathematical representation to date of a multi-terminal VSC-HVDC system, which, nonetheless, is fully flexible and easy to integrate in any modelling representation of the electrical power system. In order to test its strong modelling and simulation capabilities, a series of system simulations for both back-to-back, point-to-point and multi-terminal VSC-HVDC systems are presented.

## 1.5 Publications

The following IEEE Transactions publications are under current preparation:

1. Acha, E. and **Kazemtabrizi, B.**, “A New STATCOM Model for Power Flows using the Newton-Rapson method”, *to be submitted to IEEE Transactions on Power Systems, July 2011*
2. Acha, E. and **Kazemtabrizi, B.**, “The Incorporation of a New VSC-HVDC Link Model in Power Flows”, *to be submitted to IEEE Transactions on Power Systems, July 2011*
3. Acha, E. and **Kazemtabrizi, B.**, “A Generalized Model of the Voltage Source Converter for Multi-terminal VSC-HVDC Power Flows”, *to be submitted to IEEE Transactions on Power Systems, July 2011*
4. **Kazemtabrizi, B.** and Acha, E., “An Advanced STATCOM Model for OPF using Newton’s method”, *to be submitted to IEEE Transactions on Power Systems, August 2011*
5. **Kazemtabrizi, B.** and Acha, E., “The Incorporation of VSC-HVDC links in an OPF using Newton’s method”, *to be submitted to IEEE Transactions on Power Systems, August 2011*
6. **Kazemtabrizi, B.** and Acha, E., “Flexible Models of Multi-terminal VSC-HVDC links for OPF using Newton’s method”, *to be submitted to IEEE Transactions on Power Systems, August 2011*
7. De la Villa, A., Acha, E., **Kazemtabrizi, B.** and Gomez-Exposito, A., “An Advanced STATCOM Model for State Estimation”, *to be submitted to IEEE Transactions on Power Systems, September 2011*
8. De la Villa, A., Acha, E., **Kazemtabrizi, B.** and Gomez-Exposito, A., “The Representation of Multi-terminal VSC-HVDC in a State Estimator”, *to be submitted to IEEE Transactions on Power Systems, October 2011*

The following international textbook is in preparation under contract to be delivered to Wiley & Sons in October 2011:

Enrique Acha, Rodrigo J Garcia-Valle, Luigi Vanfretti, Antonio de la Villa, Pedro L Roncero-Sanchez and, **Behzad Kazemtabrizi**, “*VSC-FACTS, HVDC*”

*and PMU: Modelling, Analysis and Simulation in Power Grids*", John Wiley & Sons, London 2012

## 1.6 Thesis Outline

This thesis has been prepared in six chapters, including Introduction and Conclusion as such:

- Chapter 2

The principles of the Optimal Power Flow problem and its solution algorithm, Newton's method for augmented Lagrangian functions, have been thoroughly explained in this chapter. A general modelling criterion has been presented in this chapter, which is suitable for creating exclusive Lagrangians for any type of power system equipment taking advantage of their associated nodal powers. The general modelling criterion is also used to reflect the system's operational controllability using additional Lagrangians corresponding to the control equipments' associated equality constraints. This is followed by a series of carefully devised system simulations to properly depict the analytical prowess of the OPF algorithm using Newton's method for augmented Lagrangian functions. The method of handling system's empirical restrictions using exact penalty functions to create augmented Lagrangians has also been explained. The chapter closes with a succinct review of alternative OPF solution algorithms, which are not based on iterative numerical analysis techniques.

- Chapter 3

In this chapter, the model for a Static Compensator (STATCOM) aimed at OPF solutions has been introduced, which represents the STATCOM as a controllable voltage source. The solutions afforded by this model are compared with those given by the Static VAR Compensator (SVC) OPF model, an alternative and older FACTS equipment which serves the same primary function as the STATCOM. A variety of power system configurations are used for the purpose of this comparison.

- Chapter 4

In this chapter, a new and advanced model for the Voltage Source Converter for the OPF algorithm has been introduced. Contrary to conventional models, the new VSC-OPF model does not treat the VSC as a controllable voltage source behind the coupling impedance. As a result, a set of newly developed nodal active and reactive powers are introduced, which inherently include the PWM control characteristics of the VSC as exclusive state variables effectively circumventing most of the mathematical shortcomings of the VSC model based on the controllable voltage source concept. This model has been tested as a series compensator in a group of stand-alone AC network tests. Subsequently, the chapter concludes with describing the conditions whereby the new model is used to describe the behaviour of a realistic voltage source converter. This is followed by a series of radial DC system simulations in which the VSC is used to feed a DC load. Incorporating the new VSC model with a variable tap changer transformer in such system configurations will yield to modelling the STATCOM based on the new VSC modelling paradigm. However the new STATCOM-OPF model has not been addressed in this chapter.

- Chapter 5

The new VSC-OPF model presented in the previous chapter is expanded and suitably modified in order to model back-to-back, point-to-point and multi-terminal VSC-HVDC links power transmission applications. A series of simulations are presented in this chapter to illustrate the behaviour of the new VSC-HVDC OPF models. The most comprehensive mathematical representation of a multi-terminal point-to-point VSC-HVDC system based on the newly developed VSC-OPF model is presented in this chapter and it is applied to medium-size AC systems.

- Chapter 6

The general conclusions are drawn in this chapter for the whole research work. This is followed by a series of suggestions for further research in

different areas of power system analysis and modelling which may be built upon the new research ideas, concepts, methods and code assembled together in this timely piece of research.

## 1.7 References

- [1] Stevenson, W. D., Grainger, J. , *Power System Analysis*: McGraw-Hill 1994.
- [2] Acha, E., Fuerte-Esquivel, C. R., Ambriz-Perez, H., Angeles-Camacho, C., *FACTS Modelling and Simulation in Power Networks*: John Wiley & Sons Ltd., 2005.
- [3] Hingorani, G. N., Gyungyi, L., *Understanding FACTS: Concepts and Technologies of Flexible AC Transmission Systems*: IEEE, 2000.
- [4] Acha, E., Agelidis, V. G., Anaya-Lara, O., Miller, T. J. E., *Power Electronic Control in Electrical Systems*: Newnes, 2002.
- [5] Davidson, C. C., de Preville, G., "The future of high power electronics in Transmission and Distribution power systems," presented at the Power Electronics and Applications, 2009. EPE '09. 13th European Conference on,, 2009.
- [6] Deshpande, N. R., Sasi, N., Sawant, R. R., "Modeling of multilevel voltage source converter," in *Power Electronics Systems and Applications, 2004. Proceedings. 2004 First International Conference on*, 2004, pp. 24-29.
- [7] Diaz, U. A. R., Hernandez, J.H.T., "Reactive Shunt Compensation Planning by Optimal Power Flows and Linear Sensitivities," presented at the Electronics, Robotics and Automotive Mechanics Conference, 2009. CERMA '09, 2009.
- [8] Fuerte-Esquivel, C. R., Acha, E., Ambriz-Perez. H. , "A Thyristor Controlled Series Compensator Model for the Power Flow Solution of Practical Power Networks," *Power Systems, IEEE Transactions on*, vol. 15, pp. 58-64, 2000.
- [9] Gitizadeh, M., Khalilnezhad, H., "Phase Shifter Transformers Optimum Allocation in Power Systems Using a Combinational Method," presented at the Power and Energy, PECON2010, IEEE International Conference on, 2010.
- [10] Glanzmann, G., Andersson, G., "Using FACTS devices to resolve congestions in transmission grids," *CIGRE/IEEE PES, 2005. International Symposium*, pp. 347-354, 7 Oct 2005 2005.
- [11] Gotham, D. J., Heydt, G. T., "Power flow control and power flow studies for systems with FACTS devices," *Power Systems, IEEE Transactions on*, vol. 13, pp. 60-65, Feb. 1998.
- [12] Gyugi, L., "Reactive compensation. Control of shunt compensation with reference to new design concepts," in *Generation, Transmission and Distribution, IEE Proceedings*, 1981, pp. 374-381.
- [13] Gyugi, L., "Unified power-flow control concept for flexible AC transmission systems," in *Generation, Transmission and Distribution, IEE Proceedings C*, 1992, pp. 323-331.
- [14] Huang, G. M., Ping Yan, "TCSC and SVC as re-dispatch tools for congestion management and TTC improvement," presented at the Power Engineering Society Winter Meeting, 2002. IEEE, 2002.

- [15] Iliceto, F., Cinieri, E., "Comparative analysis of series and shunt compensation schemes for AC transmission systems," *Power Apparatus and Systems, IEEE Transactions on*, vol. 96, pp. 1819-1830, Nov. 1977.
- [16] Kimbark, E. W., "A New Look at Shunt Compensation," *Power Apparatus and Systems, IEEE Transactions on*, vol. PAS-102, pp. 212-218, Jan. 1983 1983.
- [17] Lockley B., P. G. (2002, Mar/Apr 2002) Static VAR Compensators: A Solution to the Big Motor/Weak System Problem? *IEEE Industry Applications*. 43-49.
- [18] Mahajan, V., "Thyristor Controlled Series Compensator," in *Industrial Technology, 2006. ICIT 2006. IEEE International Conference on*, 2006, pp. 182-187.
- [19] Noroozian, M., Petersson, A. N., Thorvaldson, B., Nilsson, B. A., Taylor, C. W., "Benefits of SVC and STATCOM for Electric Utility Application," presented at the Transmission and Distribution Conference and Exposition, IEEE PES, 2003.
- [20] Ou, Y., Singh, C., "Improvement of Total Transfer Capability Using TCSC and SVC," *Power Engineering Society General Meeting, 2001. IEEE*, vol. 2, pp. 975-947, July 25 2002.
- [21] Song, H. Y., Johns, T. A., *Flexible ac transmission systems (FACTS)*. London: The Institute for Electrical Engineers, 1999.
- [22] Wong, K. T. G., "The role of static VAR compensators in staving off voltage collapse," *Voltage Collapce (Digenst No: 1997/101), IEE Colloquium on*, pp. 5/1-5/5, 24 April 1997 1997.
- [23] Zhang, X., Handshcin, E. J., "Optimal Power Flow Control By Converter Based FACTS Controllers," presented at the AC-DC Power Transmission, 2001. Seventh International Conference on, 2001.
- [24] Zhang, Y., Zhang, Y., Wu, B., Zhou, J., "Power injection model of STATCOM with control and operating limit for power flow and voltage stability analysis," *Electric Power Systems Research*, vol. 76, pp. 1003-1010, August 2006.
- [25] Krug, D., Bernet, S., Dieckerhoff, S., "Comparison of state-of-the-art voltage source converter topologies for medium voltage applications," in *Industry Applications Conference, 2003. 38th IAS Annual Meeting. Conference Records of the*, 2003, pp. 168-175.
- [26] Gengyin, L., Ming, Z., Jie, H., Guangkai, L., Haifeng, L., "Power Flow Calculation of Power Systems Incorporating VSC-HVDC," presented at the Power System Technology, International Conference on, 2004.
- [27] Radomski, G., "Modelling and modulation of voltage source converter," presented at the Power Electronics and Motion Control Conference, 2008. EPE-PEMC 2008. 13th, 2008.
- [28] Arrillaga, J., *High Voltage Direct Current Transmission*. London: The Institute of Electrical Engineers, 1998.
- [29] Angeles-Camacho, C., Tortelli, O. L., Acha, E., Fuerte-Esquivel, C. R., "Inclusion of a High Voltage DC-Voltage Source Converter Model in a Newton-Raphson Power Flow Algoirhm," *Generation, Transmission and Distribution, IEE Proceedings*, vol. 150, pp. 691-696, Nov. 2003.

- [30] Agelidis, V. G., Demetriades, G. D., Flourentzou N., "Recent Advances in High-Voltage Direct-Current Power Transmission Systems," presented at the Industrial Technology, 2006. ICIT 2006. IEEE International Conference on,, 2006.
- [31] Pizano-Martinez, A., Fuerte-Esquivel C. R., Ambriz-Perez, H., Acha, E., "Modeling of VSC-Based HVDC Systems for a Newton-Raphson OPF Algorithm," *Power Systems, IEEE Transactions on*, vol. 22, pp. 1794-1803, Nov. 2007.
- [32] Bahrman, M. P., Johnson, B. K. (2007) The ABCs of HVDC transmission technologies. *Power and Energy Magazine, IEEE*. 32-44.
- [33] Bersesti, P., Kling, W. L., Hendriks, R. L., Vailati, R., "HVDC Connection of Offshore Wind Farms to the Transmission System," *Energy Conversion, IEEE Transactions on*, vol. 22, pp. 37-43, 2007.
- [34] Diaz, N. L., Barbosa, F. H., Trujillo, C. L., "Implementation of Nonlinear power flow controllers to control a VSC," presented at the Power Electronics and Motion Control Conference, 2008. EPE-PEMC 2008. 13th 2008.
- [35] Sarkar, S., Vijayan, P., Aliprantis, D. C., Ajarapu, V., "Effect of grid voltage unbalance on operation of a bi-directional converter," presented at the Power Symposium, 2008. NAPS ' 08. 40th North American 2008.
- [36] Pan, J., Nuqui, R., Stivastava, K., Jonsson, T., Holmberg, P., Hafner, Y. -J., "AC Grid with Embedded VSC-HVDC for Secure and Efficient Power Delivery " presented at the Energy 2030 Conference, 2008. ENERGY 2008. IEEE, 2008.
- [37] Fang, J., Gengyin, L., Zhou, M., Liang, X., "Research on the Voltage Source Converter in VSC-HVDC " presented at the Power System Technology (POWERCON), 2010 International Conference on,, 2010.
- [38] Guoqing, L., Jian, Z. , "Available Transfer Capability Calculation for AC/DC Systems with VSC-HVDC," presented at the Electrical and Control Engineering (ICECE), 2010 International Conference on,, 2010.
- [39] Westermann, D., Van Hertem, D., Kuster, A., Atmuri, R., Klockm B., Rauhala, T., "Voltage source converter (VSC) HVDC for bulk power transmission - technology and planning method," presented at the AC and DC Power Transmission, 2010. ACDC. 9th IET International Conference on,, 2010.
- [40] Azimoh, L. C., Folly, K. A., Chowdhury, S. P., "Mitigations of voltage instability in power systems," presented at the Electrical Power & Energy Conference (EPEC), 2009 IEEE, 2009.
- [41] Clark, H., Edris, A. -A., El-Gasseir, M., Epp, K., Isaacs, A., Woodford, D. (2008) Softening the Blow of Disturbances. *Power and Energy Magazine, IEEE*. 30-41.
- [42] Zhang, L., Harnefors, L., Nee, H. -P., "Interconnection of Two Very Weak AC Systems by VSC-HVDC Links Using Power-Synchronization Control," *Power Systems, IEEE Transactions on*, vol. 26, pp. 344-355, 2011.
- [43] de Alegria, I. M., Martin, J. L., Kortabarria, I., Andreu, J., Ereno, P. I., "Transmission alternatives for offshore electrical power," *Renewable and Sustainable Energy Reviews*, vol. 13, pp. 1027-1038, 2009.

- [44] Gomis-Bellmunt, O., Liang, J., Ekanayake, J., King, R., Jenkins, N., "Topologies of multiterminal HVDC-VSC transmission for large offshore wind farms," *Electric Power Systems Research*, vol. 81, pp. 271-281, 2011.
- [45] Wu, R., Dewan, S. B., Slemmon, G. R., "Analysis of an AC to DC voltage source converter using PWM with phase and amplitude control," presented at the Industry Applications Society Annual Meeting, 1989. Conference Record of the 1989 IEEE, 1989.
- [46] Shimizu, T., Fujioka, Y., Kimura, G., "DC ripple current reduction method on a single phase PWM voltage source converter," in *Power Conversion Conference - Nagaoka 1997., Proceedings of the., 1997*, pp. 237-240.
- [47] Kosterev, D. N., "Modeling synchronous voltage source converters in transmission system planning studies," *Power Delivery, IEEE Transactions on*, vol. 12, pp. 947-952, 1997.
- [48] Douangsyla, S., Indarack, P., Kanthee, A., Kando, M., Kittiratsatcha, S., Kinnares, V., "Modeling for PWM voltage source converter controlled power transfer," presented at the Communications and Information Technology, 2004. ISCIT 2004. IEEE International Symposium on, 2004.
- [49] Sun, D. I., Ashley B., Brewer B., Hughes, A., Tinney, W. F., "Optimal Power Flow by Newton's Approach," *Power Apparatus and Systems, IEEE Transactions on*, vol. PAS-103, pp. 2864-2875, 1984.
- [50] Baptista, E. C., Belati, E. A., da Costa, G. R. M., "A New Solution to the Optimal Power Flow Problem," presented at the Power Tech Proceedings, 2001 IEEE Porto, 2001.
- [51] Belati, E. A., de Sousa, V. A., Nunes, L. C. T., da Costa, G. R. M., "Newton's Method associated to the Interior Point Method for Optimal Reactive Dispatch Problem," in *Power Tech Conference Proceedings*, IEEE Bologna, 2003, p. 6.
- [52] Da Costa, G. R. M., Langona, K., Alves, D. A., "A new approach to the solution of the optimal power flow problem based on the modified Newton's method associated to an augmented Lagrangian function," *Power System Technology, 1998 Proceedings. POWERCON' 98. 1998 International Conference on.*, vol. 2, pp. 909-913, 18-21 Aug 1998.
- [53] de Souza, A. M., de Sousa, V. A., da Costa, G. R. M., "Optimal Power Flow: a Tool for Managing the Transmission Congestion," in *Power Engineering Society General Meeting, IEEE*, 2004, pp. 844-848.
- [54] Dommel, H. W., Tinney W. F., "Optimal Power Flow Solutions," *Power Apparatus and Systems, IEEE Transactions on*, vol. PAS-87, pp. 1866-1876, Oct. 1968 1968.
- [55] Lage, G. G., de Sousa, V. A., da Costa, G. R. M., "Optimal power flow solution using the penalty/modified barrier method," *Power Tech, 2009 IEEE Bucharest.*, pp. 1-6, June 28 - July 2 2009.
- [56] Pardalos, P. M., Resende, M. G. C., *Handbook of Applied Optimization*: Oxford University Press, 2002.
- [57] Rashed, A. M. H., Kelly, D. H., "Optimal Load Flow Solution Using Lagrangian Multipliers and the Hessian Matrix," *Power Apparatus and Systems, IEEE Transactions on*, vol. PAS-93, pp. 1292-1297, Sept. 1974 1974.

- [58] Santos, A., Jr., Deckmann, S., Soares, S., "A dual augmented Lagrangian approach for optimal power flow," *Power Systems, IEEE Transactions on*, vol. 3, pp. 1020-1025, Aug 1988.
- [59] Santos, A., Jr., da Costa, G. R. M., "Optimal-power-flow solution by Newton's method applied to an augmented Lagrangian function," *Generation, Transmission and Distribution, IEE Proceedings*, vol. 142, pp. 33-36, 1995.
- [60] Sasson, A. M., Vilorio, F., Aboites F., "Optimal Load Flow Solution Using the Hessian Matrix," *Power Apparatus and Systems, IEEE Transactions on*, vol. PAS-92, pp. 31-41, Jan. 1973.
- [61] Sousa, A. A., Torres, G. L., "Globally Convergent Optimal Power Flow by Trust-Region Interior-Point Methods," presented at the Power Tech, Lausanne, 2007.
- [62] Penny, J., Lindfield, G., *Numerical Methods using MATLAB*: Prentice Hall, 1999.
- [63] Atkinson, K., Weimin, H., *Theoretical Numerical Analysis: A Functional Analysis Framework*: Springer, 2005.
- [64] Allaire, G., *Numerical Analysis and Optimization: An Introduction to Mathematical Modelling and Numerical Simulation*: Oxford University Press, 2007.

## 2 Optimal Power Flow

The main body of this chapter comprises explanation of the theoretical background of the mathematical framework, namely Optimal Power Flow (OPF) algorithm, upon which models of power systems in this project are based. The OPF algorithm has been used ever since the early 1960's with a variety of solution algorithms developed to date [1]. In this chapter, the foundations of the mathematical algorithm used to formulate and solve the OPF problem has been explained in detail. The Augmented Lagrangian Function framework is chosen to formulate the OPF problem, which is then solved using Newton's method. The method's robustness and fast convergence rate is illustrated by depicting a few empirical simulations applied to both experimental and realistic power systems. The chapter then concludes with a brief section entailing to the alternative solution algorithms including meta-heuristic methods for solving the OPF problem. It should however be noted that the mathematical toolbox throughout this research has been remained the OPF Newton's method algorithm.

### 2.1 Introduction

The vast degree of density of modern interconnected power systems (networks) as well as high rises in fossil fuel prices particularly in recent years, require an effective solution for power system planners and engineers to properly cope with the ever increasing problem of economic distribution of power between generators within the network. Setting proper system operating conditions and strategies without compromising system's operational restrictions is therefore a requirement of modern robust power system design solutions [2, 3]. Consequently, in recent years, the OPF tool has become widely used for especially economic power dispatch purposes as well as determining system's optimum operating point.

The Optimal Power Flow (OPF) problem is a variant of constrained power flow problems. It is applied to the set of power flow equations that are constrained by system's operational characteristics, such as thermal and static stability limits of the transmission lines, generator and load bus voltages and phase angles, nodal active and reactive powers and depending on the system's configurations and control equipment, other associated state variables [2]. It often comprises an objective function (such as the generator's active power cost or transmission losses), which is

then subjected to power system's operational restrictions. The alleged restrictions imposed on system's state variables and on nodal power flow equations accordingly, represent the boundaries of the OPF solution space and are dubbed the constraints, which are of equality and inequality types [1-7]. A given solution to the OPF problem must always satisfy these restrictions. The OPF feasibility criteria are called the optimality conditions [3, 8-11] and are discussed in detail further in this chapter.

For a feasible solution to exist, these conditions must always be met upon reaching a solution. Consequently, optimal power flows are very effective way to determine the network's state variables that yield the best operating conditions when subjected to credible operations restrictions such as thermal or stability limits [12]. Furthermore, OPF can also be used to determine the state of a network while under the control of FACTS devices using their control characteristic as operating constraints [3]. For instance, an SVC (Static VAR Compensator), which is set to regulate the voltage of a given bus, is an additional operating constraint in the OPF formulation. In this case, the OPF solution is no longer the 'minimum cost' solution (if the objective is set to minimise generation costs) but it will yield best operating conditions that the network achieves while using SVC as a voltage regulating device. As a result it makes OPF a powerful analytical solution toolbox with application to almost any network, regardless of its configuration and equipment used.

Throughout this research the effort has been put into developing advanced models for a special group of electronically controlled devices, namely Voltage Source Converters (VSCs), which are used to regulate power system's fundamental parameters (Voltage, Phase Angles and Nodal Powers). Using the modelling criterion introduced in this chapter, various test case scenarios are deduced to properly analyse the behaviour of power networks, which may include a variety of devices including several FACTS equipment.

In the subsequent sections, the OPF mathematical formulation using Newton's method has been addressed thoroughly, followed by an extensive literature review on previous works done with regards to both devising mathematical solution algorithms.

Since the optimal power flow problem is closely inter-related to the Conventional Power Flow problems, it is only appropriate to start with outlining the general principles governing the power flow theory using Newton's method, which apply to both the OPF and CPF (Conventional Power Flow) problems.

## **2.2 An Overview of Power Flow Problem**

The primary purpose of solving conventional power flow problem is to determine the condition of the network under steady-state operation by evaluating its nodal voltage magnitudes and phase angles (voltage phasors) as well as nodal active and reactive powers and power flows of transmission lines [2, 3, 12]. Due to the complex nature of power systems, conventional algebraic solutions are not suitable for solving power flow problems and as a result, the set of non-linear equations are solved using iterative numerical analysis methods, such as Gauss-Seidel or Newton's method [12-15]. Power flow equations are particularly used in devising contingency analysis studies in the event that a change occurs in system's configuration, for instance when adding or removing a transmission line or a generator. They are also appropriate for purposes of stability studies in evaluating the condition of the system, after the presence of chief disturbances such as short circuit faults [2]. Power flow equations therefore, are suitable for determining system's conditions under which it maintains stability by determining its state variables in such a way that they agree well within their operating boundaries.

Unlike conventional power flow studies, the purpose of optimal power flow however is to evaluate the system's optimum operating point under specific conditions dictated by system's operation and equipment physical restrictions [6]. Consequently, the results obtained from an optimal power flow solution algorithm may not necessarily agree with those given by solving the set of conventional power flow equations even though both are based on the same network and subject to same operating constraints.

For reasons stated further in this chapter (section 2.3) the algorithm chosen for modelling purposes throughout this research has been the already well-established Newton's method for an Augmented Lagrangian Function [3-9, 11].

Pure Newton's method [3, 13-16] solves a given non-linear equation  $F(x) = 0$  for  $x$  using its Taylor series expansion approximation; supposing a solution vector  $x^{(i)}$  exists for function  $F(x)$  then its Taylor expansion applies as shown in equation (2.1) at iteration  $i$  converting the non-linear function  $F(x)$  to a series of linear equations:

$$F(x^{(i)}) = F(x^{(i-1)}) + F'(x^{(i-1)})\Delta x^{(i)} \quad 2.1$$

Solving  $F(x^{(i)}) = 0$  for  $x^{(i)}$  will yield to the following set of linear equations given by the matrix of first order partial derivatives of  $F$  or the Jacobian of  $F$ :

$$F(x^{(i-1)}) = -F'(x^{(i-1)})\Delta x^{(i)} \quad 2.2$$

In which we have:

$$\Delta x^{(i)} = -F'(x^{(i-1)})^{-1}F(x^{(i-1)}) \quad 2.3$$

According to equation (2.3), Newton's method is applied to almost any non-linear function provided that they are continuously differentiable over the solution space [13, 14] and that the Jacobian of  $F$  is non-singular [10]. This mathematical fact applies for both conventional as well as optimal power flow algorithms that utilise Newton's method.

In power systems analysis paradigm, the function becomes the non-linear power flow equations (nodal active and reactive powers) based on network's nodal admittance (or impedance) matrix [3, 6, 12] as shown below:

$$S = V J^* \quad 2.4$$

Replacing for system's current, for a given bus  $i$ , the following expression is written in the complex polar coordinates:

$$S_i = P_i + jQ_i = V_i \cdot \left[ \sum_k^{Nbus} Y_{ik}^* \cdot V_k^* \right] = V_i \cdot e^{j\theta_i} \cdot \sum_k^{Nbus} (G_{ik} - jB_{ik}) \cdot V_k \cdot e^{-j\theta_k} \quad 2.5$$

By implementing complex algebra to equation (2.5), the real and imaginary parts of equation (2.5) are calculated. These are shown in equations (2.6) and (2.7) and represent the nodal active and reactive powers of the system:

$$P_i = \text{Re}\{V_i \cdot e^{j\theta_i} \cdot \sum_k^{Nbus} (G_{ik} - jB_{ik}) \cdot V_k \cdot e^{-j\theta_k}\} = V_i \cdot \sum_k^{Nbus} \{V_k [G_{ik} \cos(\theta_i - \theta_k) + B_{ik} \sin(\theta_i - \theta_k)]\} \quad 2.6$$

$$Q_i = \text{Im}\{V_i \cdot e^{j\theta_i} \cdot \sum_k^{Nbus} (G_{ik} - jB_{ik}) \cdot V_k \cdot e^{-j\theta_k}\} = V_i \cdot \sum_k^{Nbus} \{V_k [G_{ik} \sin(\theta_i - \theta_k) - B_{ik} \cos(\theta_i - \theta_k)]\} \quad 2.7$$

These equations are the principal equations for modelling power system components in both conventional and optimal power flow algorithms.

Applying Newton's method (equations 2.2 and 2.3) to the set of non-linear power equations in equation (2.5) for a given vector of state variables  $x = [\theta, V]^T$  in a  $n$ -bus system, will give rise to the set of  $n$ -nodal equations shown in (2.8):

$$[\Delta S] = -[\nabla_x S] \Delta x \quad 2.8$$

Equation (2.8) is the direct result of applying Newton's method to a non-linear function (or a group of functions in this case nodal active and reactive powers), which comprises several elements.

Knowing that  $S = [P, Q]^T$  is defined as the set of nodal active and reactive powers in an arbitrary power system, the matrix of first-order partial derivatives of the nodal active/reactive power equations with respect to network's vector of state variables as shown in equation (2.9) and is called the Jacobian of  $S$  [3]:

$$J = [\nabla_x S] = \left[ \frac{dP}{dx}, \frac{dQ}{dx} \right]^T \quad 2.9$$

In an interconnected power system the vector of state variables consists of the nodal voltage magnitudes and phase angles as depicted in equation (2.10):

$$x = [\theta, V]^T \quad 2.10$$

In which  $\theta = [\theta_2, \dots, \theta_{Nbus}]^T$  is the sub-vector of phase angles (except for the Slack bus) and  $V = [V_2, \dots, V_{Nbus}]^T$  is the sub-vector of nodal voltage magnitudes (except for the Slack bus). The Slack bus is the reference bus in the power flow problem formulation and it always is chosen to be a generator bus with bulk power generation capable of handling unforeseen situations that may occur in order to maintain the system's steady state operation [2].

The matrix  $[\Delta S] = [\Delta P, \Delta Q]^T$  is called the matrix of mismatch equations and  $[\Delta x] = [\Delta \theta, \Delta V]^T$  is called the correction (or direction) vector, which in the course of the solution maintains a declining pace until its pre-defined tolerance level is reached [2, 3, 12]. Consequently the set of linear equations to be solved in iteration  $i$  via Newton's method take the form of equation (2.11) below:

$$\Delta x^{(i)} = -J^{-1(i-1)} [\Delta P, \Delta Q]^T{}^{(i-1)} \quad 2.11$$

As seen from equation (2.11), the conventional Power Flow problem is based on the co-efficient matrix of first-order partial derivatives of nodal power equations (the Jacobian), it should be noted that increasing the order of partial derivatives would result in less sparsity of the co-efficient matrix but more speed. In case of Optimal Power Flow as it will be mentioned later, a special matrix of second-order partial derivatives is used which guarantees both good sparsity and convergence speed [4, 6].

The initial conditions as required by Newton's method for both CPF and OPF, are defined depending on the types of the nodes in any arbitrary system. The voltage-

controlled buses, for instance, are those with generators (or any other voltage regulating devices) connected to them whereas load buses are those connected to loads for which the complex voltage phasors are to be determined through the power flow solution [2, 3]. The basic theory of conventional power flows is explained in a comprehensive manner in [2] and therefore it is not stressed here any further. It should be noted that focus of this research is on a variant of constrained power flow problems, namely optimal power flow. A comprehensive discussion is therefore given regarding OPF as the main mathematical toolbox of this research in the next section.

## **2.3 Optimal Power Flow Algorithm**

The general principles outlining the optimal power flow formulation and its solution algorithm based on Lagrangian functions is presented in a comprehensive fashion in this section. The problem formulation presented here is the basis of all the modelling that is carried out in this research project.

### **2.3.1 An Overview of Optimal Power Flow Problem: Formulation and Solution Algorithms**

The OPF has several applications in power systems analysis and design [1, 6]. Due to the vast complexity of today's modern power networks they are more prone to incurring instability due to even smallest undesired changes in their operation. The OPF therefore seems like a reliable tool for devising multiple assessment scenarios implemented to a power system in order to ensure its continued safe operation. For instance, strong AC couplings exist in a power network with AC line/cable interconnections, which in cases of power imbalances, due to a sudden loss of generation or line tripping in one area that causes a change in network operating frequency, are likely to induce frequency deviations to units in other areas which eventually leads to system collapse [2].

Considering the feasibility criteria of OPF, applying an economic dispatch analysis achieved by OPF algorithm to this particular system will guarantee the safe distribution of loads between multiple generating points while maintaining generation at an optimum level that agree well with system's operational as well as equipments' physical constraints, hence keeping the balance between demand and

generation at all times and minimising the possibility of equipment failure as well as other undesired dynamic responses. This very fact makes OPF an essential tool for modern network analysis, planning and design.

The OPF by definition is a constrained non-linear convex optimisation problem and therefore it belongs to the category of non-linear programming. Non-linear programming refers to the group of optimisation problems in which the objective function to be minimised (or optimised) or constraints show non-linearity [9-11]. Convexity on the other hand means that the solution space contains at least one global minimum [7, 9, 17]. It is necessary to mention that the OPF solutions carried out throughout this thesis yield the best possible solution, which from practical perspective is the optimum solution. Depending on the types of constraints used, the optimisation problems are categorised into three main groups, namely Equality Constrained Problems (ECP), Inequality Constrained Problems (ICP) and General Programming Problems [8, 10].

A general programming problem refers to those classes of optimisation problems, which contain both equality and inequality constraints. Most of the optimisation problems applied to physical systems (power networks included) are of this type.

Within the power systems paradigm, the equality constraints refer to the conditions which must hold if the system is to continue normal steady-state operation, in other words, the operation of a given power system is stable as long as the nodal power balance equations hold for each bus. Moreover, the inequality constraints are the result of implementing network's realistic operating conditions as well as equipment limits, for instance complex voltage in each node in an inter-connected power system is bounded by its upper and lower margins which are then enforced to ensure system operates within its static stability margins. Several solution methods have been proposed to solve the general programming problems. The most conventional and reliable method is to use numerical solution methods aimed at decreasing the gradient of the problem's objective function. These are collectively known as gradient-based methods. There are generally three categories of such solution algorithms for a general non-linear programming problem such as the OPF [3, 8-11].

#### I. Interior Point Methods (e.g. Logarithmic Barrier Function)

- II. Exterior Point Methods (e.g. Quadratic Penalty Function)
- III. Exact Penalty Function Methods (e.g. Augmented Lagrangian Function)

Lagrangian and penalty function methods share the same mathematical principles that aim to convert the constrained problem of OPF into a single (or a series of) unconstrained problem by penalising the objective function for points outside the feasible solution space (hence the name exterior point method) [9, 10]. The main difference between the two is that in penalty function methods (for instance in quadratic penalty function method), the objective function is penalised directly whereas in Lagrangian type methods, it is the Lagrangian function (formed via the use of Lagrangian multipliers) that is penalised. The latter has considerable numerical advantage over the former approach in that the optimal solution is reached without having to enlarge the penalty parameters of the penalty function to near infinity, a common problem in exterior point methods which introduces ill-conditioning and therefore numerical difficulties [8-10]. The augmented Lagrangian function by comparison is therefore considered as an improvement to the penalty function method, for it is only necessary to form one single unconstrained problem by combining a Lagrangian function (using multipliers) and a quadratic penalty function (using penalty parameters) together, therefore it has a better convergence rate than pure penalty function methods (obviously given the right initial conditions).

Another alternative to exterior point methods is the use of Barrier Functions [8-11, 18-22]. The barrier functions (typically logarithmic) prevent the solution points of the dual problem (unconstrained penalised function) from crossing the feasible space by setting barriers against its boundaries [9]. Because in this method the optimum is reached from within the solution space they are formally called Interior Point Methods.

Over the course of the years, comprehensive research has been carried out in the area of OPF on both methods (exterior or interior point) and there are several publications in open literature that address the problem of the OPF [1, 4-7, 18-35].

These works are normally divided into two categories; the first group pertains to the principal analysis and definition of OPF, which has been developed since the late 60s. One of the most important works done in the area of OPF formulation is the first-order gradient decent approach proposed by Dommel and Tinney in [1]. In this paper published in 1968 the principles of a Jacobian based OPF solution algorithm via Newton's method is presented, which attempts to minimise a set of linear equations developed from Lagrangian function of the system by directly evaluating a gradient of objective function. Since this method uses Jacobian terms to evaluate the state variables via Newton's method just like a conventional power flow problem (section 2.2) it gets highly complicated in real multi-node systems, it has also less convergence rate (although it maintains quadratic convergence) than higher order methods such as explicit Hessian-based solutions [4, 5].

On the other hand, applying Newton's method to explicit Hessian matrix would result in improved convergence rate at the expense of losing the higher degree of sparsity in the matrix of coefficients. The less sparsity of Hessian matrix is a mathematical fact and stems from the definition of the Hessian as being the second order partial derivatives of a function (in case of a power system, nodal powers) with respect to state variables (for instance nodal voltages or phase angles). According to definition of Hessian/Jacobian terms the non-neighbouring partial derivative terms in the Jacobian matrix are always zero but not in the Hessian matrix, which will ultimately yield to a more crowded Hessian matrix for the same system [4]. As an improvement to the Hessian approach a newly defined second order partial derivatives matrix of coefficients is introduced in [6] by direct evaluation of the Lagrangian multipliers in the system of linear equations, thus combining both Hessian and Jacobian terms to achieve better sparsity and yet better convergence rate. One of the difficulties of the method developed in [6] is in the nature of active inequality constraints, however the constraint handling has been improved in [7, 23, 26] with introducing the augmented Lagrangian function by combining multipliers and penalty functions.

From globally convergent algorithm to improvements in interior-point methods, there is a diverse range of different methods to solve the OPF problem. However in this research project the proposed solution algorithm has been the Newton's method for an augmented Lagrangian function [6, 7] combining the strong attributes of both

Newton's method and non-linear programming method of augmented Lagrangian function. The second group of papers relate to the variety of approaches (solutions) and modifications taken regarding the OPF mathematical solution algorithms [18-20, 22, 28-31, 34-36].

Most recently the trend in developing solution algorithms for OPF problem has been slightly shifted from gradient-based conventional numerical analysis (such as the augmented Lagrangian method) to direct search methods, heuristic approaches and evolutionary programming, and algorithms such as Particle Swarm Optimisation have come to light in the realm of power systems research [24, 27, 32, 33]. These so-called alternative approaches shall be considered in a separate section (section 2.5) at the end of this chapter but it should be mentioned here that analysing various approaches to the problem of optimisation is a purely mathematical argument, which is out of the scope of this research project. In the subsequent paragraphs, however, the basics of the OPF solution algorithms based on Lagrangian methods, has been presented.

### **2.3.2 Newton's Method for Augmented Lagrangian Function in Optimal Power Flow: Mathematical Toolbox**

For reasons stated above (numerical stability, improved convergence), in this research, the augmented Lagrangian function is chosen to formulate the OPF problem. The explicit Newton's method discussed in previous section is used to solve the system of linear equations formed with the matrix of second order partial derivatives of the augmented Lagrangian function as the objective function with respect to system's state variables. This method in comparison with the pure penalty function method and interior point methods has the best convergence rate possible. Furthermore it handles the constraint violations by combining multipliers and quadratic penalty functions together to achieve better reliability in finding the optimal solution [8]. All the models developed in the subsequent chapters are within such framework and therefore the sound understanding of the mathematical toolbox developed here is of paramount importance. It should be noted that the purpose of applying Newton's method is to minimise the augmented Lagrangian function and eventually determine the optimal solution.

### 2.3.2.1 Optimal Power Flow Problem Formulation: Objective Function, System State Variables Vector and the Constraints Set

The goal of the OPF algorithm is to find a series of settings for network parameters that are both feasible and yield to the optimum operating point of the system. For this purpose, the OPF must possess an objective function. Normally the objective function for an interconnected power system is chosen to be the generators' cost function, namely a quadratic function based on the generators incremental cost curve [2]. However alternative types of the objective function, such as transmission losses, reactive powers and equipment locations, may be chosen depending on the network requirements. It should be noted that the mathematical formulation described in this chapter remains generic regardless of the type of the objective function chosen, and consequently all the models developed in next chapters, are compatible as long as they are applied in Newton's method framework for any network configuration of any size and with any type of objective function. For consistency purposes, the objective function chosen throughout this research has been the non-linear generator cost function as explained in [3] and is shown in equation (2.12):

For  $N_g$  generators in a given system the cost function is defined as below:

$$F(P_g) = \sum_{j=1}^{N_g} (a_j + b_j P_{g_j} + c_j P_{g_j}^2) \quad 2.12$$

It is taken to be a quadratic function of generator's active power or  $P_g$  based on its cost curve produced by cost coefficients  $a$ ,  $b$  and  $c$ . The generators' active power schedule is initially determined through a loss-less economic dispatch analysis as explained in [2, 3].

This means that at the start of the OPF algorithm the loads are distributed in such a way that the incremental cost of generation of all the generating points remain similar (equal incremental cost criterion), in other words the rate of the generation costs with respect to changes occurring in the generators outputs is constant or  $\nabla_{P_g} F(P_g) = \text{const}$ .

This criterion provides a suitable starting condition for the OPF algorithm. The solution of the OPF algorithm however determines the final distribution of loads between the generators taking into account the system's losses as well [2].

The OPF in its most general form is formulated in equation (2.13) as a general non-linear programming problem.

For the given objective function  $f(y)$  in  $R^n$  space the following expression is written:

$$\text{Minimise } f(y) \tag{2.13}$$

Subject to

$$\begin{cases} h(x) = 0 \\ g(x) \leq 0 \end{cases}$$

Where

$h(x)$  is taken to be the set of equality constraints, and

$g(x)$  is the set of inequality constraints (operational limits)

And  $x$  is the state variables vector (primal variables) comprising of the system's nodal voltage magnitude and phase angles as well as variables associated with any FACTS equipment or transformers present in the system as shown in equation (2.14) below. They help define the system as a whole:

$$x = [\theta, V, x_{F-T}, y]^T \tag{2.14}$$

$y$  is the sub-vector of state variables associated with the objective function whose values are set to achieve the optimum. For instance for the objective function to be the generators' cost function the vector  $y = [P_g]^T$  applies, which corresponds to the

generators' active power output. In order to adhere to the conditions of the Newton's method the objective function needs to be chosen as a convex function with continuous differentiability within the OPF solution space.

System's state variables (equation 2.14) are essentially categorised into two main types, namely Control and Dependent variables [1, 3, 4, 6, 7, 23]. By definition, control variables are those whose values are set throughout the solution process in order to achieve the optimum operating point whereas dependent variables are those classes of state variables whose values depend on the condition of the system as well as control variables. For instance generating buses are of control type, because their terminal voltage is regulated by means of generator field control, as long as the generator operates within its reactive power limits (AVR works under normal operating conditions). On the other hand in the event of a violation in generator's reactive power its voltage no longer represents a control variable but its magnitude will depend on the amount of generator's violated reactive power, which is now fixed during the course of the solution. Other examples of control variables include, transformer tap ratios and phase shifter angles as well as control parameters of FACTS equipment. Moreover, load bus complex voltages are of dependent type variables whose values depend on the amount of nodal active/reactive power flows.

As seen in equation (2.13), the objective function by definition is always subject to system operating constraints. The system equality constraints are categorised into two main groups namely, Functional and Variable constraints [1]. The most important functional constraint is the system nodal power balance equation, which accounts for its normal steady-state operation.

As stated in equations (2.15) and (2.16) for a given bus ' $k$ ' the following applies:

$$\sum_i^n P_{i_k} - P_{g_k} + P_{d_k} = 0 \quad 2.15$$

For

$$k = 1, \dots, Nbuses$$

And

$$\sum_j^n Q_{j_k} - Q_{g_k} + Q_{d_k} = 0 \quad 2.16$$

For

$$k = 1, \dots, Nbuses$$

These equations state that in each node throughout the solution process, the balance between demand and generation must maintain for a continued steady-state operation (the algebraic summation of all the powers coming into and going out of the node must be equal). They hold for a normal AC system as well as FACTS-based systems. Other functional constraints are implemented, if needed, on power flow control equations (for example for active/reactive power control in a Voltage Source Converter). These particular constraints are addressed thoroughly in next chapters.

The variable constraints are exclusively used to model the control of system operation (Voltage Regulation, Phase Angle Control, Transformer Variable Tap Control) and therefore are defined on control variables. For example in case of a static VAR compensator, an additional equality constraint is added to its corresponding nodal voltage magnitude. The variable equality constraints are enforced using penalty functions.

The inequality constraints set (both on parameter and functional) are called the binding set [3] and normally comprise the generators' reactive power limits for generating buses, along with voltage and active power constraints for other buses as well as limits for additional equipment such as FACTS devices or transformers (equations 2.17-2.20):

$$Q_{G_k}^{\min} \leq Q_{G_k} \leq Q_{G_k}^{\max} \quad 2.17$$

$$P_k^{\min} \leq P_k \leq P_k^{\max} \quad 2.18$$

$$|V_k^{\min}| \angle \theta_k^{\min} \leq |V_k| \angle \theta_k \leq |V_k^{\max}| \angle \theta_k^{\max} \quad 2.19$$

$$x_{F-T}^{\min} \leq x_{F-T} \leq x_{F-T}^{\max} \quad 2.20$$

If a violation occurs throughout the course of the solution, the binding set of variables are enforced to their limits by means of exact penalty functions (penalising their Lagrangians) in order to satisfy the OPF optimality conditions [3, 9-11]. It should be noted that the functional inequalities are bounded to the system via Lagrangian multipliers only if a violation occurs in their values, whereas the functional equalities are bounded to the system throughout the solution process [3]. To add or remove any functional constraints to or from the system formulation, it may be necessary to penalise their corresponding Lagrange multipliers [3]. This fact is explained more thoroughly in further chapters, where the system operation can be described through different functional equality constraints using unique multipliers.

### 2.3.2.2 Optimal Power Flow Solution Process: Newton's method for Augmented Lagrangian Function

As mentioned earlier, the purpose of Lagrange multipliers is to convert the constrained problem of OPF into an unconstrained problem by forming a Lagrangian function.

Using Lagrange multipliers method, the problem formulation given in equation (2.13) is converted into one single unconstrained problem for the newly created augmented Lagrangian function as shown in equation (2.21) below:

$$\text{Minimise } L(x, \lambda, y, u_k) \quad 2.21$$

Where  $L$  is the new objective function and has the following general form:

$$L(x, \lambda, y, u_k) = \sum_i f_i(y) + \sum_j \lambda_j^T h_j(x) + \psi_k(u_k, g_k(x)) \quad 2.22$$

In which

$\sum f_i(y)$  is the summation of all the objective functions

$h(x)$  is the set of equality constraint equations (equations 2.15 and 2.16)

$g(x)$  is the set of inequality constraint equations

$x$  is the state variables vector that includes both control and dependent variables (equation 2.14)

$\lambda$  is the vector of equality constraint multipliers

$u$  is the vector of inequality constraint multipliers

$\psi_k(u_k, g_k(x))$  is the quadratic penalty function for corresponding active inequality constraints (active binding set).

The equality constraints are handled via the Lagrange multipliers (dual variables) that in turn, represent the sensitivity of the objective function to the changes in system's constraints [1, 3, 6, 8]. For example in case of active power balance shown in equation (2.15), its Lagrange multiplier corresponds to the changes in the objective function with respect to changes in the active power equality constraint (for each 1 MW of increase in power for instance) at the optimum operating point [2]. Consequently the Lagrange multiplier associated with a given bus 'i' is defined as below:

$$\lambda_i = \nabla_{h_i} L = \frac{df_i}{dh_i} \quad 2.23$$

Each of the system functional constraints has to be added to the system Lagrangian using its associated multiplier. The active inequality constraints are added to the system, in case of limit violations using the quadratic penalty function.

For practical purposes, it is assumed that during the course of OPF solution the inequalities remain inactive (in other words the system is assumed to work under

normal steady-state conditions) therefore the augmented Lagrangian introduced in equation (2.22) takes the following form:

$$L(x, \lambda, y) = \sum_i f_i(y) + \sum_j \lambda_j^T h_j(x) \quad 2.24$$

Equation (2.24) states that the system Lagrangian function is essentially the summation of all the objective functions along with the nodal active and reactive power equations set in equations (2.15) and (2.16). In section (2.3.4) the modelling criterion for power system components is given for properly form a Lagrangian function. By applying Newton's method to equation (2.22) the OPF is solved as a set of linear equations as such:

$$\nabla_{zz}^2 L(z) \times \Delta z = -\nabla_z L(z) \quad 2.25$$

In which 'z' is the vector of state variables as well as Lagrange multipliers (primal and dual variables vectors) as such:

$$z = [x, \lambda, y]^T \quad 2.26$$

And  $\Delta z$  is the mismatch (or correction) vector as shown in equation (2.27).

$$\Delta z = [\Delta x, \Delta \lambda, \Delta y]^T \quad 2.27$$

$\nabla_z L$  is the search direction or the gradient vector of the Lagrangian function, which should always be decreasing so as to minimise the system Lagrangian. Upon convergence of Newton's iterations, the gradient vector should be within a pre-determined tolerance typically taken to be  $1e-9$  [3].

The system of equations depicted above is illustrated with second and first order partial derivatives matrices, namely Hessian and Jacobian terms collectively comprising a coefficients matrix, taking into account the objective function and its

associated control variable as well. The matrix of coefficients should not be confused with explicit Hessian evaluation of the Lagrangian function [4, 5], which would be much less sparse. Instead, the matrix of coefficients  $\nabla_{zz}^2 L(z)$  is a combination of Hessian and Jacobian terms which maintains an acceptable degree of sparsity through using of Jacobian terms and at the same time achieves quadratic convergence rate in the Newton's loop by using higher-order partial derivative terms of the Lagrangian [6].

$$\begin{bmatrix} \nabla_{xx}^2 L(x, \lambda, y) & \nabla_x h(x)^T & \nabla_{xy}^2 L(x, \lambda, y) \\ \nabla_x h(x) & & \nabla_y h(x)^T \\ & \nabla_y h(x) & \nabla_{yy}^2 f(y) \end{bmatrix} \times \begin{bmatrix} \Delta x \\ \Delta \lambda \\ \Delta y \end{bmatrix} = - \begin{bmatrix} \nabla_x f(y) + \nabla_x h(x)^T \lambda \\ \Delta h(x) \\ \nabla_y f(y) + \nabla_y h(x)^T \lambda \end{bmatrix} \quad 2.28$$

Notice the vector of mismatch equations in the gradient vector is dubbed  $\Delta h(x)$  which corresponds to the mismatch of nodal active and reactive powers, presented in section (2.2).

If the objective function is taken to be the generators' cost function as presented in equation (2.12), then equation (2.28) is expressed in expanded form using Jacobian and Hessian terms as such:

$$\begin{bmatrix} \nabla_{\theta^2}^2 L & \nabla_{\theta V}^2 L & \nabla_{\theta \alpha}^2 L & \nabla_{\theta} h \\ \nabla_{V\theta}^2 L & \nabla_{V^2}^2 L & \nabla_{V\alpha}^2 L & \nabla_V h \\ \nabla_{x\theta}^2 L & \nabla_{xV}^2 L & \nabla_{x^2}^2 L & \nabla_x h \\ \nabla_{\theta} h & \nabla_V h & \nabla_x h & \nabla_{\lambda_{P_{g_i}}}^2 L \\ & & & \nabla_{\lambda_{P_{g_i}}}^2 L \quad \nabla_{P_{g_i}^2}^2 f(P_{g_i}) \end{bmatrix} \times \begin{bmatrix} \Delta \theta \\ \Delta V \\ \Delta x_{F-T} \\ \Delta \lambda \\ \Delta P_{g_i} \end{bmatrix} = - \begin{bmatrix} \nabla_{\theta} h(x)^T \lambda \\ \nabla_V h(x)^T \lambda \\ \nabla_{x_{F-T}} h(x)^T \lambda \\ \Delta h(x) \\ \nabla_{P_{g_i}} f(P_{g_i}) - \lambda_{P_k} \end{bmatrix} \quad 2.29$$

In which the following expressions are written for the Hessian/Jacobian terms associated with the generator cost function in equation (2.12):

For the *ith* generator connected to the *kth* bus, the system Lagrangian (ignoring the quadratic penalty function) is written as such:

$$L = a_i + b_i P_{g_i} + c_i P_{g_i}^2 + \lambda_{P_k} (\sum P_k - P_{g_i} + P_{d_i}) + \lambda_{Q_k} (\sum Q_k - Q_{g_i} + Q_{d_i}) \quad 2.30$$

Therefore calculating for the first and second partial derivatives of the following function with respect to the objective function variable, namely the generator active power output, would result in the following expressions:

$$\nabla_{\lambda_p P_{g_i}}^2 L = 0 + \nabla_{P_{g_i}} (\sum P_k - P_{g_i} + P_{d_i}) + 0 \rightarrow \quad 2.31$$

$$\nabla_{\lambda_p P_{g_i}}^2 L = -1$$

And

$$\nabla_{P_{g_i}^2}^2 L = \nabla_{P_{g_i}^2}^2 (a_i + b_i P_{g_i} + c_i P_{g_i}^2) + 0 + 0 \rightarrow \quad 2.32$$

$$\nabla_{P_{g_i}^2}^2 L = 2c_i$$

The partial derivatives of the objective function with respect to all the other variables in this particular case are zero since the generator cost function is only a function of  $P_g$ .

Equation (2.29) essentially represents the general format of OPF iterative solution via Newton's method for any type of network configuration and regardless of the equipment present. The vector of variables in equation (2.29), include all the state variables associated to the system, it also consists of the system's Lagrange multipliers whereby the equipment's constraints are bounded to create the system Lagrangian. As a result of using multipliers the Lagrangian function depicts the system's realistic behaviour characteristics in forms of functional constraints (power balance equations).

Notice that the penalty function  $\psi_{\kappa}(u_{\kappa}, g_{\kappa}(x))$  corresponding to the binding set (the set of inequality constraints) is not included in the Lagrangian function because they are not activated at the start of first iteration, in other words, active set only contains the state variables associated to the equality constraints and their corresponding multipliers (functional constraints). If a limit violation occurs during the course of

the solution, the penalty function will be activated forcing the violated inequality to its limits to satisfy the optimality conditions. Consequently the penalty function adds the set of activated inequalities to the already existing active set. The algorithm then solves the objective function for this newly updated active set.

### 2.3.2.3 Karush-Kuhn-Tucker Necessary Optimality Conditions (NOC's)

The OPF convergence criteria are expressed using the necessary optimality conditions otherwise known as the KKT conditions [1, 6, 9, 11] for a feasible solution. According to these conditions, upon convergence an optimum operating point,  $z^* = [x^*, \lambda^*, u^*]^T$ , has been definitely reached only if all the following statements are true:

1.  $\nabla_x L(z^*) \leq 0$  : The gradient vector with respect to state variables has to have reached a pre-determined tolerance level near zero (internal iterations must converge)
2.  $\nabla_\lambda L(z^*) = h(x^*) = 0$  : All equality constraint must be satisfied, in other words the network must be operating under normal working conditions
3.  $u_k^* g_k^* = 0$  : The product of the vector of inequality constraint multipliers and their corresponding inequalities must always be equal to zero (system works under normal conditions)

The last condition illustrates the feasibility of a solution, stating that for a given point to be acceptable, either of the following conclusions must always be true, if  $u_k^* = 0$ , then its corresponding inequality constraint must hold if a solution is to exist, namely  $g_k^* < 0$ . On the other hand if  $g_k^* = 0$  then its corresponding multiplier must be positive, namely  $u_k^* > 0$ , indicating that the alleged inequality has been activated during the solution process and is enforced to its limit boundaries [9]. Once again the KKT conditions emphasise the strong degree of reliability of Newton's method in terms of providing good realistic results based on system's operating constraints.

### 2.3.3 Quadratic Penalty Function in Augmented Lagrangian Method (Exact Penalty Function)

The quadratic penalty function defines an arbitrary boundary to the OPF solution space. It is only associated with active inequalities on state variables (and not functions) and has the general form illustrated in equation (2.33). In this research the quadratic penalty function  $\psi$  is not actually a pure penalty function, instead it is a penalised Lagrangian function or exact penalty function for the set of active inequalities (or the active binding set) [8]. As discussed in section (2.2), combining the Lagrangian function with a penalty function to bind the constraints to their respective limits has significant numerical advantages over pure penalty function methods where increasing the penalty parameter to near infinity to bind a value to their limits will result in ill-conditioned solutions. The quadratic penalty function binds the active inequalities, as new variable equalities, to the system Lagrangian through their associated inequalities multipliers, namely  $u$ . For the  $k$ th active inequality, the quadratic penalty function takes the following form:

$$\psi_k(u_k, \alpha, g_k(x)) = \begin{cases} u_k(g_k - g_k^{\max}) + \frac{\alpha}{2}(g_k - g_k^{\max})^2, u_k + \alpha(g_k - g_k^{\max}) \geq 0 \\ u_k(g_k - g_k^{\min}) + \frac{\alpha}{2}(g_k - g_k^{\min})^2, u_k + \alpha(g_k - g_k^{\min}) \leq 0 \\ zero \end{cases} \quad 2.33$$

The multiplier associated to active inequalities is upgraded using the expression below [3,8]:

$$u_k^i = \begin{cases} u_k^{i-1} + \alpha^{i-1}(g_k - g_k^{\max})^2, u_k^{i-1} + \alpha^{i-1}(g_k - g_k^{\max}) \geq 0 \\ u_k^{i-1} + \alpha^{i-1}(g_k - g_k^{\min})^2, u_k^{i-1} + \alpha^{i-1}(g_k - g_k^{\min}) \leq 0 \\ zero \end{cases} \quad 2.34$$

This function is essentially called the augmented Lagrangian function and has two properties: a Lagrangian function for the active inequality defined by the multiplier  $u_k$  which basically binds the active inequality to its limit boundaries within the OPF solution space, and a penalty function defined by penalty parameter  $\alpha$ , which is

used to penalise the Lagrangian function for any violations that takes place. The continuous differentiability is maintained for the augmented Lagrangian function by choosing a quadratic penalty function [9].

The function is non-zero for any violations in system state variables vector. The non-zero penalty parameter is initialised at a typically large constant, but care needs to be taken, as too large a constant would lead to ill conditioning of the coefficients matrix, which may lead to unfeasible solutions [8-11]. Nevertheless, it should maintain an increasing pace throughout the course of the solution, if there is an active binding set, according to a pre-determined criterion usually set by the user at the start of the iterative process. However upon convergence the product of the active inequality multiplier and its corresponding constraint must be zero, which means that with the act of penalty parameter the corresponding inequality constraint is enforced to its limit boundaries, and satisfied the third KKT condition namely,  $u_k(g_k - g_k^{\text{lim}}) = 0$ .

Notice that this function is added only after the Newton's iterations solves the system (internal loop) when all state variables are checked against their corresponding limits so that the violated ones may be included in the active set via their associated multipliers [3, 6, 8, 23, 26]. Should there be any violations in the constraints set the augmented Lagrangian function is then solved in another iteration of the internal loop with the active variable inequalities bounded towards their corresponding limits through the action of the penalty function [9]. The multipliers associated with active inequalities however are only updated after the internal loop using equation (2.34). This method effectively enforces the limit boundaries of the violated state variables and satisfies the third KKT necessary optimality conditions, if there is a feasible solution, otherwise the algorithm will not converge towards a solution in which case it is said that the network conditions are not realistically presented.

The pure penalty function method may be used to enforce the effects of variable equalities on certain control variables for instance voltage regulation at a given bus is achieved by penalising its corresponding nodal voltage magnitude for points other than a pre-specified value. To showcase this property in the OPF algorithm a parametric example is given in the next section.

### 2.3.4 Modelling Criterion of Power System components in OPF: A Parametric Example

Defining models for power system components in the OPF algorithm calls for careful formation of Lagrangian functions for each existing component. Consequently creating the system's Lagrangian function is the most important stage in the OPF solution algorithm and therefore it is stressed here as a parametric example. Figure (2.1) shows a simple 4-node system in which a transformer and a shunt compensator are also present.

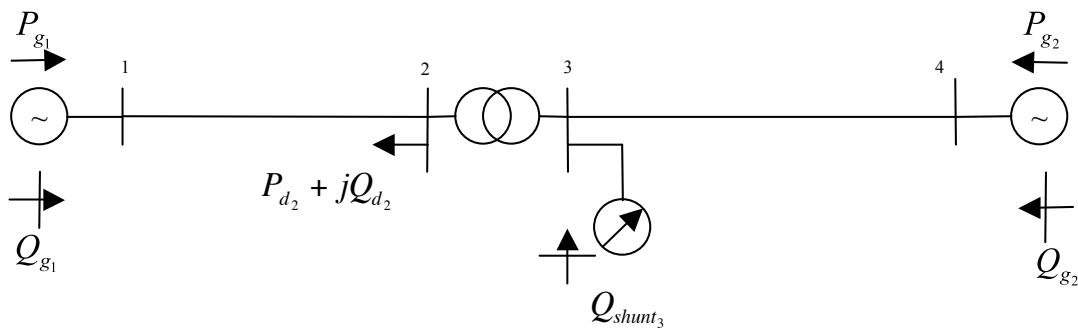


Figure 2.1 - 4-node Test System

A hierarchical solution process is given which if followed thoroughly would help to create Lagrangian functions for the most complex systems as well as the simple ones. This method has been used in the computer program developed for this research project as well and has proven its robustness against a variety of test cases.

Each system component, transmission lines, generators, shunt compensators, transformers and FACTS equipment are modelled by their complex nodal power equations in steady state operation. The nodal powers eventually form the power balance equation, which essentially states if the system is working under normal operating conditions. As a result, the power balance equation is the most important functional equality constraint in the OPF that describes the steady state behaviour of the network and needs to be bounded to the system Lagrangian using appropriate multipliers. Therefore to form the Lagrangian function properly, the power flow equations (2.6) and (2.7) has to be calculated thoroughly for all the models for system components and equipment that are connected to the system nodes. Forming the appropriate admittance matrix is crucial as the first step in determining system nodal powers. If for instance, there are FACTS and transformer devices present in



3. Forming the nodal admittance matrix for transformers and/or other equipment (including FACTS):

This system, includes one transformer and one shunt compensator each of which has their own associated admittance matrix:

Transformer (assuming it is a fixed tap transformer with tap changing facility on primary side) [37]:

$$Y_{TR} = \begin{bmatrix} Y_{TR_{22}} & -TY_{TR_{23}} \\ -TY_{TR_{32}} & T^2Y_{TR_{33}} \end{bmatrix} \quad 2.38$$

Shunt branch (assuming it is a fixed shunt susceptance for instance a capacitor bank with the susceptance value of ‘  $B_{shunt}$  ’):

$$Y_{shunt} = -jB_{shunt} \quad 2.39$$

For detailed modelling of transformers refer to chapter four and [3].

4. Calculating transformer powers and/or other equipment powers:

Based on the transformer nodal admittance matrix, its power is calculated as such for the transformer side connected to the ‘  $sth$  ’ node:

$$\begin{cases} S_{TR_s} = V_s \cdot \left[ \sum_{k=2}^3 Y_{TR_{sk}}^* \cdot V_k^* \right] = V_s e^{j\theta_s} \cdot \sum_{k=2}^3 (G_{TR_{sk}} - jB_{TR_{sk}}) \cdot V_k e^{-j\theta_k} \\ s = [2,3] \end{cases} \quad 2.40$$

And finally the calculated reactive power associated with the shunt element:

$$Q_{shunt_3} = -V_3^2 jB_{shunt_3} \quad 2.41$$

5. Calculating total nodal powers in each node:

$$P_n^{calc} = P_{TL_n} + P_{TR_n} \quad 2.42$$

$$Q_n^{calc} = Q_{TL_n} + Q_{TR_n} + Q_{shunt_n} \quad 2.43$$

6. Forming the power balance equations for the 'nth' node (Functional equality constraints set):

$$\begin{cases} P_n^{calc} - P_{g_n} + P_{d_n} = 0 \\ Q_n^{calc} - Q_{g_n} + Q_{d_n} = 0 \end{cases} \quad 2.44$$

**Step Three – Forming System Lagrangian:**

$$L_{system} = \sum_{i=1}^{n_{gen}} f_i(P_{g_i}) + \sum_{n=1}^{n_{bus}} \lambda_{p_n} (P_n^{calc} - P_{g_n} + P_{d_n}) + \sum_{n=1}^{n_{bus}} \lambda_{q_n} (Q_n^{calc} - Q_{g_n} + Q_{d_n}) \quad 2.45$$

Equation (2.45) represents the system's total Lagrangian function. It includes the effects of all the controllers and transformers that may be present in the system configuration in the form of total calculated nodal powers. This particular function is then solved using Newton's method as depicted in detail in section (2.3.2). It should be noted that in this particular example the only functional equalities are power balance equations however, there might be cases that due to the presence of power flow controllers (for instance Voltage Source Controllers) additional functional equalities have to be added to the system Lagrangian to incorporate the power regulation features associated with those controllers. This very fact is explained in detail in chapter four.

**Step Four – Linear System of Equations:**

The linear system of equations to be solved via Newton's method for the system Lagrangian formed in equation (2.45) is presented in the following equation (The general format of linear system of equations is given in equation 2.29). The

multipliers associated with equality constraints are added to the vector of state variables to form the vector ‘z’.

The linear system of equations consisting of the second order partial derivatives of the Lagrangian function with respect to vector ‘z’ and the gradient is formed as shown in equation (2.46):

$$\begin{bmatrix}
 \nabla_{\theta_i}^2 L & \nabla_{\theta_j}^2 L & \nabla_{\theta_{V_i}}^2 L & \nabla_{\theta_{V_j}}^2 L & 0 & \nabla_{\theta_i} P_i^{calc} & \nabla_{\theta_j} P_j^{calc} & \nabla_{\theta_i} Q_i^{calc} & \nabla_{\theta_j} Q_j^{calc} & 0 \\
 \nabla_{\theta_j}^2 L & \nabla_{\theta_j}^2 L & \nabla_{\theta_{V_i}}^2 L & \nabla_{\theta_{V_j}}^2 L & 0 & \nabla_{\theta_j} P_i^{calc} & \nabla_{\theta_j} P_j^{calc} & \nabla_{\theta_j} Q_i^{calc} & \nabla_{\theta_j} Q_j^{calc} & 0 \\
 \nabla_{V_{\theta_i}}^2 L & \nabla_{V_{\theta_j}}^2 L & \nabla_{V_i}^2 L & \nabla_{V_j}^2 L & \nabla_{V_{B_i}}^2 L & \nabla_{V_i} P_i^{calc} & \nabla_{V_j} P_j^{calc} & \nabla_{V_i} Q_i^{calc} & \nabla_{V_j} Q_j^{calc} & 0 \\
 \nabla_{V_{\theta_j}}^2 L & \nabla_{V_{\theta_j}}^2 L & \nabla_{V_{V_i}}^2 L & \nabla_{V_j}^2 L & 0 & \nabla_{V_j} P_i^{calc} & \nabla_{V_j} P_j^{calc} & \nabla_{V_j} Q_i^{calc} & \nabla_{V_j} Q_j^{calc} & 0 \\
 0 & 0 & \nabla_{B_{V_i}}^2 L & 0 & \nabla_{B_i}^2 L & 0 & 0 & \nabla_{B_i} Q_i^{calc} & 0 & 0 \\
 \nabla_{\theta_i} P_i^{calc} & \nabla_{\theta_j} P_i^{calc} & \nabla_{V_i} P_i^{calc} & \nabla_{V_j} P_i^{calc} & 0 & 0 & 0 & 0 & 0 & \nabla_{\lambda_{P_s}}^2 L \\
 \nabla_{\theta_j} P_j^{calc} & \nabla_{\theta_j} P_j^{calc} & \nabla_{V_j} P_j^{calc} & \nabla_{V_j} P_j^{calc} & 0 & 0 & 0 & 0 & 0 & 0 \\
 \nabla_{\theta_i} Q_i^{calc} & \nabla_{\theta_j} Q_i^{calc} & \nabla_{V_i} Q_i^{calc} & \nabla_{V_j} Q_i^{calc} & \nabla_{B_i} Q_i^{calc} & 0 & 0 & 0 & 0 & 0 \\
 \nabla_{\theta_j} Q_j^{calc} & \nabla_{\theta_j} Q_j^{calc} & \nabla_{V_j} Q_j^{calc} & \nabla_{V_j} Q_j^{calc} & 0 & 0 & 0 & 0 & 0 & 0 \\
 0 & 0 & 0 & 0 & 0 & \nabla_{\lambda_{P_s}}^2 L & 0 & 0 & 0 & \nabla_{P_s}^2 f(P_{s_i})
 \end{bmatrix}
 \times
 \begin{bmatrix}
 \Delta\theta_i \\
 \Delta\theta_j \\
 \Delta V_i \\
 \Delta V_j \\
 \Delta B_i \\
 \Delta\lambda_{P_i} \\
 \Delta\lambda_{P_j} \\
 \Delta\lambda_{Q_i} \\
 \Delta\lambda_{Q_j} \\
 \Delta P_{s_i}
 \end{bmatrix}
 =
 \begin{bmatrix}
 \nabla_{\theta_i} L \\
 \nabla_{\theta_j} L \\
 \nabla_{V_i} L \\
 \nabla_{V_j} L \\
 \nabla_{B_i} L \\
 \Delta P_i^{calc} \\
 \Delta P_j^{calc} \\
 \Delta Q_i^{calc} \\
 \Delta Q_j^{calc} \\
 \nabla_{P_s} f(P_{s_i}) - \lambda_p
 \end{bmatrix}
 \tag{2.46}$$

If there are any violations, the active set is augmented and the system Lagrangian is expanded by the quadratic penalty function thus creating an augmented Lagrangian function which is then solved via Newton’s method. It should be noted here that the process for forming the Lagrangian function is irrespective to the type of the objective function and therefore can be used for any type of OPF.

### ***Step Five – Control of System Operation***

The quadratic penalty is also used to enforce equality constraints on certain control variables. For instance, in the case of the system shown in Figure (2.1), the control variable in node 3 is obviously its nodal voltage namely, ‘V<sub>3</sub>’.

Assuming that the shunt compensator is used to fix the nodal voltage magnitude in node 3 to a specified value will result in the introduction of a variable equality constraint in the form of equation (2.47) below:

$$V_3 - V_{spec} = 0 \quad 2.47$$

Equation (2.47) essentially states that during the solution process the incremental changes in the voltage magnitude in node 3 should be infinitesimal. Therefore it is necessary to nullify its associated increment in the system of linear equations. To enforce the equality constraint on voltage magnitude in node 3 it is necessary to penalise it for other than zero increments, this is done by constructing a quadratic penalty function shown in equation (2.48):

$$\phi(V_3) = \frac{1}{2} \varphi (V_3 - V_{spec})^2 \quad 2.48$$

It is clearly seen from the expression in equation (2.48) that the penalty function is non-zero for all nodal voltage magnitudes except the specified value.

If the penalty factor ‘ $\varphi$ ’ is chosen to be sufficiently large (its value does not change throughout the solution process), then by adding its derivatives to the corresponding Hessian and gradient terms the nodal voltage magnitude in node 3 is essentially enforced to the specified value.

The first and second derivatives of the penalty function associated with ‘ $V_3$ ’ are added to the linear system of equations given in equation (2.46) resulting in a zero increment in ‘ $\Delta V_3$ ’.

$$\begin{cases} \frac{d\phi(V_3)}{dV_3} = \varphi(V_3 - V_{spec}) \\ \frac{d^2\phi(V_3)}{dV_3^2} = \varphi \end{cases} \quad 2.49$$

The concept of enforcing variable equality constraints via quadratic penalty functions is used several times throughout this research and will again be explained in greater detail in the next chapter where models for shunt compensators are introduced for the OPF algorithm.

**Step Six – Augmented Lagrangian Function:**

If the quadratic penalty function is activated to enforce the violated variables to their limit boundaries, equation (2.45) changes as shown below:

Assuming after global iteration ‘1’, a violation occurs in the amount of the voltage in node 2 (which is a PQ load node so its voltage magnitude is a dependant variable and therefore prone to limit violation), the quadratic penalty function according to definition in equation (2.33) is activated as such:

If  $V_2^{(2)} > V_2^{\max}$ :

(The number in parentheses represents the iteration step)

$$L_{\text{system}}^{\text{Aug}^{(2)}} = \sum_{i=1}^{n_{\text{gen}}} f_i^{(2)}(P_{g_i}) + \sum_{n=1}^{n_{\text{bus}}} \lambda_{p_n} (P_n^{\text{calc}} - P_{g_n} + P_{d_n}) + \sum_{n=1}^{n_{\text{bus}}} \lambda_{q_n} (Q_n^{\text{calc}} - Q_{g_n} + Q_{d_n}) + u_2^{(2)}(V_2^{(2)} - V_2^{\max}) + \frac{\alpha_2^{(2)}}{2}(V_2^{(2)} - V_2^{\max})^2 \quad 2.50$$

In which case the Hessian/Jacobian self-terms in the matrix of coefficients associated with node 2 in equation (2.46) would take the following forms:

Jacobian Self-Element/Gradient:

$$\nabla_{V_2} L_{\text{system}}^{\text{Aug}^{(2)}} = \sum_{n=1}^{n_{\text{bus}}} \lambda_{p_n} \cdot \nabla_{V_2} P_n^{\text{calc}^{(2)}} + \sum_{n=1}^{n_{\text{bus}}} \lambda_{q_n} \cdot \nabla_{V_2} Q_n^{\text{calc}^{(2)}} + u_2^{(2)} + \alpha_2^{(2)}(V_2^{(2)} - V_2^{\max}) \quad 2.51$$

Hessian Self-Element:

$$\nabla_{V_2}^2 L_{\text{system}}^{\text{Aug}^{(2)}} = \sum_{n=1}^{n_{\text{bus}}} \lambda_{p_n} \cdot \nabla_{V_2}^2 P_n^{\text{calc}^{(2)}} + \sum_{n=1}^{n_{\text{bus}}} \lambda_{q_n} \cdot \nabla_{V_2}^2 Q_n^{\text{calc}^{(2)}} + \alpha_2^{(2)} \quad 2.52$$

Equations (2.51) and (2.52) clearly show the effectiveness of the quadratic penalty function in enforcing the voltage in node 2 to its limit boundaries. Equation (2.52) essentially nullifies the increments in the amount of voltage in node 2 in the correction vector via the penalty parameter ‘ $\alpha$ ’, which is a very large constant.

Equation (2.51) on the other hand penalises the gradient vector and prevents it from deviating anymore from the limit boundaries of the solution space. The quadratic method is effective as the penalty parameter increases however by combining the penalty function method and the multiplier ' $u_2$ ' to bind the violated variable to its limits the need for increasing the penalty parameter towards near infinity decreases. This method therefore is not prone to ill conditioning due to very large values in the penalty parameter ' $\alpha$ ' [8, 9].

Eventually, the Lagrangian function attributed to this particular system is solved via Newton's method by forming the set of linear equations shown in equation (2.29) for a gradient vector that leads to the optimum solution. The optimum obtained through Newton's method must then satisfy the KKT conditions stated in previous section.

### **2.3.5 Summary of Newton's Method for an Augmented Lagrangian Function**

The main reasons for choosing Newton's method to minimise the augmented Lagrangian function are the fast convergence rate of this particular solution method and its better reliability in comparison with pure penalty function methods. However it is fair to say that the numerical reliability of the Newton's method depends mostly on initial conditions, if they are not chosen properly there could be several undesired ramifications such as producing a near singular Hessian matrix during the Newton's internal loop iterations which would lead to non-feasible solutions. Below is a summary of key points of using Newton's method for an augmented Lagrangian function, as the main mathematical toolbox of this research project:

1. Solution time is proportional to network size (the bigger the system, the more time it needs to converge; however network size does not alter the convergence characteristic)
2. The state variables are divided into two categories: control (generators' voltage and active powers; transformers' tap ratios or phase shifters' angles) and dependent (loads' voltage magnitudes; phase angles)

3. Equality constraints are divided into two types: Functional and Variable, Functional constraints are bounded to the system Lagrangian via Lagrange multipliers whereas Variable constraints are bounded using penalty functions; Both functional and variable constraints are used to control and depict the system operation realistically
4. For each functional equality constraint there is an equality multiplier and for each active inequality constraint there is an inequality multipliers (dual variables)
5. Active inequality constraints are added to the system Lagrangian using their associated multipliers, their violated values are then enforced to their associated limits via the use of penalty functions
6. Solution algorithm consists of solving a set of linear equations based on Newton's method which minimises the system's Lagrangian Function
7. It gives robust practical solutions (for system operators and real time simulation) and applies to all of the optimisation problems regarding OPF
8. Quadratic convergence rate depends on the nature of the initial conditions
9. The objective function sensitivity to constraints is dealt with through the multipliers
10. Hessian might be singular which yields to no solutions (if the initial conditions are badly selected)
11. The Karush-Kuhn-Tucker necessary optimality conditions (NOC's) guarantee a minimum for the objective function although they cannot guarantee a global minimum; they also define the convergence rate of the algorithm towards a solution point

12. The solution is within the operational characteristics of the system and any violation will be dealt with automatically within the algorithm and active inequalities will be forced to their limits (no external tuning is required)

A complete flow chart for the OPF solution process for augmented Lagrangian function via Newton's method has been given in section (2.5). Notice that the flowchart is an improved version of the one given in [3], which better illustrates several stages pertaining OPF via Newton's method. The flowchart in section (2.5) can also be used for such cases that systems with control equipment (for instance FACTS devices or VSC converters) are present to control given system parameters. The process outlining the incorporation of control features into the OPF algorithm has been discussed briefly in this chapter, however it will be re-emphasised in subsequent chapters where models for FACTS devices are explicitly developed for the OPF algorithm. For now a few practical case scenarios involving real and experimental power systems have been presented below in a more comprehensive manner to depict the crucial role of the OPF in defining network's conditions.

## **2.4 Optimal Power Flow Scenarios applied to Power Systems**

In this section multiple case scenarios are presented separately to depict the OPF characteristics and solutions when applied to real power systems. The OPF formulation based on Newton's method for Lagrangian functions developed in this chapter is the basis of a computer simulation program that is created for the purposes of optimal power analysis in this research project.

In the following section, several assessment scenarios are devised based on a variety of interconnected power systems where a general OPF solution is implemented without any FACTS devices. In the subsequent chapters with the introduction of mathematical models associated to different FACTS equipments, FACTS-based OPF is however applied. For consistency purposes, it is assumed that the aim in solving the OPF in these scenarios is the economic assessment of the system and therefore the objective function to be minimised is chosen to be the generators' cost functions as shown in equation (2.12). The hierarchical solution process to construct the system Lagrangian that is introduced in section (2.3.4) is applied in the

following test scenarios to properly model the steady-state behaviour of each system within the optimal power flow algorithm.

Five case scenarios have been presented to assess the various characteristics of the OPF and its robustness in dealing with almost any power system configuration. These scenarios comprise 8-, 9-, 11-, 14- and 30-node systems two of which are IEEE test cases (14 and 30 bus systems). In the subsequent sub-sections each system is introduced and their corresponding OPF simulation results are presented. The data pertaining to each system is presented in a separate section in Appendix II.

### **2.4.1 8-node System**

The first case scenario is for an 8-node system as shown in figure (2.2). Unless otherwise stated the assumptions below apply to all the case scenarios presented in this chapter.

- Base power is 100 MVA
- Bus 1 is taken to be the Slack bus with voltage upper limit of 1.5 p.u.
- System objective function is taken to be the generators' cost curves
- Generators initial active dispatch is given by the lossless economic dispatch at the start of the OPF algorithm
- All the multipliers are initiated at zero
- The powers injection to the node is determined by a negative sign whereas power leaving a node by a positive sign

A general OPF is run for the system given in figure (2.2) with the aim to determine the optimum operating point of this system. The OPF is run to minimise the objective function, which is taken to be the generators' cost curve functions as given in equation (2.12). There are no controllers or shunt compensators present in the system. Applying the OPF algorithm to such a network to obtain the optimum operating point requires solving equation (2.29) via Newton's method, in which the system Lagrangian has the general form of equation (2.44) at the start of the OPF iterative process. It should be noted however that all the state variables are within their operational limits which if violated are enforced to their corresponding boundaries via the use of the quadratic penalty function shown in equation (2.33), with the dual variables for the violated inequalities being updated at the end of each

global iteration via equation (2.34). Upon convergence the solution is only deemed feasible if it satisfies all the KKT optimality conditions otherwise it will be rejected. The corresponding nodal active and reactive powers are included in the system Lagrangian through their associated multipliers. As mentioned earlier the nodal powers required to form the functional equality constraints corresponding to the power balance equations are formed via system's associated admittance matrix and the complex apparent power equation as explained extensively in the parametric example shown in section (2.3.4). The OPF is formulated for the 8-node system as below:

- System's objective function:

$$f_i = 60 + 3.4P_{G_i} + 0.004P_{G_i}^2 \quad 2.53$$

- Constraints set:

$P_G(p.u.)$	$Q_G(p.u.)$
$0.1 \leq P_{G_1} \leq 2.0$	$-5.00 \leq Q_{G_1} \leq 5.00$
$0.1 \leq P_{G_2} \leq 2.0$	$-3.00 \leq Q_{G_2} \leq 3.00$

**Table 2.1 – Generators Constraints Set**

- Transformers and Other Controllers:

<b>Transformer No.</b>	<b>Sending Bus</b>	<b>Receiving Bus</b>	<b><math>X_t</math> (p.u)</b>	<b>Tap (primary)</b>
1	3	6	0.05	1.0
2	5	7	0.05	1.0

**Table 2.2 - Fixed Tap Transformer Data**

The following results have been obtained by solving the OPF problem for the 8-bus system under given constraints after 4 global iterations.

- OPF Results:

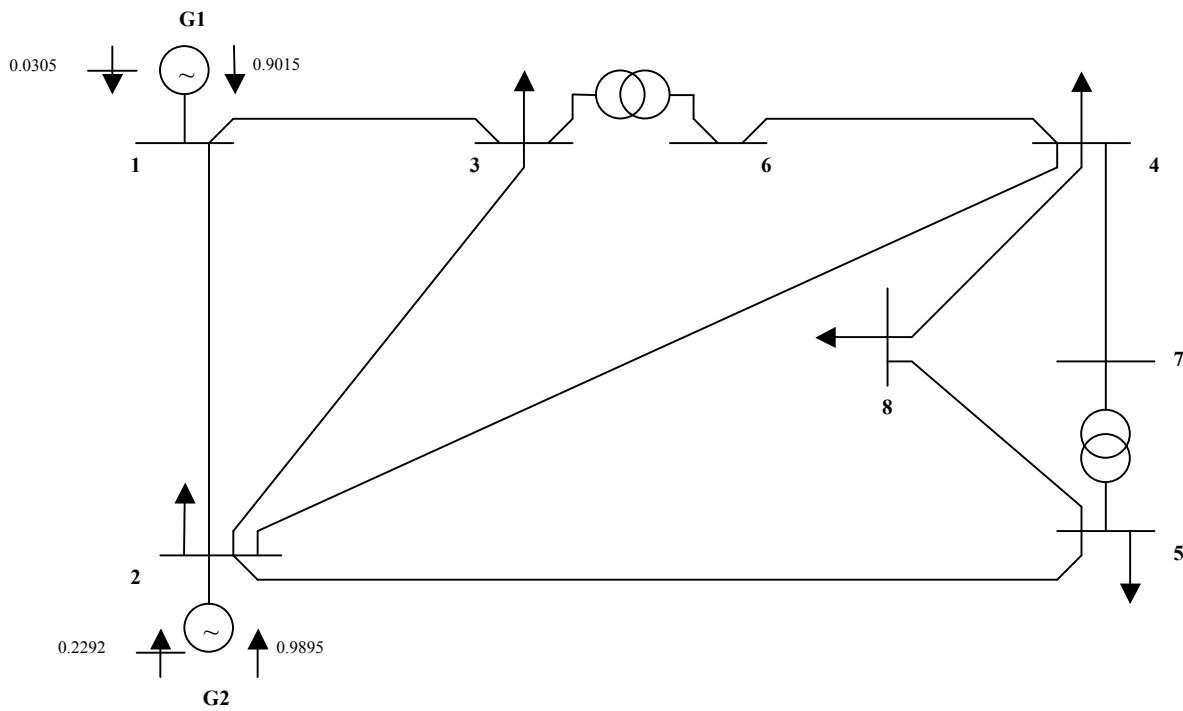


Figure 2.2 – 8-node Test System

Generator No.	Active Power Dispatch (p.u.)	Reactive Powers (p.u.)	Optimal Cost of Generation \$/hr	Optimal Value of Total Generation
1	0.9015	0.0305	399.0173	834.6291 \$/hr
2	0.9895	0.2292	435.6118	

Table 2.3 - Generators' Optimal Power Flow Dispatch

Line No.	Send	Rec	Sending End (p.u.)		Receiving End (p.u.)		Incurred Losses (p.u.)
			$P_i$	$Q_i$	$P_j$	$Q_j$	
1	1	2	+0.5410	-0.0066	-0.5362	-0.0525	+0.0048-j0.0591
2	1	3	+0.3605	+0.0371	-0.3518	-0.0706	+0.0087-j0.0335
3	2	3	+0.2994	+0.0477	-0.2947	-0.0808	+0.0047-j0.0331
4	2	4	+0.3839	+0.0370	-0.3764	-0.0617	+0.0075-j0.0246
5	2	5	+0.6425	+0.0969	-0.6284	-0.0899	+0.0141+j0.0070
6	6	4	+0.1965	-0.0003	-0.1961	-0.0217	+0.0003-j0.0220
7	4	7	+0.0454	-0.0003	-0.0453	-0.0280	+0.0001-j0.0283
8	4	8	+0.1272	+0.0337	-0.1265	-0.0601	+0.0006-j0.0265
9	8	5	-0.0735	-0.0399	+0.0737	+0.0178	+0.0002-j0.0221

**Table 2.4 - System Optimal Power Flow**

Transformer No.	Sending End (p.u.)		Receiving End (p.u.)	
	$P_s$	$Q_s$	$P_r$	$Q_r$
1	+0.1965	+0.0014	-0.1965	+0.0003
2	-0.0453	-0.0279	+0.0453	+0.0280

**Table 2.5 - Calculated Transformers Powers (at optimum)**

Bus No.	1	2	3	4	5	6	7	8
Multiplier \$/hr	4.12	4.19	4.33	4.36	4.38	4.34	4.37	4.40

**Table 2.6 - Incremental Generation Costs (Multipliers)**

- Results Discussion:

The results obtained here state that under steady state operation the economic way to operate the system is within these specific conditions as determined by the OPF solution. Consequently operating the generators outside these optimal boundaries means that the system is deviated from its optimal operating point. The optimum value for the objective function with respect to all the constraints has been calculated to \$834.63 per hour of fuel consumption. As seen from the voltages, the voltage magnitude at node 2 has reached its upper limit and is therefore fixed at that value by the use of augmented Lagrangian method using the combination of multipliers and penalty parameters in the quadratic penalty function defined in equation (2.33). It is very important to know that the amount of objective function is dependent on the system configuration and therefore it may differ for the same generators if there is a change in its configuration, for instance if a power controller

or shunt compensator is added. This fact is addressed thoroughly in the following chapters where power regulators such as Voltage Source Converters are added to the similar systems that are presented here.

### 2.4.2 9-node System

The next system to be tested for the OPF is a 9-node system with the configuration shown in figure (2.3). The assumptions mentioned in the previous case scenario also apply for this system with the exception that the upper limit for the slack bus voltage is reduced to 1.1 per unit of voltage magnitude. There are three machines in this system each of which are assigned their own distinct objective function. According to the OPF formulation the optimum operating point achieved by solving the OPF in such a system would be the summation of the optimum values of all the objective functions included in the system (equations 2.24 and 2.45).

Two test runs are presented for this system: firstly the 9-node system is simulated without any compensators and the results are given, however in a next test run a shunt compensator similar to the one in section (2.3.4) is added to node 9 for purposes of fixing its voltage to 1.0 per unit.

The OPF is run again for the compensated system and the results for each case scenario are compared. It is expected that the system should behave better when the compensator is in place with the voltage profile improved. The purpose of this simulation is to show that the OPF solution process and modelling criteria introduced in this chapter are suitable for portraying the system behaviour characteristics in a variety of different circumstances.

The OPF problem is formulated as such for the 9-node system shown in figure (2.3):

- System's objective functions:

$$f_1 = 150 + 5P_{G_1} + 0.1100P_{G_1}^2 \quad 2.54$$

$$f_2 = 600 + 1.2P_{G_2} + 0.0850P_{G_2}^2 \quad 2.55$$

$$f_3 = 335 + P_{G_3} + 0.1225P_{G_3}^2 \quad 2.56$$

- Constraints set:

$P_G(p.u.)$	$Q_G(p.u.)$
$0.1 \leq P_{G_1} \leq 2.5$	$-3.00 \leq Q_{G_1} \leq 3.00$
$0.1 \leq P_{G_2} \leq 3.0$	$-3.00 \leq Q_{G_2} \leq 3.00$
$0.1 \leq P_{G_3} \leq 2.7$	$-3.00 \leq Q_{G_3} \leq 3.00$

**Table 2.7 - Generators Constraints Set**

- Transformers and other controllers:

<b>Transformer No.</b>	<b>Sending Bus</b>	<b>Receiving Bus</b>	$X_t$ <b>(p.u)</b>	<b>Tap (primary)</b>
1	1	4	0.0576	1.0
2	3	6	0.0586	1.0
3	2	8	0.0625	1.0

**Table 2.8 - Fixed Tap Transformers Data**

- Compensator connecting transformer (Test Run Two only):

<b>Transformer No.</b>	<b>Compensated Bus</b>	$X_t$ <b>(p.u.)</b>	<b>Tap (primary)</b>
4	9	0.0500	1.0

**Table 2.9 - Fixed Tap Connecting Transformer Data**

The OPF is run for the 9-node system and is converged to the following results after 4 global iterations.

- OPF Results:

- Test Run One: Uncompensated System

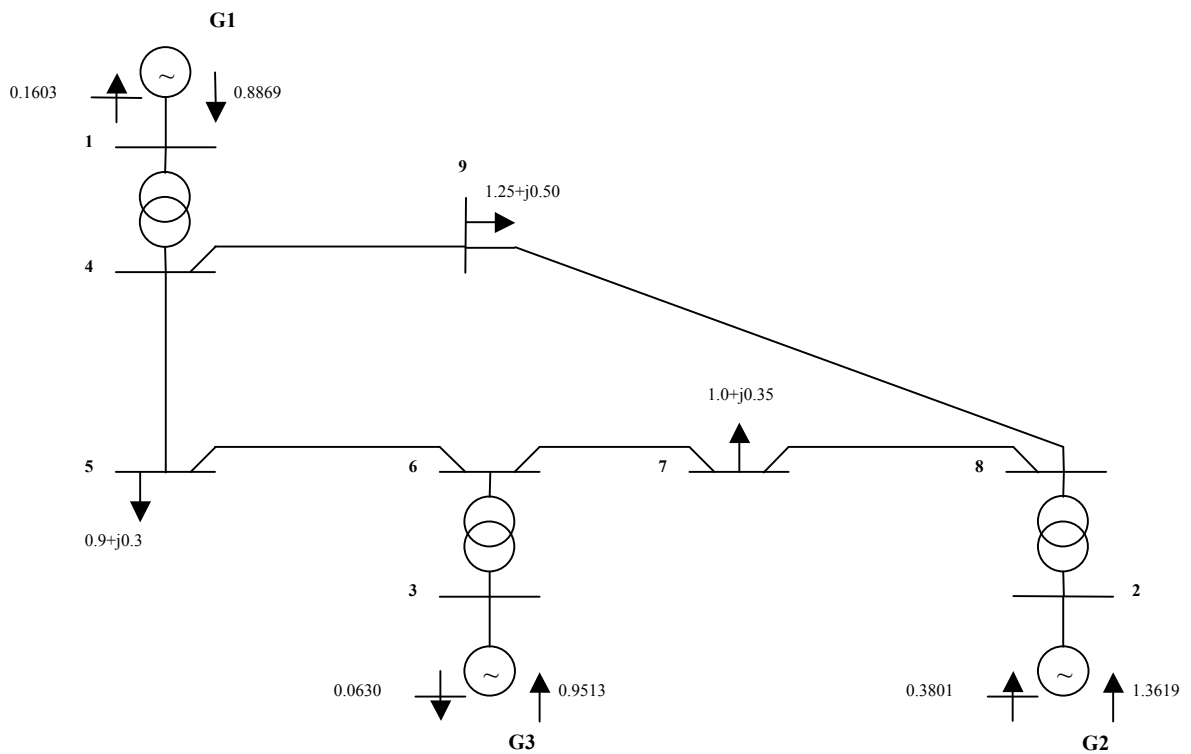


Figure 2.3 - 9-node Test System (Optimal Power Flow Solution)

Generator No.	Active Power Dispatch (p.u.)	Reactive Powers (p.u.)	Optimal Cost of Generation \$/hr	Optimal Value of Total Generation
1	0.8869	-0.1603	1458.7059	5337.2536 \$/hr
2	1.3619	0.3801	2339.9148	
3	0.9513	-0.0630	1538.6328	

Table 2.10 - Generators Optimal Power Flow Dispatch

Mathematical Modelling of Multi-terminal VSC-HVDC Links in Power Systems using  
Optimal Power Flows

---

Line No.	Send	Rec	Sending End (p.u.)		Receiving End (p.u.)		Incurred Losses (p.u.)
			$P_i$	$Q_i$	$P_j$	$Q_j$	
1	4	5	+0.6386	-0.1850	-0.6321	+0.0476	+0.0065-j0.1374
2	5	6	-0.2679	-0.3476	+0.2713	-0.0420	+0.0034-j0.3869
3	6	7	+0.6800	-0.0669	-0.6752	-0.1344	+0.0047-j0.2013
4	7	8	-0.3248	-0.2156	+0.3257	+0.0510	+0.0009-j0.1646
5	8	9	+1.0362	+0.2259	-1.0023	-0.3874	+0.0339-j0.1615
6	9	4	-0.2477	-0.1126	+0.2483	-0.0190	+0.0006-j0.1316

**Table 2.11 - System Optimal Power Flow**

Transformer No.	Sending End (p.u.)		Receiving End (p.u.)	
	$P_s$	$Q_s$	$P_r$	$Q_r$
1	+0.8869	-0.1603	-0.8869	+0.2039
2	+0.9513	-0.0630	-0.9513	+0.1090
3	+1.3619	+0.3801	-1.3619	-0.2768

**Table 2.12 - Calculated Transformer Powers (at optimum)**

Bus No.	1	2	3	4	5	6	7	8	9
Multiplier \$/hr	24.51	24.35	24.31	24.52	24.93	24.31	24.55	24.36	25.84

**Table 2.13 - Incremental Generation Costs (Multipliers)**

○ Test Run Two: Compensated System

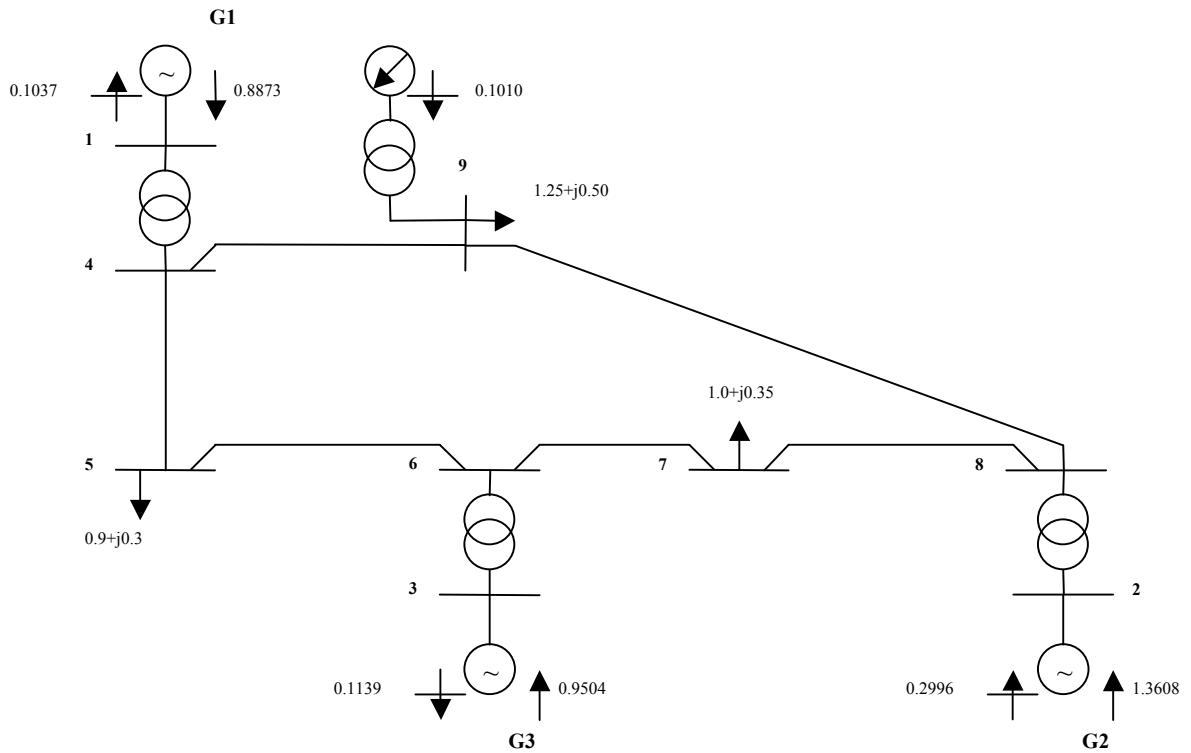


Figure 2.4 - 9-node Compensated Test System (Optimal Power Flow Solution)

Generator No.	Active Power Dispatch (p.u.)	Reactive Powers (p.u.)	Optimal Cost of Generation \$/hr	Optimal Value of Total Generation
1	0.8873	-0.1037	1459.6768	5333.3883 \$/hr
2	1.3608	0.2996	2337.2439	
3	0.9504	-0.1139	1536.4676	

Table 2.14 - Generators Optimal Power Flow Dispatch

Mathematical Modelling of Multi-terminal VSC-HVDC Links in Power Systems using  
Optimal Power Flows

---

Line No.	Send	Rec	Sending End (p.u.)		Receiving End (p.u.)		Incurred Losses (p.u.)
			$P_i$	$Q_i$	$P_j$	$Q_j$	
1	4	5	+0.6370	-0.1252	-0.6306	-0.0109	+0.0064-j0.1361
2	5	6	-0.2694	-0.2891	+0.2724	-0.0927	+0.0030-j0.3818
3	6	7	+0.6780	-0.0693	-0.6731	-0.1235	+0.0049-j0.1929
4	7	8	-0.3269	-0.2265	+0.3279	+0.0675	+0.0010-j0.1590
5	8	9	+1.0329	+0.1281	-1.0003	-0.2907	+0.0326-j0.1626
6	9	4	-0.2497	-0.1088	+0.2503	-0.0214	+0.0006-j0.1302

**Table 2.15 - System Optimal Power Flow**

Transformer No.	Sending End (p.u.)		Receiving End (p.u.)	
	$P_s$	$Q_s$	$P_r$	$Q_r$
1	+0.8873	-0.1037	-0.8873	+0.1466
2	+0.9504	-0.1139	-0.9504	+0.1602
3	+1.3608	+0.2996	-1.3608	-0.1956
4	+0.0000	+0.1010	-0.0000	-0.1005

**Table 2.16 - Calculated Transformer Powers (at optimum)**

Bus No.	1	2	3	4	5	6	7	8	9
Multiplier \$/hr	24.52	24.33	24.28	24.52	24.93	24.28	24.53	24.33	25.72

**Table 2.17 - Incremental Generation Costs (Multipliers)**

- Results Discussion:

From the results above it is clearly inferred that the OPF is a very effective tool in ascertaining system's operating conditions under different constraints. Comparing the results obtained by the OPF in Test Run One to the ones obtained for Test Run Two, it is seen that the presence of the shunt compensator at node 9 has little effect on moving the system's optimum operating point, which is understandable considering that the objective function was chosen to the generator's active power generation. Chart (2.1) illustrates this very fact that despite the presence of a shunt compensator the system's optimum operating point has so little deviations and the OPF eventually converged to the same operating point albeit with little changes in the amounts of active and reactive powers in the system given by tables (2.13) and (2.17). It should however be noted that node 9 has the highest incremental cost of generation which means it would be more expensive to generate for every megawatt

of power that is consumed in node 9. This is because that this node is physically located in farthest location than the other nodes.

However the changes occurred in system's voltage profile as well as the amounts of reactive power produced by the generators are more conspicuous. Chart (2.2) shows the reactive power generation/consumption by the generators in each test run.

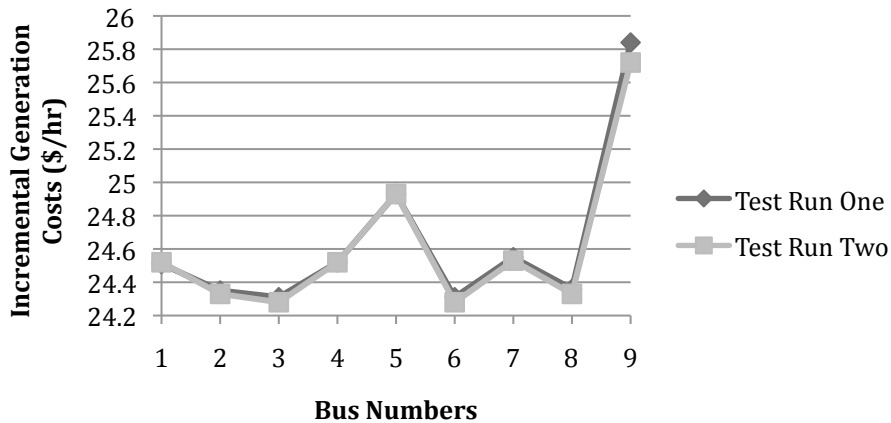


Chart 2.1 - Incremental Cost Price Comparison – Minimal Deviation from Optimum Operating Point

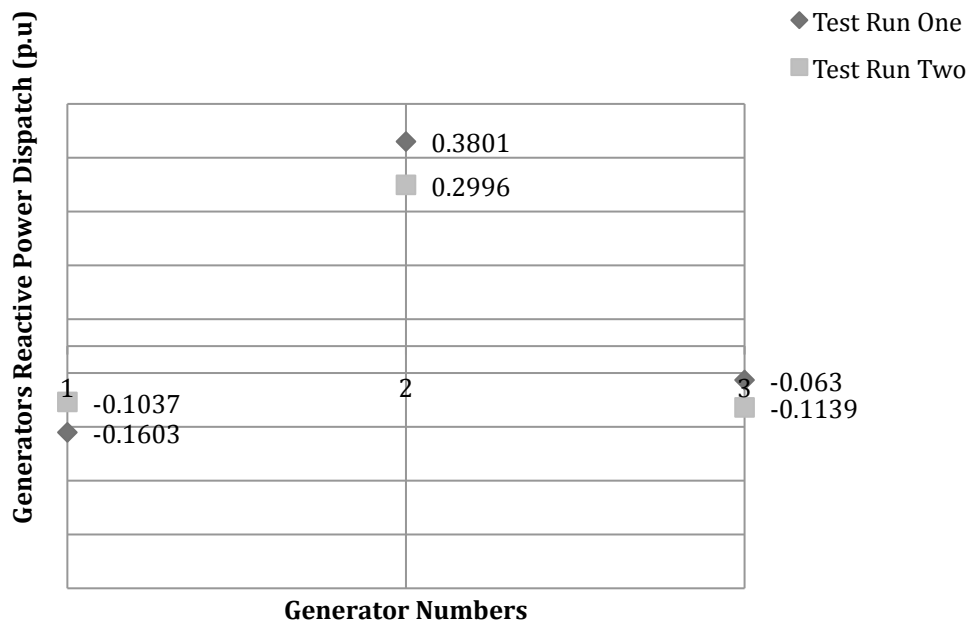


Chart 2.2 - Generators Reactive Power Dispatch

As shown in chart (2.2), generator in node 2 provides the main bulk of reactive power to the system with the other two generators acting as sink nodes for the remainder of reactive power that is not consumed by the system loads. From the

OPF results obtained for each test run, it is seen that the amount of reactive power in generator 2 has decreased from 38.01 MVARs to 29.96 MVARs due to the presence of the shunt compensator in node 9.

The results show that given the conditions set by the constraints at the start of the simulation, continuous optimum operation of the generators in the 9-node system, costs approximately 5340 \$/hr of fuel consumption provided that the generators power dispatch remain as the values obtained here. Deviating from this point will result in higher costs of active power generation. Obviously if the conditions of the system changed or if the system configuration changed in any way by adding or removing components which will result in a change in the calculated nodal powers in the power balance equation (equations 2.15 and 2.16), the optimum point of operation would be different from the ones obtained in this case scenario.

Test run 2 shows that by applying shunt reactive compensation in node 9, a more relaxed voltage profile can be achieved. The voltage profile for each test run is shown in chart (2.3).

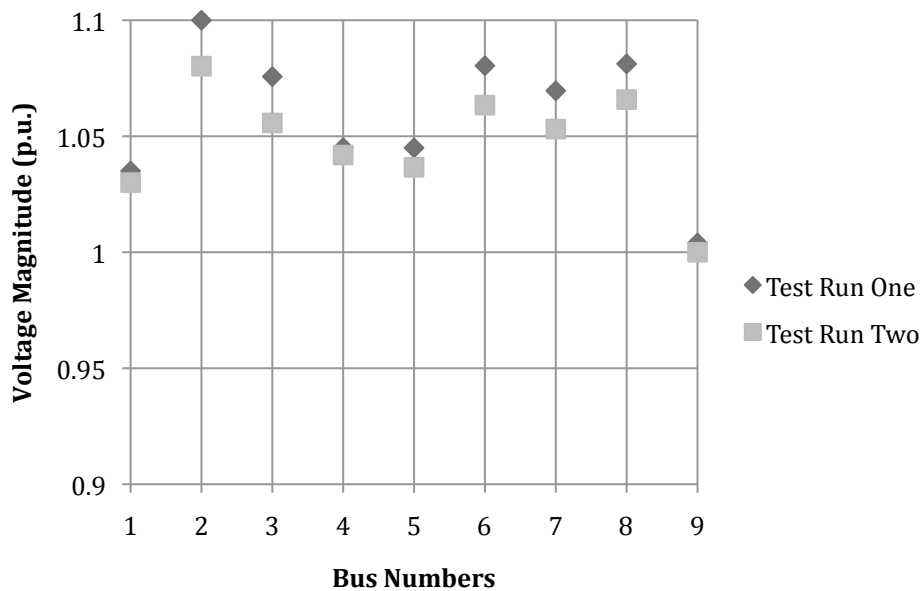


Chart 2.3 - 9-node System Voltage Profile (in per unit)

In both cases the OPF is converged in 4 iterations and the KKT optimality conditions are satisfied. In order to include the effects of shunt compensator a new variable equality constraint (on node 9 voltage magnitude) is added to the system

constraints set via the use of penalty functions added to the corresponding Hessian and Jacobian entries to nullify the terms associated with the increments of the voltage magnitude in node 9 effectively fixing its value to 1.0 per unit (see section 2.3.4).

### 2.4.3 11-node System

A modification of the 8-node system is represented in this next case scenario. The modified system consists of 11 nodes and three identical generators similar to the ones used for the 8-node system. However, apart from the generators, two dedicated shunt compensators act as voltage regulators in nodes 6 and 7.

The OPF is formulated for the 11-node system via the following tables:

- System's objective functions:

$$f_i = 60 + 3.4P_{G_i} + 0.004P_{G_i}^2 \quad 2.57$$

- Constraints set:

$P_G(p.u.)$	$Q_G(p.u.)$
$0.1 \leq P_{G_1} \leq 2.5$	$-5.00 \leq Q_{G_1} \leq 5.00$
$0.1 \leq P_{G_2} \leq 2.7$	$-3.00 \leq Q_{G_2} \leq 3.00$
$0.1 \leq P_{G_3} \leq 1.5$	$-3.00 \leq Q_{G_3} \leq 3.00$

**Table 2.18 - Generators Constraints Set**

- Transformers and other controllers:

Transformer No.	Sending Bus	Receiving Bus	$X_t$ (p.u)	Tap (primary)	Compensators Bus
1	3	6	0.0500	0.987	6
2	5	7	0.0500	0.957	7

**Table 2.19 - Fixed Tap Transformers Data and Shunt Compensators**

The OPF is run for the following system and is converged after four iterations:

- OPF Results:

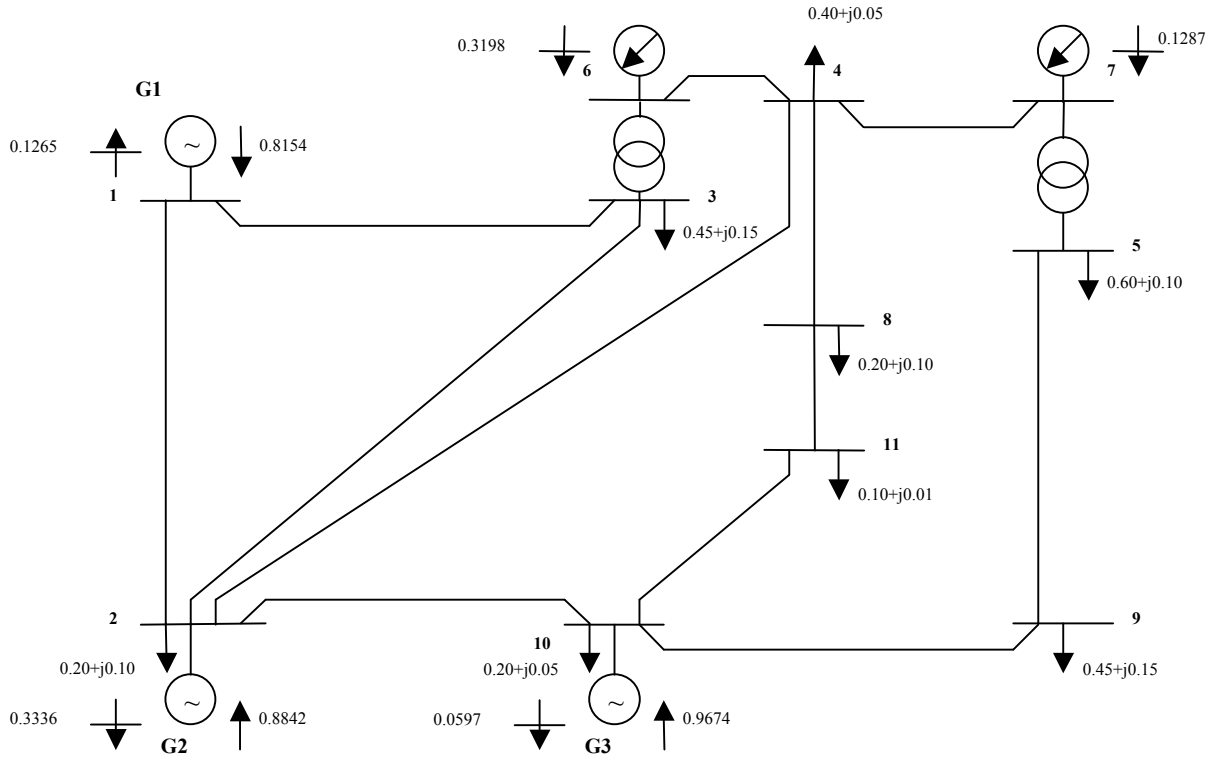


Figure 2.5 - 11-node Test System (Optimal Power Flow Solution)

Generator No.	Active Power Dispatch (p.u.)	Reactive Powers (p.u.)	Optimal Cost of Generation \$/hr	Optimal Value of Total Generation
1	0.8154	-0.1265	363.8156	1182.0488 \$/hr
2	0.8842	-0.3336	391.8911	
3	0.9674	-0.0597	426.3420	

Table 2.20 - Generators Optimal Power Flow Dispatch

Transformer No.	Sending End (p.u.)		Receiving End (p.u.)	
	$P_s$	$Q_s$	$P_r$	$Q_r$
1	+0.2271	-0.3229	-0.2271	+0.3293
2	-0.1652	-0.1805	+0.1652	+0.1831

**Table 2.21 - Transformers Calculated Powers (at optimum)**

Bus No.	1	2	3	4	5	6	7	8	9	10	11
Multiplier \$/hr	4.05	4.11	4.26	4.31	4.39	4.27	4.39	4.34	4.35	4.17	4.19

**Table 2.22 - Incremental Generation Costs (Multipliers)**

Shunt Device	Bus No.	Reactive Power Compensation (p.u.)
1	6	0.3198 (capacitive)
2	7	0.1287 (capacitive)

**Table 2.23 - Shunt Reactive Powers (Compensators)**

- Results Discussion:

Like the prior simulation case scenarios the OPF converges in four iterations. Its results state that at optimum the cost of generation would be approximately 1182 \$/hr for the system. The incremental cost of generation for nodes follow a similar pattern with each node contributing to approximately 4.3 \$/hr of increase in cost for each 1 MW of power increase. Similar to the 9-node system, in this particular case scenario the shunt compensators are set to regulate the voltage magnitudes in nodes 6 and 7. However the shunt compensators in this system are set to regulate the voltage magnitude within a more relaxed range rather than just fixing them to a pre-determined value. As mentioned earlier, equality constraints on control variables are enforced by defining specific penalty functions (in the 9-node system a penalty function was defined to enforce the voltage magnitude of node 9 to 1.0 per unit), however in this case because the shunt compensators are free to regulate the voltage within a range rather than fixing their magnitude to a pre-determined value there is no need to penalise the voltage magnitudes in nodes 6 and 7 so long as they do not violate their limits.

The results obtained here shows that there is no violation in the voltage magnitudes and upon convergence all the variables are within their specified limits and the OPF result satisfies the KKT conditions.

The next two case scenarios are taken from IEEE test systems (14- and 30-node systems), the OPF algorithm developed in this research and presented in this chapter is applied to these realistic power networks. The purpose of applying the OPF algorithm to IEEE test systems is to illustrate the robustness of the OPF algorithm and formulation, which has been developed and presented in this chapter in dealing with realistic systems.

For simplicity purposes only the final OPF results are mentioned here, it should be noted that the comprehensive system data for all the systems simulated in this chapter is given in Appendix II. The data for IEEE test systems presented in this chapter and all the other chapters can be found online in the following web address:

University of Washington, Power Systems Test Case Archives:  
(<http://www.ee.washington.edu/research/pstca>)

#### **2.4.4 IEEE 14-node System**

The IEEE 14-node system is shown in figure (2.6) illustrating the generators economic power dispatch as obtained by the OPF. The OPF is converged in 3 iterations and the following results are obtained. The voltage limits are set to 1.06 and 0.9 per unit for load buses and 1.15 and 0.9 for all other buses including the reference bus. There are five identical generators operating in the system with the following expression for their cost curves as objective functions:

$$f_i = 0.2 + 0.3P_{G_i} + 0.01P_{G_i}^2 \quad 2.58$$

A shunt compensator similar to the one introduced in the parametric example and present in two previous case scenarios, is tasked to regulate the voltage at node 9.

- OPF Results:

Generator No.	Active Power Dispatch (p.u.)	Reactive Powers (p.u.)	Optimal Cost of Generation \$/hr	Optimal Value of Total Generation
1	+0.5083	-0.0144	41.2811	215.5123 \$/hr
2	+0.5156	+0.1051	42.2527	
3	+0.5366	+0.1831	45.0885	
4	+0.5183	+0.0388	42.6156	
5	+0.5306	+0.1179	44.2742	

Table 2.24 - Generators Optimal Power Flow Dispatch

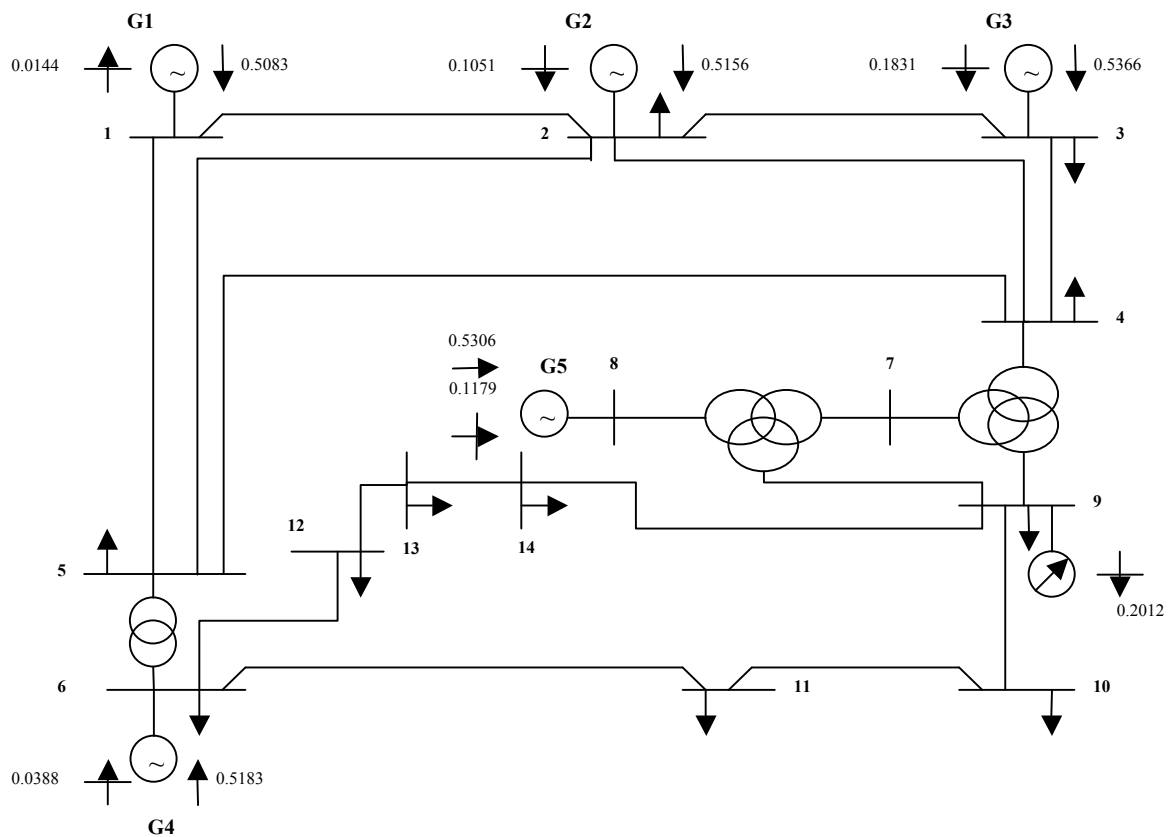


Figure 2.6 - 14-node Test System (Optimal Power Flow Solution)

Transformer No.	Sending End	Receiving End	Sending End (p.u.)		Receiving End (p.u.)	
			$P_s$	$Q_s$	$P_r$	$Q_r$
1	4	7	-0.1502	-0.0069	+0.1502	+0.0115
2	4	9	+0.0155	+0.0232	-0.0155	-0.0228
3	5	6	-0.0305	+0.1541	+0.0305	-0.1480
4	7	8	-0.5306	-0.0707	+0.5306	+0.1179
5	7	9	+0.3804	+0.0592	-0.3804	-0.0439

**Table 2.25 - Transformer Calculated Powers (at optimum)**

Bus No.	1	2	3	4	5	6	7	8	9	10	11	12	13	14
Multiplier \$/hr	1.32	1.33	1.37	1.36	1.35	1.34	1.36	1.36	1.36	1.37	1.36	1.36	1.36	1.37

**Table 2.26 - Incremental Generation Cost (Multipliers)**

Shunt Device	Bus No.	Reactive Power Compensation (p.u.)
1	9	0.2021 (capacitive)

**Table 2.27 - Shunt Reactive Powers (Compensators)**

- Results Discussion:

The results obtained from the OPF algorithm indicate that the optimum operating point of the system costs approximately 215 \$/hr of generators' fuel consumption. There are no violations in the system and the OPF is converged in four iterations.

### 2.4.5 IEEE 30-node System

The IEEE 30-node system is a familiar test system in academic papers and therefore it has been tested here to showcase the capability of the OPF algorithm. The system is a section of the US power system and its data can be found in the *power systems tests case archive* at the following address (University of Washington: <http://www.ee.washington.edu/research/pstca>). This system consists of 6 generators, 34 transmission lines, 7 transformers feeding 30 loads in the network and 2 shunt compensators in nodes 10 and 24. A general layout of the 30-node system illustrating the OPF solution is given in figure (2.7). The original system operates in 132/33 KV range. The OPF algorithm produces its results in per unit and the appropriate bases need apply in order to generate the voltage levels in kilo volts. Choosing an arbitrary base level for the system power is however redundant since

the OPF algorithm gives the final economic distribution of powers in per unit. It is assumed that all generators operate within a similar output voltage level and a similar base MVA has been adopted for the whole system regardless of the voltage levels to maintain consistency and simplify objective function calculations.

The OPF algorithm is applied to this system with the following expressions defining the systems objective functions:

$$f_1 = 2.00P_{G_1} + 0.02P_{G_1}^2 \quad 2.59$$

$$f_2 = 1.75P_{G_2} + 0.0175P_{G_2}^2 \quad 2.60$$

$$f_3 = 1.00P_{G_3} + 0.0625P_{G_3}^2 \quad 2.61$$

$$f_4 = 3.25P_{G_4} + 0.083P_{G_4}^2 \quad 2.62$$

$$f_5 = 3.00P_{G_5} + 0.025P_{G_5}^2 \quad 2.63$$

$$f_6 = 3.00P_{G_6} + 0.025P_{G_6}^2 \quad 2.64$$

- OPF Results:

The OPF algorithm is applied to the system and it has been observed that it converges in 5 iterations. There is a voltage violation in nodes 12 and 24 where the OPF algorithm has successfully enforced their corresponding magnitudes to 1.05 per unit (the upper limit). Voltages in other nodes remained within their respective limits. The 30-node system is a good example of how the quadratic penalty function method combined with the Lagrangian multipliers effectively act together to satisfy the KKT conditions. The OPF results are detailed in tables (2.29-2.32).

Mathematical Modelling of Multi-terminal VSC-HVDC Links in Power Systems using  
Optimal Power Flows

---

Generator No.	Active Power Dispatch (p.u.)	Reactive Powers (p.u.)	Optimal Cost of Generation \$/hr	Optimal Value of Total Generation
1	+0.5770	+0.0053	181.9648	967.1601 \$/hr
2	+0.7451	+0.1619	227.556	
3	+0.2865	+0.2594	79.9660	
4	+0.6968	+0.4167	266.7753	
5	+0.2883	-0.1871	107.2659	
6	+0.2801	-0.0488	103.6320	

**Table 2.28 - Generators Optimal Power Flow Dispatch**

Transformer No.	Sending End	Receiving End	Sending End (p.u.)		Receiving End (p.u.)	
			$P_s$	$Q_s$	$P_r$	$Q_r$
1	6	9	+0.0654	+0.0870	-0.0654	-0.0847
2	6	10	+0.0920	+0.0262	-0.0920	-0.0213
3	9	11	-0.2883	+0.2122	+0.2883	-0.1871
4	9	10	+0.3537	-0.1276	-0.3537	+0.1422
5	4	12	+0.1601	+0.1890	-0.1601	-0.1740
6	12	13	-0.2801	+0.0593	+0.2801	-0.0488
7	28	27	+0.1731	+0.0394	-0.1731	-0.0284

**Table 2.29 - Transformers Calculated Powers (at optimum)**

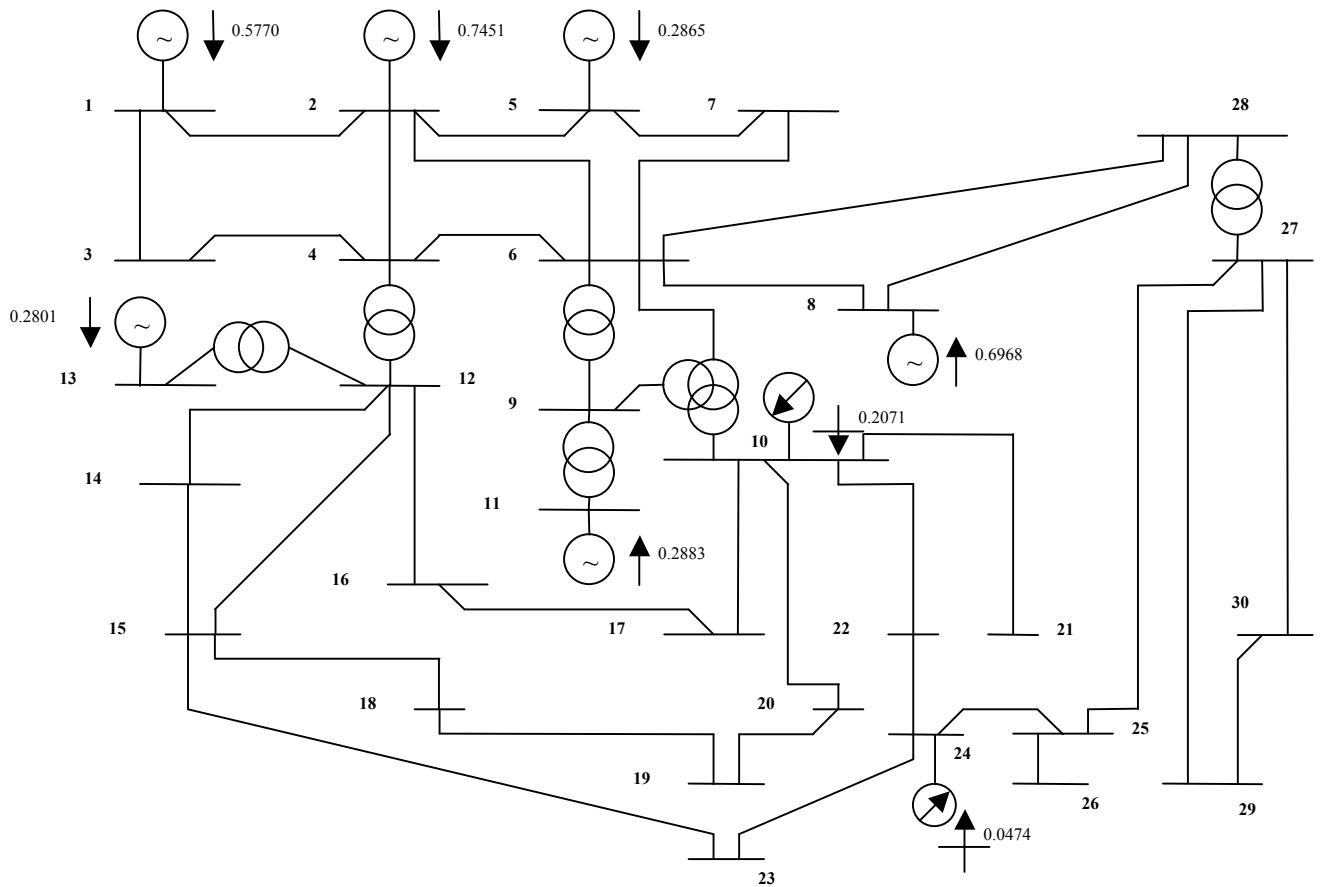


Figure 2.7 - 30-node Test System (Optimal Power Flow Solution)

Bus No.	1	2	3	4	5	6	7	8	9	10	11	12	13	14	15
Multiplier	4.31	4.36	4.40	4.42	4.58	4.44	4.52	4.41	4.44	4.44	4.44	4.40	4.40	4.47	4.49
\$/hr															

Table 2.30 - Incremental Generation Costs (Multipliers) - First 15 nodes

Bus No.	16	17	18	19	20	21	22	23	24	25	26	27	28	29	30
Multiplier	4.45	4.46	4.54	4.55	4.52	4.49	4.48	4.52	4.52	4.51	4.59	4.47	4.45	4.59	4.67
\$/hr															

Table 2.31 - Incremental Generation Costs (Multipliers) - Second 15 nodes

Shunt Device	Bus No.	Reactive Power Compensation (p.u.)
1	10	0.2071 (capacitive)
2	24	0.0474 (capacitive)

Table 2.32 - Shunt Reactive Powers (Compensators)

- Results Discussion:

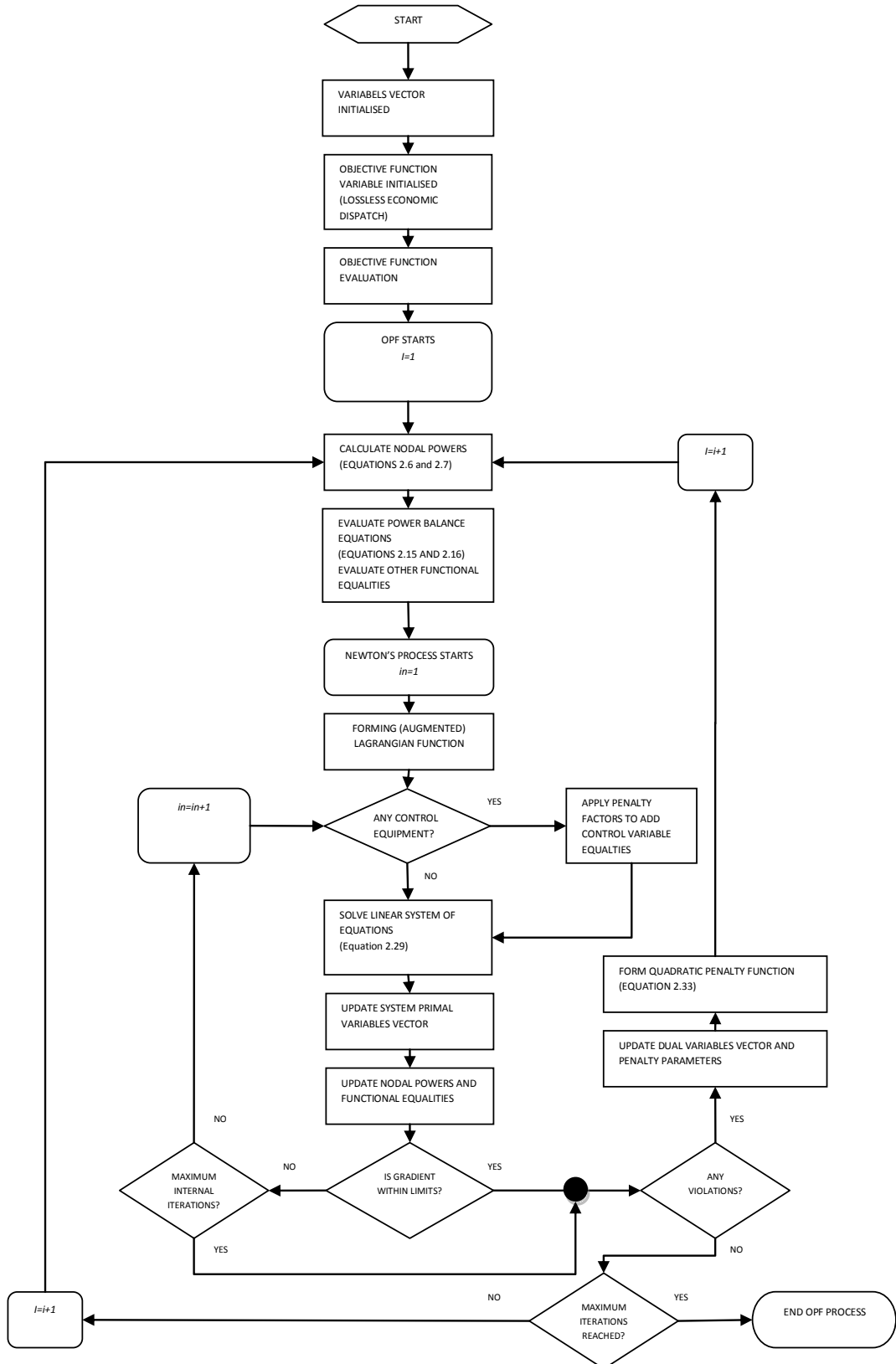
As shown in the 9-node case scenario, it can be observed here that the shunt compensators at buses 10 and 24 provide reactive power requirements locally improving the system's voltage profile at these buses. There are six machines in this system four of which operate as over-excited synchronous generators providing reactive power whereas the remaining two that are connected to nodes 11 and 13 respectively provide only active power and absorb reactive power therefore as the OPF algorithm dictates, achieving optimum operating point of the system does not depend on these two machines operation in the over-excited region. However if the voltages in nodes 11 and 13 were to be fixed by controlling the field current of their machines (by including two additional variable equalities) the results would have been different. Once again these results confirm the flexibility of the OPF formulation and the modelling criterion introduced in this chapter in dealing with a variety of operational circumstances.

The result obtained here state that in order for the system to operate economically it is required to spend 967 \$/hr, deviating from this point would obviously generate bigger values for the objective function.

It is clearly inferred from the results shown in table (2.30) and (2.31) that it would be costlier to generate power to nodes that are physically located farther from the points of generation. For instance the cost of increasing demand by 1 MW in node 30 costs approximately 4.67\$, whereas in comparison it costs less to transmit 1 MW increase in power to node 26 which physically is closer to the nearest point of generation, namely node 8. As it is seen from the case scenarios presented in this section, the OPF algorithm is a very useful tool in analysing the system's behaviour under different circumstances for example for purposes of economic distribution of loads between different generators (economic dispatch). For instance from the results it can be observed that for improving economic performance of the system it may be useful to add local condensers to provide active power locally to the more isolated nodes (node 30). One of the main purposes of this project is to study systems that are used for the purpose of connecting autonomous generating facilities that are remotely located from each other in an optimum fashion that is both economical and improves the reliability of the system. In chapter 4 the principles of

modelling for Voltage Source Converters that are useful for creating VSC-HVDC interconnections are explained. These VSC-HVDC inter-links are then used to connect remotely located areas of local generation-consumption (micro-grids). The OPF algorithm is then used to devise the optimum operating points of such systems under a variety of circumstances and conditions. In the next section the OPF solution process is given in a flow chart.

## 2.5 Optimal Power Flow Formulation: A Flow Chart



## 2.6 Alternative Solution Algorithms for OPF including Meta-Heuristics

Apart from the already well established Newton's method for augmented Lagrangian function, there are a handful of alternative solution algorithms for solving complex optimisation problems such as the OPF that are not necessarily based on numerical methods. The groups of alternative OPF solution algorithms are mostly based on either Fuzzy mathematical methods [24] or Meta-heuristic algorithms that are generic and can be applied to a variety of practical programming problems (from engineering type problems to finance and economics as well as biology) including the OPF [10]. Because they are purely based on direct search methods inspired by natural phenomena, they are particularly useful for devising global optimisation algorithms because unlike numerical methods such as the Newton's method, they allow for temporary expansions of the solution space therefore the possibility of being trapped in a neighbourhood of local minima is little in such solution algorithms [17]. Examples of Meta-heuristics include Ant Colony Systems, Tabu Search methods, Simulated Annealing, Variable Neighbourhood Search and Particle Swarm Optimisation [10, 27, 32, 33, 38]. The PSO algorithm particularly has shown to be very effective in solving OPF problem in being able to reach a global solution [32], however it should be noted that such globally convergent solution algorithms are time consuming and therefore it is not practical for real time simulation applications. The modelling criterion for conventional programming methods such as the augmented Lagrangian function as explained in this chapter can still be used in Meta-heuristic approaches as well for formulating the optimisation problem however the difference is in the solution algorithm chosen. There can either be conventional algorithms such as Newton's method, which are fast and more reliable or the slower but globally convergent algorithms such as PSO can be used to solve a non-linear programming problem such as the OPF. As mentioned earlier the scope of this project is not to investigate the features of different mathematical programming approaches for the OPF but to use one to develop robust models in order to be used in power system analysis scenarios.

## 2.7 Conclusion

The augmented Lagrangian function as a very effective tool for converting a constrained non-linear programming problem such as the OPF into an unconstrained simpler programming problem is presented thoroughly in this chapter. The solution algorithm for solving the OPF is chosen to be the Newton's method due to its strong convergence characteristic and its flexibility in applying to almost any power system with any configuration as well as equipment present. The OPF via Newton's method consists essentially of two parts, one is the internal iteration loop which is the main loop for minimising the Lagrangian function using a system of linear equations (Hessian/Jacobian terms) whereas on the other hand the state variables limit check process is carried out in the outer loop where, if necessary, the effects of violated constraints are added to the system Lagrangian using quadratic penalty functions. It is shown that using a combination of multipliers to include the effects of equality constraints as well as active inequality constraints and quadratic penalty function to account for constraints' limit violations are more effective than merely using pure penalty function methods which are prone to numerical ill-conditioning.

There are two categories of equality constraints: variable and functional. Variable equalities are always on control variables and are enforced to the system formulation using penalty functions (just like active inequalities). Functional equalities, on the other hand, are power flow control equations that describe the state of operation in a system. The most important functional equality constraints are the power balance equations, which need to hold for the entirety of the OPF solution process. The functional equalities are added to the system formulation using their associated Lagrangian multipliers.

The purpose of presenting the numerical simulations in this chapter was to depict the robustness of the Newton's method in solving the OPF problem in different situations. Moreover the OPF algorithm has been applied to two case scenarios involving realistic power systems.

There is however other alternative approaches to the Newton's method, which are mostly based on Heuristic search methods. These methods, while similar to conventional optimisation approaches in formulating the constrained optimisation

problem (using Lagrangian functions or penalty functions) of the OPF, are different in solution. The augmented Lagrangian function still is used to formulate the OPF problem however the solution algorithm applied to the OPF is different from the Newton's method. They take more time to converge; nevertheless they mostly reach a global solution.

## 2.8 References

- [1] Dommel, H. W., Tinney W. F., "Optimal Power Flow Solutions," *Power Apparatus and Systems, IEEE Transactions on*, vol. PAS-87, pp. 1866-1876, Oct. 1968 1968.
- [2] Stevenson, W. D., Grainger, J. , *Power System Analysis*: McGraw-Hill 1994.
- [3] Acha, E., Fuerte-Esquivel, C. R., Ambriz-Perez, H., Angeles-Camacho, C., *FACTS Modelling and Simulation in Power Networks*: John Wiley & Sons Ltd., 2005.
- [4] Sasson, A. M., Vilorio, F., Aboytes F., "Optimal Load Flow Solution Using the Hessian Matrix," *Power Apparatus and Systems, IEEE Transactions on*, vol. PAS-92, pp. 31-41, Jan. 1973.
- [5] Rashed, A. M. H., Kelly, D. H., "Optimal Load Flow Solution Using Lagrangian Multipliers and the Hessian Matrix," *Power Apparatus and Systems, IEEE Transactions on*, vol. PAS-93, pp. 1292-1297, Sept. 1974 1974.
- [6] Sun, D. I., Ashley B., Brewer B., Hughes, A., Tinney, W. F., "Optimal Power Flow by Newton's Approach," *Power Apparatus and Systems, IEEE Transactions on*, vol. PAS-103, pp. 2864-2875, 1984.
- [7] Santos, A., Jr., da Costa, G. R. M., "Optimal-power-flow solution by Newton's method applied to an augmented Lagrangian function," *Generation, Transmission and Distribution, IEE Proceedings*, vol. 142, pp. 33-36, 1995.
- [8] Bertsekas, D. P., *Constrained Optimization and Lagrange Multiplier Methods*: Academic Press, 1982.
- [9] Bazaraa, M. S., Sherali, H. D., Shetty C. M., *Nonlinear Programming: Theory and Algorithms*: John Wiley and Sons, Inc., 1993.
- [10] Pardalos, P. M., Resende, M. G. C., *Handbook of Applied Optimization*: Oxford University Press, 2002.
- [11] Ruszczyński, A., *Nonlinear Optimization*: Princeton University Press, 2006.
- [12] Acha, E., Agelidis, V. G., Anaya-Lara, O., Miller, T. J. E., *Power Electronic Control in Electrical Systems*: Newnes, 2002.
- [13] Penny, J., Lindfield, G., *Numerical Methods using MATLAB*: Prentice Hall, 1999.
- [14] Atkinson, K., Weimin, H., *Theoretical Numerical Analysis: A Functional Analysis Framework*: Springer, 2005.
- [15] Allaire, G., *Numerical Analysis and Optimization: An Introduction to Mathematical Modelling and Numerical Simulation*: Oxford University Press, 2007.
- [16] Betts, J. T., *Practical Methods for Optimal Control Using Nonlinear Programming*: Society for Industrial and Applied Mathematics, 2001.

- [17] Venkataraman, P., *Applied Optimization with MATLAB Programming*: John Wiley and Sons, 2002.
- [18] Baptista, E. C., Belati, E. A., da Costa, G. R. M., "A New Solution to the Optimal Power Flow Problem," presented at the Power Tech Proceedings, 2001 IEEE Porto, 2001.
- [19] Belati, E. A., de Sousa, V. A., Nunes, L. C. T., da Costa, G. R. M., "Newton's Method associated to the Interior Point Method for Optimal Reactive Dispatch Problem," in *Power Tech Conference Proceedings*, IEEE Bologna, 2003, p. 6.
- [20] de Souza, A. M., de Sousa, V. A., da Costa, G. R. M., "Optimal Power Flow: a Tool for Managing the Transmission Congestion," in *Power Engineering Society General Meeting, IEEE*, 2004, pp. 844-848.
- [21] de Sousa, V. A., Baptista, E. C., da Costa, G. R. M., "Optimal Power Flow via Interior-Exterior Method," *Power Engineering Society General Meeting, 2007. IEEE*, pp. 1-6, 24-28 June 2007.
- [22] Lage, G. G., de Sousa, V. A., da Costa, G. R. M., "Optimal power flow solution using the penalty/modified barrier method," *Power Tech, 2009 IEEE Bucharest*, pp. 1-6, June 28 - July 2 2009.
- [23] Santos, A., Jr., Deckmann, S., Soares, S., "A dual augmented Lagrangian approach for optimal power flow," *Power Systems, IEEE Transactions on*, vol. 3, pp. 1020-1025, Aug 1988.
- [24] Abdul-Rahman, K. H., Shahidehpour, S. M., "A Fuzzy-based Optimal Reactive Power Control," *Power Systems, IEEE Transactions on*, vol. 8, pp. 662 - 679, May 1993.
- [25] Granville, S., Rodrigo de Miranda Alves, A., "Active-Reactive Coupling in Optimal Reactive Dispatch: A Solution via Karush-Kuhn-Tucker Optimality Conditions," *Power Systems, IEEE Transactions on*, vol. 9, pp. 1774-1779, Nov 1994.
- [26] Da Costa, G. R. M., Langona, K. , Alves, D. A., "A new approach to the solution of the optimal power flow problem based on the modified Newton's method associated to an augmented Lagrangian function," *Power System Technology, 1998 Proceedings. POWERCON' 98. 1998 International Conference on*, vol. 2, pp. 909-913, 18-21 Aug 1998.
- [27] Yuryevich, J., Po Wong, K., "Evolutionary Programming Based Optimal Power Flow Algorithm," *Power Systems, IEEE Transactions on*, vol. 14, pp. 1245-1250, November 1999.
- [28] Almeida, K. C., Salgado, R., "Optimal Power Flow Solutions under Variable Load Conditions," *Power Systems, IEEE Transactions on*, vol. 15, pp. 1204-1211, Nov 2000.
- [29] Kim, B. H., Baldick, R., "A Comparison of Distributed Optimal Power Flow Algorithms," *Power Systems, IEEE Transactions on*, vol. 15, pp. 599-604, May 2000.
- [30] Lima, F. G. M., Soares, S., Santos, A., Jr., Akmeida, K. C., Galiana, F. D., "Numerical experiments with an optimal power flow algorithm based on parametric techniques," *Power Systems, IEEE Transactions on*, vol. 16, pp. 374-379, Aug 2001.
- [31] Sousa, A. A., Torres, G. L., "Globally Convergent Optimal Power Flow by Trust-Region Interior-Point Methods," presented at the Power Tech, Lausanne, 2007.

- [32] Yang, B., Zhao, Z., "Survey on Applications of Particle Swarm Optimization in Electric Power Systems," in *Control and Automation, IEEE International Conference on*, Guangzhou, China, 2007, pp. 481-486.
- [33] Abido, M. A., "Multiobjective particle swarm optimization for optimal power flow problem," presented at the Power System Conference, 2008. MEPCON 2008. 12th International Middle-East, 2008.
- [34] Zhiguang, H., Quanyuan J., "Nonlinear weighted multiple centrality corrections interior point method for optimal power flow," presented at the Sustainable Power Generation and Supply, 2009. SUPERGEN '09. International Conference on, 2009.
- [35] Quanyuan, J., Guangchao G., Chuangxin G., Yijia C., "An Efficient Implementation of Automatic Differentiation in Interior Point Optimal Power Flow," *Power Systems, IEEE Transactions on*, vol. 25, pp. 147-155, Feb. 2010 2010.
- [36] Hong, Y.-Y., Liao, C.-M., Lu, T-G., "Application of Newton optimal power flow to assessment of VAR control sequences on voltage security: case studies for a practical power system," in *Generation, Transmission and Distribution, IEE Proceedings C*, 1993, pp. 539-544.
- [37] Acha, E., Ambriz-Perez, H., Fuerte-Esquivel, C. R., "Advanced transformer control modeling in an optimal power flow using Newton's method," *Power Systems, IEEE Transactions on*, vol. 15, pp. 290-298, Feb 2000.
- [38] Mori, M., Matsuzaki, O., "A rule-based tabu search technique for power system decomposition," *Power Engineering Society Summer Meeting, 2000. IEEE*, vol. 4, pp. 1990-1995, 2000.

### **3 Optimal Power Flow Modelling for Shunt FACTS Controllers**

The principles pertaining the modelling of shunt reactive FACTS controllers are extensively explained in the following chapter. Modelling of FACTS controllers is carried out using the same generic criteria developed in previous chapter for modelling various power system components within the OPF algorithm. The models developed are then solved using Newton's method for a variety of different configurations. Even though the first part of this chapter comprises a general overview of FACTS modelling within the Augmented Lagrangian Function framework for different devices (Series, Shunt and Hybrid), the main area of focus has remained the shunt reactive compensator. Models for both Thyristor Controlled Reactor (TCR) based Static VAR Compensator (SVC) and the more advanced Voltage Source Converter (VSC) based Static Compensator (STATCOM) have been presented accordingly. Furthermore, for the first time a comparison study has been carried out for both models in several real and experimental power systems to fully depict the robustness of the models and their ability to cope with different circumstances in optimising the system performance while maintaining the steady state voltage profile and eventually improving system stability.

#### **3.1 Introduction**

In this research project a power system is seen as an actively managed system having full flexibility in power flow regulation and voltage control by using power electronics based controllers otherwise known as FACTS (Flexible AC Transmission Systems). The seamless control of power systems' fundamental parameters, namely nodal voltage magnitude and phase angle is essential for the continuous steady state operation of the system [1]. The flexibility and enhanced stability margins brought about by FACTS make them essential elements of modern power systems design in almost any voltage level making understanding the operational characteristics of FACTS devices and controllers one of the most important concepts in power systems research.

Recent developments in the area of power electronics design and development have spawned a new breed of fully controlled semi-conductors such as GTOs (Gate Turn-

Off Thyristors) and IGBTs (Insulated Gate Bipolar Transistor) with turn-off capability [2]. Such devices have considerable advantage over the conventional Thyristors in that their turn-off compatibilities do not depend on the line current and they can be turned on and off at anytime [1].

IGBT valves switched with Pulse Width Modulation (PWM) schemes for instance are mainly used in medium voltage self-commutated controllers such as Voltage Source Converters (VSCs) providing independent bi-directional active and reactive power control capability on the AC side (four quadrant operation) as well as bi-directional DC power control [1-3]. In contrast, a Thyristor-controlled Current Source Converter (CSC), only provides active power support while consuming reactive power, so their AC current is always lagging [1, 2]. Sinusoidal PWM (SPWM) is used to switch the valves at rates higher than fundamental frequency therefore reducing the levels of low-order harmonics albeit at the cost of increasing switching losses [1].

The FACTS controllers are essentially grouped into two main categories based on the type of the power electronics used in them, namely the Variable Impedance Type and the Switching Converter Type [1, 2, 4, 5]. Most of the newer more advanced FACTS controllers belong to the latter category. For example the Voltage Source Converter introduced in [1] is a controller device capable of providing direct active and reactive power support depending on the application it is providing to the system [2]. It can be used as an active series capacitor in form of a Static Series Synchronous Controller (SSSC) for improving the transmission line's total transfer capability (TTC) or it can be used as a Synchronous Voltage Source (SVS) to provide shunt compensation in STATCOM for fast nodal voltage support at its point of connection by consuming/delivering reactive power and hence keeping the voltage levels at an acceptable range [1, 2, 6].

The variable impedance type category is however, the group of FACTS devices that are generally based on line-commutated Thyristor Controlled Reactor (TCR) valves in parallel with fixed capacitor/reactor groups that compared to the converter type FACTS are less reliable and generate more low-order harmonics [1, 2, 5, 7, 8]. An SVC is a typical example of this particular type of FACTS equipment, which contains a TCR valve in parallel with a switched (mechanical or electronic)

capacitor bank for providing reactive power compensation [1, 9-11]. The Thyristor Controlled Series Capacitor (TCSC) is used for long transmission line impedance compensation and is generally a fixed capacitor bank again in parallel with a TCR valve, which is then connected typically in mid-point in series with the impedance of the compensated long transmission line providing fast series impedance compensation and improving the line's active power transfer capability [1, 12, 13].

In both SVC and TCSC, unlike the VSC based controllers such as the STATCOM, the act of compensation is carried out by manipulation of the TCR's thyristors' firing angles [8, 14, 15]. Due to the firing angle control of the TCR, these controllers tend to have a net reactive impedance which is either inductive or capacitive depending on the value of the firing angle as well as the application they are used in and therefore they are called the variable impedance type FACTS controllers [1, 2, 8, 10, 14, 15]. The variable impedance type FACTS controllers are modelled simply as variable shunt or series impedances in power flow studies.

VSC-based controllers such as the STATCOM or SSSC, on the other hand, provide direct active/reactive power compensation via controlling the amplitude and phase angle of their associated voltage injections at their points of compensation achieved through Pulse Width Modulation switching or any other means [1, 2]. For example a STATCOM regulates the voltage at its point of connection by controlling the amplitude of its converter voltage relative to the nodal voltage of bus to which it is connected much like a synchronous condenser [1, 4, 6, 9, 16]. Moreover the SSSC controls the active power transmission capacity by injecting a controllable series voltage at its point of connection which then can control the net phase angle difference between the sending and receiving ends of the transmission line, essentially increasing (or decreasing) the total active power transmission capacity of the line [4]. Some FACTS controllers can be a combination of both series and shunt controllers and are called Hybrid (or Combined) Controllers [1]. The most important Hybrid Controller is the Unified Power Flow Controller (UPFC) first proposed in [17], which is a combination of a STATCOM and a SSSC. Since the UPFC is essentially based on VSCs it belongs to the category of switching converter type FACTS controllers. The UPFC in principle is used to control all the fundamental parameters in a power system, namely the voltage magnitude, phase angle and power flow [1]. The shunt converter provides voltage regulation by

providing shunt reactive compensation exactly as a STATCOM whereas the series converter provides phase angle compensation and line impedance compensation through injecting a controllable series voltage to the compensated transmission line it is set to control [1, 2]. The categorisation of FACTS controllers is a very useful tool in identifying the operational principles of different FACTS devices when it comes to their modelling in power flow studies. For example, knowing that the SVC is a conventional thyristor-controlled variable impedance FACTS controller is helpful in order to model the SVC as a variable shunt susceptance in power flow studies as done in [10]. The two main categories of FACTS devices along with their respective controllers and their applications are summarised in [1].

Regardless of which type of FACTS controllers present in the system they have a discernible influence on the operation of the system in steady state. Therefore one of the most important aspects of solving the OPF problem is to assess the conditions of the system while under the control of FACTS equipment. For instance electronically controlled shunt compensators may be used to regulate voltages in load buses in modern power systems. Applying OPF in such a system will yield to the optimum settings in which the system operates while maintaining voltages constant at regulated buses in forms of active equality constraints.

In the next section the concept of modelling FACTS equipment for power flow studies is explained. This is followed by a brief literature review on the most important works done in the area of FACTS-OPF modelling.

### **3.2 An Overview of FACTS Modelling for Power Flow Studies (Conventional and Optimal)**

Considering current advancements in the fields of Flexible AC Transmission Systems, there has been a lot of research material published in the area of FACTS modelling in power systems particularly with relations to OPF algorithms [4, 10, 16, 18-21]. The FACTS models for power flow studies are essentially categorised into two groups of steady state and dynamic models. Steady-state models of FACTS equipment are used in conventional as well as optimal power flow study scenarios that are formulated and solved via numerical analysis algorithms such as Newton's method. Depending on the operational principles of the FACTS controller, the

steady-state models are either Power Injection Models (PIM) or Variable Impedance Models [22]. For example in [10] a variable shunt susceptance power flow model for the SVC has been presented for both conventional and optimal power flow algorithms. The SVC model is developed in such a way that it can be used in power flow solution algorithms that are solved via Newton's method. Furthermore, In [14] a similar variable series impedance model has been developed for conventional power flow solved via Newton's method for the TCSC.

However, almost all modern VSC-based FACTS controllers are modelled as power injections at their points of connection [22]. In other words, the FACTS device is purely modelled as series or shunt voltage-dependent power injections depending on its type and operational characteristics. A voltage source converter in this paradigm is therefore modelled as a controllable voltage source injecting an amount of active/reactive power based on its source voltage and phase angle [5]. Since VSC type controllers provide independent active and reactive power support in the AC side there can be various control strategies for a power flow model of such devices [1]. The model can be configured to provide direct voltage control or direct power control depending on its application and operational principles. Developing power injection models (or sometimes controllable voltage source models) for switching converter type FACTS controllers has become the subject of much study in the past years with publications on models developed for both conventional and optimal power flow algorithms becoming more and more common [4, 7, 19, 20, 22, 23].

For instance in [4], the STATCOM is presented as a controllable shunt voltage source which injects a controllable reactive power to its point of connection, moreover, in the same paper the SSSC is modelled as a series voltage source with which the net transmission capacity of the compensated line is controlled. Hybrid FACTS controllers in this way can easily be modelled as a group of series/shunt power injections. For instance an early version of UPFC power injection modelling for conventional power flow studies has been given in [24] and its OPF counterpart in [5, 19]. The UPFC-OPF model introduced in [5] is devised for Newton's method for augmented Lagrangian function which means that the UPFC is modelled as an exclusive Lagrangian, whereas in [19] the OPF algorithm for which the model is developed is not mentioned.

Although the power injection model is a fairly accurate account of the operational characteristics of the switching converter type FACTS controller, it lacks a fundamental parameter, namely it is unable to properly model the converter's internal switching losses [22]. Furthermore the effects of the converter PWM control in providing active and reactive powers are ignored (modulation ratios). To include the effects of PWM switching as well as converter's internal losses and DC link losses, a new and more advanced model for VSCs has been created. The converter's PWM control is represented in form of a complex tap ratio with a controllable magnitude and phase angle. This model, appropriately called the compound transformer model, has been developed as part of this research for OPF algorithm and is the building block of VSC-HVDC system models, which are presented, in the next two chapters. In the next section, the FACTS-OPF modelling application in power system study scenarios is investigated in more detail by simulating SVC and STATCOM incorporated systems.

There have been other useful publications regarding other types of FACTS equipment, for instance regarding power flow models for Thyristor Controlled Series Compensator (TCSC) a power flow model in Newton's method has been described in [14] as well as [20] and [23], which contain power injection models (based on controllable voltage sources) for Voltage Source Converters and VSC-HVDC systems. In the next chapter a more comprehensive study on different models for VSC based systems will be presented.

### **3.3 Shunt Compensator Modelling in OPF using Newton's method for Augmented Lagrangian Function**

In this section, models developed for SVC and STATCOM controllers, suitable for OPF algorithm using Newton's method for Lagrangian functions, are elaborately depicted. The difference between SVC and STATCOM is in the nature of their operation [1]. Even though both provide reactive power compensation, SVC operation is based on injecting a reactive current (either capacitive or inductive) in the system by switching capacitors. However STATCOM regulates voltage directly by the operation of its VSC. The converter will control its output voltage and inject or consume reactive power to and from the system, more like a synchronous condenser [1]. Therefore SVC model is based on a shunt variable susceptance

whereas STATCOM model is based on controllable voltage source. Furthermore, as an advantage to SVC, the STATCOM can be configured to provide active power to its point of connection through an energy storage device such as a large capacitor (not the DC voltage source capacitor in VSC) or battery or a group of fuel cells [1, 4, 16]. The active power control capability of the STATCOM is presented for the first time within the OPF algorithm in the model developed in this chapter and its effectiveness is tested.

Shunt compensation is a necessity in modern power systems, which feed several kinds of loads in order to keep a constant voltage profile and ensure good power quality for the consumer. There are two possible cases in shunt compensation [1, 2, 5, 9-11, 16]:

1. The voltage is sagging due to excessive reactive consumption caused by heavy industrial loads; in this case the compensator will inject reactive power to its point of control to compensate the needed reactive power and keep the voltage magnitude constant
2. In some unlikely cases the voltage starts increasing dramatically which may have been caused due to load rejection, Ferranti effects in open end lines are also a main cause of voltage increase; in such peculiar situations the compensator starts consuming the excess reactive power in order to preclude the voltage from increasing any more

SVC comprises two sets of legs, one set includes capacitor banks, which can be switched on or off, and the other contains TCR valves (or Thyristor Controlled Reactor valves). Whenever there is a need for reactive power the TCR's switching angle will increase making SVC's current more capacitive and vice versa [8, 10]. STATCOM comprises a VSC behind connecting shunt transformer impedance (or reactance) [16] typically between 0.1 to 0.15 per unit [1] (In empirical examples presented in this chapter the STATCOM model's coupling impedance has a value of 0.05 per unit). VSC may also be connected to energy storage to provide active power control or account for small switching losses that occur in realistic converters [1]. STATCOM will then provide the required reactive power dispatch to the system through operation of the VSC. The converter voltage is controlled to provide reactive power compensation at the point of connection; the STATCOM model can

also be configured to provide direct reactive power rather than voltage regulation to the point of connection. The STATCOM's main advantage towards the SVC is that it is capable of providing capacitive compensation even in very low voltage levels and therefore provides a more promising platform on which the system can remain stable [1].

It should be noted that SVC and STATCOM operation principles are discussed in detail in several publications [1, 2, 5, 6, 10, 16, 25] and will not be discussed here any further. In this section the principles outlining the modelling criteria for SVC and STATCOM is however presented. It is stressed here that because of the vital application of shunt compensators in improving system stability by regulating the voltage developing OPF models for such devices is of paramount importance when studying FACTS based systems.

### **3.3.1 STATCOM OPF Formulation (Controllable Voltage Source Model)**

The mathematical approach developed in previous chapter for formulating the OPF problem by forming an augmented Lagrangian function is used to model the STATCOM operation here.

The STATCOM regulates reactive power by controlling its converter voltage magnitude much like a synchronous condenser [1, 16], it is therefore modelled as a controllable voltage source with close to zero active power exchange (converter voltage is in phase with the system nodal voltage) with the system (neglecting the ohmic losses as well as presence of any sort of energy storage units) [4, 16, 22].

The power balance equations given in previous chapter (Equations 2.15 and 2.16) also apply in a system with STATCOM taking into account the effects of STATCOM reactive power output (which is voltage dependent) in the reactive power balance equation as explained thoroughly in the parametric example of chapter two. The STATCOM controllable voltage source model is the first model with an additional functional equality constraint that is presented in this research. The functional equality constraint is on STATCOM's output reactive power, which is a function of its output converter voltage. Equation (3.2) shows the exclusive Lagrangian formed out of STATCOM's reactive power constraint. The state variables vector associated with the STATCOM are the voltage magnitude and

phase angle of the controllable voltage source representing STATCOM's voltage source converter as such:

$$z_{statcom} = [\delta_{conv}, V_{conv}, \lambda_{qconv}]^T \quad 3.1$$

The vector of variables in equation (3.1) is used to form the STATCOM Lagrangian function in equation (3.2).

$$L_{conv}(x, \lambda) = \lambda_{qconv} (Q_{conv} - Q_{specified}) \quad 3.2$$

This function should account for the STATCOM's control constraints, which is on converter's output reactive power as shown in equation (3.3):

$$Q_{conv} - Q_{specified} = 0 \quad 3.3$$

In addition to the functional constraint in equation (3.3), STATCOM can be configured for direct voltage regulation, in which case it behaves exactly like a synchronous condenser with zero active power output.

The direct voltage regulation shows itself as a variable equality constraint on STATCOM's output voltage as shown in equation (3.4).

$$V_i - V_{specified} = 0 \quad 3.4$$

As explained in chapter two the variable equality constraints are enforced throughout the OPF solution process using exclusive quadratic penalty functions in forms of equation (3.5).

$$\phi(V_i) = \frac{1}{2} \varphi(V_i - V_{specified})^2 \quad 3.5$$

This function is defined in such a way that penalises the system Lagrangian for points outside the pre-specified nodal voltage for node  $i$ . It should be stressed here that STATCOM's converter voltage should not be penalised as it is assumed that STATCOM regulates voltage with the free operation of the converter, therefore penalising the converter's voltage along with the nodal voltage at which point the STATCOM is connected will produce inaccurate results. The controllable voltage source model shown in figure (3.1) represents the operation of the VSC in the STATCOM device (designated here as  $k$ ) as an adjustable (or controllable) voltage phasor, namely  $V_{conv(k)} \angle \delta_{conv(k)}$ , which should not be confused with the system's vector of voltage phasors.

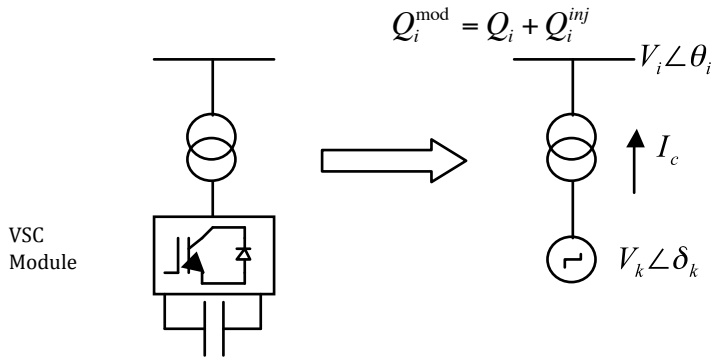


**Figure 3.1 - STATCOM Controllable Voltage Source Model**

According to figure (3.1) the STATCOM regulates the voltage magnitude by injecting currents to its point of compensation. The converter output reactive power thus takes the form of equation (3.6):

$$Q_{conv} = \text{Im}\{V_k I_c^*\} = V_k \cdot \sum_{j=k}^i V_j \cdot [G_{kj} \sin \theta_{kj} - B_{kj} \cos \theta_{kj}] \quad 3.6$$

Substituting for the vector of state variables pertaining the STATCOM's converter shown in equation (3.1), equation (3.6) is re-written as such:

$$Q_{conv} = -V_{conv}^2 B_c - V_{conv} V_i [G_c \sin(\delta_{conv} - \theta_i) - B_c \cos(\delta_{conv} - \theta_i)] \quad 3.7$$

This equation represents the STATCOM's reactive power behind the connecting transformer, namely  $Y_c$ . The injected reactive power element calculated at node  $i$  will however take the form of equation (3.8) below:

$$Q_i^{inj} = -V_i^2 B_c - V_i V_{conv} [G_c \sin(\theta_i - \delta_{conv}) - B_c \cos(\theta_i - \delta_{conv})] \quad 3.8$$

Consequently, the Lagrangian function associated to the STATCOM operation takes the following form:

$$L_{statcom}(x, \lambda) = \lambda_{q_i} (Q_i^{mod} - Q_{g_i} + Q_{d_i}) + \lambda_{q_{conv}} (Q_{conv} - Q_{specified}) \quad 3.9$$

Where

$Q_i^{mod} = Q_i + Q_i^{inj}$  is the total calculated nodal power taking into account the contribution of the STATCOM at node 'i' as well

$Q_{conv}$  is the reactive power flow between converter and compensated bus

$Q_{specified}$  is the pre-determined reactive power in order to be maintained for a fix voltage profile

$V_i$  is the nodal voltage to be regulated by STATCOM

$V_{specified}$  is the pre-determined voltage magnitude to be set by the user

$Q_i^{mod} = Q_i^{system} + Q_{conv}$  is the newly formed injected nodal reactive power at the point of compensation

Consequently, the system of linear equations presented in equation (2.29) in chapter two is solved for the newly updated system Lagrangian including the STATCOM's exclusive Lagrangian.

If the STATCOM is set to regulate reactive power at its point of connection, equation (3.3) will become active (equation 3.2 is added to the system Lagrangian) whereas the converter voltage is set free to accept any value, albeit within limits, depending on the amount of injected reactive power. This is essentially different from when the STATCOM is operating under voltage regulation mode, where the reactive power control constraint is deactivated (by penalising its multiplier, namely  $\lambda_{q_{conv}}$ ) and the nodal voltage at the compensated bus (equation 3.4) is fixed to a pre-determined value via penalty function given in equation (3.5) (See the parametric example in chapter two). One of the main differences between a STATCOM controllable voltage source model and a generator model is that the functional constraint on the reactive power in a generator is normally deactivated during the normal operation of the generator and is only activated to enforce the generator's reactive power to its binding limits [5], whereas in a STATCOM model equation (3.3) may be activated throughout the OPF solution process to represent the reactive power control feature of the STATCOM.

The expanded exclusive system of equations in forms of Hessian and Jacobian terms associated with the STATCOM power injection model is therefore presented in its most general form in equation (3.10).

$$\begin{bmatrix} \frac{\partial^2 L}{\partial \theta^2} & \frac{\partial^2 L}{\partial \theta \partial V} & \frac{dQ_i^{\text{mod}}}{d\theta} & \frac{dQ_{conv}}{d\theta} \\ \frac{\partial^2 L}{\partial V^2} & \frac{\partial^2 L}{\partial V \partial \theta} & \frac{dQ_i^{\text{mod}}}{dV} & \frac{dQ_{conv}}{dV} \\ \frac{\partial V \partial \theta}{dQ_i^{\text{mod}}} & \frac{\partial V \partial \theta}{dQ_{conv}} & & \\ \frac{d\theta}{dQ_{conv}} & \frac{dV}{dQ_{conv}} & & \end{bmatrix} \times \begin{bmatrix} \Delta \theta \\ \Delta V \\ \Delta \lambda_{q_i} \\ \Delta \lambda_{q_{conv}} \end{bmatrix} = - \begin{bmatrix} \nabla_{\theta} L \\ \nabla_V L \\ \Delta Q_i^{\text{mod}} \\ Q_{conv} - Q_{spec} \end{bmatrix} \quad 3.10$$

Through Newton's iterative method the system of linear equations is solved iteratively for vector of state variables. After the internal iterations is finished the values for state variables as well as their associated Lagrangians, are checked against the system limits to determine and update the active set. The violated inequalities are enforced to their boundaries using the quadratic penalty function.

### 3.3.2 SVC OPF Formulation (Variable Susceptance Model)

Unlike STATCOM, which is based on voltage source converters, SVC is merely a capacitor bank controlled by static thyristor switches (or TCR's) and therefore its mathematical model is based on a variable shunt susceptance [10]. By varying the amount of shunt susceptance, SVC will either inject or consume reactive power to or from its point of compensation [9]. The variable shunt susceptance model is shown in figure (3.2):

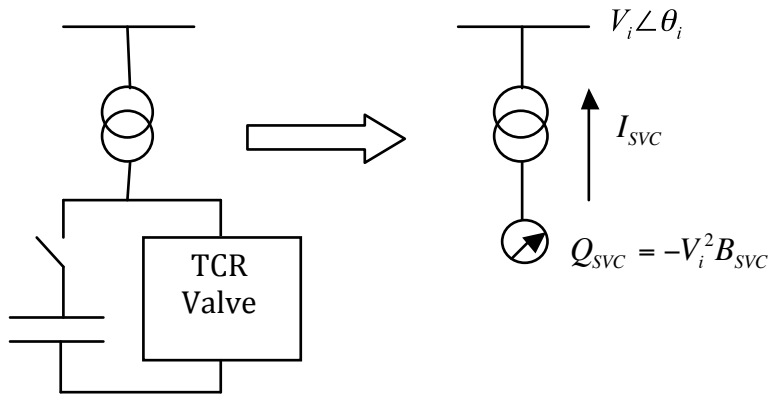


Figure 3.2 - SVC Variable Susceptance Model

SVC is modelled as a variable shunt susceptance connected to the point of compensation via an impedance [5]. As shown in equation (3.11), the nodal reactive power in an SVC-connected node is a function of SVC's shunt susceptance and not the voltage. This adds a new functional equality constraint to the set of constraints in the OPF formulation to include the effects of the SVC.

$$Q_{SVC} = -V_i^2 B_{SVC} \quad 3.11$$

Therefore SVC's exclusive Lagrangian takes the following form:

$$L_{SVC} = -\lambda_{SVC} V_i^2 B_{SVC} \quad 3.12$$

Notice that unlike the STATCOM Lagrangian in equation (3.2), the SVC susceptance model cannot provide direct reactive power support since its reactive

power function depends on the SVC's susceptance, namely  $B_{SVC}$  and not the nodal voltage magnitude. It is best to think of the SVC as a variable capacitor and not a synchronous generator [10].

The SVC operation in voltage regulation mode is however, defined by creating a new variable constraint on the nodal voltage of the SVC compensated bus, namely  $V_i$  in figure (3.2) as shown in equation (3.13).

$$V_i - V_{specified} = 0 \quad 3.13$$

The SVC enters voltage regulation mode by penalising the nodal voltage at its point of connection just like the STATCOM.

It is noted that the SVC compensated bus is modelled as a PVQ load bus in SVC feasible operation space, whereas the STATCOM regulated bus, is modelled as a PV generating bus (as if a generator is connected) within its limits. If for some reason the STATCOM reactive power violates limits, the compensated bus is changed into a generator PQ bus in which case the voltage is free to take up any value depending on the value of the violated reactive power. However if the SVC somehow violates its limits (of the variable shunt susceptance), its associated bus is converted to a special form of load PQ bus where the reactive power injected from the SVC is fixed at  $Q_{SVC} = -B_{lim} \times V_i^2$ . The SVC is not to be modelled as a generator PQ bus outside of its limit boundaries because its reactive power is then merely a function of the bus voltage magnitude and doesn't reflect the effects of the variable shunt susceptance limit which clearly produces inaccurate results [5, 10].

The models presented in this section for both SVC and STATCOM are the simplest form of modelling FACTS controllers, which properly include their control characteristics. However as an improvement to both power injection model and variable impedance model, the mathematical models developed in this research that are presented in the following chapters, are considered as the most advanced models for voltage source converters that are capable of illustrating the operational behaviour of VSC based controllers such as STATCOM's in their most detailed form. In chapter four the new concept of modelling VSC as a combination of a

power injection model and a variable impedance model is introduced. The VSC model is then used to model VSC-HVDC schemes as well as stand alone AC systems. For now this chapter concludes with several test case scenarios depicting the behaviour characteristics the two OPF models developed for STATCOM and SVC.

### **3.4 Optimal Reactive Power Control in Power Systems**

In the following section, the concept of optimal reactive power control is introduced by presenting a few test case scenarios. The 8-node system as the benchmark example is presented first. Both SVC variable susceptance model and STATCOM controllable voltage source model are implemented to this system. Subsequently, the STATCOM model is applied to IEEE 30-node system in order to illustrate the optimal reactive control in a realistic power system configuration. For comparison studies the shunt controller models, where applicable, are replaced by the STATCOM model in the 30-node system. The objective function is again chosen to be the generators' cost functions. The OPF is applied in a variety of distinct case scenarios to best reflect the realistic operating conditions in a given power system and generate a good comparison platform. The purpose of the OPF is then to determine the optimum operating points while utilising the shunt controllers to regulate the flow of reactive power and achieve an improved voltage profile in the system.

#### **3.4.1 Compensated 8-node System**

Two distinctive scenarios are presented in this section; one entails an SVC connected to the system in order to provide indirect shunt reactive support whereas in the other, the SVC is replaced by a STATCOM. Subsequently, both SVC and STATCOM OPF models have been put to test and a comparison between the results of the two has been made to draw appropriate conclusions.

The main difference between the STATCOM and SVC is not in the nature of their purpose but in their operation. The STATCOM is basically a Voltage Source Converter that is connected to the compensated bus through connecting impedance whereas the SVC is a collection of TCR's in parallel with switched capacitor banks. Both provide reactive power compensation and regulate voltage at their point of

connection to improve voltage profile and consequently overall stability of the system.

The system Lagrangian is augmented by the exclusive Lagrangian terms corresponding to STATCOM and SVC models presented in equations (3.2) and (3.12) respectively. For simulation purposes, the controllers are added to bus 4. In case of the SVC an additional connecting transformer is required to attach the SVC model to node 4, however the STATCOM model does not require such configuration and can be connected to its point of compensation directly. The reason is that the STATCOM is modelled as a synchronous condenser behind connecting impedance. The voltage in bus 4 is then controlled by the operation of the shunt compensators, namely SVC and STATCOM. Consequently the OPF program is run and results below are obtained.

There are essentially three different cases:

1. Case One: SVC is connected but not regulating voltage at bus 4
2. Case Two: SVC is connected and is regulating voltage at bus 4
3. Case Three: STATCOM is connected and is regulating voltage at bus 4

It should be noted that STATCOM OPF model is capable of both direct and indirect voltage regulation, which for the consistency purposes the former mode is chosen in the simulations.

### **1. Case One**

The OPF solution for compensated 8-bus system (with SVC) is shown in figure (3.3) (all the initial conditions remain the same as in chapter two simulations; the objective function is also the same and therefore is not mentioned here again).

The OPF is run knowing that the SVC is free to regulate the voltage at node 4 within its allowable boundaries. The OPF converges in 3 iterations and the following results are obtained:

Generator No.	Active Power Dispatch (p.u.)	Reactive Powers (p.u.)	Optimal Cost of Generation \$/hr	Optimal Value of Total Generation
1	0.9010 (0.9015)	-0.0138 (0.0305)	398.826 (399.0173)	834.2731 (834.6291) \$/hr
2	0.9891 (0.9895)	0.0572 (0.2292)	435.4471 (435.6118)	

**Table 3.1 - Generator's Optimal Power Flow Dispatch (the amounts in parentheses belong to the uncompensated case)**

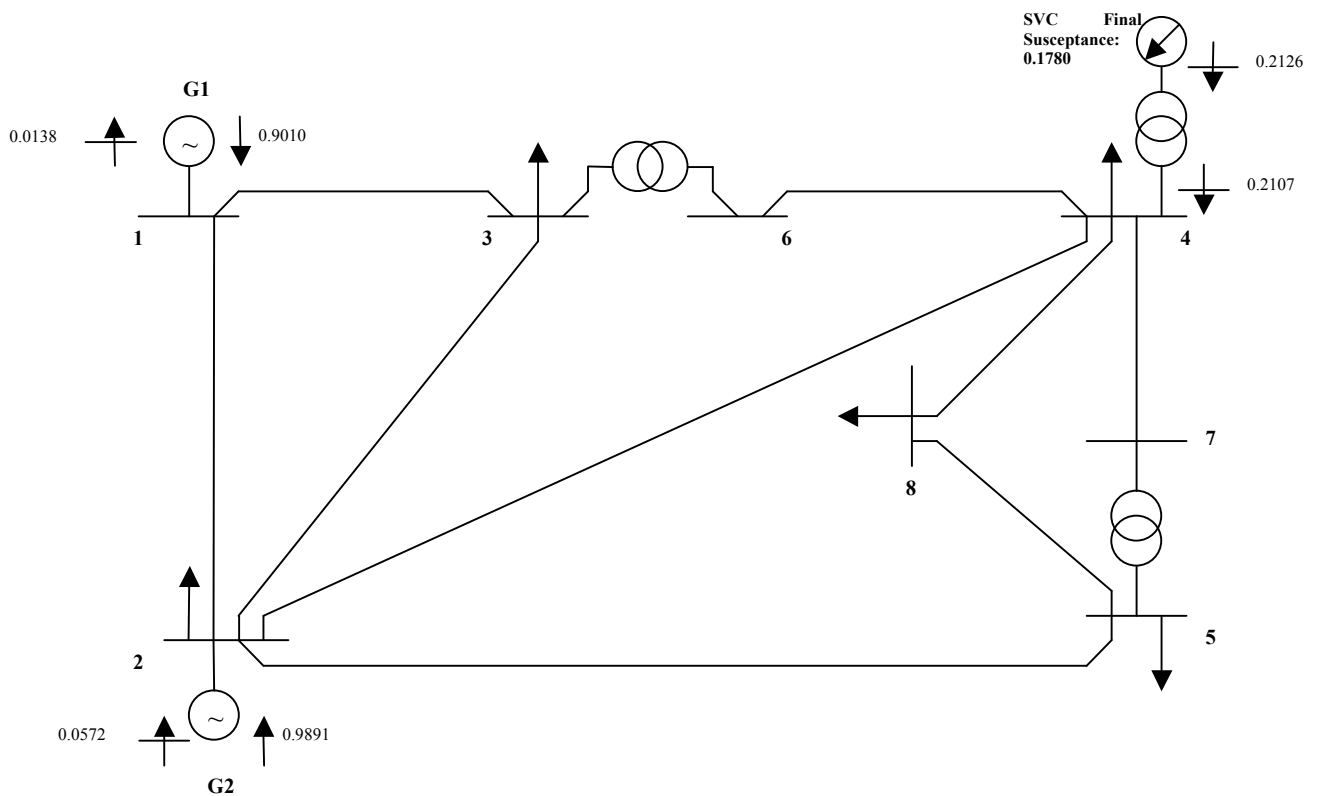


**Figure 3.3 - 8-node System OPF Solution (SVC Case One)**

Transformer No.	Sending End (p.u.)		Receiving End (p.u.)	
	$P_s$	$Q_s$	$P_r$	$Q_r$
1	+0.2005	-0.0746	-0.2005	+0.0766
2	-0.0447	-0.0632	+0.0447	+0.0634

**Table 3.2 - Calculated Transformer Powers (at optimum)**

Bus No.	1	2	3	4	5	6	7	8
Multiplier	4.12	4.19	4.33	4.35	4.37	4.33	4.37	4.39
\$/hr								

Table 3.3 - Incremental Generation Costs

SVC No.	Reactive Power (per unit)	Variable Shunt Susceptance (per unit)
1	0.2126 (capacitive)	0.1780

Table 3.4 - SVC Operation (Case One)

- Results Discussion:

As seen in chart (3.1) the overall voltage profile of the system compared to the uncompensated case in chapter two, has increased particularly in node 4 where the SVC is connected. The increase in voltage profile is mainly due to SVC's reactive power generation at its point of connection. The voltage magnitude in node 4 has increased from 1.0707 per unit obtained from solving the general OPF problem in previous section to 1.0833 per unit. Table (3.4) shows the amount of reactive power generation by the SVC at the end of the OPF solution process as 21.26 MVARs of capacitive reactive power (21.07 MVARs of which reaches node 4) maintaining a value of 0.1780 per unit for the variable shunt susceptance.

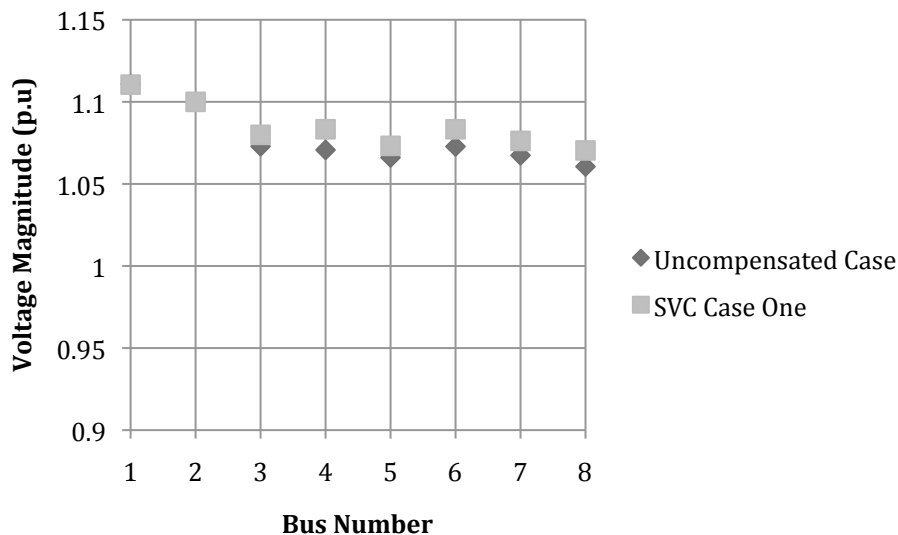


Chart 3.1 - 8-node System Nodal Voltage Comparison (Uncompensated Case vs. SVC Case One)

There is an improvement, albeit strikingly small, in value of the objective function when compared to the results from the uncompensated system solution, which means that the presence of the SVC for improving the

voltage profile has slightly decreased the amount of active power flows in the system and the generators accordingly which then improves the optimum operating point of the system even further. However it should be noted that the operation of the SVC, or any other shunt compensators, have little effect in the amount of active power flow in the system. Unless there is an energy storage facility connected to the shunt compensator the active power exchange between it and the system would be nearly zero per unit. The active power control capability only applies to the shunt controllers that are based on voltage source converters such as the STATCOM. The SVC can provide neither direct reactive nor active power support to its point of connection.

The shunt compensation capability of the SVC OPF model may be better presented in an extreme operating condition where the amount of reactive power demand/excess in node 4 is extremely heavy. To illustrate the robustness of the SVC OPF model in being able of depicting the shunt compensation behaviour properly, the reactive power in bus 4 is permitted to vary between ranges of -45 MVARs (excess in reactive power) to +45 MVARs (demand of reactive power) and subsequently the SVC OPF model is put to test for each case. Table (3.5) illustrates the SVC OPF model behaviour when subjected to a variable reactive power schedule in node 4. As shown in this table, it is clear that the SVC OPF model is capable of maintaining the voltage magnitude within its limit boundaries (0.9 to 1.1 per unit) even if subjected to extreme operating conditions where lack or heavy usage of reactive power is noticeable in the system. The solutions obtained by the OPF algorithm must agree with the KKT optimality conditions and therefore must maintain the constraints within their corresponding limits.

Reactive Power Demand/Excess	$V_4$ (p.u)	$Q_{SVC}$ (p.u)	$B_{SVC}$ (p.u)	$\sum_i f_i$ (\$/hr)
-45 MVARs	1.0841	0.2729 (inductive)	-0.2377	834.2716
-15 MVARs	1.0841	0.0239 (inductive)	-0.0203	834.2716
Zero MVARs	1.0841	0.1752 (capacitive)	+0.1469	834.2716
+15 MVARs	1.0833	0.3150 (capacitive)	+0.2615	834.2730
+45 MVARs	1.0834	0.6274 (capacitive)	+0.5077	834.2729

**Table 3.5 - SVC Model Reactive Compensation Capability in OPF**

The KKT conditions set by the OPF algorithm ensure that the SVC always operates within its linear boundaries ( $-0.75 \leq B_{SVC} \leq +0.75$  per unit), which in turn is enforced to represent the operating limits of the SVC used in this simulation. The SVC shunt susceptance is initialised at an arbitrary value (in this simulation it is  $B_{SVC}^{ini} = 0.5$  per unit). If the network operation is so extreme that the SVC shunt susceptance is violated, the OPF then discards the given solution as being not feasible under realistic steady state operation. This behaviour again shows the strong robustness of OPF algorithm in depicting network's realistic conditions via utilising operating constraints. As seen in table (3.5), in extreme cases of reactive power excess (-45 and -15 MVARs), the SVC model is actually consuming excess amounts of reactive power in order to prevent any over-voltages. Such situations can properly model undesirable circumstances such as load rejection or open end lines in which extreme amounts of excess reactive power would bring about over-voltages in the system. The purpose of applying SVC OPF model is therefore to determine the conditions of operation by which the system not only maintains stability but also operates at an optimum level. If the above reactive power conditions happen in the system without the operation of the SVC, the voltage profile obviously deviates more severely which may bring the system's nodal voltage profile dangerously close to its limits and consequently bring about system voltage collapse. The extreme voltage variations due to the changing nature of the reactive power demand in bus 4 are shown in table (3.6).

Reactive Power Demand/Excess	$V_4$ (p.u)	$\sum_i f_i$ (\$/hr)
-45 MVARs	<b>1.1000</b>	<b>896.740</b>
-15 MVARs	1.0826	834.279
Zero MVARs	1.0737	834.486
+15 MVARs	1.0646	835.027
+45 MVARs	1.0458	837.171

**Table 3.6 - Voltage Magnitude Variations at the presence of no SVC**

The more reactive power changes, the more it affects the nodal voltage at bus 4, which is more remarkable at either ends of the reactive power range. If the variation in reactive power perpetuates, the voltage magnitude in node

4 eventually goes over the limits (as it is the case in -45MVARs range where the OPF algorithm enforced the nodal voltage magnitude in node 4 to its upper limit, namely 1.1 per unit). Table (3.6) clearly illustrates the crucial role the SVC as a shunt reactive controller plays in maintaining a fixed voltage profile in the 8-node system.

## 2. Case Two

In this scenario, the SVC is set to control the voltage magnitude at node 4 to be always 1.1 per unit whatever the system conditions may be. The voltage regulation feature of SVC is represented in the OPF algorithm as a variable equality constraint on nodal voltage at bus 4 as depicted in equation (3.12). As mentioned in chapter two, the equality constraints (variable and functional) are used in the OPF for the purpose of representing equipment control facilities used in the system. In case of a shunt compensator capable of voltage regulation, the nodal voltage at the compensated bus becomes another equality constraint that needs to be added to the set of constraints. The voltage is then enforced to its pre-determined value via the use of a quadratic penalty function similar to the one introduced in chapter two. The penalty function contains the penalty factor, which is a typically large number. By adding the first and second order derivatives of the penalty function defined for the nodal voltage magnitude in node 4, to the corresponding Hessian/Jacobian terms in the system of linear equations, the algorithm essentially enforces the nodal voltage magnitude in node 4 to a pre-determined value, namely 1.1 per unit (See control of system operation in chapter two). The OPF algorithm is then run to obtain results reflecting this new condition. Tables (3.7 – 3.10) illustrate the results by the OPF algorithm while the SVC is controlling the voltage at bus 4. It should be noted that in this scenario the reactive power demand is taken to be 5 MVARs, namely the default reactive power conditions at bus 4. The OPF is converged in four iterations; the solution is shown in figure (3.4).

Generator No.	Active Power Dispatch (p.u.)	Reactive Powers (p.u.)	Optimal Cost of Generation \$/hr	Optimal Value of Total Generation
1	0.9028	-0.0218	399.5602	834.7574 \$/hr
2	0.9886	-0.2152	435.1970	

Table 3.7 - Generators Optimal Power Flow Dispatch (SVC Regulating Voltage)

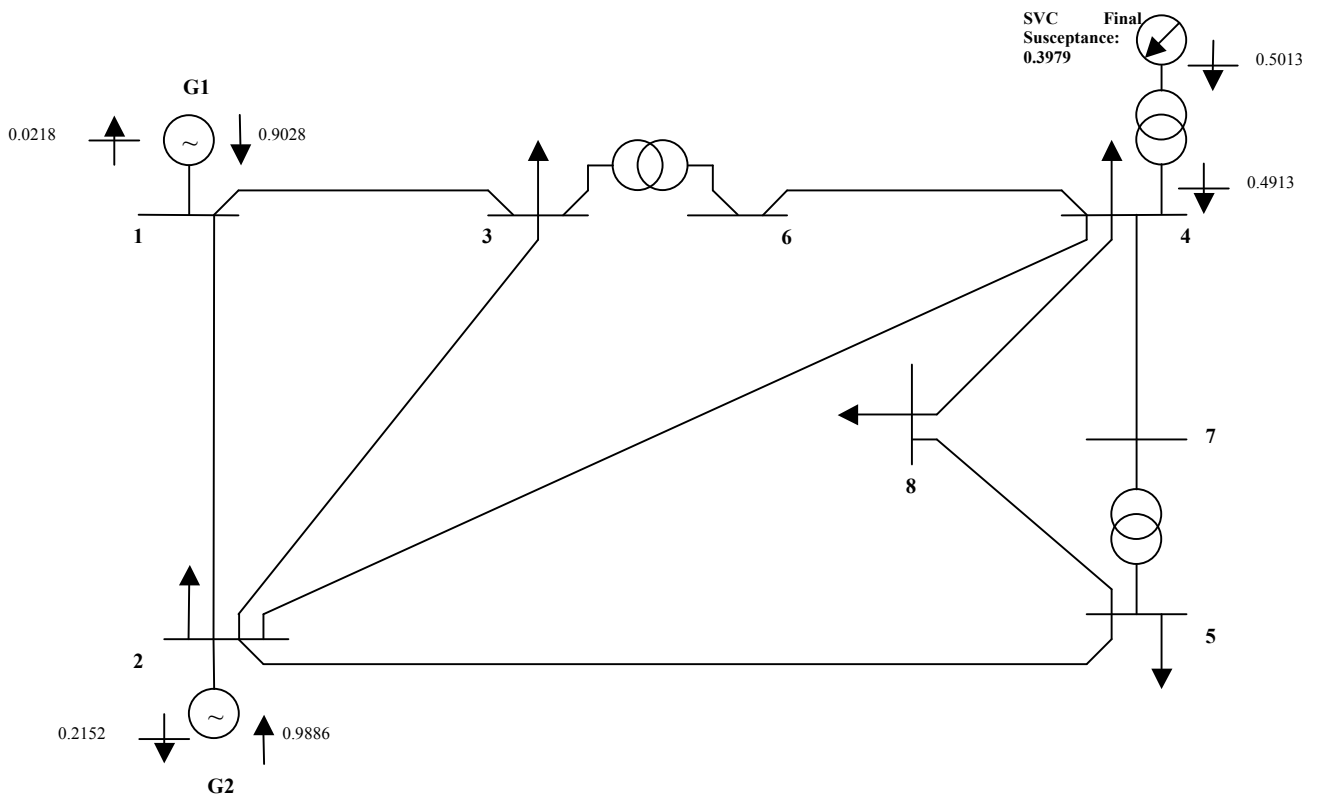


Figure 3.4 - 8-node System OPF Solution (SVC Case Two)

Transformer No.	Sending End (p.u.)		Receiving End (p.u.)	
	$P_s$	$Q_s$	$P_r$	$Q_r$
1	+0.2062	-0.1708	-0.2062	+0.1738
2	-0.0437	-0.1106	+0.0437	+0.1112

Table 3.8 - Calculated Transformer Powers (at optimum)

Bus No.	1	2	3	4	5	6	7	8
Multiplier	4.12	4.19	4.34	4.36	4.38	4.34	4.37	4.40
\$/hr								

Table 3.9 - Incremental Generation Costs

SVC No.	Reactive Power (per unit)	Variable Shunt Susceptance (per unit)
1	0.5013 (capacitive)	0.3979

Table 3.10 - SVC Operation (Case Two)

- Results Discussions:

Once again the results obtained here by the OPF algorithm shows how the SVC OPF model is capable of improving the overall voltage profile of the system which consequently has a direct effect on improving system's performance in terms of voltage stability and power quality. The SVC generates 50.13 MVARs of reactive power (49.13 MVARs of which is injected to node 4) to keep the voltage magnitude at node 4 fixed at 1.1 per unit. The voltage regulation capability is modelled as a new variable equality, which is then added to the system of equations through a special penalty function. The system voltage profile compared to Case One has been improved as shown in chart (3.2) below.

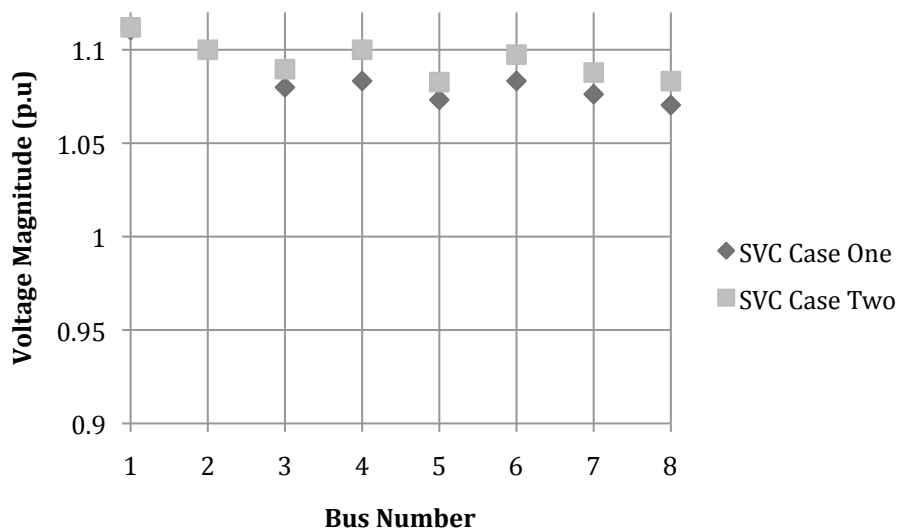


Chart 3.2 - 8-node System Voltage Comparison (SVC Case One vs. SVC Case Two)

### 3. Case Three

In this case scenario the SVC is replaced by a STATCOM at bus 4. The STATCOM OPF voltage source model that is presented previously is used in the algorithm to regulate voltage at bus 4. Since the STATCOM model represents connecting impedance, there is no need for an additional connecting transformer as it was the case with the SVC model. It should be noted that for the purposes of simulation the STATCOM converter's impedance is taken to be 0.05 per unit.

The STATCOM voltage regulation feature is once again added as a variable equality with appropriate corresponding penalty function to enforce its magnitude to the pre-determined value of 1.1 per unit. Assuming the same initial conditions for the 8-node system, as well as the same objective function presented in chapter two, the OPF is run for the STATCOM model, which again converged after four iterations. It has been immediately observed that when in voltage control mode, STATCOM produces the exact same results as for the SVC, illustrated in tables (3.7 – 3.10), which indicates that as long as STATCOM and SVC are working within their limits, their voltage regulation features have similar effects on the operation of the network as given by the OPF results, despite the difference in their methods of modelling.

The STATCOM converter is injecting 50.13 MVARs of reactive power, 49.13 MVARs of which are consumed by node 4 to keep the voltage fixed at 1.1 per unit.

The STATCOM OPF model however, can be re-configured to provide active power compensation to the system. In order to study the potential applications of VSC-based controllers in a real power system, it is assumed that STATCOM's converter is used as a means to connect an energy storage device to bus 4.

In order to add active power flow control capability to the STATCOM OPF model, it is only necessary to add a new functional constraint to STATCOM Lagrangian in equation (3.9) in form of equation (3.14) as such:

$$L_{P_{conv}} = \lambda_{P_{conv}} (P_{conv} - P_{specified}) \quad 3.14$$

The active power regulation might indicate the presence of energy storage devices connected to STATCOM's converter as well. Once again assuming same initial conditions and knowing that STATCOM is set to inject 10 MWs of active power, the following results are obtained:

The OPF is converged in three iterations with the following results:

Generator No.	Active Power Dispatch (p.u.)	Reactive Powers (p.u.)	Optimal Cost of Generation \$/hr	Optimal Value of Total Generation
1	0.8529	-0.0262	379.0879	791.4470 \$/hr
2	0.9338	-0.1926	412.3590	

**Table 3.11 - Generators Optimal Power Flow Dispatch**

Transformer No.	Sending End (p.u.)		Receiving End (p.u.)	
	$P_s$	$Q_s$	$P_r$	$Q_r$
1	+0.1675	-0.1622	-0.1675	+0.1645
2	-0.0600	-0.1056	+0.0600	+0.1063

**Table 3.12 - Calculated Transformers Powers (at optimum)**

Bus No.	1	2	3	4	5	6	7	8
Multiplier \$/hr	4.08	4.15	4.28	4.30	4.32	4.29	4.32	4.34

**Table 3.13 - Incremental Generation Costs**

STATCOM No.	Converter's Reactive Power (per unit)	Injected Reactive Power at node 4
1	+0.4675	-0.4584

**Table 3.14 - STATCOM Operation at optimum (Voltage Regulation Mode)**

The goal of this exercise was to indicate the effects of local active power regulation on system's total performance. The optimal power flow solution has also been shown in figure (3.5). It is also observed that by utilising STATCOM's voltage source converter, the system provides 10MWs of active power at bus 4 locally, which decreases the system total active generation resulting in a significant drop in the final value of the objective function to 791.4 \$/hr from 834.7 \$/hr in previous scenarios. Since the STATCOM's active power exchange with the system has little influence in the voltage variations occurring in the system and particularly at node 4, the system's voltage profile remains the same as before.

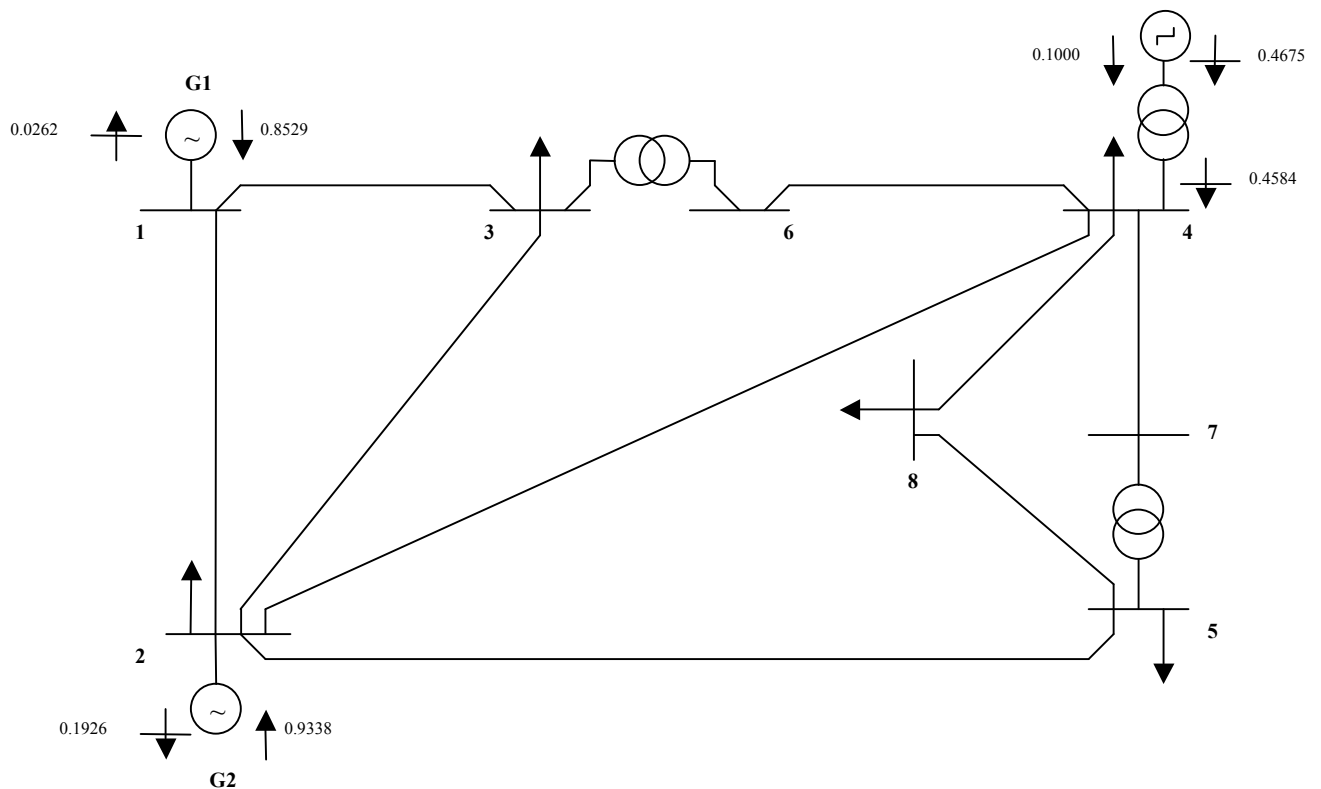
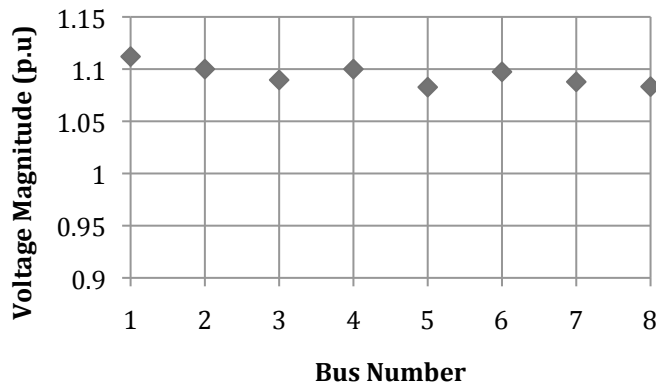


Figure 3.5 - 8-node System OPF Solution with STATCOM in place of SVC

The system's voltage profile for the SVC and STATCOM cases while regulating voltage at node 4 to 1.1 per unit has been presented in chart (3.3). It is clearly observed that both controllers follow the same pattern in regulating the voltage, which is what initially was expected.



**Chart 3.3 - STATCOM Model vs. SVC Model Voltage Regulation Modes produce the exact same results**

It proves from the last simulation scenario that the presence of STATCOM is advantageous to the SVC since STATCOM's connecting converter can provide both active and reactive power to its point of connection should the need arise and the possible facilities are available (for example if the converter is connected to a micro-generator). This very fact shows one of the most important benefits of using converter based FACTS devices instead of more conventional variable impedance types [4].

The voltage source converter power control characteristics are investigated more thoroughly in next two chapters where a new and advanced model for VSC is described. It is clearly shown here that using VSC based FACTS such as STATCOM has the benefit of providing a smoother and more comprehensive control capability to the system whereby the system's reliability is improved even further [1]. As it is shown in this simulation providing local active power regulation is seamlessly realised through connecting local sources of energy via VSCs. In next chapters the VSC-HVDC links suitable for such interconnections are thoroughly investigated and the appropriate OPF models are developed and tested. In the next section the STATCOM controllable voltage source model is applied to the IEEE 30-node system to illustrate its operational characteristics in dealing with a realistic power system configuration.

### **3.4.2 Compensated IEEE 30-node System**

The IEEE 30-node system was introduced in previous chapter. It is shown from the system data (both in chapter two and Appendix II) that the IEEE 30-node system possesses two shunt compensators in nodes 10 and 24. The general OPF simulation

carried out in chapter two regarded these shunt compensators as fixed capacitors, with shunt susceptance values of 0.19 and 0.043 per unit respectively. However, for the purposes of simulation here, the shunt compensator in node 24 is replaced with a fully functional STATCOM voltage source model.

The STATCOM is allowed to operate freely within the permitted nodal voltage range of 0.9-1.05 per unit and the OPF is run, which has converged in 9 iterations. There have been voltage magnitude violations in nodes 9, 10 and 12, in which the OPF has successfully bounded the violated voltage magnitude to its upper limit, namely 1.05 per unit, using the quadratic penalty function.

Furthermore, in another run, the STATCOM is tasked with maintaining the voltage magnitude at node 24 to 1.00 per unit, which is done by introducing a new variable equality constraint for voltage magnitude in node 24 in the OPF formulation. As there have been no violations in the amounts of voltages in the system, the OPF converges in three iterations this time. It is observed that by varying the voltage between 0.095-1.05 the STATCOM effectively manages to maintain the voltage and prevent a collapse. The results for the STATCOM simulation in the 30-node system have been presented in table (3.15) below:

Bus No.	Target Voltage (p.u.)	Obtained Voltage (p.u.)	STATCOM's converter's voltage (p.u.)	Converter's reactive power (p.u.)	Calculated injected reactive power (p.u.)	SVC's injected reactive power (p.u.)
24	$0.9 \leq V_{24} \leq 1.05$	1.0356	1.0406	0.1029 (capacitive)	0.1024 (capacitive)	0.1022 (capacitive)
24	$V_{24} = 1.00$	1.000	1.0022	0.0446 (capacitive)	0.0445 (capacitive)	0.0446 (capacitive)

**Table 3.15 - STATCOM and SVC Comparison in IEEE 30-node System (Compensation at node 24)**

In both cases the results for simulating the same configuration with the SVC is also given for comparison (note that in this case scenario the SVC variable impedance model is directly connected to node 24 and is not behind a connecting transformer). As it is seen from the table, the SVC produces the exact same results which again stresses the fact that both devices provide the same compensation capability within their operating range albeit they are completely different in terms of operation and modelling [1].

The STATCOM can also be configured to control reactive power at the point of connection. In another test run for the 30-node system, the STATCOM is controlling the reactive power at node 24 to be exactly 0.1 per unit and the OPF is run once more. According to the STATCOM modelling criteria presented in section (3.3.1), the reactive power control is modelled as a functional constraint in the form of equation (3.3), which in turn deactivates equation voltage control in equation (3.4). As a result, the nodal voltage magnitude in node 24 is no longer penalised whereas the STATCOM reactive power constraint is added to the system Lagrangian throughout the solution process.

The OPF is run and the following results are obtained after seven iterations:

<b>Bus No.</b>	<b>Target Converter's Reactive Power (p.u.)</b>	<b>Obtained Voltage (p.u.)</b>	<b>STATCOM's converter's voltage (p.u.)</b>	<b>Converter's reactive power (p.u.)</b>	<b>Calculated injected reactive power (p.u.)</b>
24	0.1000	1.0354	1.0402	0.1000 (capacitive)	0.0995 (capacitive)

**Table 3.16 - STATCOM controlling reactive power at node 24**

For the purpose of controlling the reactive power of the converter, the last rows and columns pertaining the STATCOM's functional equality constraint on its reactive power must be included in the system of linear equations as depicted in equation (3.10). As before, the influence of the exact penalty function is conspicuous in dealing with voltage violations in nodes 9, 10 and 12 all of which are effectively bounded by the OPF algorithm to their upper limits of 1.05 per unit. As seen from table (3.16), the STATCOM model this time fixes the amount of reactive power its converter is producing to 0.1 per unit effectively freeing the system voltage, however both converter's reactive power and the system voltage must be within their limits otherwise the algorithm may reject the solution as it may not satisfy the KKT optimality conditions. The results presented in table (3.16) resemble to a great deal to those obtained in table (3.15) when STATCOM is not regulating the voltage, which means that the STATCOM model's effect on nodal voltage is closely interrelated with its reactive power control capability. It is therefore imperative that the nodal voltage be freed to take up a value depending on the value of the reactive power, which is set by the user; otherwise the STATCOM's voltage source

representation will not produce accurate results. In both cases the objective function takes the minimum value of approximately 967\$ per hour of fuel consumption.

### 3.5 Conclusions

The OPF models for two types of the most important shunt controllers have been developed and presented in this chapter. The SVC-OPF model as mentioned in [10] is modelled as a variable shunt susceptance within its boundary region for realistic results. The STATCOM, on the other hand, is modelled as a shunt power injection to its point of connection. The STATCOM's converter's power is a function of its voltage and comprises its exclusive functional equality constraint. However, the STATCOM can also be configured to directly regulate nodal voltage magnitude at its point of compensation in which case there is no need for an additional functional equality constraint, even though an additional variable constraint on the compensated nodal voltage magnitude is necessary. Because the STATCOM's converter reactive power as well as the nodal injected reactive power is a function of the nodal voltage magnitude of the compensated bus, they are closely interrelated and therefore they cannot be activated in conjunction with each other. The STATCOM, unlike the SVC, is modelled as a controllable voltage source in its entire region of operation. The model developed here for the STATCOM is the simplest form of power injection model for a shunt VSC-based controller. It effectively represents the operation of the voltage source converter in form of a controllable voltage/power source. It should be noted that this model, although effective, lacks some fundamental features, mostly it does not model the internal switching losses of the VSC and takes no account of the PWM control of the converter. For these reasons a new model is developed for the VSC as the building block of almost all modern switching converter type FACTS controllers, including the STATCOM, which can then be used to model both STATCOM and SSSC as well as VSC-HVDC systems. This model, dubbed the compound transformer model is introduced in the next chapter. The OPF models developed in this chapter and subsequent chapters are for steady-state operation only.

### 3.6 References

- [1] Hingorani, G. N., Gyungyi, L., *Understanding FACTS: Concepts and Technologies of Flexible AC Transmission Systems*: IEEE, 2000.

- [2] Acha, E., Agelidis, V. G., Anaya-Lara, O., Miller, T. J. E., *Power Electronic Control in Electrical Systems*: Newnes, 2002.
- [3] Krug, D., Bernet, S., Dieckerhoff, S., "Comparison of state-of-the-art voltage source converter topologies for medium voltage applications," in *Industry Applications Conference, 2003. 38th IAS Annual Meeting. Conference Records of the*, 2003, pp. 168-175.
- [4] Zhang, X., Handshcin, E. J., "Optimal Power Flow Control By Converter Based FACTS Controllers," presented at the AC-DC Power Transmission, 2001. Seventh International Conference on, 2001.
- [5] Acha, E., Fuerte-Esquivel, C. R., Ambriz-Perez, H., Angeles-Camacho, C., *FACTS Modelling and Simulation in Power Networks*: John Wiley & Sons Ltd., 2005.
- [6] Qingguang, Y., Li, P., Liu, W., Xie, X., "Overview of STATCOM Technologies," presented at the Electric Utility Deregulation, Restructuring and Power Technologies, 2004.
- [7] Angeles-Camacho, C., Tortelli, O. L., Acha, E., Fuerte-Esquivel, C. R., "Inclusion of a High Voltage DC-Voltage Source Converter Model in a Newton-Raphson Power Flow Algorithm," *Generation, Transmission and Distribution, IEE Proceedings*, vol. 150, pp. 691-696, Nov. 2003.
- [8] Glanzmann, G., Andersson, G., "Using FACTS devices to resolve congestions in transmission grids," *CIGRE/IEEE PES, 2005. International Symposium*, pp. 347-354, 7 Oct 2005 2005.
- [9] Wong, K. T. G., "The role of static VAR compensators in staving off voltage collapse," *Voltage Collapse (Digenst No: 1997/101)*, *IEE Colloquium on*, pp. 5/1-5/5, 24 April 1997 1997.
- [10] Ambriz-Perez, H., Acha, E., Fuerte-Esquivel, C. R., "Advanced SVC Models for Newton-Raphson Load Flow and Newton Optimal Power Flow Studies," *Power Systems, IEEE Transactions on*, vol. 15, pp. 129-136, 2000.
- [11] Lockley B., P. G. (2002, Mar/Apr 2002) Static VAR Compensators: A Solution to the Big Motor/Weak System Problem? *IEEE Industry Applications*. 43-49.
- [12] Ou, Y., Singh, C., "Improvement of Total Transfer Capability Using TCSC and SVC," *Power Engineering Society General Meeting, 2001. IEEE*, vol. 2, pp. 975-947, July 25 2002.
- [13] Huang, G. M., Ping Yan, "TCSC and SVC as re-dispatch tools for congestion management and TTC improvement," presented at the Power Engineering Society Winter Meeting, 2002. IEEE, 2002.
- [14] Fuerte-Esquivel, C. R., Acha, E., Ambriz-Perez. H. , "A Thyristor Controlled Series Compensator Model for the Power Flow Solution of Practical Power Networks," *Power Systems, IEEE Transactions on*, vol. 15, pp. 58-64, 2000.
- [15] Mahajan, V., "Thyristor Controlled Series Compensator," in *Industrial Technology, 2006. ICIT 2006. IEEE International Conference on*, 2006, pp. 182-187.
- [16] Zhang, Y., Zhang, Y., Wu, B., Zhou, J., "Power injection model of STATCOM with control and operating limit for power flow and voltage stability analysis," *Electric Power Systems Research*, vol. 76, pp. 1003-1010, August 2006.

- [17] Gyugi, L., "Unified power-flow control concept for flexible AC transmission systems," in *Generation, Transmission and Distribution, IEE Proceedings C*, 1992, pp. 323-331.
- [18] Hong, Y.-Y., Liao, C.-M., Lu, T.-G., "Application of Newton optimal power flow to assessment of VAR control sequences on voltage security: case studies for a practical power system," in *Generation, Transmission and Distribution, IEE Proceedings C*, 1993, pp. 539-544.
- [19] Noroozian, M., Angquist, L., Ghandhari, M., Andersson, G., "Use of UPFC for Optimal Power Flow Control," *Power Delivery, IEEE Transactions on*, vol. 12, pp. 1629-1934, October 1997.
- [20] Pizano-Martinez, A., Fuerte-Esquivel C. R., Ambriz-Perez, H., Acha, E., "Modeling of VSC-Based HVDC Systems for a Newton-Raphson OPF Algorithm," *Power Systems, IEEE Transactions on*, vol. 22, pp. 1794-1803, Nov. 2007.
- [21] Diaz, U. A. R., Hernandez, J.H.T., "Reactive Shunt Compensation Planning by Optimal Power Flows and Linear Sensitivities," presented at the Electronics, Robotics and Automotive Mechanics Conference, 2009. CERMA '09, 2009.
- [22] Gotham, D. J., Heydt, G. T., "Power flow control and power flow studies for systems with FACTS devices," *Power Systems, IEEE Transactions on*, vol. 13, pp. 60-65, Feb. 1998.
- [23] Gengyin, L., Ming, Z., Jie, H., Guangkai, L., Haifeng, L., "Power Flow Calculation of Power Systems Incorporating VSC-HVDC," *Power System Technology, International Conference on*, pp. 1562-1566, Nov. 21-24 2004.
- [24] Nabavi-Niaki, A., Iravani, M. R., "Steady-State And Dynamic Models of Unified Power Flow Controller (UPFC) For Power System Studies," *Power Systems, IEEE Transactions on*, vol. 11, pp. 1937-1943, November 1996.
- [25] Noroozian, M., Petersson, A. N., Thorvaldson, B., Nilsson, B. A., Taylor, C. W., "Benefits of SVC and STATCOM for Electric Utility Application," presented at the Transmission and Distribution Conference and Exposition, IEEE PES, 2003.

## **4 Advanced Voltage Source Converter Model in Optimal Power Flow algorithm using the Compound Transformer Concept**

In this chapter, the principles of modelling the power converters, particularly the fully controlled self-commutated Voltage Source Converter (VSC), in the Optimal Power Flow algorithm using Newton's method for augmented Lagrangian function, has been explained. The new power injection modelling method uses an advanced concept called the Compound Transformer Model whereby the VSC is effectively modelled as a transformer with controllable variable complex tap ratio. Mathematically, it has been shown that the Pulse Width Modulation (PWM) attributes for controlling a voltage source converter can properly be represented by the operation of the compound transformer's complex tap ratio. Therefore, the compound transformer has been introduced as a suitable, more accurate mathematical platform to describe the operation of the VSC and VSC-based systems for the purposes of optimal power flow analysis. Accordingly, a new set of nodal active and reactive power injections for the VSC operation in the network in the form of a compound transformer has been developed and presented. The new modelling approach is advantageous over the conventional controllable voltage source models since it explicitly includes the control capabilities of the VSC in the form of state variables in the OPF mathematical formulation. Two categories of simulations follow the mathematical formulation of the new compound transformer model. In the first set of simulations the compound transformer has been tested as a stand-alone device and several OPF simulations have been carried out to verify its robustness in controlling power system parameters, namely voltage and active power in both ends of the transformer. In the second set, its operation as a voltage source converter feeding a DC load has been tested and verified. The DC active power regulation is achieved via the phase angle compensation of the compound transformer's variable phase shifter. The latter set of simulations is crucial for further High Voltage Direct Current Transmission system models based on VSCs (VSC-HVDC) presented in the next chapter. It has been shown that the VSC compound transformer model concept is a major improvement over the previous controllable voltage source modelling approach. It yields a more realistic and elaborate description of the operation of the actual voltage source converters in power system applications.

## 4.1 Introduction

Power converters have been playing a decisive role in modern power system configurations for decades now. They are essentially used to convert DC power to AC power in a power network in order to meet certain operating conditions, for instance, synchronising autonomous AC grids with each other or transferring bulk amounts of active power over longer distances, where the active power transfer capacity is severely impaired due to the operational restrictions of a typical High Voltage AC Transmission (HVAC) line [1, 2]. However, with the advancements in the power electronics technologies and the emergence of renewable sources of energy (for instance Wind and Solar Power), which are more susceptible to voltage and frequency deviations and affect the overall power quality of the system, the need for reliable operation of the power system free from voltage imbalances and other dynamic issues seems obvious. Sensitive industrial loads such as induction machines that require a constant source of reactive power compensation as well as loads that operate in variable frequency and voltage ranges all exert undesired effects on the steady state operation of the network decreasing its reliability and power quality [3]. Unfortunately, conventional power converters that are based on semi-controlled semi-conductors such as thyristors, require line-commutation and therefore provide limited controllability and flexibility in adopting more advanced power network configurations, for instance in connecting variable speed induction machines to the AC grid [3]. On the other hand, relative simplicity in control strategies applied to newer breed of power electronics devices such as IGBTs or GTOs have led to the introduction of fully controlled self-commutated power converters whereby the output voltage waveform is controlled in both phase angle and magnitude using flexible switching schemes such as Pulse Width Modulation (PWM) [2, 4, 5]. These converters in turn have been used in many applications ranging from fast and reliable interconnection of remotely located distributed generation sources to the power grid to synchronising autonomous AC grids with each other in High Voltage Direct Current transmission systems [6, 7]. Furthermore, almost all of the modern FACTS controllers, namely the switching converter type FACTS controllers such as the STATCOM or UPFC are based on self-commutated voltage source converters that provide fast and reliable voltage/power control for the system [8].

There are generally two categories of power converters, regardless of the type of power electronics device (fully or semi controlled) used in them and only with respect to the type of their DC source [2]. They can be configured as either Voltage Source Converters (VSC) or Current Source Converters (CSC). Self-commutated converters can operate as both CSCs and VSCs, whereas the line-commutated converters can only operate as CSCs [2, 8]. The two categories of power converters are shown in figures (4.1) and (4.2) respectively [8].

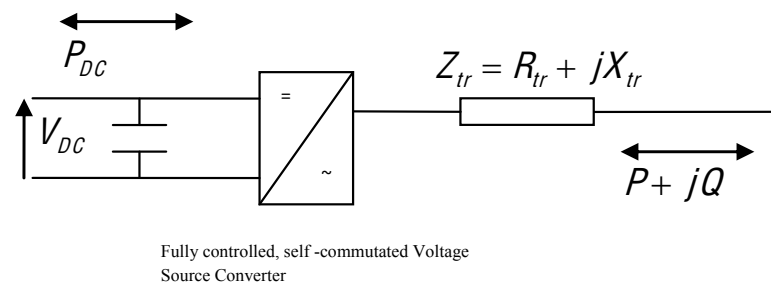


Figure 4.1 - Voltage Source Converter - Fully Controlled Self Commutated Converter

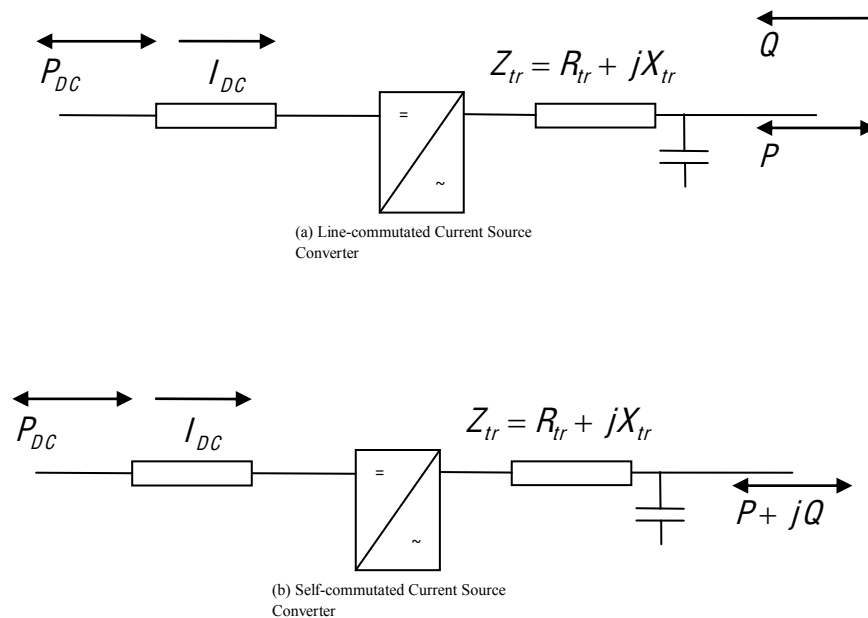


Figure 4.2 - Current Source Converter - (a) Fully Controlled Line Commutated Converter (b) Fully Controlled Self Commutated Converter

As it is seen in figure (4.1), the VSC possesses a DC voltage source (typically a large/medium capacitor) whose voltage polarity in the DC side never changes and therefore the direction of the power flow to and from the converter is controlled by changing the direction of the DC current [2, 8]. It should be noted that the bi-directional DC current in a VSC requires adding anti-parallel diodes to the fully controlled semi-conductor used for conversion (either GTOs or IGBTs in most recently made converters) to provide a return path for the current from the AC side to the DC side to realise rectification [8, 9]. As a result, all practical voltage source converter topologies include valves with a fully controlled semi-conductor (GTO or IGBT) coupled with anti-parallel diodes [10]. By contrast, in a CSC the DC current has only one direction and it is the changing in the DC voltage polarity that governs the direction of the power flow to and from the converter [2, 8]. Conventional line-commutated converters utilise thyristors, which have both forward and reverse voltage blocking capabilities [8].

The VSCs are more flexible and introduce better controllability in the system than the CSCs since they utilise fully controlled power electronics and therefore are self-commutated [4, 9]. As it is seen from figure (4.1), the VSC provides bi-directional active and reactive power in the AC side as well as bi-directional active power in the DC side [2]. As a result, the VSCs operate in all four quadrants of the P-Q plane [2, 3]. In comparison, if a CSC is based on semi controlled power electronics (for instance thyristors), then it requires reactive power from the AC side to achieve commutation and therefore is incapable of operating in four quadrants of the P-Q plane and it can only operate in two quadrants (consuming reactive power) [8]. If a CSC is based on fully controlled power electronics devices, it can too provide bi-directional active and reactive power on the AC side, however most bi-directional self-commutated converters are VSCs.

Fully controlled self-commutated voltage source converters constitute a major part of this research and therefore their associated operational principles followed by their potential applications in modern power systems are adequately explained further in this section. The CSC operation and applications are therefore out of the scope of this project and will not be mentioned here any further.

In a voltage source converter, the active and reactive powers between the converter and the AC system are controlled by altering the phase angle and voltage magnitude of the converter's voltage against the AC system voltage using PWM for switching fully-controlled semi-conductors (for example IGBTs) [4, 11-13]. Unlike conventional line-commutated converters, in a PWM-controlled voltage source converter both active and reactive power flows between the converter and the AC system are regulated independently, which results in improving system reliability and delivered power quality [2, 3, 5, 8, 11, 13, 14].

In an actual PWM-controlled voltage source converter, the active power flow as well as its direction is controlled by regulating the incurred phase angle difference between the converter's output voltage and the AC system voltage [3, 8, 11-13]. Moreover, the voltage magnitude is also controlled in a PWM-controlled VSC by changing the amplitude modulation index of the converter [2, 8, 12-14]. On the other hand, the VSC controls the reactive power through controlling the converter voltage magnitude (up to its capacitive rating) against the AC system voltage much like a synchronous condenser [4, 8, 12, 14, 15]. If the converter voltage output is bigger than the AC system voltage, the converter then supplies reactive power to the system and vice versa [11, 12]. The seamless reactive power controllability in voltage source converters makes them ideal for interconnecting to weaker systems stronger ones without the need for additional reactive power compensators.

Since the VSC provides both active and reactive power flows to the system it is appropriate to assume that from the power system perspective, the voltage source converter is seen as an ideal voltage source, for instance a synchronous condenser, behind coupling impedance (or reactance) [4]. In fact, the voltage source converters have been modelled as controllable voltage sources (hence active and reactive power injections) almost in every power flow study scenario [4, 5, 9, 11, 13, 14, 16, 17].

However, in this project an alternative path for modelling the VSC in power flow studies, more specifically in optimal power flow analysis, has been chosen, which is not based on ideal controllable voltage sources.

Considering the fact that the instantaneous power has to remain equal between AC and DC sides of an actual voltage source converter [8], then a voltage source converter can validly be thought of as an ideal transformer behind coupling impedance. The transformer, dubbed the compound transformer, is a relatively new concept in modelling power converters and has certainly never been used to model a VSC before. The concept stems from the fact that introducing a variable phase shifter angle and assuming a variable transformer ratio control the voltage phasors in either sides of this “compound device” in both phase angle and magnitude just like a real voltage source converter. Subsequently, the nodal active and reactive powers are controlled in a compound transformer exactly like an actual voltage source converter. Essentially, the rectifier or inverter operation of the voltage source converter is chosen based on the direction of the nodal power injections for the compound transformer model.

In this chapter, a comprehensive analysis has been carried out for the new compound transformer model and it has been shown that this new modelling criterion is capable of portraying the most accurate and elaborate representation of the operational principles of a real voltage source converter. It will also be mentioned later that modelling the operation of an actual VSC as a compound transformer has an important mathematical advantage over the conventional controllable voltage source models, since it explicitly includes the effects of PWM control characteristics of the converter into the OPF formulation.

## 4.2 Compound Transformer Concept

The compound transformer shown in figure (4.3a), in itself is a special kind of electronically controlled FACTS device, which possesses the capabilities of an On-Load Tap Changer (OLTC) and an electronically controlled Phase Shifting Transformer (PST) simultaneously [18]. It is observed that such a device is capable of providing the means to control network’s fundamental parameters, namely active power flow and voltage magnitude in sending and receiving ends.

The phase shifter facility in the compound transformer, essentially resembles the operation of a Phase Angle Regulator (PAR), which provides phase angle compensation with the amount of  $\pm\varphi_{ps}$  by injecting a controllable series voltage

with adjustable phase angle and magnitude, namely,  $V^{inj} \angle \alpha^{inj} = |\pm V^{inj}| e^{\pm j\alpha^{inj}}$  to the line [8, 18, 19]. Ultimately, the phase angle regulator in the compound transformer model controls the amount of active power across the line by regulating the incurred phase angle difference between the sending and receiving ends of the line,  $\theta_{sr} \pm \varphi_{ps}$  in figure (4.3a) [8, 15, 18, 20, 21]. On the other hand, if the PAR is coupled with an OLTC, then the nodal voltage magnitudes in the line are also controlled directly by a continuous tap magnitude ratio,  $T$ .

Consequently, by combining the controlling facilities of both PAR and OLTC together, the compound transformer can essentially be thought of as an ideal transformer with an incurred continuous variable complex tap ratio with the value of  $m_{ps} = T \angle \pm \varphi_{ps} = |T| e^{\pm j\varphi_{ps}}$  as shown in figure (4.3a) [12, 18, 20].

As seen in figure (4.3b), the complex tap ratio effectively controls the nodal voltages in both magnitude and phase angle, which yields to full control in both nodal active and reactive powers. For consistency purposes, it is assumed that the tap changer facility of the OLTC and subsequently the compound transformer is located at the primary side of the transformer. All the impedance calculations are therefore carried out with reference to the primary side for subsequent models introduced in this chapter and the following chapter.

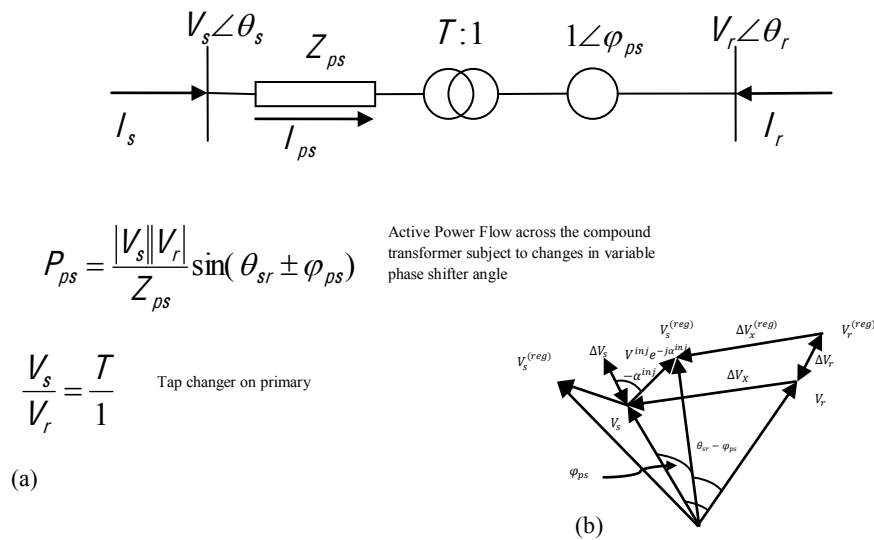


**Figure 4.3 - Compound Transformer - (a) The variable phase shifter ratio models both active power and nodal voltage magnitude controls (b) Phasor diagram for leading operation**

It should be noted that the reactive power in a compound transformer model configuration is regulated indirectly through the nodal voltage magnitude adjustments. Much like a practical OLTC, It is then up to the system to provide necessary reactive power requirements to account for the pre-determined voltage magnitude at the point of control [8]. Consequently, in terms of OPF mathematical formulation, the effects of the OLTC (direct voltage regulation) is formulated as a variable equality constraint on the voltage magnitude at which bus it is set to regulate much like the STATCOM/SVC OPF models presented in chapter three. However, care needs be taken so as not to violate the limits of the tap changer magnitude in the complex tap ratio of the compound transformer. For practical VSC-HVDC OPF modelling the direct voltage regulation capability of the compound transformer will also be subject to the VSC's capacitive ratings.

### **4.3 VSC Compound Transformer Model for Optimal Power Flow Algorithm via Newton's Method**

Considering the operational principles of the compound transformer device introduced in figure (4.3a), it is obvious that it provides an appropriate framework for elaborate modelling of the operating principles of the PWM-controlled voltage source converter using its controllable variable complex tap ratio.

The VSC in power flow analysis is traditionally modelled as a controllable voltage source behind coupling impedance (or reactance), which injects controllable active and reactive power (as functions of its converter voltage) to the AC system [5, 11].

However the conventional power flow modelling approach of the VSC has a fundamental drawback in that it does not model the converter's internal switching losses, which in case of PWM control due to the relative high switching frequency may increase [8]. Furthermore, it ignores the role of PWM control characteristics (phase shifting and line voltage magnitude adjustments) in regulating system parameters [14, 22].

As mentioned in [14], since conventional voltage source converter power injection models do not include the effects of PWM amplitude modulation ratio as well as the switching losses, there is no way of verifying whether these values are within limits

if such models are used for OPF analysis. Therefore, they do not provide accurate grounds for describing the operation of a real voltage source converter for the purposes of optimal power flow analysis.

Unlike the conventional controllable voltage source models proposed in [5, 11, 14] though, the compound transformer model presented in this chapter, takes into account the effects of the PWM control in a VSC in form of a controllable variable complex tap, namely  $m_{ps} = T \angle \varphi_{ps}$ , as shown in figure (4.4a).

On the other hand, as an improvement to the model concept shown in figure (4.3a), the compound transformer used to model the voltage source converters explicitly comprises the converter's internal switching losses as a shunt ohmic resistance in parallel with a shunt susceptance representing the DC capacitor (DC source/sink voltage).

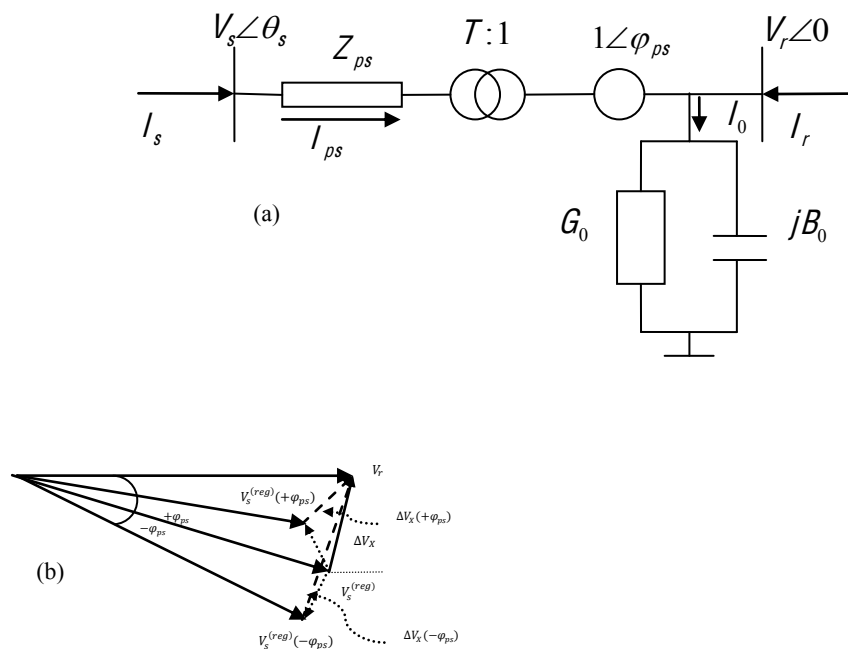


**Figure 4.4 - (a) VSC Compound Transformer Model (b) Phasor diagram for converter's lagging operation and control on primary**

The new model provides common grounds for modelling VSC-based systems such as Unified Power Flow Controller (UPFC), Solid State Synchronous Controller (SSSC) and VSC-HVDC transmission links. Accordingly, the compound transformer model developed in this chapter is used for modelling VSC-HVDC

transmission systems for back-to-back, point-to-point and multi-terminal configurations in next chapter.

The operational principles of the compound transformer model are presented in form of a phasor diagrams in figure (4.4b) for converter's leading operation and basic voltage and power control modes on primary. The power and voltage control on secondary follows the same principles and therefore have not been shown. It should be noted that in figure (4.4b), it has been assumed that the receiving end voltage has zero phase angle. According to figure (4.4a), the compound transformer's active power flow between nodes  $s$  and  $r$  is defined as such (temporarily ignoring the shunt branch):

$$P_{ps} = \frac{|V_s||V_r|}{Z_{ps}} \sin(\theta_s - \theta_r \pm \varphi_{ps}) \quad 4.1$$

In which the following relationship between the sending and receiving voltages apply:

$$|V_s| = T|V_r| \quad 4.2$$

Equation (4.1) essentially states that in the compound transformer, the active power flow is regulated, by varying the controllable phase shift  $\varphi_{ps}$  to obtain the required phase angle difference suitable for achieving a pre-specified control target for  $P_{ps}$ . This is basically similar to controlling the phase angle difference between the converter's voltage and the AC system voltage in a PWM-controlled voltage source converter [11]. The phase shifter angle operation has been shown in forms of series voltage injections to the primary voltage in the phasor diagram in figure (4.4b). Furthermore, the nodal voltage magnitude in the compound transformer model is controlled using the variable tap changer magnitude ratio  $T$ . Equation (4.2) therefore is a mathematical representation of the VSC PWM amplitude modulation index that can take up any value within the converter's physical and operational boundaries [13, 14]. Ultimately, both from equations (4.1) and (4.2) as well as phasor diagram in figure (4.4b) it is clear that the operation of the variable complex tap ratio in the compound transformer would result in a controllable output voltage

in both phase angle and magnitude and eventually by controlling these parameters both active and reactive powers are controlled.

A direct benefit of modelling the voltage source converter, as a compound transformer with coupling impedance (which models the converter's connection transformer) is that the resultant value of the complex tap ratio phasor is explicitly included in the derived calculated nodal active and reactive power injections in both ends of the compound model. This means that throughout the course of the OPF solution process, the algorithm chooses the optimum tap magnitude ratio as well as the phase angle difference values associated with the desired voltage magnitude and the active power flows in either side of the converter. Defining an explicit control variable in form of the complex tap ratio guarantees that the control targets are achieved in the OPF without violating the complex tap ratio's respective limits, since they have to satisfy the KKT optimality conditions (particularly the third condition). Consequently, the results obtained from the compound transformer model is much more accurate than the conventional voltage source power injection models.

#### 4.3.1 Derived Nodal Power Flows in Compound Transformer Model

According to the single line diagram representation of the compound transformer model shown in figure (4.4a), the admittance matrix pertaining the compound model is calculated as such taking into account the shunt branch as well:

$$Y_T = \begin{bmatrix} Y & -(T\angle\varphi_{ps})Y \\ -(T\angle -\varphi_{ps})Y & T^2Y + Y_0 \end{bmatrix} \quad 4.3$$

In which the following self- and mutual-elements of the series transformer admittance matrix are defined:

$$Y = G_{ss} + jB_{ss} = -G_{sr} - jB_{sr} \quad 4.4$$

And

$$G = G_{ss} = \frac{R_{ps}}{R_{ps}^2 + X_{ps}^2} \quad 4.5$$

$$B = B_{ss} = \frac{-X_{ps}}{R_{ps}^2 + X_{ps}^2} \quad 4.6$$

The complex apparent power for the compound transformer model is calculated as the product of the nodal voltage magnitudes in primary and secondary with the complex conjugates of the currents flowing in each node as presented in equation (4.7).

$$\begin{bmatrix} S_s \\ S_r \end{bmatrix} = \begin{bmatrix} V_s & \\ & V_r \end{bmatrix} \begin{bmatrix} I_s \\ I_r \end{bmatrix}^* \quad 4.7$$

Replacing for complex conjugate currents with the relation  $I^* = Y_T^* V^*$ , equation (4.7) is re-written in polar coordinates, as such:

$$\begin{bmatrix} S_s \\ S_r \end{bmatrix} = \begin{bmatrix} V_s e^{j\theta_s} & \\ & V_r e^{j\theta_r} \end{bmatrix} \begin{bmatrix} Y^* & -TY^* e^{-j\varphi_{ps}} \\ -TY^* e^{+j\varphi_{ps}} & T^2 Y^* + Y_0^* \end{bmatrix} \begin{bmatrix} V_s e^{-j\theta_s} \\ V_r e^{-j\theta_r} \end{bmatrix} \quad 4.8$$

Which eventually yields the two general expressions corresponding the complex nodal apparent powers for primary and secondary sides of the compound transformer model in polar coordinates:

Sending end (primary side):

$$S_s = V_s^2 Y^* - TV_s V_r Y^* e^{j(\theta_s - \theta_r - \varphi_{ps})} \quad 4.9$$

Receiving end (secondary side):

$$S_r = (T^2 Y^* + Y_0^*) V_r^2 - TV_r V_s Y^* e^{j(\theta_r - \theta_s + \varphi_{ps})} \quad 4.10$$

By performing basic complex algebra on equations (4.9) and (4.10) taking into account equations (4.4-4.6) associated with the converter's admittance matrix and knowing that the shunt branch admittance is defined as  $Y_0 = G_0 + jB_0$ , the nodal active and reactive powers for the sending and receiving ends of the compound transformer model are, in polar form, calculated as shown in equations (4.11-4.14). Note that the details of calculations leading to the nodal powers are presented in Appendix I of this thesis and therefore will not be mentioned here.

Powers at sending end (or primary side):

$$P_s = V_s^2 G - TV_s V_r [G \cos(\theta_{sr} - \varphi_{ps}) + B \sin(\theta_{sr} - \varphi_{ps})] \quad 4.11$$

$$Q_s = -V_s^2 B - TV_s V_r [G \sin(\theta_{sr} - \varphi_{ps}) - B \cos(\theta_{sr} - \varphi_{ps})] \quad 4.12$$

Powers at receiving end (or secondary side):

$$P_r = V_r^2 (G_0 + T^2 G) - TV_r V_s [G \cos(\theta_{sr} - \varphi_{ps}) - B \sin(\theta_{sr} - \varphi_{ps})] \quad 4.13$$

$$Q_r = -V_r^2 (B_0 + T^2 B) - TV_r V_s [-G \sin(\theta_{sr} - \varphi_{ps}) - B \cos(\theta_{sr} - \varphi_{ps})] \quad 4.14$$

The calculated nodal powers presented in equations (4.11-4.14) essentially define the operation of the VSC in form of the compound transformer model's active and reactive power injections and therefore they have to be taken into account in the compound transformer exclusive Lagrangian when modelling the VSC in the OPF algorithm. It should be noted that these nodal power equations take into account the VSC internal switching losses in form of  $P_0 = G_0 V_r^2$ .

### 4.3.2 Compound Transformer OPF Formulation

The OPF general formulation presented in chapter two applies for the compound transformer model as well. This means that all the equality constraints particularly the power balance equations, which define the steady state operation of the system

must hold. The newly defined power injections, namely equations (4.11-4.14) are therefore included in the system's power balance equations.

The compound transformer model is formulated in the OPF by defining a new vector of state variables, containing the control variables of the transformer complex tap ratio as presented in equation (4.15).

$$z_{ps} = [\varphi_{ps}, T, \lambda_{\varphi_{ps}}]^T \quad 4.15$$

As mentioned earlier, the compound transformer is developed to model the operation of VSC and VSC-based systems in particular. Therefore its control constraints are the same as the VSC control capabilities, namely, seamless control on active power flow in both ends as well as nodal voltage magnitude.

Consequently, The compound transformer's operating constraints are defined on its active power flow as well as the nodal voltage magnitude at either ends of the transformer.

The active power flow constraint is defined as a new functional equality for the compound transformer model's active power flow, namely equation (4.16).

$$P_{ps} - P_{specified} = 0 \quad 4.16$$

Furthermore, the voltage control constraint is defined as a variable equality on the voltage magnitude of the *ith* side of the compound transformer model as such:

$$V_i - V_{specified} = 0 \quad 4.17$$

When the compound transformer model is used to model the operation of a real voltage source converter, equations (4.16) and (4.17), essentially define the boundary region of the OPF solution space at the presence of the converter. Furthermore, the multiplier term  $\lambda_{\varphi_{ps}}$  in equation (4.15) corresponds to the

compound transformer's exclusive active power functional equality constraint shown in equation (4.16), which is used to activate its associated Lagrangian function.

In addition to these equalities, the following nodal power balance equations must hold for both sides of the compound transformer model:

$$\begin{aligned} P_i^{calc} - P_{g_i} + P_{d_i} &= 0 & 4.18 \\ i &\in [s, r] \end{aligned}$$

And

$$\begin{aligned} Q_i^{calc} - Q_{g_i} + Q_{d_i} &= 0 & 4.19 \\ i &\in [s, r] \end{aligned}$$

In which  $P_i^{calc}$  and  $Q_i^{calc}$  are the total calculated injected powers at  $i$ th node connected to the compound transformer, which include the model's nodal active and reactive power injections in equations (4.11 – 4.14) (See parametric example in chapter two). All the state variables associated with the compound transformer model have to be within their respective limits. Eventually, the functional equalities defined in equations (4.16) as well as (4.18) and (4.19) are added to the system of equations by defining the compound transformer model's Lagrangian as such:

$$L_{PS} = \sum_{i \in [s, r]} \lambda_{p_i} (P_i^{calc} - P_{g_i} + P_{d_i}) + \sum_{j \in [s, r]} \lambda_{q_j} (Q_j^{calc} - Q_{g_j} + Q_{d_j}) + \lambda_{\varphi_{ps}} (P_{ps} - P_{spe}) \quad 4.20$$

In which

$P_i^{calc}$  and  $Q_j^{calc}$  are the total calculated nodal active and reactive powers of the either ends of the compound transformer model

$P_{g_i}$  and  $Q_{g_j}$  are the active and reactive power generation of the converter's corresponding buses

$P_{d_i}$  and  $Q_{d_j}$  are the active and reactive power demands of the converter's corresponding buses

$P_{spe}$  is the amount of regulated active power flow to be achieved based on system's operation and requirements

$P_{ps}$  is the active power flow within the compound transformer (in case of a VSC it is bi-directional in both DC and AC sides of the converter)

The Lagrangian function in equation (4.20) is used to model the operation of the voltage source converter in the OPF algorithm. It should be noted that at the start of the OPF solution process, it is assumed that all constraints are within limits so the exact penalty function corresponding to violated inequalities (equation 2.33) is not activated and therefore is not shown in equation (4.20). However, the functional equality constraint corresponding to the compound transformer's active power flow (equation 4.16) may be activated throughout the OPF solution process only if the transformer is tasked with controlling the active power. The functional inequalities associated with the generator's active and reactive powers are not activated at the start of the OPF solution process and will only be added to the system should a violation occur in their respective values.

On the other hand, if need be, the variable equality constraint on the compound transformer's voltage magnitude defined in equation (4.17) is included in the OPF formulation using the special quadratic penalty function shown in equation (4.21).

$$\phi(V_i) = \frac{1}{2} \varphi (V_i - V_{specified})^2 \quad 4.21$$

In which,  $\varphi$  is the large pre-defined penalty factor which is fixed throughout the solution process.

The penalty function defined in equation (4.21) effectively penalises the nodal voltage magnitude for points other than the target voltage magnitude dictated by system operating requirements. The voltage consequently is enforced to the target value, by adding the first and second partial derivatives of the penalty function to

their corresponding Hessian and Jacobian terms in the linear system of equations associated with the compound transformer model (equation 4.23).

The compound model's control parameters associated with the complex tap of the transformer are naturally bounded to their physical and operational limits as shown in equation (4.22) by the use of exact quadratic penalty functions. The augmented Lagrangian approach, therefore, guarantees reaching an optimum operating point, which is well within the system's operational and physical boundaries by satisfying the third KKT optimality conditions.

$$|T^{\min}| \angle \varphi_{ps}^{\min} < |T| \angle \varphi_{ps} < |T^{\max}| \angle \varphi_{ps}^{\max} \quad 4.22$$

When it comes to checking limit violations, the compound transformer's control variables have priority over their associated nodal power injections simply because of the fact that the latter are functions of the former. Generally if the complex tap ratio is not violated, then it is most likely that a violation in the amount of nodal active and reactive power injections will not occur unless the network conditions dictate a violation. For instance in case of voltage control, the network's reactive power demand (for a specified voltage magnitude) might violate the compound transformer's nodal reactive power limit in which case, its amount is enforced towards its limit boundaries using appropriate Lagrangian multipliers.

The system of linear equations presented in equation (4.23) is developed exclusively for the compound model presented in figure (4.4a). It should be noted that the partial derivatives of the matrix of coefficients, namely Hessian and Jacobian terms, are calculated with respect to the matrix of state variables  $z = [\theta, V, T, \varphi_{ps}, \lambda_p, \lambda_q, \lambda_{\varphi_{ps}}]^T$ .

The linear system of equations presented in equation (4.23) comprises the second order partial derivatives of the newly updated Lagrangian function, containing the compound transformer's exclusive Lagrangian in equation (4.20), with respect to the vector of state variables  $z$ , which in turn includes the exclusive variables associated with the compound transformer model that is shown in equation (4.15). This linear system of equations is then solved within the OPF, using Newton's

iterative method introduced in chapter two. It should be noted that the expressions for the exclusive terms of second order partial derivatives with respect to the compound transformer model's state variables are presented in Appendix I of this thesis.

$$\begin{bmatrix} \nabla_{\theta^2}^2 L & \nabla_{\theta V}^2 L & \nabla_{\theta \varphi}^2 L & \nabla_{\theta T}^2 L & \nabla_{\theta} P^{calc} & \nabla_{\theta} Q^{calc} & \nabla_{\theta} P_{ps}^{(k)} \\ \nabla_{V\theta}^2 L & \nabla_{V^2}^2 L & \nabla_{V\varphi}^2 L & \nabla_{VT}^2 L & \nabla_V P^{calc} & \nabla_V Q^{calc} & \nabla_V P_{ps}^{(k)} \\ \nabla_{\varphi\theta}^2 L & \nabla_{\varphi V}^2 L & \nabla_{\varphi^2}^2 L & \nabla_{\varphi T}^2 L & \nabla_{\varphi} P^{sr} & \nabla_{\varphi} Q^{sr} & \nabla_{\varphi} P_{ps}^{(k)} \\ \nabla_{T\theta}^2 L & \nabla_{TV}^2 L & \nabla_{T\varphi}^2 L & \nabla_{T^2}^2 L & \nabla_T P^{sr} & \nabla_T Q^{sr} & \nabla_T P_{ps}^{(k)} \\ \nabla_{\theta} P^{calc} & \nabla_V P^{calc} & \nabla_{\varphi} P^{sr} & \nabla_T P^{sr} & 0 & 0 & 0 \\ \nabla_{\theta} Q^{calc} & \nabla_V Q^{calc} & \nabla_{\varphi} Q^{sr} & \nabla_T Q^{sr} & 0 & 0 & 0 \\ \nabla_{\theta} P_{ps}^{(k)} & \nabla_V P_{ps}^{(k)} & \nabla_{\varphi} P_{ps}^{(k)} & \nabla_T P_{ps}^{(k)} & 0 & 0 & 0 \end{bmatrix} \times \begin{bmatrix} \Delta\theta \\ \Delta V \\ \Delta\varphi_{ps} \\ \Delta T \\ \Delta\lambda_p \\ \Delta\lambda_q \\ \Delta\lambda_{\varphi_{ps}} \end{bmatrix} = - \begin{bmatrix} \nabla_{\theta} L \\ \nabla_V L \\ \nabla_{\varphi_{ps}} L \\ \nabla_T L \\ \Delta P^{calc} \\ \Delta Q^{calc} \\ (P_{ps}^{(k)} - P_{ps}^{specified}) \end{bmatrix} \quad 4.23$$

The upper indicator ( $k$ ) in equation (4.23) denotes compound transformer model mode of power control, which essentially determines whether the power regulation is on the sending end or the receiving end of the compound transformer model. The upper indicator  $sr$  denotes the exclusive nodal power injections associated with the compound transformer. The compound transformer OPF formulation is consequently used to model the operation of the voltage source converter within the OPF algorithm, guaranteeing that the VSC PWM control characteristics, namely the compound transformer's controllable variable complex tap ratio, is kept within limits by satisfying the KKT conditions upon reaching an optimum.

### 4.3.3 Compound Transformer Model Modes of Operation

The compound model possesses four inherent control modes (modes of operation) inferred from its functional and variable equalities introduced in equations (4.16) and (4.17).

It can be set to any one of these four control modes by activating its corresponding control equalities on its voltage and active power flow. The compound transformer modes of operation are presented in table (4.1) below.

Mode	Control State	Power Equality	Voltage Equality
No Control	Mode 1	Deactivate Lagrangian Function	Remove Penalty Function
Voltage Only	Mode 2	Deactivate Lagrangian Function	Add Penalty Function
Power Only	Mode 3	Activate Lagrangian Function	Remove Penalty Function
Voltage/Power	Mode 4	Activate Lagrangian Function	Add Penalty Function

**Table 4.1 - Compound Transformer Model Modes of Operation**

As seen from table (4.1), in order to activate any of the control modes it is only necessary to activate their corresponding control equalities. For example, regarding the compound model shown in figure (4.4a), if the compound transformer model is set to control the voltage at node  $s$ , its associated voltage magnitude will be penalised for points other than the target voltage using the penalty function presented in equation (4.21). Moreover, the power control mode in the compound transformer model requires the activation of the Lagrangian function associated with the compound transformer's power flow equations shown in equation (4.24).

$$L_{\lambda_{\varphi_{ps}}} = \lambda_{\varphi_{ps}} (P_{ps}^{(k)} - P_{specified}) \quad 4.24$$

The term  $(k)$  essentially takes two values, namely 1 and 2. If  $k = 1$ , then it means that the transformer is regulating power at primary, whereas if  $k = 2$  it indicates that it is regulating power at secondary. For instance, regarding the compound model in figure (4.4a), it is assumed that the converter is regulating power at its primary side (or node  $s$ ), the Lagrangian function associated with converter's power control then takes the shape of equation (4.25).

$$L_{\lambda_{\varphi_{ps}}} = \lambda_{\varphi_{ps}} (P_{ps}^{(1)} - P_{specified}) = \lambda_{\varphi_{ps}} (P_s - P_{specified}) \quad 4.25$$

Similarly for power control on the secondary side, equation (4.25) is altered as such:

$$L_{\lambda_{\varphi_{ps}}} = \lambda_{\varphi_{ps}} (P_{ps}^{(2)} - P_{specified}) = \lambda_{\varphi_{ps}} (P_r - P_{specified}) \quad 4.26$$

The power at primary or secondary can either be negative or positive, which essentially determines the direction of the power from sending to receiving end or vice versa.

In case of a VSC, the positive and negative signs in the compound transformer model would correspond to the inverting and rectifying operation of the converter. If the power sign at the AC side were positive (or if the power at DC side were negative) then the converter would act as a rectifier, whereas if the power sign at the AC side were negative (or if the power sign at the DC side were positive) then the converter acts as an inverter. The power control constraint in equation (4.24) guarantees bi-directionality of the active power flow to and from the converter in the compound transformer model.

The compound transformer model can also be configured to control both power and voltage concurrently (which is its default mode of operation in most VSC-based system simulations such as VSC-HVDC links), in which case both control equalities on voltage and converter's active power flow are activated and their associated control constraints have to be added to the OPF formulation using their associated penalty/Lagrangian functions. It should be noted that the Lagrangian associated with the functional equality constraint on compound transformer's active power, namely equation (4.24), is active throughout the solution process. However, if the compound transformer is set to regulate voltage only or if it does not control any network parameters, then this equation is effectively deactivated using an appropriate quadratic penalty function to penalise its associated multiplier, namely  $\lambda_{\varphi_{ps_i}}$ . It then becomes active only if there is a power limit violation in either side of the converter.

Eventually, by referring to table (4.1), nine distinct control combinations are derived for the compound transformer model (and subsequently for VSC compound model operation) as seen in table (4.2).

VSC Control Mode	Voltage Control	Power Control
1.0.0.	N/A	N/A
2.1.0.	Sending End	N/A
2.2.0.	Receiving End	N/A
3.1.0.	N/A	Sending End
3.2.0.	N/A	Receiving End
4.1.1.	Sending End	Sending End
4.1.2.	Sending End	Receiving End
4.2.1.	Receiving End	Sending End
4.2.2.	Receiving End	Receiving End

**Table 4.2 - Compound Transformer Model Control Modes**

These control combinations correspond to whichever state variable the compound transformer model is controlling and whether its associated value is regulated on the its sending end or receiving end. The 3-digit notation is a practical way of identifying the compound model modes of operation and will be referred to several times throughout this chapter and next.

#### 4.4 AC Stand-alone Operation Tests

In order to properly test the compound transformer model's various modes of operation, a simple system test comprising 4-nodes has been devised. The compound transformer model is tested as a stand-alone device, whose operation can be interpreted as a series power regulator connecting the generator to node 3 via the impedance with the value of  $Z_1 = R_1 + jX_1$ , feeding the load in node 3 while providing fast nodal voltage and power support via the variable complex tap phasor. The data for the 4-node system is found under system data in Appendix II and therefore will not be mentioned here. For consistency purposes, however, it is necessary to mention that the objective function has taken to be the same as the objective function in the 8-node system that was featured in previous chapters. Moreover, It should be noted that the results depicted in the following system tests are in per unit. The purpose of running the OPF algorithm is as always, indentifying the optimum point of operation in which the generators' fuel cost is at minimum. Where applicable, the compound transformer is tasked with regulating the voltage magnitude and/or active power flow to 1.0 per unit. The OPF solution for the 4-node system is obtained by solving the exclusive system of linear equations pertaining to the compound model shown in equation (4.23) via Newton's iterative

process, taking into account the limits on the complex tap in equation (4.22). The control modes are selected by referring to table (4.1) in order to activate/deactivate the control constraints on active power (equation 4.16) and/or nodal voltage magnitude (equation 4.17). In the following OPF simulations, the compound transformer model is tested in several modes of operations and the results are presented in figures (4.5-4.11) respectively.

#### 4.4.1 Control Mode: 1.0.0.

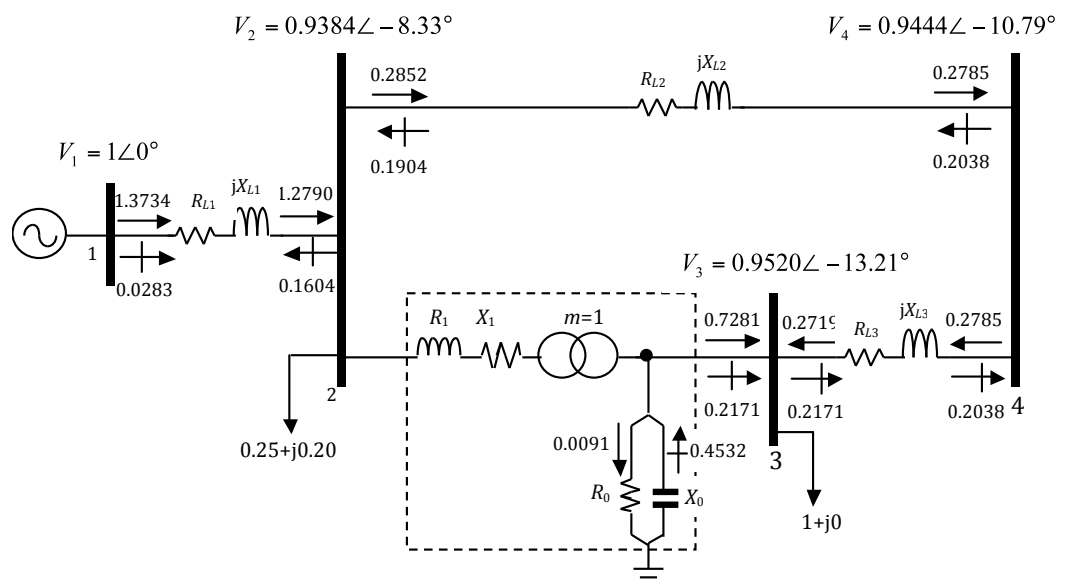


Figure 4.5 - Compound Transformer as a series compensator (No Control)

**4.4.2 Control Mode: 2.1.0.**

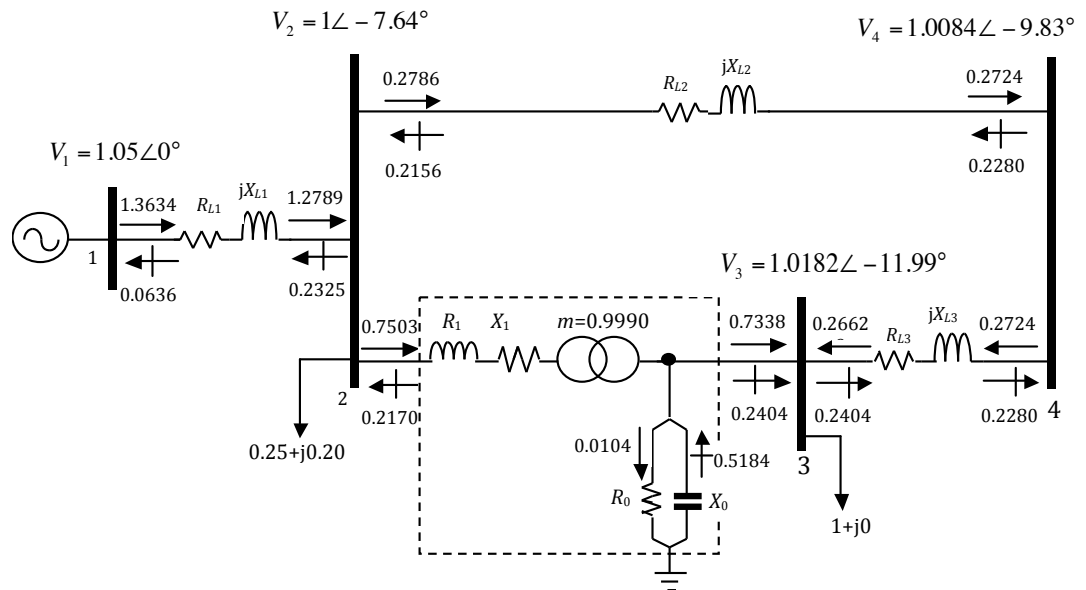


Figure 4.6 - Compound Transformer as a series compensator (Voltage Control on primary)

**4.4.3 Control Mode: 2.2.0.**

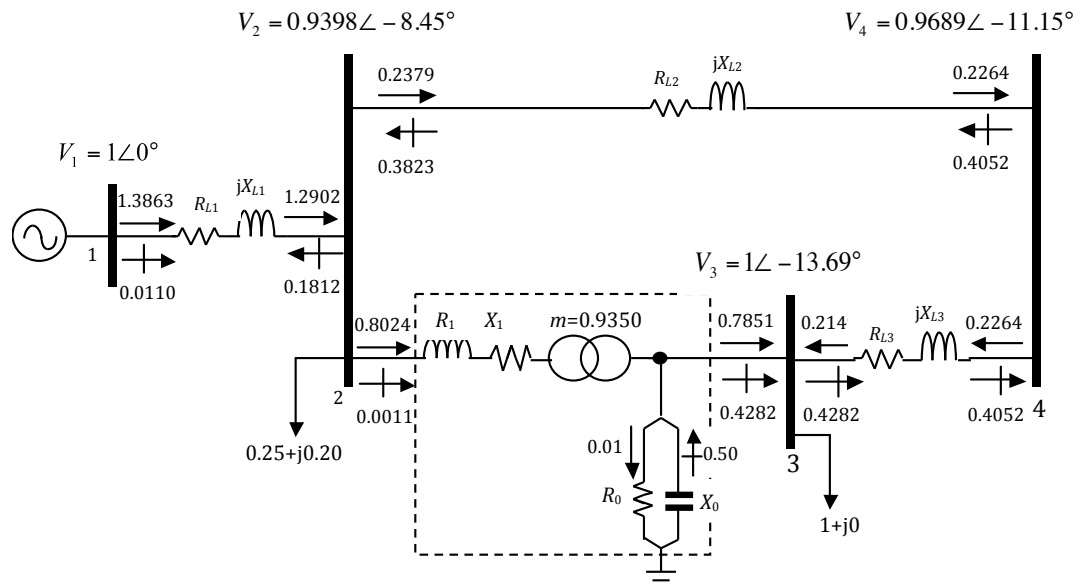


Figure 4.7 - Compound Transformer as a series compensator (Voltage Control on secondary)

**4.4.4 Control Mode: 3.1.0.**

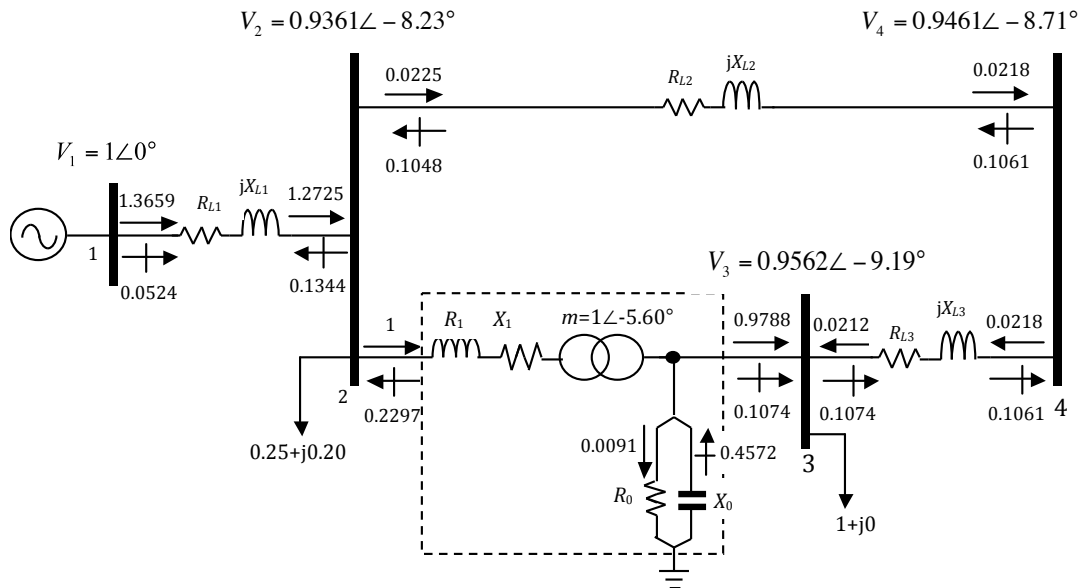


Figure 4.8 - Compound Transformer as a series compensator (Power Control on primary)

**4.4.5 Control Mode: 3.2.0.**

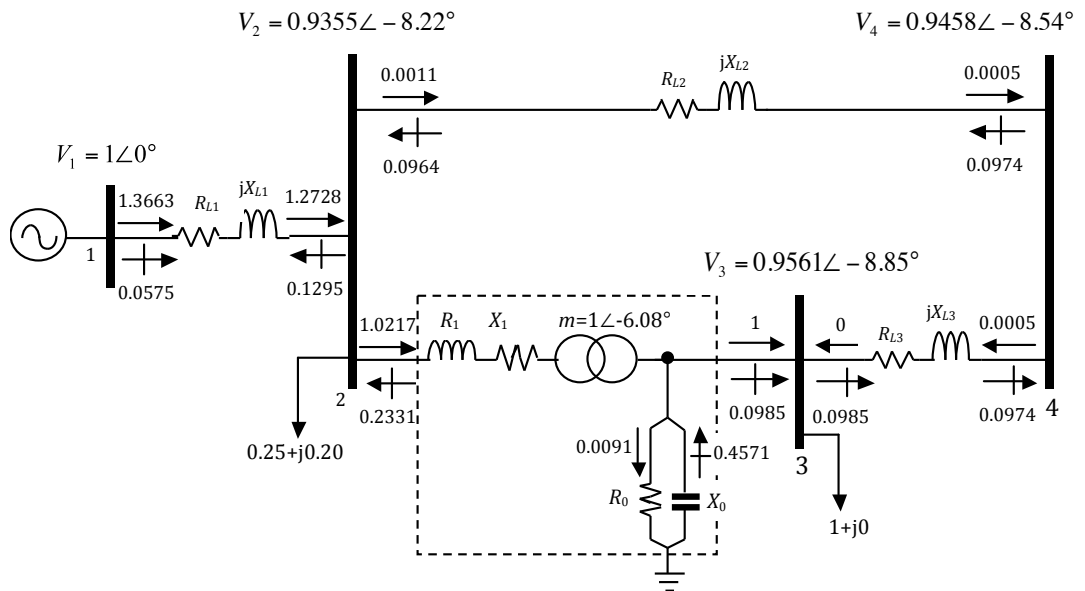


Figure 4.9 - Compound Transformer as a series compensator (Power Control on secondary)

#### 4.4.6 Control Mode: 4.2.2.

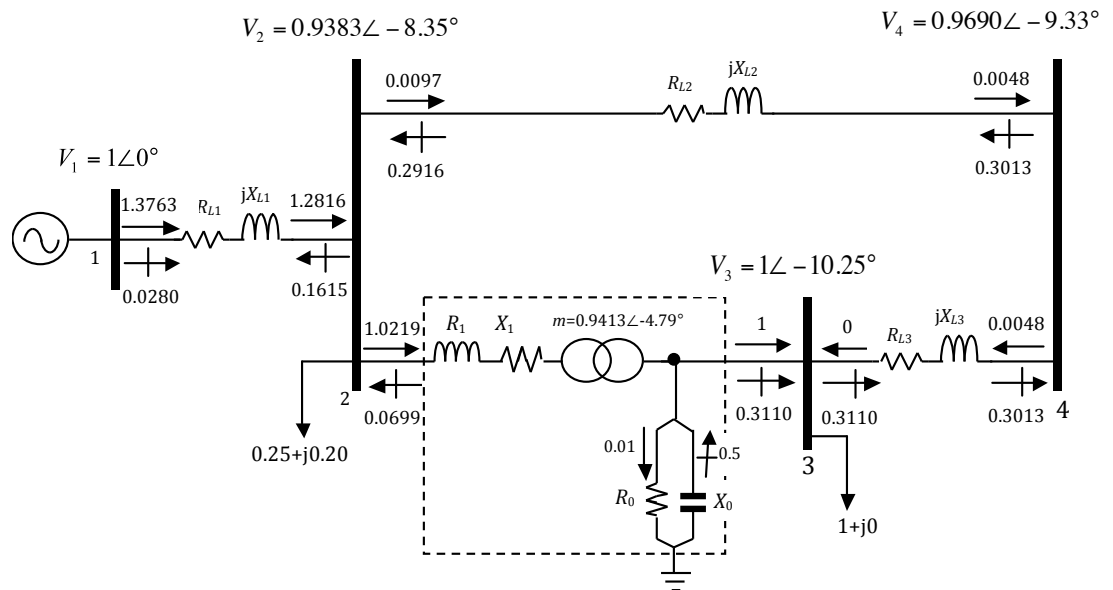


Figure 4.10 - Compound Transformer as a series compensator (Power on secondary; Voltage on secondary)

#### 4.4.7 Control Mode: 4.2.1.

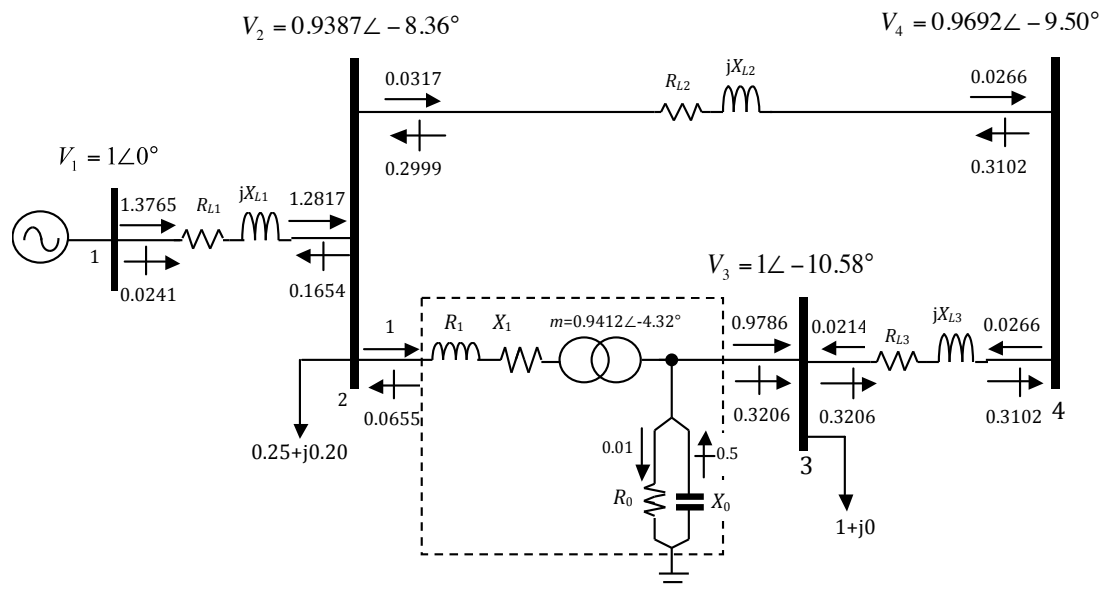


Figure 4.11 - Compound Transformer as a series compensator (Power on primary; Voltage on secondary)

#### 4.4.8 Results Discussion

Several control modes depicted in table (4.2) are successfully tested for the new compound transformer model in the 4-node AC system above.

Evidently, the compound transformer model in such a system configuration does behave like a series compensator. The compound transformer's phase shifter variations are responsible for active power flow loop control between nodes 2, 3 and 4. In particular, the power flowing across the transmission line between nodes 2 and 4 is largely affected by the operation of the compound transformer model, and whether the compound transformer is controlling active power or not. The reactive power flow, on the other hand is indirectly controlled by the compound transformer's tap changer ratio variations.

Table (4.3) summarises the compound model's modes of operation in the depicted 4-node system as such:

Control Mode	$T\angle\varphi_{ps}$	$V_2\angle\theta_2$	$V_3\angle\theta_3$	$f_{g_1}$ \$/hr
1.0.0.	$1\angle 0.0^\circ$	$0.9384\angle -8.33^\circ$	$0.9520\angle -13.21^\circ$	602.397
2.1.0.	$0.9990\angle 0.0^\circ$	$1\angle -7.64^\circ$	$1.0182\angle -11.99^\circ$	597.893
2.2.0.	$0.9350\angle 0.0^\circ$	$0.9398\angle -8.45^\circ$	$1\angle -13.69^\circ$	608.237
3.1.0.	$1\angle -5.60^\circ$	$0.9361\angle -8.23^\circ$	$0.9562\angle -9.19^\circ$	599.029
3.2.0.	$1\angle -6.08^\circ$	$0.9355\angle -8.22^\circ$	$0.9561\angle -8.85^\circ$	599.110
4.2.2.	$0.9413\angle -4.79^\circ$	$0.9383\angle -8.35^\circ$	$1\angle -10.25^\circ$	603.730
4.2.1.	$0.9412\angle -4.32^\circ$	$0.9387\angle -8.36^\circ$	$1\angle -10.58^\circ$	603.790

**Table 4.3 – Compound Transformer Model's Modes of Operation as a Series Compensator in the 4-node System Simulations**

It can be seen that in every mode of operation, the variable complex tap phasor, namely  $m_{ps} = T\angle\varphi_{ps}$  takes a different value (as obtained by the OPF algorithm), which corresponds to its associated control mode (either 1,2,3 or 4). The direction of the power flow to or from the transformer's ends depend on the network operating conditions as well as the compound transformer model's own modes of operation. In case of reactive power flow, the amount and direction of the power depends on the transformer's voltage control constraint, whether it's controlling the voltage or not and on which side it is set to maintain the voltage.

It should be mentioned again that the compound model modes of operation are selected via adding or removing appropriate penalty terms to activate/deactivate the associated control constraints on voltage or active power as seen in table (4.1).

Whenever the converter is set to regulate the voltage, the tap changer has to be operational, whereas in power control mode the phase shifter has to operate to provide the required phase angle difference associated with the target value of active power. On the other hand, whenever the compound transformer model is set to control both voltage magnitude and active power simultaneously, the variable complex tap phasor in the compound model becomes operational. Since the compound transformer's complex tap is included in the vector of state variables, its limit boundaries has to be checked after finishing each internal loop so that it can satisfy the third KKT optimality condition. Notice that the variable complex tap ratio inequality constraints have priority over the nodal voltage and power flow inequalities of the compound transformer model. Eventually, through the process of limit check the results obtained by the OPF guarantee that the equipments' physical limits are not violated. Charts (4.1) and (4.2) show the performance of the compound model in voltage and power control modes (including modes 4.1.2. and 4.1.1. which were not included in the simulations) via the operation of the tap changer ratio as well as the phase shifter angle respectively. Notice that both values are kept well within their specified limit boundaries by the OPF algorithm.

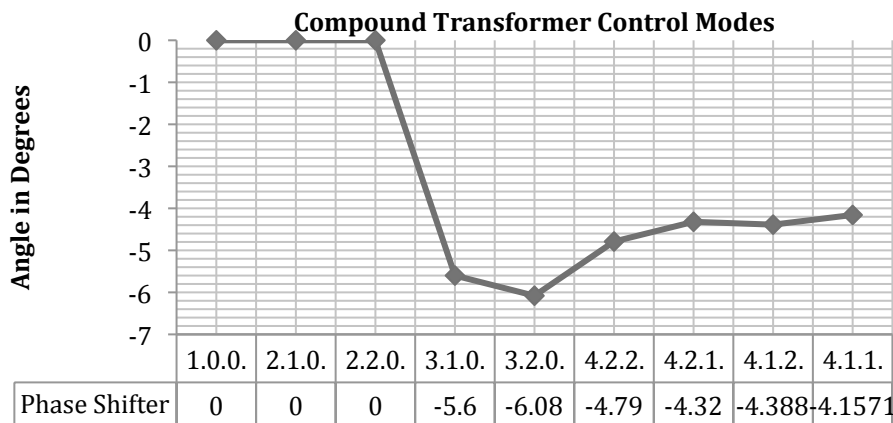


Chart 4.1 - Compound Model's Phase Shifter Angle Variations in the 4-node System Simulations (within limits)

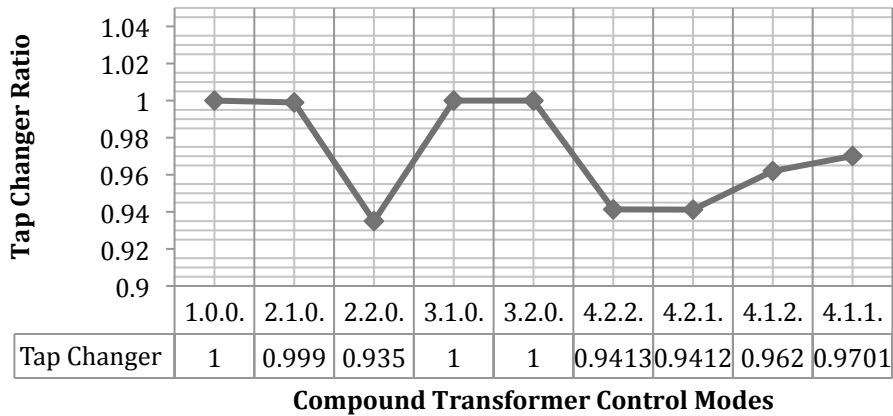


Chart 4.2 - Compound Model's Tap Changer Ratio Variations in the 4-node System Simulations (within limits)

In mode 1 (no control) both phase shifter and tap changer can either be operational in which case their final values are dictated by the OPF algorithm otherwise they can be fixed to their initial values as it is the case here using appropriate penalty functions.

The objective function value varies between approximately 597\$/hr to 608\$/hr in different control modes, which clearly indicates the fact that the final value of the objective function and in turn the 4-node system's final dispatch depends on the compound transformer's behaviour in the system.

## 4.5 DC Stand-alone Operation Tests

The compound transformer model can be used to model a voltage source converter for supplying DC loads, which are defined as a real power demand,  $P_d$ . Since the DC node (compound transformer's receiving end) has only a real voltage component, the required phase angle difference to achieve the target value of the real power supplied to the DC load is achieved via the operation of the phase shifter in the compound transformer. By using the appropriate penalty functions to deactivate its associated increments in the linear system of equations the OPF algorithm essentially ignores the DC bus phase angle component. Consequently, the "true" conditions of a DC bus can be properly accommodated in the compound transformer model without the need for introducing additional connection buses or exclusive state variables.

One of the major benefits of using compound transformer in DC system tests is the ability to properly model the operation of VSC-FACTS controllers such as the STATCOM provided that the VSC compound transformer model is coupled with a coupling transformer. The system simulations that are presented in this section can be reconfigured as a STATCOM-OPF model if it is assumed that the coupling transformer leakage reactance is added to the reactance of the transmission line connecting the VSC compound transformer model to the generator. The DC tests presented in the following sections also form the basics of OPF modelling pertaining to the more complex multi-terminal VSC-HVDC systems that are mentioned in next chapter.

In order to regulate the power at DC bus to the required amount (demand in DC bus), the functional equality constraint associated with the compound transformer model's active power, which was mentioned in equation (4.16), is simplified to the form of equation (4.27) as such:

$$P_r - P_d = 0 \quad 4.27$$

Which in turn would create the Lagrangian function for active power regulation at the DC bus as presented in equation (4.28). The Lagrangian function then is added to the VSC compound model's Lagrangian function (equation 4.20) and will be included in the system of linear equations.

$$L_{\varphi_{ps}} = \lambda_{\varphi_{ps}} (P_r - P_d) \quad 4.28$$

In the following case scenarios the VSC compound transformer model is used to supply (interconnect) a DC load at the converter's DC side bus using the functional equality shown in equation (4.28) in order to maintain the active power at that node to a pre-determined value (the DC load demand). The reactive power in the DC bus naturally comes to zero since there is no source of reactive power demand at this bus.

#### 4.5.1 Case One

In the OPF solution shown for the AC system presented in figure (4.12), the power network is supplying a DC load at 100 MWs using a VSC compound transformer model.

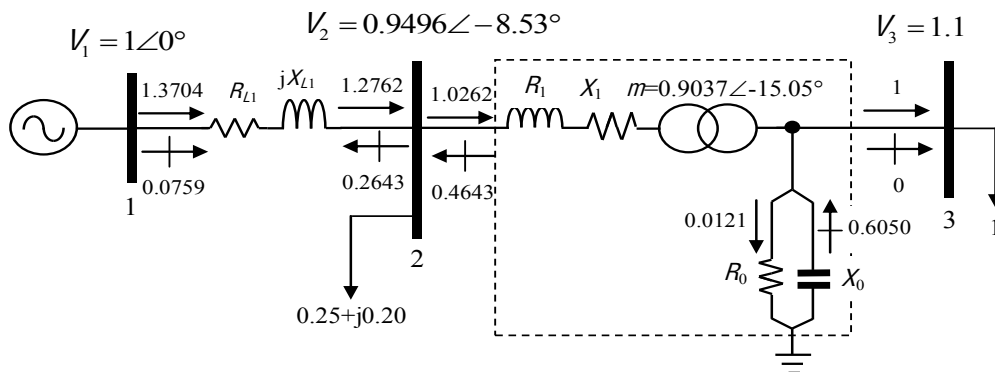


Figure 4.12 – Compound Transformer feeding the DC Load

The voltage at the DC node is kept constant at the value of 1.1 per unit at all times using its associated penalty function introduced in equation (4.21). The power is regulated at the DC bus to 100 MWs using the Lagrangian function in equation (4.28) to bind the functional equality in equation (4.27) to the system Lagrangian. As a result, the VSC compound model is operating in mode 4, and therefore phase shifter and tap changer are both operational. The OPF is run for the same objective function as in previous test cases and is converged in three iterations.

As it is seen from figure (4.12), the VSC has successfully kept the active power at 100 MWs at the DC load bus with the phase shifter taking a value of 15.05 degrees. The voltage at the DC bus has also been maintained at 1.1 per unit. As expected, there is no reactive power flow at the converter's DC side bus. Furthermore, the converter's internal ohmic losses have arrived at 1.21 MWs.

The generator's optimum power flow dispatch is shown in figure (4.12) to be at approximately 137 MWs of active power and 7.59 MVARs of reactive power. The reason why there is so little of reactive power generation is that most of the reactive power is generated by the voltage source converter that feeds the reactive requirements in node 2 with the rest being the losses in the system. The objective function final value (optimal value of generation) has arrived at 601.03 \$/hr. It

should be noted that the generator cost data is the same as previous case. The rest of the system data is presented in Appendix II.

#### 4.5.2 Case Two

The AC network in figures (4.13) as well as (4.14), is used to supply 100 MWs of demand at the DC node (node 3) using the voltage source converter compound transformer model. For consistency purposes, the same objective function as before applies for the generators in this system. Furthermore, the compound transformer is tasked with maintaining the voltage magnitude at the DC bus to 1.1 per unit. The power constraint at the DC node is again added to the system Lagrangian and subsequently included in the system of linear equations using the Lagrangian function in equation (4.28). The following sets of simulations have been carried out for the case two:

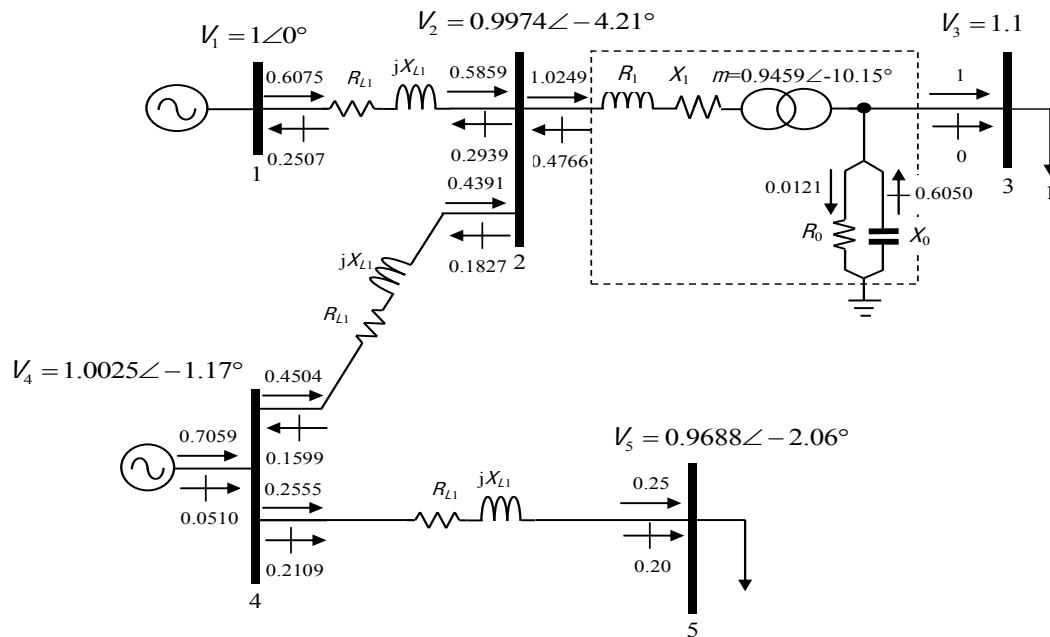
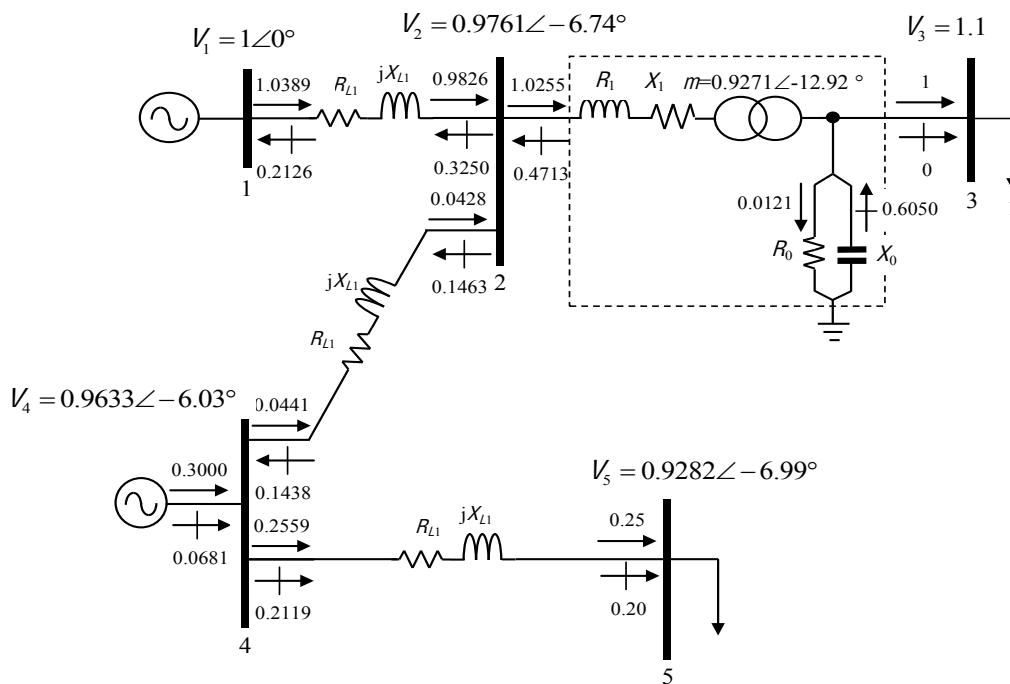


Figure 4.13 – VSC Compound Transformer feeding the DC Load



**Figure 4.14 – VSC Compound Transformer feeding the DC Load (Generator 2 active power schedule limited to 0.3 per unit)**

In both case scenarios the generators' active power distribution is obtained by the OPF algorithm, however in second attempt, the generation capacity in second machine which is connected to node 4 is extremely limited (30 MWs maximum) and therefore the bulk of the active power in the system is being generated by the first generator (slack bus generator).

By comparing the results from two simulations it can be seen that even though the power flow distribution has changed in the system, it has limited effect on the power flow inside the converter, since the compound transformer model has isolated the DC load from the rest of the system. It is imperative to note that the capability of isolating loads from system disturbances is one of the most vital roles a voltage source converter and subsequently a VSC-based interconnection system can play in increasing system stability margins [2].

The active power of the second generator is kept fixed to its upper limit, namely 30 MWs by activating its corresponding functional inequality constraint. The first generator, however, is still free to take up any value of active power dispatch, albeit within limits. Noticeably, there is no reactive power flow in node 3, which is expected since this node supplies the DC load, however the converter supplies

reactive power to node 2 from where it is distributed amongst the network's transmission lines. Once again it is stressed that the power demand in the DC bus is satisfied via the operation of the phase shifter angle, whereas the voltage is regulated through the operation of the tap changer.

The operation of the complex tap ratio for all three DC test cases has been summarised in table (4.4).

DC Test Case	Complex Tap Ratio	AC Side Voltage	DC Side Voltage
Case One	$0.9037\angle -15.05$	$0.9496\angle -8.53$	$1.1\angle 0.0$
Case Two - 1	$0.9459\angle -10.15$	$0.9974\angle -4.21$	$1.1\angle 0.0$
Case Two - 2	$0.9271\angle -12.92$	$0.9761\angle -6.74$	$1.1\angle 0.0$

**Table 4.4 - VSC Compound Model DC Load Test Results**

It should be noted that the VSC compound transformer model in a VSC-HVDC transmission system behaves exactly as it is depicted here in the DC test simulations providing both voltage and active power control requirements to the converter's DC as well as AC nodes. Consequently, the compound transformer model provides a strong mathematical tool to properly model any VSC-HVDC transmission system in any configuration (Back to Back, Point-to-Point and Multi-terminal) and for any purpose simply via the operation of the variable complex tap in the compound transformer model.

## 4.6 5-node Benchmark System Test: Changes in System Conditions

In this section, the compound transformer model has been tested in the 5-node benchmark system in [12] in order to precisely determine its potential influence on deviating the optimum operating point in the OPF algorithm. The compound transformer in this system acts as a series compensator regulating active power across the line connecting between nodes "Lake" and "Main".

According to the system data presented in Appendix II, the active power demand in "Main" is 40 megawatts, which, in normal operation, where no active power regulation is carried out, is provided by the system through the lines connected to "Main". The optimum active power flow solution as obtained by the OPF algorithm

at “Main” in the 5-node benchmark system has been presented in figure (4.15) below.

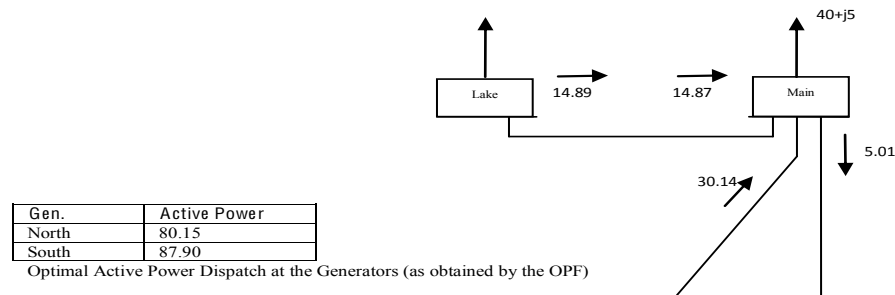


**Figure 4.15 - Partial OPF Solution for the normal 5-node Benchmark system; Notice the active power flow between “Lake” and “Main”**

However, by connecting the compound transformer between “Lake” and “Main” the active power transferred between these nodes can be regulated seamlessly using the phase shifter angle variations in the compound model.

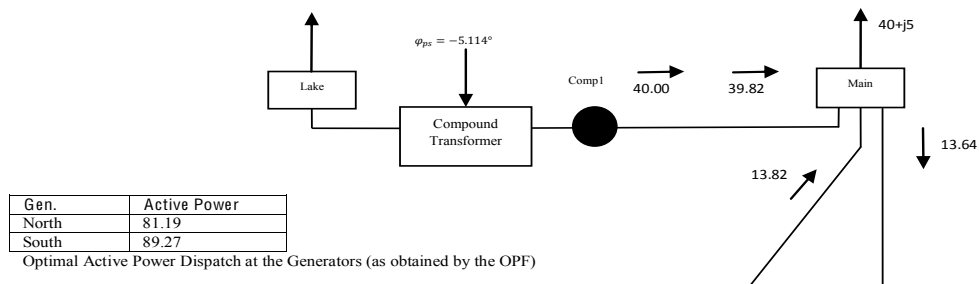


**Figure 4.16 - Partial OPF Solution for the 5-node Benchmark system with the compound transformer regulating power between "Lake" and "Main"**

Within the OPF algorithm, setting the power control constraint requires activation of equation (4.16) via adding its Lagrangian in equation (4.24) to the system Lagrangian. The compound transformer model is added to the system configuration using the dummy bus “Comp1” and the OPF is run for operating mode 3.2 (power control on receiving end). The OPF converges in 6 iterations with the results shown in figure (4.16).

As it can be seen from the results obtained by the OPF shown in figure (4.16), the compound transformer has successfully regulated the amount of active power between “Lake” and “Main” to 40 MWs, with the active power at “Main” arriving at 39.82 MWs to support the active power demand there. The compound

transformer model has regulated the pre-determined amount of active power by varying its phase shifter angle to -5.114 degrees, which means that the overall incurred phase angle difference between voltage phase angles in “Lake” and “Main” has been shifted by approximately 5 degrees resulting in increasing the power flow to 40 MWs from previously 14.87 MWs in the first test run in figure (4.15). A significant shift in the bulk of active power flow between the transmission lines connected to “Main” is noticeable by comparing the OPF results shown in figures (4.15) and (4.16). The bulk of active power now flows in the line connecting “Lake” and “Main”.

On the other hand, comparing the results in figures (4.15) and (4.16) shows that in the second test run the generators active power dispatch particularly in “South” has been increased, which indicates that using the compound transformer model to regulate the power while adding more flexibility to the system operation comes at the price of increasing the objective function final value by approximately 1%, from 748 \$/hr to 757 \$/hr. However, this increase in the objective function value (generators’ increase in fuel consumption) is justified by the fact that the compound transformer model improves system stability margins by improving its controllability in active power flow.

The main reason as to why the cost function increases in the second test run, in other words why the optimal power flow does not converge towards the same point, is that by using the compound transformer to regulate active power between “Lake” and “Main”, a new functional equality constraint is introduced, which is suitable for controlling the active power along the transmission line between these two nodes. Therefore, by simply adding the new functional constraints, the boundaries of the solution region will change from that of the first test run where no power regulating devices are present. It is precisely due to the change of boundaries of the solution region that there is less degree of freedom for the cost function variations during the course of the solution process that ultimately yields a different optimum operating point. It is imperative to note that FACTS controllers are tasked with improving system stability by actively controlling the system parameters. However, applying the OPF in each system depends on the conditions of that system alone, which are essentially the constraints, which the optimisation problem’s objective functions are subjected to.

On the other hand, if the compound transformer had been used in mode 1 the results would have been similar to those in figure (4.15), since the OPF boundary regions would have remained the same as before.

## 4.7 Conclusion

In this chapter an advanced model for the voltage source converter in optimal power flow has been introduced. The model is based on the fact that the operation of a PWM-controlled VSC can be modelled more precisely as a compound transformer device with controllable complex tap phasor to include the characteristics of the PWM control in the OPF mathematical formulation.

Based on the operational principles of a PWM-controlled VSC, the complex tap ratio variations accurately model the voltage and phase angle control of the converter's output voltage phasor giving rise to independent active and reactive power control. Furthermore, by adding a shunt branch to the equivalent circuit of the compound transformer, the converter's internal switching losses are modelled as a shunt resistive branch, whereas the DC bus capacitor is modelled as a shunt susceptance.

The new model is essentially different from previous modelling approaches [5, 11, 14, 16], which often regard the VSC as a controllable voltage source much like a synchronous condenser behind coupling impedance (or reactance) [4].

The active power in the compound transformer model is controlled via the variations in the amount of variable phase shifter angle in the compound transformer, which is capable of achieving control targets by way of phase angle control much like a real PWM-controlled voltage source converter. The voltage relations between the sending and receiving side of the compound transformer is controlled via the variable tap changer ratio, which in case of a PWM-controlled VSC, corresponds to the amplitude modulation index [13, 14] of the converter. This gives rise to indirect reactive power control by way of direct nodal voltage magnitude control.

The bi-directional power flow control is also maintained by selecting the appropriate modes of operation in the compound transformer. The active power

control entails activating the active power functional equality constraint, which remains active throughout the solution process. However, in certain modes of operation where no active power regulation is desired, penalising its corresponding multiplier will deactivate the Lagrangian function associated with the active power control constraint.

The behaviour characteristics of the model developed in this chapter within the OPF algorithm has been tested thoroughly in a variety of simulations aimed at portraying different circumstances under which the compound transformer may be chosen to operate. In the AC stand-alone tests, the compound model has been tested as a stand-alone device with the purpose to verify whether all the control modes work properly. In the DC tests, the compound transformer models the operation of a voltage source converter used to feed a DC load. Using the phase shifter angle compensation in the compound transformer model, it has been observed that the new VSC model is capable of providing the required amount of active power to the DC node regardless of the changes in system conditions at the AC side, which means that the new VSC compound transformer model is capable of isolating the DC loads from the AC network. This particular characteristic of the compound transformer model plays a vital role in performing OPF calculations in systems with VSC-HVDC links. In the next chapter the details of modelling the VSC-HVDC systems using the new compound transformer model are explained.

## 4.8 References

- [1] Arrillaga, J., *High Voltage Direct Current Transmission*. London: The Institute of Electrical Engineers, 1998.
- [2] Acha, E., Agelidis, V. G., Anaya-Lara, O., Miller, T. J. E., *Power Electronic Control in Electrical Systems*: Newnes, 2002.
- [3] Sarkar, S., Vijayan, P., Aliprantis, D. C., Ajarapu, V., "Effect of grid voltage unbalance on operation of a bi-directional converter," presented at the Power Symposium, 2008. NAPS '08. 40th North American 2008.
- [4] Diaz, N. L., Barbosa, F. H., Trujillo, C. L., "Implementation of Nonlinear power flow controllers to control a VSC," presented at the Power Electronics and Motion Control Conference, 2008. EPE-PEMC 2008. 13th 2008.
- [5] Gengyin, L., Ming, Z., Jie, H., Guangkai, L., Haifeng, L., "Power Flow Calculation of Power Systems Incorporating VSC-HVDC," *Power System Technology, International Conference on*, pp. 1562-1566, Nov. 21-24 2004.
- [6] Lawrence, R., Middlekauff, S. (2005, Jan-Feb ) The new guy on the block: Applying distributed generation tools in power design systems. *Industry Applications Magazine, IEEE*. 54-59.

- [7] Leon, A. E., Solsona, J. A., Valla, M. J., "Control Strategy for hardware simplification of voltage source converter-based power applications," *Power Electronics, IET*, vol. 4, pp. 39-50, January 2011.
- [8] Hingorani, G. N., Gyungyi, L., *Understanding FACTS: Concepts and Technologies of Flexible AC Transmission Systems*: IEEE, 2000.
- [9] Radomski, G., "Modelling and modulation of voltage source converter," presented at the Power Electronics and Motion Control Conference, 2008. EPE-PEMC 2008. 13th, 2008.
- [10] Krug, D., Bernet, S., Dieckerhoff, S., "Comparison of state-of-the-art voltage source converter topologies for medium voltage applications," in *Industry Applications Conference, 2003. 38th IAS Annual Meeting. Conference Records of the*, 2003, pp. 168-175.
- [11] Angeles-Camacho, C., Tortelli, O. L., Acha, E., Fuerte-Esquivel, C. R., "Inclusion of a High Voltage DC-Voltage Source Converter Model in a Newton-Raphson Power Flow Algorithm," *Generation, Transmission and Distribution, IEE Proceedings*, vol. 150, pp. 691-696, Nov. 2003.
- [12] Acha, E., Fuerte-Esquivel, C. R., Ambriz-Perez, H., Angeles-Camacho, C., *FACTS Modelling and Simulation in Power Networks*: John Wiley & Sons Ltd., 2005.
- [13] Guoqing, L., Jian, Z. , "Available Transfer Capability Calculation for AC/DC Systems with VSC-HVDC," presented at the Electrical and Control Engineering (ICECE), 2010 International Conference on,, 2010.
- [14] Pizano-Martinez, A., Fuerte-Esquivel, C. R., Ambriz-Perez, H., Acha, E., "Modeling of VSC-Based HVDC Systems for a Newton-Raphson OPF Algorithm," *Power Systems, IEEE Transactions on*, vol. 22, pp. 1794-1803, Nov. 2007.
- [15] Zhang, X., Handshcin, E. J., "Optimal Power Flow Control By Converter Based FACTS Controllers," presented at the AC-DC Power Transmission, 2001. Seventh International Conference on, 2001.
- [16] Wei, X., Chow, J. H., Fardanesh, B., Edris, A., "A common modeling framework of voltage-sourced converters for loadflow, sensitivity, and dispatch analysis," in *Power Engineering Society General Meeting, 2003, IEEE*, 2003, pp. 2569-2575.
- [17] Sreejaya, P., Iyer, S. R., "Optimal reactive power flow control for voltage profile improvement in AC-DC power systems," presented at the Power Electronics, Drives and Energy Systems (PEDES) & 2010 Power India, 2010 Joint International Conference on, 2010.
- [18] Nabavi Niaki, S. A., "A novel steady-state model and principles of operation of phase-shifting transformer comparable with FACTS new devices," in *Power Systems Technology, 2002. Proceedings. PowerCon 2002. International Conference on*, 2002, pp. 1450-1457.
- [19] Gitizadeh, M., Khalilnezhad, H., "Phase Shifter Transformers Optimum Allocation in Power Systems Using a Combinational Method," presented at the Power and Energy, PECON2010, IEEE International Conference on, 2010.
- [20] Momoh, J., A., Zhu, J., Z., "A new approach to optimal power flow with phase shifter," in *Systems, Man, and Cybernetics, 1998. 1998 IEEE International Conference on*, 1998, pp. 4794-4799.

- [21] Verboomen, J., Van Hertem, D., Schavemaker, P., H., Kling, W., L., Belmas, R., "Phase shifting transformers: principles and applications," in *Future Power Systems, 2005 International Conference on*, 2005.
- [22] Zhang, Y., Zhang, Y., Wu, B., Zhou, J., "Power injection model of STATCOM with control and operating limit for power flow and voltage stability analysis," *Electric Power Systems Research*, vol. 76, pp. 1003-1010, August 2006.

## **5 Advanced Mathematical Modelling of Back-to-Back, Point-to-Point and Multi-terminal VSC-HVDC Transmission Systems in OPF using Newton's Method**

This chapter introduces a new optimal power flow model for the High Voltage Direct Current Transmission systems that are based on Voltage Source Converters (VSC-HVDC). The model is suitable for OPF solutions for Lagrangian functions using Newton's iterative method. The compound transformer concept introduced in previous chapter has been used to model back-to-back, point-to-point and multi-terminal VSC-HVDC transmission systems. Since voltage source converters are capable of regulating network parameters independently, the VSC-HVDC systems are particularly suitable for safe and reliable integration of autonomous operating AC grids, such as local generation based micro-grids with each other and the utility grid. Furthermore, due to the PWM control of the voltage source converters, these self-commutated converters are capable of safe grid-integration of renewable sources of energy where the output voltage is prone to variations in both frequency and magnitude. Consequently, the VSC-HVDC systems are becoming an integral part of many modern power system designs, where flexibility of operation is a paramount necessity. They advantage the conventional line-commutated converter, due to their capability of controlling all the system parameters, which eventually help to improve system reliability and increase stability margins. Throughout this chapter, using the compound transformer concept, a comprehensive model for VSC-HVDC systems are developed within the OPF algorithm and tested against a variety of system conditions to verify its operational robustness. It has been observed that the compound transformer model is perfectly capable of simulating the HVDC power transmission at a common DC node. However, in order to fully realise the potential of compound transformers in modelling point-to-point HVDC systems, they are modified in such a way that they inherently include the DC link transmission losses. The models described in this chapter constitute the most realistic representation of a VSC-HVDC system within the OPF algorithm.

## 5.1 Introduction

The High Voltage Direct Current (HVDC) transmission systems that are based on fully controlled self-commutated Voltage Source Converters, dubbed VSC-HVDC system, are the newest advent in DC power transmission technology [1-7]. As stated in previous chapter, benefits of HVDC transmission over High Voltage AC transmission (HVAC), is mostly conspicuous in bulk power transmission over long distances (more than 700 km), where the impedance of the AC system plays a significant role in limiting its total transfer capability and at the same time reduces system stability margins by being more prone to frequency and/or voltage deviations due reactive power consumption by the AC transmission lines [1, 6-9]. As a result, since the AC system requires reactive power for maintaining the voltage, in an HVAC power transmission system, reactive power compensators are installed in several locations in order to ensure system's perpetual steady state operation [2].

The bulk power transmission capability is particularly severely limited in case of underground/submarine HVAC cables, due to the presence of highly capacitive currents generated by cables, which in turn reduces the permissible transfer distance to a few tens of kilometres [10]. By contrast, an HVDC cable exerts no capacitive charge and therefore there are virtually no distance limitations for HVDC submarine/underground cables except for the natural distance limit imposed by the cable's physical restrictions (for instance thermal limits) [9]. Consequently, the HVDC transmission systems are the ideal choice for transferring a large amount of generated active power from remotely located sources of energy, for instance offshore wind farms [6, 10-13].

On the other hand, HVAC interconnections require synchronous operation between their respective AC segments. A disturbance in a given segment may affect the operation of the rest of the system and introduce difficulties in recovery process of the system [14]. For example in case of active power imbalances in a segment the induced frequency deviations may be in such great extent that some systems may never recover towards a steady state point of operation [15]. Given enough generation capacity, an HVDC system is practically impervious to such implications

and therefore is a much more desired option for creating safe interconnections between multiple isolated AC systems [6, 8].

There are two technologies for HVDC power transmission systems, namely Current Source Converter based (CSC-HVDC) and the more advanced, more efficient Voltage Source Converter based (VSC-HVDC) [1, 3-5, 7, 8].

Most high power HVDC converters are in fact designed based on thyristor-controlled converters (for example a current source converter or CSC), which require commutation by the AC system [1, 6, 7]. Consequently, these line-commutated converters require a source of reactive power for commutation between valves and therefore are incapable of providing reactive power to the AC system, a great feat in the otherwise self-commutated converters [3, 6, 8, 9, 16, 17]. They are also susceptible to generating high levels of low order harmonics, which requires installing AC filters, which in turn provide the required reactive power compensation to the line-commutated converter in a conventional HVDC system [4, 6, 8]. Considering the shortcomings of the line-commutated converters, the voltage source converter, therefore, seems like an ideal choice for introducing both voltage and active power controllability to an interconnected power system [8, 18]. Consequently, the VSC-based systems are more beneficial than the conventional thyristor-controlled systems.

Similar to an individual voltage source converter, which is based on fully controlled power electronics (GTO or IGBT), the VSC-HVDC system parameters, namely active power flow as well as nodal voltages can also be controlled through fast pulse width modulation (PWM) schemes for switching the fully controlled power electronics [1, 3-6, 8, 10, 16-20]. The PWM essentially controls the converters' active and reactive power flows by controlling the phase angle and magnitude of the converters nodal voltage against the AC system voltage respectively [4, 6, 16, 17]. As mentioned in chapter four, with VSC-HVDC systems, the bi-directional independent active power flow control on the AC side of the converters, essentially improves system reliability by realising four-quadrant power control operation [3, 4, 6, 21].

The most significant aspect of seamless active power regulation capability of VSC-HVDC is that they can be utilised to link autonomous power networks (either distribution systems or industrial loads or even renewable sources of energy) to create an interconnected web of independently operating systems without the need for re-synchronisation [1, 6, 8].

One of the key advantages of VSC-HVDC tie lines in segmented power systems is that they improve power flow flexibility within the interconnected network; through seamless active power flow control the system's total active power can then be optimally dispatched between segments in such a way that that agrees well within the network's stability limits [8, 15]. Provided that there is enough generation capacity in a segmented system, the VSC-HVDC active power control capability is particularly helpful to circumvent system-wide frequency collapses in case of undesired disturbances, since the active power is transmitted through the converters in a controlled manner and the disturbed section is effectively isolated from the rest of the system by the converters. This feature is mostly useful in connecting local power networks [22] or to create DC hubs in order to convert large scale AC networks into a series of smaller, more manageable segments [8, 15].

On the other hand, the system voltage stability may also increase in light of the fact that VSC-HVDC systems, unlike conventional HVDC systems, are capable of providing reactive power to the AC system as well eliminating the need for sources of reactive power compensation to achieve successful commutation [1, 4, 9, 10, 16]. In the voltage source converter, utilising PWM amplitude modulation ratio can directly control the system voltage magnitude.

Due to utilising fast switching frequencies in PWM-controlled converters, the VSC-HVDC system, in comparison with a conventional HVDC system, generates lower levels of low order harmonics and therefore contributes to lowering the costs of construction by requiring smaller harmonics filters [1, 3, 4, 12, 23]. The only downside of high PWM switching frequencies is that the converter's internal switching losses may increase significantly. As a result, in this project the internal switching losses are included in the mathematical OPF model of VSC-HVDC systems as a shunt resistive branch.

The VSC-HVDC systems are used in both back-to-back and point-to-point systems much like a conventional HVDC transmission system. A point-to-point VSC-HVDC system is a DC transmission system in which the DC power flows through a DC transmission line between two separate points, whereas a back-to-back VSC-HVDC system is a DC transmission system in which there is no DC transmission line and the converter stations are virtually connected together. Since there is practically no limitation on the number of terminals in VSC-HVDC systems they can be used to form multi-terminal configurations for virtually any number of terminals [6, 8].

Furthermore, due to independent active and reactive power control in VSC-HVDC systems, a weak AC system can seamlessly be connected to a stronger system (for example the utility grid) in such a fashion that system stability may not be compromised [4, 24]. A weak AC system may be categorised as a low inertia system in which there are no (or few) generators present [24]. Connecting such systems to a strong system, for instance the utility grid, using conventional HVDC systems without means of increasing system generation capacity is virtually impossible since the thyristor-based converters would not be capable of line-commutation [1]. However, since a VSC-HVDC system generates voltage waveform by means of PWM, they can be used as interconnection systems for weaker AC grids without jeopardising the voltage stability [24].

The VSC-HVDC systems can also be used to interconnect renewable sources of energy such as offshore wind farms that are susceptible to voltage/frequency deviations to the utility grid [4, 6, 8, 10, 11, 13]. In case of an offshore wind farm, for instance, the VSC-HVDC system is tasked with regulating the system frequency using seamless active power control while at the same time supplying reactive power to the induction generators in the offshore wind farm realising a stable voltage output [11].

Fast and reliable voltage regulation realised through PWM switching coupled with the need for no reactive power compensation to achieve commutation in voltage source converter essentially leads to producing a stable output voltage waveform impervious to any deviations in the voltage magnitude which may bring about instability in the system. Consequently from the power system working perspective,

the VSC-HVDC system is much more beneficial over the conventional HVDC transmission links.

The major benefits of VSC-HVDC transmission systems over the more conventionally used CSC-HVDC systems (based on line commutated converters) as well as HVAC are categorised in the following [1, 3-6, 8-10, 13, 16, 18, 21, 23, 24]:

1. They are capable of performing four quadrant power operation due to their bi-directional independent active and reactive power regulations
2. They yield improved voltage stability margins due to the direct voltage control capability of the voltage source converter; useful in interconnecting power grids that are most susceptible to voltage magnitude variations, for instance weak AC grids, distributed energy systems and micro-grids
3. They yield improved frequency stability margins through seamless active power transfer regulation between different autonomous segments provided that enough generation resources are available
4. They are practically free of commutation failure even in systems with small generation capacity (weak AC grid, passive loads) due to the self-commutating capability of the voltage source converter
5. They produce smaller levels of harmonics due to the higher semi-conductor switching frequencies used by the PWM control but they introduce high frequency harmonics that require special attention
6. They have faster response time than conventional HVDC to the system dynamics of the higher PWM switching frequency
7. They are useful for grid-connection of renewable sources of energy, where a stable output voltage waveform is desired

In the following sections, a detailed mathematical model for VSC-HVDC transmission systems, based on the compound transformer model has been

presented for back-to-back, point-to-point and multi-terminal VSC-HVDC configurations. It has been shown that using compound transformers, the VSC-HVDC transmission system can effectively be modelled within the optimal power flow algorithm and all of its operational characteristics, namely active power flow control as well as nodal voltage magnitude control, will be included in the system of equations as explicit state variables. Furthermore, the models described in this chapter are suitable for multi-terminal configurations, where more than two converter stations (or terminals) are used to link multiple AC systems to each other. Unlike conventional HVDC, there is virtually no restriction on the number of terminals in a multi-terminal VSC-HVDC topology and models presented in this chapter can be expanded to incorporate however many number of terminals required.

## **5.2 Advanced Back-to-Back VSC-HVDC Mathematical Model in Optimal Power Flow Algorithm using Compound Transformer Model**

In the following section, the compound transformer model developed in previous chapter has been used and expanded to model high voltage direct current transmission systems based on voltage source converters in the OPF algorithm. The mathematical formulation of the compound transformer model has remained similar to previous chapter for back-to-back configurations, however in order to include the DC link losses, the OPF formulation is modified for modelling point-to-point DC power transmission (VSC-HVDC with DC link present). The additional reactive power constraint, to ensure a zero reactive power in the DC bus is also added to the system formulation for all VSC-HVDC models. The operation of the VSC-HVDC modelled with compound transformer is governed by selecting proper equality constraints on voltage and active powers which are in turn based on the system requirements as well as limits. In the following sub-sections, the OPF formulation regarding back-to-back VSC-HVDC systems has been presented.

### **5.2.1 Back-to-Back VSC-HVDC Compound Model's OPF Formulation**

The back-to-back VSC-HVC system typically comprises two converter stations, one acting as a rectifier, converting AC power into DC, whereas the other acts as an inverter, converting DC power to AC. Back-to-back HVDC links are mostly used to synchronise two different AC networks operating in different frequencies to each other [1]. However, they may also be used to facilitate a safe, reliable and flexible interconnection between multiple isolated AC grids [1, 7, 8].

Bi-directional independent active and reactive power control on the AC side will give the voltage source converter stations the ability to effectively control the network parameters in order to achieve network operational requirements and maintain stability even when feeding the most sensitive loads.

The simplest configuration of a VSC-HVDC system is a back-to-back configuration comprised of two converters, namely a rectifier and an inverter. Throughout this research a VSC-HVDC system comprising of only two VSC stations is called a Two-terminal system. Any VSC-HVDC system comprising of more than two voltage source converter stations is however called a Multi-terminal system. In the following section, the mathematical formulation of both two- and multi-terminal back-to-back VSC-HVDC systems within the optimal power flow algorithm using the compound transformer Lagrangian function has been explained thoroughly and the required modes of operation to achieve a realistic HVDC power have been elaborated.

#### **5.2.1.1 Two-terminal Back-to-Back VSC-HVDC OPF Model using Compound Transformer**

In order to form a two-terminal back-to-back VSC-HVDC link, two compound transformers (shown in figure 4.4a) representing two voltage source converter stations are connected to each other through their receiving ends, which then act as a common DC bus as shown in figure (5.1).

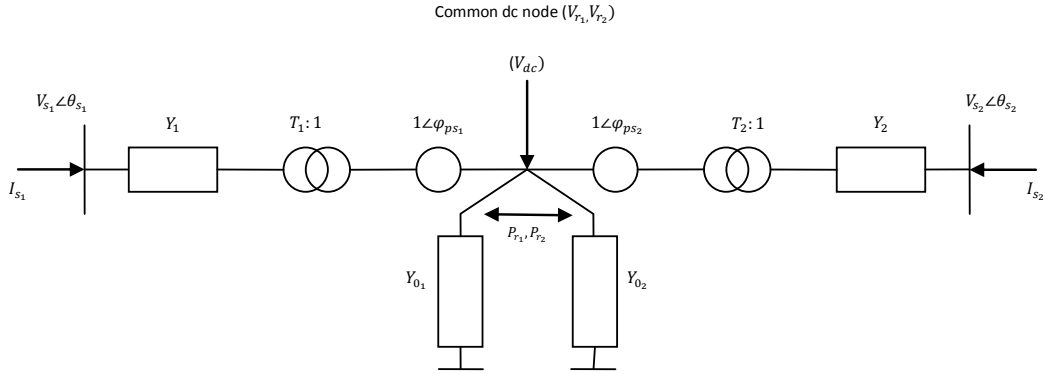


**Figure 5.1 – Two-terminal Back-to-Back VSC-HVDC Compound Transformer Model (Notice that the common node is at the receiving ends)**

As mentioned in previous chapter, the active power regulation at the DC bus is obtained via the operation of the phase shifter in the compound transformer. As seen from figure (5.1), the nodal admittance matrix for the two-converter system is derived based on the compound transformer's nodal admittance matrix given in equation (4.3) in polar coordinates:

$$Y_{T_2} = \begin{bmatrix} Y_1 & & -T_1 Y_1 e^{j\varphi_{ps1}} & \\ & Y_2 & & -T_2 Y_2 e^{j\varphi_{ps2}} \\ -T_1 Y_1 e^{-j\varphi_{ps1}} & & T^2 Y_1 + Y_{0_1} & \\ & -T_2 Y_2 e^{-j\varphi_{ps2}} & & T^2 Y_2 + Y_{0_2} \end{bmatrix} \quad 5.1$$

Referring to the general expression for the complex nodal apparent power for the compound transformer presented in equation (4.8) for an individual compound transformer, the complex nodal apparent powers for the two-terminal back-to-back VSC-HVDC in figure (5.1) are calculated as follows:

$$\begin{bmatrix} S_{s_1} \\ S_{s_2} \\ S_{r_1} \\ S_{r_2} \end{bmatrix} = \begin{bmatrix} V_{s_1} e^{j\theta_{s_1}} & & & \\ & V_{s_2} e^{j\theta_{s_2}} & & \\ & & V_{r_1} e^{j\theta_{r_1}} & \\ & & & V_{r_2} e^{j\theta_{r_2}} \end{bmatrix} \times \begin{bmatrix} Y_1^* & & -T_1 Y_1^* e^{-j\varphi_{ps1}} & \\ & Y_2^* & & -T_2 Y_2^* e^{-j\varphi_{ps2}} \\ -T_1 Y_1^* e^{j\varphi_{ps1}} & & T_1^2 Y_1^* + Y_{0_1}^* & \\ & -T_2 Y_2^* e^{j\varphi_{ps2}} & & T_2^2 Y_2^* + Y_{0_2}^* \end{bmatrix} \begin{bmatrix} V_{s_1} e^{-j\theta_{s_1}} \\ V_{s_2} e^{-j\theta_{s_2}} \\ V_{r_1} e^{-j\theta_{r_1}} \\ V_{r_2} e^{-j\theta_{r_2}} \end{bmatrix} \quad 5.2$$

Eventually the complex nodal apparent powers for each converter station are derived from equation (5.2).

Sending End:

$$S_{s_1} = V_{s_1}^2 Y_1^* - T_1 V_{s_1} V_{r_1} Y_1^* e^{j(\theta_{s_1} - \theta_{r_1} - \varphi_{ps_1})} \quad 5.3$$

And

$$S_{s_2} = V_{s_2}^2 Y_2^* - T_2 V_{s_2} V_{r_2} Y_2^* e^{j(\theta_{s_2} - \theta_{r_2} - \varphi_{ps_2})} \quad 5.4$$

Receiving End:

$$S_{r_1} = (T_1^2 Y_1^* + Y_{0_1}^*) V_{r_1}^2 - T_1 V_{r_1} V_{s_1} Y_1^* e^{j(\theta_{r_1} - \theta_{s_1} + \varphi_{ps_1})} \quad 5.5$$

And

$$S_{r_2} = (T_2^2 Y_2^* + Y_{0_2}^*) V_{r_2}^2 - T_2 V_{r_2} V_{s_2} Y_2^* e^{j(\theta_{r_2} - \theta_{s_2} + \varphi_{ps_2})} \quad 5.6$$

Ultimately, given equations (5.3-5.6), the nodal active and reactive powers for the two-terminal VSC-HVDC system is developed in a similar fashion as for an individual compound transformer presented in equations (4.11-4.14) and therefore they will not be repeated here. Notice that the DC bus voltage is defined with the general expression,  $V_{r_i} \angle \theta_{r_i}$ , however since the DC bus voltage does not have an angle, The angle  $\theta_{r_i}$ , is accordingly penalised to properly constitute the conditions of the DC bus voltage.

In order to include the two-terminal back-to-back VSC-HVDC link model to the optimal power flow formulation a new vector of state variables is defined and added to the vector of system state variables:

$$z_{ps} = [\varphi_{ps_i}, T_i, \lambda_{\varphi_{ps_i}}]^T \quad 5.7$$

Each compound transformer representing the converter stations possesses its own control-constraints on both nodal voltages as well as active power flows. Knowing

that a real voltage source converter is capable of four-quadrant power flow operation, the compound transformers in a two-terminal back-to-back VSC-HVDC system should also be capable of injecting/consuming both active and reactive power to and from the AC system.

For the  $i$ th compound transformer in a two-terminal configuration the following constraints are defined on active power as well as nodal voltage magnitude.

The functional equality on compound transformer's active power flow for the  $l$ th side of the  $i$ th compound transformer:

$$P_{ps_i}^{(l)} - P_{spe_i} = 0 \quad 5.8$$

( $l \in [1,2]$  with 1 corresponds to sending and 2 to receiving ends of the compound transformer)

The nodal voltage variable equality constraint in the  $j$ th side of the  $i$ th compound transformer:

$$V_{j_i} - V_{spe_i} = 0 \quad 5.9$$

Consequently, the functional equality constraint on the power is added to the system Lagrangian using its associated Lagrangian multiplier, namely  $\lambda_{\varphi_{ps_i}}$ . Furthermore, should the need arises, the variable equality constraint is added to the system formulation by using the appropriate pure penalty functions as explained in previous chapters. The penalty function used to enforce the nodal voltage variable equality constraint is similar to the general quadratic pure penalty function given in equation (4.21) in chapter four. It is added to the system Lagrangian only if the compound transformers are regulating the voltages. The general modes of operation of a back-to-back VSC-HVDC system are further explained later on in this chapter. It should be noted that apart from the exclusive control constraints for the compound transformer modes of operation the normal system constraints, namely the power balance equations must also hold for normal steady state operation throughout the OPF solution process.

The Lagrangian function for a two-terminal back-to-back VSC-HVDC system comprising of two compound transformers is shown in equation (5.10).

$$L_{PS} = \sum_{j=1}^2 \sum_{i=s}^r \lambda_{p_{i_j}} (P_{i_j}^{calc} - P_{g_{i_j}} + P_{d_{i_j}}) + \sum_{m=1}^2 \sum_{k=s}^r \lambda_{q_{k_m}} (Q_{k_m}^{calc} - Q_{g_{k_m}} + Q_{d_{k_m}}) + \sum_{n=1}^2 \lambda_{p_{ps_n}} (P_{ps_n}^{(l)} - P_{spe_n}) \quad 5.10$$

$P_{i_j}^{calc}$  is the total calculated active power in the  $i$ th side of the  $j$ th converter including its exclusive nodal active power

$Q_{k_m}^{calc}$  is the total calculated reactive power in the  $k$ th side of the  $m$ th converter including its exclusive nodal reactive power (the compound model's nodal reactive power at the DC bus is maintained at zero by an additional constrained explained further in this chapter)

$P_{ps_n}^{(l)}$  is the  $n$ th compound transformer power flow on its  $l$ th side ( $l \in [1,2]$ )

By selecting the active power control constraints for both compound transformers at their receiving ends (DC bus) throughout the solution process, the DC power flow balance between the two converters are obtained. The variable phase shifter angle is responsible to compensate for the required phase angle difference between the converters and the AC system so that the required DC active power flow requirements are met.

### 5.2.1.2 Multi-terminal Back-to-Back VSC-HVDC OPF Model using Compound Transformer

The back-to-back multi-terminal VSC-HVDC compound transformer model has been shown in figure (5.2).

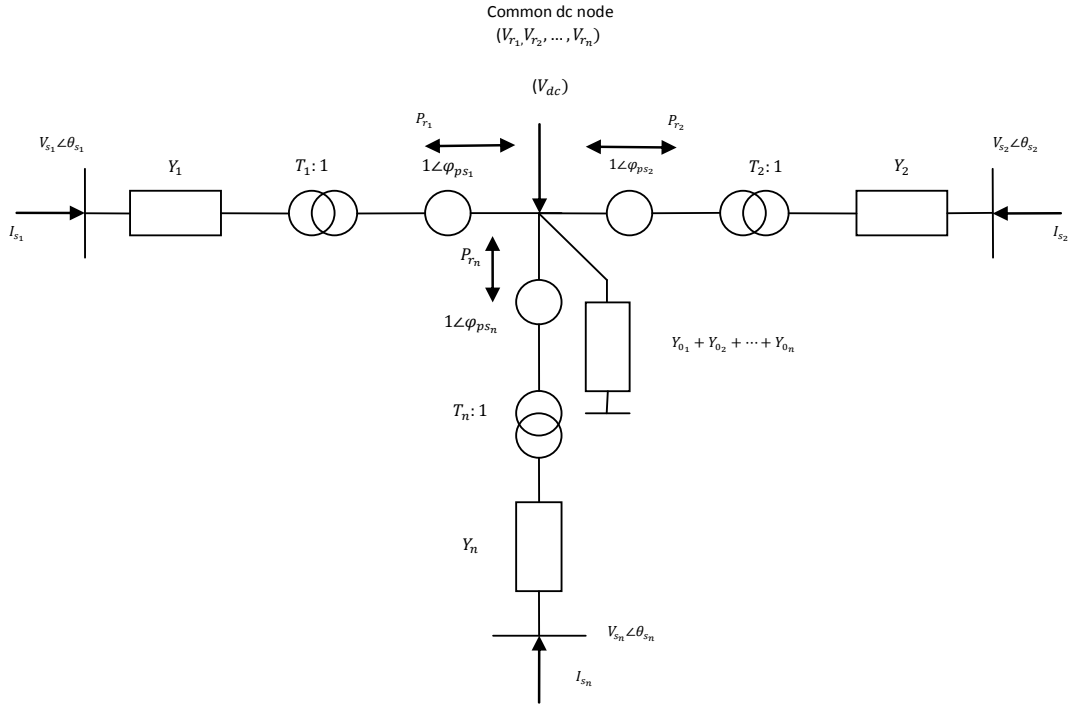


Figure 5.2 - Multi-terminal Back-to-Back VSC-HVDC Compound Transformer Model Configuration

The admittance matrix for a multi-terminal back-to-back VSC-HVDC system is constructed similarly to the two-terminal system in figure (5.1) and is shown in equation (5.11).

$$Y_{T_n} = \begin{bmatrix} Y_1 & & \dots & -T_1 Y_1 e^{j\varphi_{ps_1}} & & \dots \\ & Y_2 & & & -T_2 Y_2 e^{j\varphi_{ps_2}} & \\ \vdots & & \ddots & \vdots & & \ddots \\ -T_1 Y_1 e^{-j\varphi_{ps_1}} & & & Y_n & & -T_n Y_n e^{j\varphi_{ps_n}} \\ & -T_2 Y_2 e^{j\varphi_{ps_2}} & & & T_1^2 Y_1 + Y_{0_1} & \dots \\ \vdots & & \ddots & & \vdots & T_2^2 Y_2 + Y_{0_2} \\ & & & -T_n Y_n e^{j\varphi_{ps_n}} & & \ddots \\ & & & & & T_n^2 Y_n + Y_{0_n} \end{bmatrix} \quad 5.11$$

This equation is essentially an expansion of equation (5.1), instead of forming a  $4 \times 4$  matrix; the admittance matrix for back-to-back multi-terminal VSC-HVDC is expanded to incorporate a  $2n \times 2n$  matrix for  $n$  converters.

Equation (5.11) therefore is the generalisation of the admittance matrix in equation (5.1) that is valid for a multi-terminal back-to-back VSC-HVDC system for any number of converters.



Eventually for  $ncomp > 2$  converters in a multi-terminal VSC-HVDC system modelled by compound transformers, equation (5.10) is expanded as such:

$$L_{PS} = \sum_{j=1}^{ncomp} \sum_{i=s}^r \lambda_{p_i} (P_{i_j}^{calc} - P_{g_{i_j}} + P_{d_{i_j}}) + \sum_{m=1}^{ncomp} \sum_{k=s}^r \lambda_{q_{k_m}} (Q_{k_m}^{calc} - Q_{g_{k_m}} + Q_{d_{k_m}}) + \sum_{n=1}^{ncomp} \lambda_{\varphi_{ps_n}} (P_{ps_n}^{(l)} - P_{spe_n}) \quad 5.15$$

The Lagrangian function in equation (5.15) is the most general format of the system Lagrangian function in a power system incorporating a multi-terminal back-to-back VSC-HVDC.

### 5.2.2 Reactive Power Constraint

For a realistic representation of HVDC systems, it is imperative that the total reactive power injection at DC bus remains zero, which means that there should not be any reactive power at the DC side of the converter model. As mentioned earlier, the compound transformer models the characteristics of PWM control in the voltage source converter, however, it is incapable of limiting the reactive power injection at DC bus to zero. This is because the tap changer ratio, namely  $T$  is responsible for direct voltage magnitude regulations (on either ends of the compound transformer), which means that the reactive power flow is free to vary within the system's permitted operational limits as long as there is no voltage/tap changer ratio limit violation, in other words, the direct voltage regulation feature of the tap changer has an indirect effect on the amount of reactive power needed for the system to maintain that voltage making the DC side bus act as a type PV bus.

Consequently, if there is no constraint on this amount of power, the converter model draws reactive power from the system and ultimately the converter itself. Therefore, in order to circumvent the effects of reactive power consumption by the DC side bus in the compound transformer model, the shunt susceptance of the converter therefore needs to be variable, acting much like an SVC (Static VAR Compensator), to compensate for the excess reactive power injected to the DC bus, converting it to a type PVQ bus, with Q always set to zero per unit.

In order to properly model the reactive power constraint at the DC side bus (or receiving end), the vector of state variables in equations (4.15) and subsequently in (5.7) needs to be augmented by the value of the variable shunt susceptance of the

compound model, namely,  $B_0$ . The variable shunt susceptance is then constrained within the VSCs' capacitive range, which means that the system voltage regulation is subject to the converters' capacitive range.

The receiving end reactive power is added to the system formulation as a functional equality as shown in equation (5.16).

$$Q_r = 0 \quad 5.16$$

Adding a new functional equality constraint to the system formulation means creating a new Lagrangian in form of equation (5.17) using the multiplier and  $\lambda_B$ .

$$L_{Q_r} = \lambda_B (Q_r - 0) \quad 5.17$$

Eventually, the vector of state variables will be expanded to incorporate the new variable shunt susceptance as well as the reactive power constraint's multiplier.

$$z_{ps} = [\varphi_{ps}, T, \lambda_{\varphi_{ps}}, B_0, \lambda_B]^T \quad 5.18$$

Consequently, the following state variables need to be initiated at the start of OPF algorithm in order to properly model the behaviour of a VSC-HVDC system modelled by compound transformers for both back-to-back and point-to-point applications.

By adding the reactive power constraint the Lagrangian function in equation (5.15) takes the following form:

$$L_{PS} = \sum_{j=1}^{ncomp} \sum_{i=s}^r \lambda_{p_i} (P_{i_j}^{calc} - P_{g_{ij}} + P_{d_{ij}}) + \sum_{m=1}^{ncomp} \sum_{k=s}^r \lambda_{q_{km}} (Q_{k_m}^{calc} - Q_{g_{km}} + Q_{d_{km}}) + \sum_{n=1}^{ncomp} \lambda_{\varphi_{ps_n}} (P_{ps_n}^{(l)} - P_{spe_n}) + \sum_{\alpha=1}^{ncomp} \lambda_{B_\alpha} (Q_{r_\alpha} - 0.0) \quad 5.19$$

### 5.2.3 Linear System of Equations

The OPF linear system of equations is formed with respect to the Lagrangian introduced in equation (5.19) for a multi-terminal back-to-back VSC-HVDC system as such:

For the  $i$ th converter station equation (4.23) is re-written as such:

$$\begin{bmatrix}
 \nabla_{\theta^2}^2 L & \nabla_{\theta V}^2 L & \nabla_{\theta \varphi}^2 L & \nabla_{\theta T}^2 L & \nabla_{\theta B_0}^2 L & \nabla_{\theta} P^{calc} & \nabla_{\theta} Q^{calc} & \nabla_{\theta} P_{ps}^{(k)} & \nabla_{\theta} Q_r^{calc} \\
 \nabla_{V\theta}^2 L & \nabla_{V^2}^2 L & \nabla_{V\varphi}^2 L & \nabla_{VT}^2 L & \nabla_{VB_0}^2 L & \nabla_V P^{calc} & \nabla_V Q^{calc} & \nabla_V P_{ps}^{(l)} & \nabla_V Q_r^{calc} \\
 \nabla_{\varphi\theta}^2 L & \nabla_{\varphi V}^2 L & \nabla_{\varphi^2}^2 L & \nabla_{\varphi T}^2 L & \nabla_{\varphi B_0}^2 L & \nabla_{\varphi} P^{sr} & \nabla_{\varphi} Q^{sr} & \nabla_{\varphi} P_{ps}^{(l)} & \nabla_{\varphi} Q_r^{calc} \\
 \nabla_{T\theta}^2 L & \nabla_{TV}^2 L & \nabla_{T\varphi}^2 L & \nabla_{T^2}^2 L & \nabla_{TB_0}^2 L & \nabla_T P^{sr} & \nabla_T Q^{sr} & \nabla_T P_{ps}^{(l)} & \nabla_T Q_r^{calc} \\
 \nabla_{B_0\theta}^2 L & \nabla_{B_0 V}^2 L & \nabla_{B_0 \varphi}^2 L & \nabla_{B_0 T}^2 L & \nabla_{B_0}^2 L & \nabla_{B_0} P^{sr} & \nabla_{B_0} Q^{sr} & \nabla_{B_0} P_{ps}^{(l)} & \nabla_{B_0} Q_r^{calc} \\
 \nabla_{\theta} P^{calc} & \nabla_V P^{calc} & \nabla_{\varphi} P^{sr} & \nabla_T P^{sr} & \nabla_{B_0} P^{sr} & 0 & 0 & 0 & 0 \\
 \nabla_{\theta} Q^{calc} & \nabla_V Q^{calc} & \nabla_{\varphi} Q^{sr} & \nabla_T Q^{sr} & \nabla_{B_0} Q^{sr} & 0 & 0 & 0 & 0 \\
 \nabla_{\theta} P_{ps}^{(l)} & \nabla_V P_{ps}^{(l)} & \nabla_{\varphi} P_{ps}^{(l)} & \nabla_T P_{ps}^{(l)} & \nabla_{B_0} P_{ps}^{(l)} & 0 & 0 & 0 & 0 \\
 \nabla_{\theta} Q_r^{calc} & \nabla_V Q_r^{calc} & \nabla_{\varphi} Q_r^{calc} & \nabla_T Q_r^{calc} & \nabla_{B_0} Q_r^{calc} & 0 & 0 & 0 & 0
 \end{bmatrix}
 \times
 \begin{bmatrix}
 \Delta\theta \\
 \Delta V \\
 \Delta\varphi_{ps} \\
 \Delta T \\
 \Delta B_0 \\
 \Delta\lambda_p \\
 \Delta\lambda_q \\
 \Delta\lambda_{\varphi_{ps}} \\
 \Delta\lambda_B
 \end{bmatrix}
 = -
 \begin{bmatrix}
 \nabla_{\theta} L \\
 \nabla_V L \\
 \nabla_{\varphi_{ps}} L \\
 \nabla_T L \\
 \nabla_{B_0} L \\
 \Delta P^{calc} \\
 \Delta Q^{calc} \\
 (P_{ps}^{(l)} - P_{specified}) \\
 (Q_r - 0.0)
 \end{bmatrix}
 \quad 5.20$$

By iteratively solving equation (5.20) the OPF generates the system optimum operating point whilst at the same time adhering to the compound transformer exclusive control constraint to control system operation. The reactive power constraint guarantees that there would be no reactive power flow in the DC bus. It should be reminded that the exclusive state variables associated with the compound transformer are checked against any limit violations and should the need arises they are enforced towards their respective boundaries using exact penalty functions. It should be noted that equation (5.16) is true for both two- and multi-terminal back-to-back VSC-HVDC configurations.

### 5.2.4 Back-to-Back VSC-HVDC Compound Model's Modes of Operation

In order to properly model the operation of a VSC-HVDC system, the compound models used need to be operated in either power only or combined power/voltage control modes via activating the appropriate voltage/power control constraints (equations 5.8 and 5.9) as shown in table (5.1).

Mode	Control State	Power Equality	Voltage Equality
Power Only	Mode 3	Activate Lagrangian Function	Remove Penalty Function
Voltage/Power	Mode 4	Activate Lagrangian Function	Add Penalty Function

**Table 5.1 - Back-to-Back VSC-HVDC Compound Model's Plausible Modes of Operation**

Generally, in a typical VSC-HVDC system, one converter is tasked with controlling the voltage at the DC bus whereas the other converter is tasked with controlling the active power flow. However, when the voltage source converters are modelled as compound transformers, both devices have to be set to power control mode in order to facilitate DC power flow transfer as shown in figure (5.3) below.

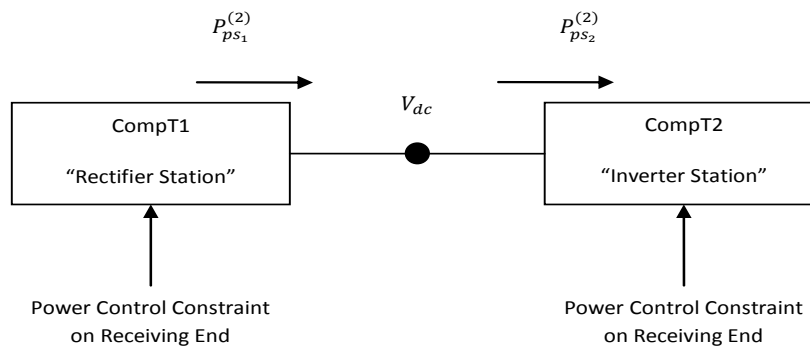


**Figure 5.3 - A two-station Back-to-Back VSC-HVDC System modelled with Compound Transformers (Notice the Active Power Control Constraints are on the receiving ends)**

In the following configuration for a back-to-back VSC-HVDC system, the first compound model dubbed “CompT1” acts as a rectifier station with an active power flow injecting to the DC bus.

Therefore its associated power control constraint corresponding to the compound transformer’s active power flow is activated; hence equation (5.8) is re-written as follows:

$$P_{ps_1}^{(2)} - P_{spe_1} = -P_{r_1} - P_{spe_1} \quad 5.21$$

The minus sign in the above equation indicates that the power is flowing from the converter to the DC node, thus realising rectification.

On the other hand the second compound model, namely “CompT2” behaves as an inverter, and therefore its associated functional equality on its power flow is re-written as such:

$$P_{ps_2}^{(2)} - P_{spe_1} = +P_{r_2} - P_{spe_1} \quad 5.22$$

The plus sign indicates that the active power is entering the second converter from the DC node, hence achieving inverting operation. The power signs here are merely notations, which are used so as to determine the direction of the active power flow to and from the converters. If the power enters the converter from the DC bus, hence if the converter operates as an inverter, the sign would be positive, whereas if it flows out of the converter and to the DC bus, hence if it operates as a rectifier, the sign would be negative. This notation method has been used infrequently throughout this chapter to better describe the rectification and inversion operation of the voltage source converter models.

In the following example, in order to preserve the rectifier-inverter operation and thus preserving a unidirectional DC power, “CompT1” has to inject power to the DC node, whereas “CompT2” has to receive power from the DC node and therefore their associated powers are negative and positive respectively. Consequently, choosing positive signs for both converters will obviously yield to inaccurate or even unfeasible solutions. In order to bind the functional equality constraints for converters’ active powers, their associated Lagrangians are activated and added to the system Lagrangian as shown in equations (5.23) and (5.24).

The rectifier station:

$$L_{\lambda_{\varphi_{ps_1}}} = \lambda_{\varphi_{ps_1}} (P_{ps_1}^{(2)} - P_{spe_1}) = \lambda_{\varphi_{ps_1}} (-P_{r_1} - P_{spe_1}) \quad 5.23$$

And the inverter station:

$$L_{\lambda_{\varphi_{ps_2}}} = \lambda_{\varphi_{ps_2}} (P_{ps_2}^{(2)} - P_{spe_1}) = \lambda_{\varphi_{ps_2}} (+P_{r_2} - P_{spe_1}) \quad 5.24$$

In order to maintain the active power balance in DC node, thus preserving the normal steady state operating conditions in the system, both converters are constrained towards a similar amount of pre-determined active power flow, namely  $P_{spe_1}$ . Since there is no DC link losses in a back-to-back configuration maintaining the active power balance at the DC node is done simply by selecting equal functional constraints for each rectifier-inverter set of converters (equations 5.23 and 5.24).

However, in a point-to-point VSC-HVDC system where the active power is flowing through a DC transmission link from one converter to the other, the situation is changed, since now there is the element of DC transmission losses that need to be taken into account. Mathematically, the calculated nodal powers developed for the back-to-back VSC-HVDC compound model (equation 5.13 and 5.14) is incapable of maintaining the power balance in such systems. However, by expanding the compound transformer model in such a way that it accounts for the DC transmission losses inherently, the active power balance is maintained. This fact is further explained later where the mathematical model for the expanded compound transformer model is introduced. Referring to the example in figure (5.3), if the rectifier station, is tasked with keeping the voltage magnitude at DC node to a certain pre-determined amount, its mode of operation is set to 4.2.2., whereas the inverter station operates in mode 3.2.0. with no voltage regulation.

In accordance with the mathematical formulation of the compound transformer model, the second station is also capable of regulating the voltage in its sending end (hence the AC node), and its mode of operation can be changed to 4.1.2. indicating that it regulates voltage in its AC side bus realising indirect reactive power control in the AC side. The different permitted control modes for a back-to-back VSC-HVDC compound transformer model are summarised in table (5.2) below:

<b>Converters' Plausible Control Modes</b>	<b>Voltage Control</b>	<b>Power Flow Control</b>
3.2.0.	N/A	DC Node
4.1.2.	AC Node	DC Node
4.2.2.	DC Node	DC Node

**Table 5.2 - Back-to-Back VSC-HVDC Converter Station's Control Modes**

### **5.3 Optimal Power Flow Control in Back-to-Back VSC-HVDC Transmission Systems**

In order to achieve network's optimum operating performance as well as minimise generation costs the optimal power flow algorithm has been carried out for the back-to-back VSC-HVDC compound transformer model in the following system simulations. The VSCs are used to control the active power between various autonomous sections in such a fashion that it agrees with system's operational restrictions. Consequently, in the VSC-HVDC compound transformer OPF models, the equality constraints associated with the compound transformers' active power flows are used to optimally control the active power between the independent sections defining new boundaries on the OPF solution space. Furthermore, they determine the direction of the flow of power from one converter to the other in the back-to-back VSC-HVDC system (as well as point-to-point systems). As mentioned in previous chapter, the voltage and active power control characteristics of a voltage source converter are modelled through the variable complex tap ratio in the compound transformers. Therefore, in voltage/power control modes, the complex tap ratio has to be free to take up any values according to its associated control constraint (whether on the voltage or active power) otherwise the system is incapable of controlling the state variable and the OPF will generate inaccurate results.

The OPF algorithm for the HVDC systems modelled with compound transformers is initialised similarly to the other FACTS-OPF scenarios with the exception of the slack bus. Since the HVDC links multiple sections in a power network in an asynchronous manner, correct implementation of the optimal power flow algorithm (as well as conventional power flow algorithms) calls for selection of multiple slack buses in the system, which essentially gives rise to several fully decoupled OPFs that are solved for one single Lagrangian function pertaining to the whole system. This fact has been explained more clearly with the assistance of the following key test scenarios. The data for all of the following system simulations has been given in Appendix II. The objective function is the same as in equation (2.53) for the 8-node benchmark system.

### 5.3.1 Two-terminal Back-to-Back VSC-HVDC

Figure (5.4) illustrates an OPF solution for a two-terminal back-to-back VSC-HVDC link. Each AC grid represents an independent AC grid with its own machine. The back-to-back VSC-HVDC system is used to connect the autonomous operating AC grids to each other in a controlled manner. The power is therefore being transferred through the VSC-HVDC link from node 1 to node 5 (infinite bus). Both nodes 1 and 5 are taken to be slack buses for their respective AC grids. In order to add the back-to-back compound transformer model to the system OPF formulation, its associated exclusive Lagrangian presented in equation (5.19), is added to the system overall Lagrangian. The power balance equations associated with each compound transformer as well as the active power flow constraint and the DC reactive power constraint is included in this Lagrangian function. The complex nodal apparent powers associated with the back-to-back VSC-HVDC compound transformer model are calculated by solving equation (5.2). Consequently the nodal active and reactive powers associated with each compound transformer, namely equations (5.3-5.6), are derived from complex nodal apparent powers. The OPF is then solved for the two-terminal back-to-back system by solving the linear system of equations shown in equation (5.20) taking into account the vector of state variables pertaining to the compound transformers' controllable complex tap phasor (equation 5.7).

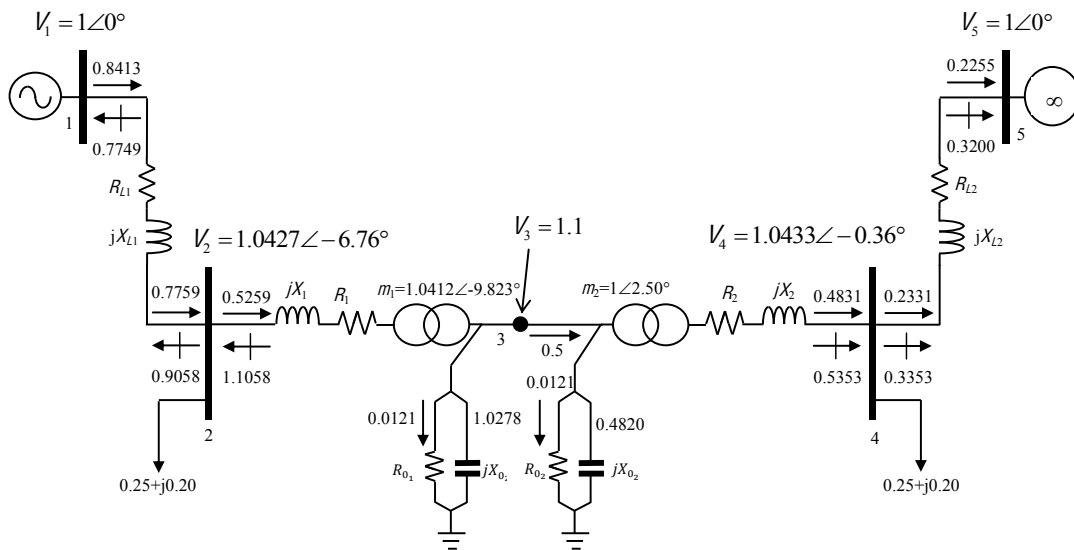


Figure 5.4 - Two-terminal Back-to-Back VSC-HVDC Compound Transformer Model OPF Solution (node "5" is the infinite bus)

According to the control equality constraints on both the converters' active power flows as well as their nodal voltage magnitudes the compound transformers' modes of operation are selected by activating the appropriate Lagrangian/penalty functions as shown in table (5.3). The rectifier station is also tasked with maintaining the DC nodal voltage magnitude to 1.1 per unit.

Converter	Mode of Operation	Power Equality	Voltage Equality	Power/Voltage Control
Rectifier Station	4.2.2.	Activate Lagrangian Function	Add Penalty Function	DC Node
Inverter Station	3.2.0.	Activate Lagrangian Function	Remove Penalty Function	DC Node

**Table 5.3 - Two-terminal Back-to-Back VSC-HVDC Compound Transformer Model Modes of Operation**

In order to activate the power equality constraint (equation 5.8) it is only necessary to add its corresponding Lagrangian to the system Lagrangian function using the appropriate multipliers, namely  $\lambda_{\varphi_{ps_i}}$ , which remains active throughout the solution process.

The voltage variable equality (equation 5.9), on the other hand, is added to the system formulation by penalising nodal voltage magnitude at the DC bus using a pure penalty function that has been described previously.

As seen from figure (5.4), the back-to-back system is connected between nodes 2 and 4 with node 3 being the DC node. Through activating the compound transformers' functional equalities on active power, the VSC-HVDC link regulates the DC power to 0.5 per unit. It should be noted that the objective function for the infinite bus corresponds to the value of the work whereas the objective function in node 1 corresponds to the cost of fuel generation. The OPF is run for the above system converging in three iterations and the following observations are immediately made following the results:

- Generator in node 1 generates 0.80 per unit of active power
- The power arriving at the inverter station in the back-to-back system is fixed to 0.5 per unit
- The power arriving at the infinite bus is approximately 0.22 per unit

- The phase angles in both slack buses must be penalised (towards zero or an arbitrary value) in order for the OPF algorithm to converge (requirement for multiple slack buses)
- The voltage and powers in the VSC-HVDC system is being controlled through the operation of the variable complex tap ratio

The cost functions as obtained by the OPF have been summarised in table (5.4) below.

Slack Bus	Generator	Infinite Bus	Overall Cost Function
1	359.531 \$/hr	N/A	344.909 \$/hr
5	N/A	14.622 \$/hr	

**Table 5.4 – System Optimum Cost (in \$/hr)**

It has been observed from table (5.4), that approximately for each 360 \$/hr spending on the generation cost, 14.6 \$/hr has been turned into work. The rest accounts for the cost of consumption by the network loads in nodes 2 and 4 as well as transmission losses bringing the overall cost of fuel generation to 344.9 \$/hr at the optimum operating point and taking into account the compound transformers' control constraints on powers and voltages. The voltage at the DC node, as mentioned before, has been set to 1.1 per unit by penalising its associated nodal voltage magnitude within the OPF solution process. No violations in the state variables vector as well as functions have been observed.

In order to reverse the direction of the active power transfer through the back-to-back VSC-HVDC system (from node 5 to node 1) it is only necessary to alter the signs in the power control constraints associated with the compound transformers as explained in section (5.3.2).

In this case, the output power in the first converter (nodes 2 and 3) has to be set to positive (indicating inversion), whereas the output power in the second converter (nodes 4 and 3) has to be set to negative (indicating rectification) in their corresponding power control constraints in a similar fashion as in equations (5.21) and (5.22) so as to maintain a power transfer between nodes 5 and 1. The OPF solution for the case where power is directed from node 5 to node 1 (now the infinite bus) is shown in figure (5.5). The rest of the system data remains intact

including the compound transformers' modes of operation in table (5.3) with a minor exception that this time it is the inverter station that is tasked with maintaining the voltage at the DC bus (since the power is now being transferred from node 5 to 1). Therefore, even though the system is symmetrical and even though no change in the converters' modes of operations are made, due to the reversal of the DC current, the functional equality constraints on the converters' active powers in fact did change. Consequently, the OPF expectedly converges towards a different optimum operating point than in the first test run as observed in table (5.5).

Slack Bus	Generator	Infinite Bus	Overall Cost Function
1	N/A	16.832 \$/hr	349.109 \$/hr
5	365.941 \$/hr	N/A	

Table 5.5 - System Optimum Cost (in \$/hr)

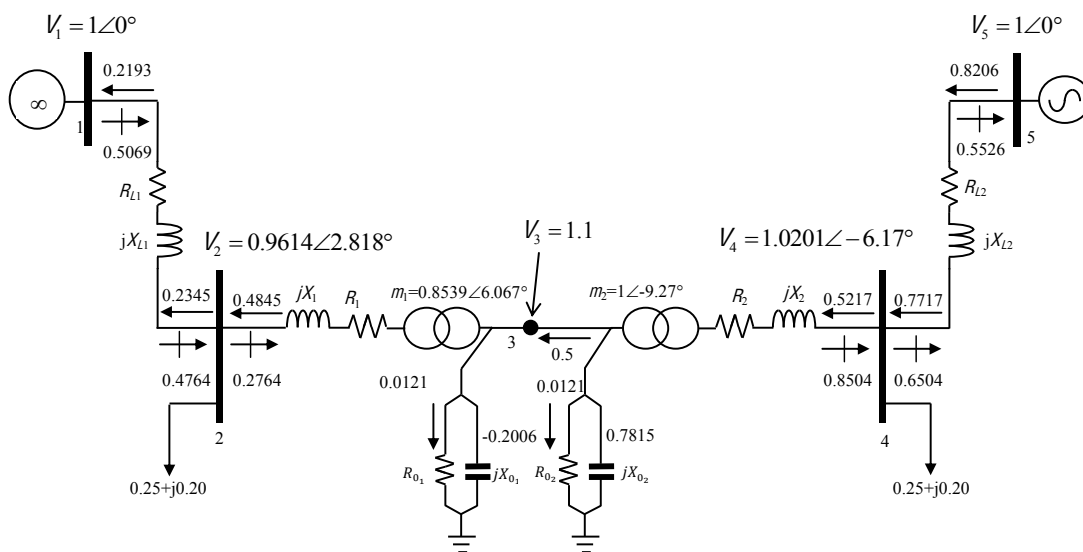


Figure 5.5 - Two-terminal Back-to-Back VSC-HVDC Compound Transformer Model OPF Solution (node "1" is the infinite bus)

If, however, the constraints remain the same as in the first test run (the modes of operation interchange), the OPF then converges towards exactly the same operating point as obtained in the first test run.

There are other plausible modes of operation with which the back-to-back VSC-HVDC system in the above example can operate. For instance, the second converter can be set to regulate the voltage in node 4, whereas the first converter is used to

regulate the voltage in node 3, namely the DC node. In any case, selecting a mode of operation for the compound transformers is done by activating or removing the appropriate associated Lagrangian functions (in case of active power control) or pure penalty function (in case of nodal voltage magnitude control) to or from the system Lagrangian and the linear system of equations respectively (See sections 5.3.2).

The reactive power at the DC node has been remained zero for both of the above system simulations by activating equation (5.16).

### 5.3.2 Multi-terminal Back-to-Back VSC-HVDC

An OPF solution for a multi-terminal back-to-back VSC-HVDC interconnection link has been presented in figure (5.6) below.

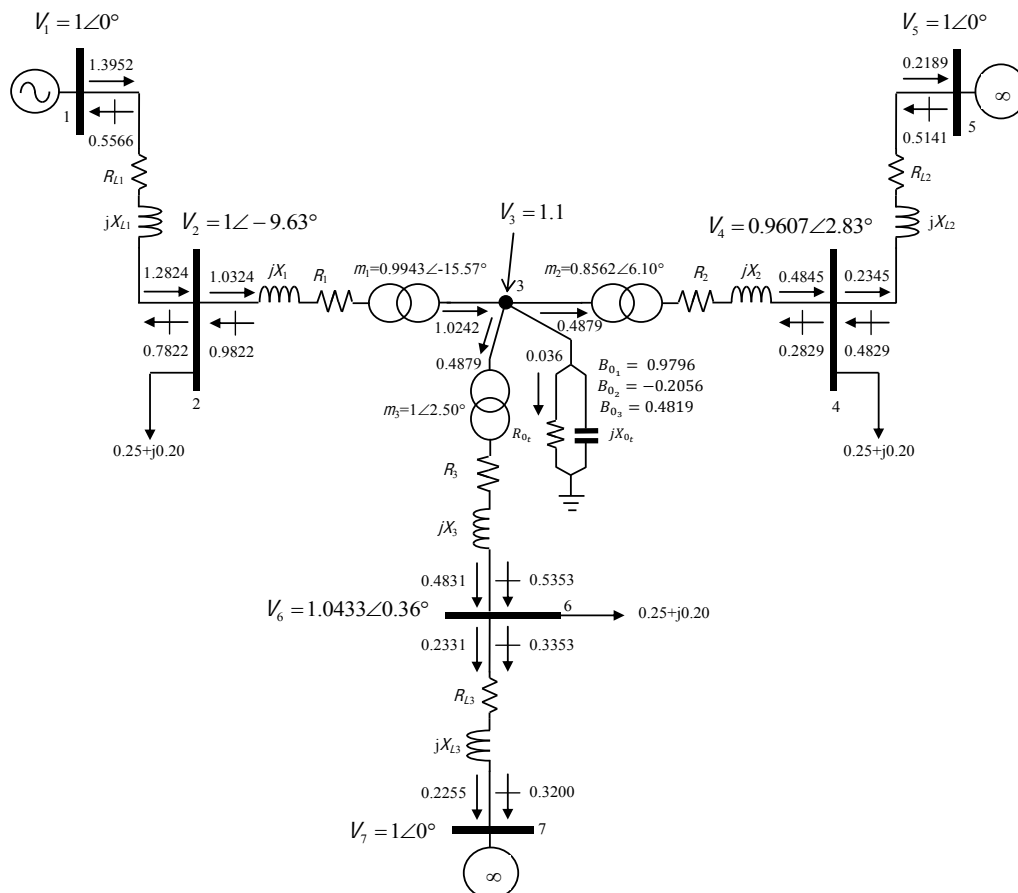


Figure 5.6 - Multi-terminal Back-to-Back VSC-HVDC Compound Transformer Model OPF Solution (nodes “5” and “7” are infinite buses) (notice the variable shunt susceptance values in per unit)

The multi-terminal back-to-back VSC-HVDC link shown in figure (5.6) consists of three voltage source converters modelled by compound transformers. It has been used to interconnect three autonomous AC grids with each other to deliver power generated in node 1 to nodes 5 and 7, which are taken as infinite buses in this particular example. The converter connected between nodes 2 and 3 act as a rectifier, whereas the other two converters act as inverters. The voltage at the DC bus is regulated at 1.1 per unit and the power leaves the rectifier at 1 per unit entering the inverters at 0.5 per unit each. Notice that the shunt branches of the three converters are grouped together and placed (artificially) at bus 3, thus giving rise to the values of power flows at this node. The OPF algorithm converged in four iterations with no violations in the state variables or functions. Similar to two-terminal test runs, the OPF is initialised by setting three slack buses in the system, namely nodes 1, 5 and 7 to solve three decoupled AC power flows.

The Lagrangian function exclusive to the compound transformers for a back-to-back multi-terminal system such as the one in figure (5.6) is formed using equation (5.19). Consequently, the linear system of equations in equation (5.20) is formed to solve the OPF. The converters' modes of operation as dictated by the network operational requirements in terms of active power flow as well as nodal voltage magnitude regulation are selected according to table (5.6).

Converter	Mode of Operation	Power Equality	Voltage Equality	Voltage Control	Power Control
VSC1 (nodes 2-3)	4.1.2.	Activate Lagrangian Function	Add Penalty Function	AC Node (node 2)	DC Node
VSC2 (nodes 4-3)	4.2.2.	Activate Lagrangian Function	Add Penalty Function	DC Node	DC Node
VSC3 (nodes 6-3)	3.2.0.	Activate Lagrangian Function	Remove Penalty Function	N/A	DC Node

**Table 5.6 - Multi-terminal Back-to-Back VSC-HVDC Compound Transformer Model Modes of Operation (notice that the rectifier station is tasked with maintaining the voltage at the AC side)**

According to the results obtained by the OPF, at the optimum operating point, the system draws approximately 1.4 per unit of active power from node 1 to be delivered to nodes 5 and 7 respectively. VSC1 is tasked with maintaining the voltage magnitude at its AC side, whereas the DC node voltage is fixed by VSC2. VSC3 does not regulate voltage magnitudes at either its AC or DC sides. Upon

convergence, approximately 0.23 per unit of active power arrives at both nodes 5 and 7, with the rest of the power dispatch being consumed by loads in each independent AC grid segment. The rest of the generated active power accounts for the transmission losses. The active power is being distributed between the AC segments according to a pre-determined criterion via each converter station. Consequently, the rectifier station, namely VSC1, is tasked with regulating the active power at the DC side at 1 per unit, 0.5 per unit of which is directed towards VSC2 and the remaining 0.5 per unit towards VSC3 through the action of the inverter stations. By activating active power flow constraints similar to equation (5.8), each converter maintains its target active power flow in accordance with the mentioned criterion.

The cost functions associated with the OPF solution depicted in figure (5.6) are shown in table (5.7) below, notice that the synchronous machines in nodes 5 and 7 act as motors not generators.

Slack Bus	Generator	Infinite Bus	Overall Cost Function
1	612.247 \$/hr	N/A	581.187 \$/hr
5	N/A	16.437 \$/hr	
7	N/A	14.622 \$/hr	

**Table 5.7 - System Optimum Cost (in \$/hr)**

As shown in table (5.7), the overall cost function as obtained by the OPF is 581.18 \$/hr of generator fuel consumption at the slack node.

- Operational Flexibility:

To verify the flexibility of operation brought to the system by the presence of the multi-terminal VSC-HVDC compound transformer models, two different case scenarios, other than the one already presented, have been devised, which are shown in figures (5.7) and (5.8) respectively.

It has been assumed, that each autonomous AC grid in figure (5.6) has a variable demand pattern that has to be addressed accordingly by the voltage source converters in the back-to-back VSC-HVDC interconnection link. It has also been

assumed that all the generators are capable of addressing the demands variations within their respective limits.

Consequently, through activating and/or deactivating appropriate equalities (on voltage and/or active power) the voltage source converters respond to the changes in the network operational requirements. Conspicuously, solving the OPF for each case scenario then yields the best operating point for the system, subject to those particular restrictions.

The required active power flow dispatch at the DC node for each converter has been shown in table (5.8) for the three case scenarios. OPF solution presented in figure (5.6) pertains to case one.

Case Scenario	VSC1	VSC2	VSC3
One	-1.0	+0.5	+0.5
Two	-1.0	-0.5	+1.5
Three	+1.0	-0.5	-0.5

**Table 5.8 - The Multiple Test Case Scenarios Required Active Power Dispatch (at the DC node)**

The positive and negative signs denote the direction of the DC active power dispatch between the three converters, as it is required by the system. For consistency purposes, the compound transformers' control modes are assumed to remain similar to those in table (5.6) for all three case scenarios. The optimal power dispatch for the three machines along with the final cost is shown in table (5.9) for the three case scenarios (the powers are in per unit). Machine 1 is connected to node 1, Machine 2 to node 5 and Machine 3 to node 7. The negative sign in the machines' power dispatch indicate that they are receiving active power, hence act as motors not generators.

Case Scenario	Machine 1	Machine 2	Machine 3	Optimum Cost (\$/hr)
One	+1.3952	-0.2189	-0.2255	581.187 \$/hr
Two	+1.3952	+0.8345	-1.1513	690.486 \$/hr
Three	-0.6964	+0.8384	+0.8206	573.307 \$/hr

**Table 5.9 - System Optimal Power Flow Dispatch (in per unit)**

The variable complex tap ratio final position as obtained by the OPF has been illustrated in table (5.10) for all three case scenarios.

Case Scenario	VSC1	VSC2	VSC3
One	$0.994\angle -15.57$	$0.856\angle +6.10$	$1.000\angle +2.50$
Two	$0.994\angle -15.57$	$1.029\angle -9.65$	$1.000\angle +13.67$
Three	$0.911\angle +10.78$	$1.036\angle -9.75$	$1.000\angle -9.27$

**Table 5.10 - Operation of Complex Tap Ratio for the three Converter Stations**

It is observed from table (5.9) that the OPF converges towards different operating points for each case scenario, which is due to the changing in mainly the active power constraints. In the first case scenario, the power is being delivered from node 1 to infinite buses 5 and 7 with the voltage source converters regulating the power at the DC node according to table (5.8).

However, in the second case scenario, the active power control constraints change slightly to reflect on the conditions of the system. It is assumed that the demand in the third slack node, namely node 7 has been increased. The network therefore responds to this increase in demand by configuring the voltage source converters in such a way so that the amount of active power arriving at the third converter increases to 1.5 per unit. This is done by changing the conditions of the active power constraints of the three compound transformers in the OPF algorithm (increasing their specified powers). It is therefore observed that this increase in power would result in a different final power dispatch at the optimum.

The power is now being transferred through the back-to-back VSC-HVDC interconnection link from both nodes 1 and 5 towards node 7 with the amounts given in table (5.9) (See figure 5.7).

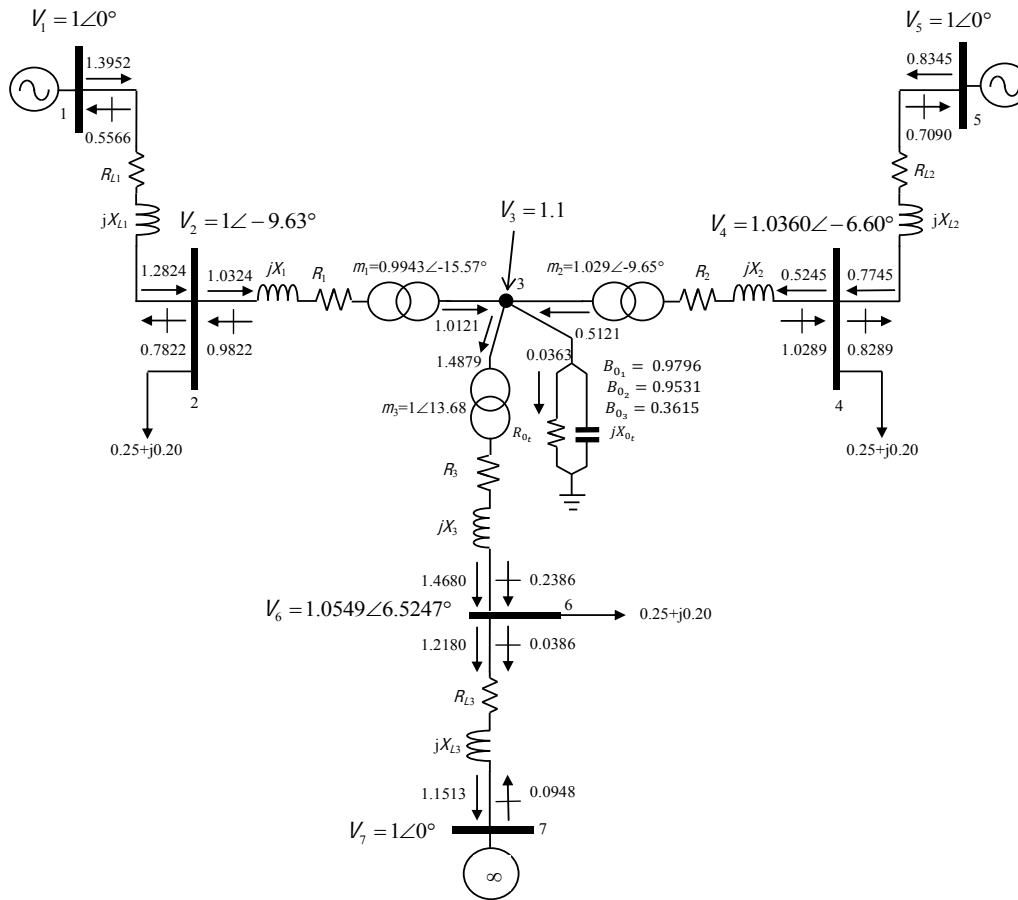


**Figure 5.7 – Multi-terminal Back-to-Back VSC-HVDC Compound Transformer Model Test Case Two OPF Solution**

Similarly by changing the operational requirements of the network for the third time in the final case scenario (figure 5.8), the voltage source converters are again reconfigured to respond accordingly (again by referring to table 5.8) and therefore the OPF will converge towards a different operating point.

By ensuring that the KKT conditions are always satisfied upon convergence and adhering to the control equality constraints set at the start of the solution process, the final power dispatch given by the OPF is the optimum operating point of the network in which the system maintains stability and improved reliability through the operation of the voltage source converters.

As seen from table (5.10) the variable complex tap ratio associated with each compound transformer takes a different value, which depends on the nature of their control mode. For instance, since the third converter, VSC 3, does not regulate voltage, its associated variable tap ratio remains constant, which indicates that its



sort of system demand in terms of both active power transfer capacity and voltage regulation requirements. By simply selecting the appropriate mode of operation, depicted in table (5.2) for each compound transformer, the above meshed system operates in a variety of circumstances and adapts to any change in the active power demand thanks to the power and voltage control capabilities of the compound transformers. The OPF then yield to an optimum point within which the network maintains steady state operation under the set circumstances.

### 5.3.3 Multi-terminal Back-to-Back VSC-HVDC: Four Terminals Meshed

The voltage source converters are used in a multi-terminal back-to-back configuration to connect the four independent AC grids to each other forming a four-terminal meshed system whose OPF solution is depicted in figure (5.9).

As seen from figure (5.9), the multi-terminal system is being used to transfer the power generated by Machines 1,2 (nodes 1 and 5) to Machines 3,4 (nodes 7 and 9).

VSC1 as well as VSC2 act as rectifiers regulating active power at their DC sides to 1 per unit, whereas VSC3 and VSC4 act as inverters receiving 1 per unit DC active power flow. Furthermore, VSC3 and VSC4 are tasked with regulating the voltage at the AC side, whereas VSC1 and VSC2 are maintain the voltage at the DC side giving rise the following modes of operation in table (5.11).

Converter	Mode of Operation	Power Equality	Voltage Equality	Voltage Control	Power Control
VSC1 (nodes 2-3)	4.2.2.	Activate Lagrangian Function	Add Penalty Function	D C Node	DC Node
VSC2 (nodes 4-3)	4.2.2.	Activate Lagrangian Function	Add Penalty Function	DC Node	DC Node
VSC3 (nodes 6-3)	4.1.2.	Activate Lagrangian Function	Add Penalty Function	AC Node (node 6)	DC Node
VSC4 (nodes 8-3)	4.1.2.	Activate Lagrangian Function	Add Penalty Function	AC Node (node 8)	DC Node

**Table 5.11 - Multi-terminal Back-to-Back VSC-HVDC Compound Transformer Model Modes of Operation for the Four-terminal Meshed**



The compound transformer's modes of operation have been selected in such a way that the operation of the system remains symmetrical as it is seen from figure (5.9).

The above example can be used to model a Wind Farm power transfer system. The power from two wind farms, namely nodes 1 and 5 are eventually being delivered to the utility grid, nodes 7 and 9 after being distributed optimally and symmetrically throughout the network. Later in this chapter a similar interconnection system based on multi-terminal point-to-point VSC-HVDC model is applied to a realistic system configuration that is based on the IEEE 14-bus test system.

## **5.4 Advanced Point-to-Point VSC-HVDC Compound Model's OPF Formulation using Expanded Compound Transformer Model**

Most of the HVDC systems require long DC transmission lines for transferring bulk DC power between at least two points within a given power system. Throughout this research, such systems are said to fulfil point-to-point power transmission applications. The modelling criterion of a point-to-point VSC-HVDC transmission system using the compound model, however, differs from that of the back-to-back systems in its active power flow constraint, since it needs to account for the DC losses occurring at the DC transmission link. In the following section, the compound transformer model has been expanded to incorporate the effects of the DC transmission losses in point-to-point power transmission applications for VSC-HVDC systems.

### **5.4.1 Problem of Point to Point active power control in Compound Transformer Model**

Referring to the complex nodal powers derived for the compound transformer model in back-to-back configurations, namely equations (5.13) and (5.14), it has been clearly observed that the compound transformer model is only capable of controlling active power at its own point of connection, namely either its sending (primary) or receiving (secondary) ends. This means that the compound transformer model is not capable of maintaining the power balance between two nodes separated by a transmission line. Even though not being able to maintain power balance between two separate points is not an issue for local power regulation applications and back-to-back connections (synchronising various AC sections or connecting a

weak network to a strong one), it poses a dilemma in point-to-point HVDC applications where DC links/cables are added to the system configuration. A two-terminal point-to-point VSC-HVDC system has been presented in figure (5.10).

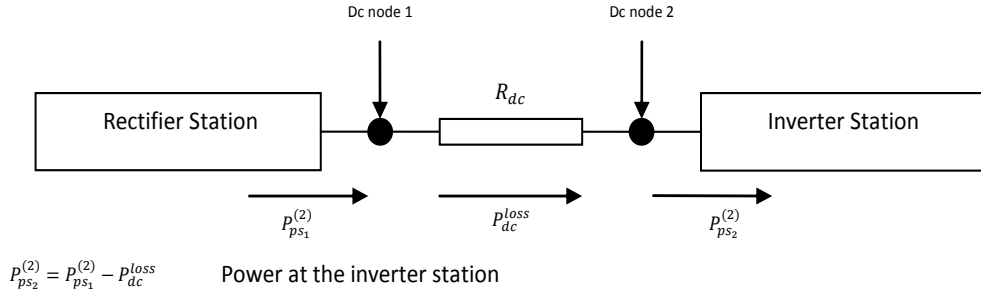


**Figure 5.10 - Two-terminal Point-to-Point VSC-HVDC System (Notice the DC power losses in the DC transmission line)**

It is obvious that the power transferred through the DC link in such a system will incur some, albeit, very small DC losses due to the conductors' resistance towards the DC current, namely  $P_{dc} = R_{dc} I_{dc}^2$ . For DC power transmission from rectifier to inverter, the following functional equality constraints are defined:

The Rectifier station:

$$P_{ps_1}^{(2)} - P_{spe_1} = -P_{r_1} - P_{spe_1} \quad 5.25$$

The Inverter station:

$$P_{ps_2}^{(2)} - P_{spe_2} = +P_{r_2} - P_{spe_2} \quad 5.26$$

Basic circuit theory suggests that the following power balance equation must be satisfied at the inverter station:

$$P_{r_2} = P_{r_1} - P_{dc}^{losses} \quad 5.27$$

Within the optimal power flow formulation paradigm, this means that the inverter's functional equality must be constrained towards the amount shown in equation

(5.27), which essentially requires knowing the DC transmission losses in advance (as a separate state variable). However, it is virtually impossible to determine the DC transmission losses at the start of the OPF algorithm. Furthermore, one of the requirements of maintaining a HVDC power transmission is activating both functional equalities on converters' active powers simultaneously (See section 5.2.4).

Since the DC losses are unknown at the start of the OPF solution process and there is no way to initialise them without knowing the power flows, the functional equality at the inverter station cannot be activated accurately. Therefore using compound transformer model for modelling point-to-point VSC-HVDC systems will generate inaccurate results due to ill conditioning of the OPF solution space. The only possible scenario for modelling a point-to-point VSC-HVDC operation with compound transformer model is to bind both powers at a pre-determined amount by adding their corresponding Lagrangians to the system Lagrangian. However, due to incurred losses in the DC transmission link, the OPF algorithm simply ignores the active power equalities and sets the powers for both converters in such a way that the DC losses are also included so that the power balance in equation (5.23) is not violated. It is quite obvious that this form of modelling is unreliable because the algorithm no longer is within the chosen set of equality constraints and therefore its results are not accurate results even if they converge to a possible solution.

Knowing that controlling the amount of active power flow between voltage source converters is one of the most essential applications of VSC-HVDC systems particularly in forming interconnections between various autonomous segments, including such strong characteristics in their mathematical models becomes equally important. In the next section the VSC compound transformer model has been expanded to incorporate the effects of DC line losses.

### 5.4.2 Expanded Compound Transformer Model Reduced Admittance Matrix and Derived Nodal Powers

The expanded compound transformer model used to model the point-to-point VSC-HVDC transmission systems is shown in figure (5.1) below:

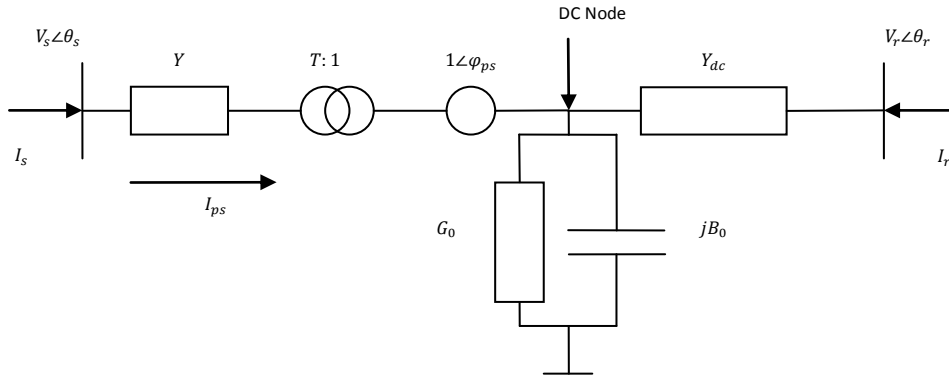


Figure 5.11 - The Expanded (Augmented) Compound Transformer Model

The DC transmission link has been added to the compound transformer model using a dummy bus called “DC-node”.

Based on the single line diagram representation shown in figure (5.11), the admittance matrix is derived as shown in equation (5.28) below:

$$Y_T = \begin{bmatrix} Y & -(T \angle \varphi_{ps})Y & \\ -(T \angle -\varphi_{ps})Y & T^2 Y + Y_0 + Y_{dc} & -Y_{dc} \\ & -Y_{dc} & Y_{dc} \end{bmatrix} \quad 5.28$$

Using Kron’s reduction technique, presented in [14], to mathematically eliminate “DC-node”,  $Y_T$  is converted into a reduced matrix comprising the effects of DC line/cable. In this way the expanded model will retain the form of a two-node model presented in the previous section. It should be noted that for the OPF algorithm, the expanded model is still seen as a two-node transformer model.

A proper point-to-point VSC-HVDC system is therefore formed, by connecting a compound transformer (figure 4.4a) as well as an expanded compound transformer (figure 5.11) to each other. This particular configuration, while it maintains the effects of a DC line/cable in form of internal series resistance, is still seen by the OPF algorithm as a back-to-back system. Consequently, if using expanded compound model, the system in figure (5.10) takes the shape of figure (5.12).

The power in the first converter can now be easily fixed to a pre-determined amount using its Lagrangian, knowing that it inherently includes the DC losses as well. In this way the active power control features can easily be added taking into account the DC losses in the calculated injected powers as internal losses of the expanded model.

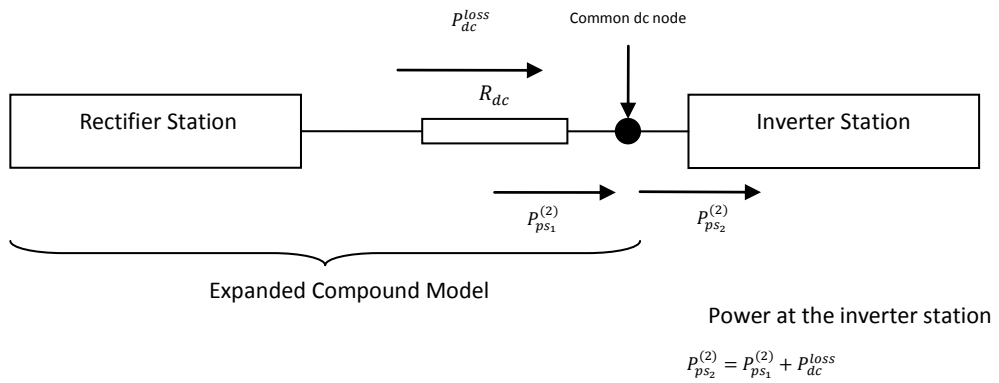


**Figure 5.12 - Expanded Compound Transformer Model Reconfiguration (Notice the shift in output power controls and the power balance at the common DC node)**

Referring to the expanded model presented in figure (5.11), the new reduced matrix, dubbed  $Y_T'$  is shown in equation (5.29).

$$Y_T' = \frac{1}{K} \begin{bmatrix} Y(Y_0 + Y_{dc}) & -(T\angle\varphi_{ps})YY_{dc} \\ -(T\angle -\varphi_{ps})YY_{dc} & Y_{dc}(T^2Y + Y_0) \end{bmatrix} \quad 5.29$$

In which

$$K = T^2Y + Y_0 + Y_{dc} \quad 5.30$$

According to the new admittance matrix presented in equation (5.29), the power flows used to derive the expanded model have to be re-calculated to incorporate the effects of DC line/cable by re-calculating the nodal complex apparent powers. The equation for calculating nodal complex apparent powers for the compound transformer model presented in equations (4.7) is re-written for the expanded model's admittance matrix in equation (5.29) as such:

$$\begin{bmatrix} S_s \\ S_r \end{bmatrix} = \begin{bmatrix} V_s & \\ & V_r \end{bmatrix} \begin{bmatrix} I_s \\ I_r \end{bmatrix}^* \quad 5.31$$

Substituting for the complex conjugate currents with the product of the reduced admittance matrix and the expanded model's nodal voltages, equation (5.31) is re-written as such in polar coordinates:

$$\begin{bmatrix} S_s \\ S_r \end{bmatrix} = \begin{bmatrix} V_s e^{j\theta_s} & \\ & V_r e^{j\theta_r} \end{bmatrix} \frac{1}{K^*} \begin{bmatrix} Y^*(Y_0^* + Y_{dc}^*) & -TY^*Y_{dc}^*e^{-j\varphi_{ps}} \\ -TY^*Y_{dc}^*e^{+j\varphi_{ps}} & (T^2Y^* + Y_0^*)Y_{dc}^* \end{bmatrix} \begin{bmatrix} V_s e^{-j\theta_s} \\ V_r e^{-j\theta_r} \end{bmatrix} \quad 5.32$$

By comparing equation (5.32) with the nodal power equations for the normal compound transformer model (equation 4.7), the effects of DC link/cable in form of admittance  $Y_{dc}$  is discernible. However, it should be noted that in a real DC line there is no series reactance and therefore for purposes of simulation the DC line's series reactance has to be set to zero.

Ultimately, by solving equation (5.32) for the nodal complex apparent powers, the general expressions for active and reactive nodal powers for the expanded model are derived as shown in equations (5.33-5.36) for the sending and receiving ends of the expanded compound transformer model.

Powers at sending end (or primary side):

$$P_s = V_s^2 G_{eq1} - TV_s V_r [G_{eq1dc} \cos(\theta_{sr} - \varphi_{ps}) + B_{eq1dc} \sin(\theta_{sr} - \varphi_{ps})] \quad 5.33$$

$$Q_s = -V_s^2 B_{eq1} - TV_s V_r [G_{eq1dc} \sin(\theta_{sr} - \varphi_{ps}) - B_{eq1dc} \cos(\theta_{sr} - \varphi_{ps})] \quad 5.34$$

Powers at receiving end (or secondary side):

$$P_r = V_r^2 G_{eq2} - TV_r V_s [G_{eq2dc} \cos(\theta_{sr} - \varphi_{ps}) - B_{eq2dc} \sin(\theta_{sr} - \varphi_{ps})] \quad 5.35$$

$$Q_r = -V_r^2 B_{eq2} - TV_r V_s [-G_{eq2dc} \sin(\theta_{sr} - \varphi_{ps}) - B_{eq2dc} \cos(\theta_{sr} - \varphi_{ps})] \quad 5.36$$

The equivalent conductance and susceptance terms shown in the above equations entail the changes in the admittance matrix of the expanded compound transformer. They are basically the re-defined reduced admittance matrix terms for the expanded compound transformer model to include the DC transmission line's admittance. The precise calculations yielding the equivalent admittance terms for the expanded model are carried out and presented in next section.

#### 5.4.3 Equivalent Admittance Elements for the Expanded Compound Transformer in Rectangular and Polar Forms

The equivalent admittance elements, pertaining to the reduced admittance matrix, in nodal active and reactive power flows presented in equations (5.33-5.35) are calculated by solving equation (5.32) for the complex nodal apparent powers in sending and receiving ends of the expanded compound transformer shown in figure (5.11). By doing simple matrix algebra equation (5.32) will result in the following equations:

Complex apparent nodal power at sending end:

$$S_s = (K^*)^{-1} (V_s e^{j\theta_s}) [Y^* V_s^* (Y_0^* + Y_{dc}^*) e^{-j\theta_s} - TV_r^* Y_{dc}^* e^{-j(\varphi_{ps} + \theta_r)}] \rightarrow S_s = \underbrace{(K^*)^{-1}}_1 \underbrace{[Y^* (Y_0^* + Y_{dc}^*) V_s^2]}_2 - \underbrace{TV_r^* Y_{dc}^* V_s^* e^{j(\theta_s - \theta_r - \varphi_{ps})}}_4 \quad 5.37$$

Complex apparent nodal power at receiving end:

$$S_r = (K^*)^{-1} (V_r e^{j\theta_r}) [-TY_{dc}^* V_s^* e^{j(\varphi_{ps} - \theta_s)} + Y_{dc}^* V_r^* (T^2 Y^* + Y_0^*) e^{-j\theta_r}] \rightarrow S_r = (K^*)^{-1} \underbrace{[-TV_r^* Y_{dc}^* V_s^* e^{j(\theta_r - \theta_s + \varphi_{ps})}]}_5 + \underbrace{Y_{dc}^* V_r^2 (T^2 Y^* + Y_0^*)}_3 \quad 5.38$$

From equations (5.37) and (5.38), the following self- and mutual complex nodal powers are derived in polar coordinates.

Self-Sending End:

$$S_{ss} = \underbrace{(K^*)^{-1}}_1 \underbrace{[Y^* (Y_0^* + Y_{dc}^*) V_s^2]}_2 \quad 5.39$$

Self-Receiving End:

$$S_{rr} = \underbrace{(K^*)^{-1}}_1 \underbrace{[Y_{dc}^* V_r^2 (T^2 Y^* + Y_0^*)]}_3 \quad 5.40$$

Mutual Send and Receive:

$$S_{sr} = \underbrace{(K^*)^{-1}}_1 \underbrace{[-TV_s V_r^* Y^* Y_{dc}^* e^{j(\theta_s - \theta_r - \varphi_{ps})}]}_4 \quad 5.41$$

Mutual Receive and Send:

$$S_{rs} = \underbrace{(K^*)^{-1}}_1 \underbrace{[-TV_r V_s^* Y^* Y_{dc}^* e^{j(\theta_r - \theta_s + \varphi_{ps})}]}_5 \quad 5.42$$

Solving for  $(K^*)^{-1}$  term:

Referring to equation (5.30) it is known that:

$$K = T^2 Y + Y_0 + Y_{dc} \quad 5.43$$

Therefore its complex conjugate is defined in rectangular form as such:

$$K^* = \underbrace{(T^2 G + G_0 + G_{dc})}_{\Delta'} - j \underbrace{(T^2 B + B_0 + B_{dc})}_{\Delta''} \quad 5.44$$

And its inverse:

$$(K^*)^{-1} = (\Delta' - j\Delta'')^{-1} = \frac{\Delta' + j\Delta''}{\Delta'^2 + \Delta''^2} = \Delta_R + j\Delta_I \quad 5.45$$

Solving for  $\Delta_R$  and  $\Delta_I$  will yield to the following equations:

$$\Delta_R = \frac{\Delta'}{\Delta'^2 + \Delta''^2} = \frac{T^2G + G_0 + G_{dc}}{|K|^2} \quad 5.46$$

And

$$\Delta_I = \frac{\Delta'}{\Delta'^2 + \Delta''^2} = \frac{T^2B + B_0 + B_{dc}}{|K|^2} \quad 5.47$$

Solving sub-equation (2) in equation (5.39), the following auxiliary admittance elements are derived with respect to the expanded compound model's sending end:

$$\begin{cases} G_{11} = G(G_0 + G_{dc}) - B(B_0 + B_{dc}) \\ B_{11} = -G(B_0 + B_{dc}) - B(G_0 + G_{dc}) \end{cases} \quad 5.48$$

In which

$Y = G + jB$  is the coupling admittance of the expanded compound transformer

$Y_0 = G_0 + jB_0$  is the shunt admittance of the expanded compound transformer

$Y_{dc} = G_{dc} + jB_{dc}$  is the series line admittance of the expanded compound transformer (to simulate a DC transmission line  $B_{dc}$  must be set at zero)

Subsequent sub-equations (3), (4) and (5) are also solved similarly yielding to the following auxiliary admittance terms:

Sub-equation (4):

$$\begin{cases} G_{12} = GG_{dc} - BB_{dc} \\ B_{12} = -(GB_{dc} + BG_{dc}) \end{cases} \quad 5.49$$

Solving for mutual Send-Receive complex nodal apparent powers in polar form:

$$S_{sr} = (\Delta_R + j\Delta_I)(-TV_s V_r)[G_{12} + jB_{12}](\cos(\theta_{sr} - \varphi_{ps}) + j\sin(\theta_{sr} - \varphi_{ps})) \rightarrow \quad 5.50$$

$$\begin{cases} P_{sr} = (-TV_s V_r)\{(\Delta_R G_{12} - \Delta_I B_{12})\cos(\theta_{sr} - \varphi_{ps}) - (\Delta_R B_{12} + \Delta_I G_{12})\sin(\theta_{sr} - \varphi_{ps})\} \\ Q_{sr} = (-TV_s V_r)\{(\Delta_R B_{12} + \Delta_I G_{12})\cos(\theta_{sr} - \varphi_{ps}) + (\Delta_R G_{12} - \Delta_I B_{12})\sin(\theta_{sr} - \varphi_{ps})\} \end{cases}$$

Sub-equation (3):

$$\begin{cases} G_{22} = G_{dc}[T^2 G + G_0] - B_{dc}[T^2 B + B_0] \\ B_{22} = -B_{dc}[T^2 G + G_0] - G_{dc}[T^2 B + B_0] \end{cases} \quad 5.51$$

Solving for self sending and receiving end powers:

Sending End:

$$S_{ss} = (\Delta_R + j\Delta_I)(G_{11} + jB_{11})V_s^2 \rightarrow \quad 5.52$$

$$\begin{cases} P_{ss} = (\Delta_R G_{11} - \Delta_I B_{11})V_s^2 \\ Q_{ss} = (\Delta_I G_{11} + \Delta_R B_{11})V_s^2 \end{cases}$$

Receiving End:

$$S_{rr} = (\Delta_R + j\Delta_I)(G_{22} + jB_{22})V_r^2 \rightarrow \quad 5.53$$

$$\begin{cases} P_{rr} = (\Delta_R G_{22} - \Delta_I B_{22})V_r^2 \\ Q_{rr} = (\Delta_I G_{22} + \Delta_R B_{22})V_r^2 \end{cases}$$

Sub-equation (5):

$$\begin{cases} G_{21} = GG_{dc} - BB_{dc} \\ B_{21} = -(GB_{dc} + BG_{dc}) \end{cases} \quad 5.54$$

$$\begin{cases} G_{12} = G_{21} \\ B_{12} = B_{21} \end{cases}$$

Solving for mutual Receive-Send power:

$$S_{rs} = (\Delta_R + j\Delta_I)(-TV_r V_s)[G_{21} + jB_{21}](\cos(\theta_{rs} + \varphi_{ps}) + j\sin(\theta_{rs} + \varphi_{ps})) \rightarrow \quad 5.55$$

$$\begin{cases} P_{rs} = (-TV_s V_r)\{(\Delta_R G_{21} - \Delta_I B_{21})\cos(\theta_{sr} + \varphi_{ps}) - (\Delta_R B_{21} + \Delta_I G_{21})\sin(\theta_{sr} + \varphi_{ps})\} \\ Q_{rs} = (-TV_s V_r)\{(\Delta_R B_{21} + \Delta_I G_{21})\cos(\theta_{sr} + \varphi_{ps}) + (\Delta_R G_{21} - \Delta_I B_{21})\sin(\theta_{sr} + \varphi_{ps})\} \end{cases}$$

Ultimately, comparing equations (5.50), (5.52), (5.53) and (5.55) with the complex nodal active and reactive powers in equations (5.33-5.36), the following equivalent admittance terms are derived.

Self-elements:

$$\begin{cases} G_{eq1} = \Delta_R G_{11} - \Delta_I B_{11} \\ B_{eq1} = \Delta_R B_{11} + \Delta_I G_{11} \\ G_{eq2} = \Delta_R G_{22} - \Delta_I B_{22} \\ B_{eq2} = \Delta_R B_{22} + \Delta_I G_{22} \end{cases} \quad 5.56$$

Mutual elements:

$$\begin{cases} G_{eq1dc} = \Delta_R G_{12} - \Delta_I B_{12} \\ B_{eq1dc} = \Delta_R B_{12} + \Delta_I G_{12} \\ G_{eq2dc} = \Delta_R G_{21} - \Delta_I B_{21} \\ B_{eq2dc} = \Delta_R B_{21} + \Delta_I G_{21} \end{cases} \quad 5.57$$

The re-defined self- and mutual elements of the reduced matrix help define the new nodal active and reactive powers, with which the Lagrangian function for the expanded compound transformer model is created.

#### 5.4.4 The Expanded Compound Transformer Constraints Set within the OPF

The normal functional as well as variable equality constraints for the compound transformer apply in the expanded form as well. These constraints include the steady-state power balance equations as well as the expanded compound model's

active power control constraint. The expanded model may also be used to regulate nodal voltage magnitude at its points of connection, which means that the variable equality constraint on the expanded model's nodal voltages may be activated should the need arises. The reactive power constraint in equation (5.16) also applies in case of the expanded compound transformer model for maintaining a zero reactive power flow in point-to-point VSC-HVDC models.

### 5.4.5 The Expanded Compound Transformer Exclusive Lagrangian

The general format of the exclusive Lagrangian function for the expanded compound transformer model in figure (5.11) is similar to that of the compound transformer model shown in equation (4.20) taking into account the new re-defined nodal active and reactive powers (equations 5.33-5.36) in the power balance equations and the new reactive power functional equality constraint as shown below.

$$L_{PS} = \sum_{i \in [s,r]} \lambda_{p_i} (P_i^{calc} - P_{g_i} + P_{d_i}) + \sum_{j \in [s,r]} \lambda_{q_j} (Q_j^{calc} - Q_{g_j} + Q_{d_j}) + \lambda_{\varphi_{ps}} (P_{ps} - P_{spe}) + \lambda_B (Q_r - 0.0) \quad 5.58$$

Eventually, the linear system of equations containing the second order partial derivatives of the Lagrangian with respect to the state variables vector in equation (5.18) is formed.

$$\begin{bmatrix} \nabla_{\theta}^2 L & \nabla_{V}^2 L & \nabla_{\theta\varphi}^2 L & \nabla_{\theta T}^2 L & \nabla_{\theta B_0}^2 L & \nabla_{\theta} P^{calc} & \nabla_{\theta} Q^{calc} & \nabla_{\theta} P_{ps}^{(k)} & \nabla_{\theta} Q_r^{calc} \\ \nabla_{V\theta}^2 L & \nabla_{V^2}^2 L & \nabla_{V\varphi}^2 L & \nabla_{VT}^2 L & \nabla_{VB_0}^2 L & \nabla_V P^{calc} & \nabla_V Q^{calc} & \nabla_V P_{ps}^{(k)} & \nabla_V Q_r^{calc} \\ \nabla_{\varphi\theta}^2 L & \nabla_{\varphi V}^2 L & \nabla_{\varphi^2}^2 L & \nabla_{\varphi T}^2 L & \nabla_{\varphi B_0}^2 L & \nabla_{\varphi} P^{sr} & \nabla_{\varphi} Q^{sr} & \nabla_{\varphi} P_{ps}^{(k)} & \nabla_{\varphi} Q_r^{calc} \\ \nabla_{T\theta}^2 L & \nabla_{TV}^2 L & \nabla_{T\varphi}^2 L & \nabla_{T^2}^2 L & \nabla_{TB_0}^2 L & \nabla_T P^{sr} & \nabla_T Q^{sr} & \nabla_T P_{ps}^{(k)} & \nabla_T Q_r^{calc} \\ \nabla_{B_0\theta}^2 L & \nabla_{B_0 V}^2 L & \nabla_{B_0\varphi}^2 L & \nabla_{B_0 T}^2 L & \nabla_{B_0^2}^2 L & \nabla_{B_0} P^{sr} & \nabla_{B_0} Q^{sr} & \nabla_{B_0} P_{ps}^{(k)} & \nabla_{B_0} Q_r^{calc} \\ \nabla_{\theta} P^{calc} & \nabla_V P^{calc} & \nabla_{\varphi} P^{sr} & \nabla_T P^{sr} & \nabla_{B_0} P^{sr} & 0 & 0 & 0 & 0 \\ \nabla_{\theta} Q^{calc} & \nabla_V Q^{calc} & \nabla_{\varphi} Q^{sr} & \nabla_T Q^{sr} & \nabla_{B_0} Q^{sr} & 0 & 0 & 0 & 0 \\ \nabla_{\theta} P_{ps}^{(k)} & \nabla_V P_{ps}^{(k)} & \nabla_{\varphi} P_{ps}^{(k)} & \nabla_T P_{ps}^{(k)} & \nabla_{B_0} P_{ps}^{(k)} & 0 & 0 & 0 & 0 \\ \nabla_{\theta} Q_r^{calc} & \nabla_V Q_r^{calc} & \nabla_{\varphi} Q_r^{calc} & \nabla_T Q_r^{calc} & \nabla_{B_0} Q_r^{calc} & 0 & 0 & 0 & 0 \end{bmatrix} \times \begin{bmatrix} \Delta\theta \\ \Delta V \\ \Delta\varphi_{ps} \\ \Delta T \\ \Delta B_0 \\ \Delta\lambda_p \\ \Delta\lambda_q \\ \Delta\lambda_{\varphi_{ps}} \\ \Delta\lambda_B \end{bmatrix} = - \begin{bmatrix} \nabla_{\theta} L \\ \nabla_V L \\ \nabla_{\varphi} L \\ \nabla_T L \\ \nabla_{B_0} L \\ \Delta P^{calc} \\ \Delta Q^{calc} \\ (P_{ps}^{(k)} - P_{specified}) \\ (Q_r - 0.0) \end{bmatrix} \quad 5.59$$

Using this model, the VSC-HVDC links are modelled properly for point-to-point applications. The OPF is solved for the above linear system of equations using Newton's iterative process, taking into accounts the additional equalities as well as

power balance equations. In the following section, the principles of modelling a point-to-point VSC-HVDC system using the expanded compound transformer have been described in greater detail.

#### 5.4.6 Point-to-Point VSC-HVDC System OPF Formulation using Expanded Compound Transformer

A point-to-point VSC-HVDC configuration is shown in figure (5.13) below:

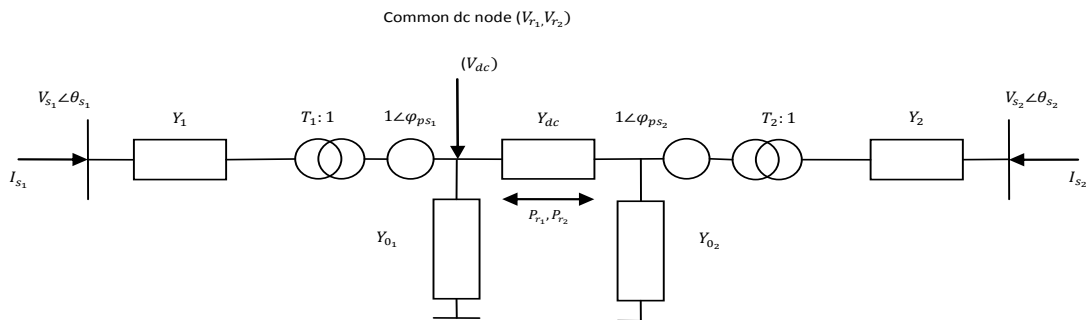
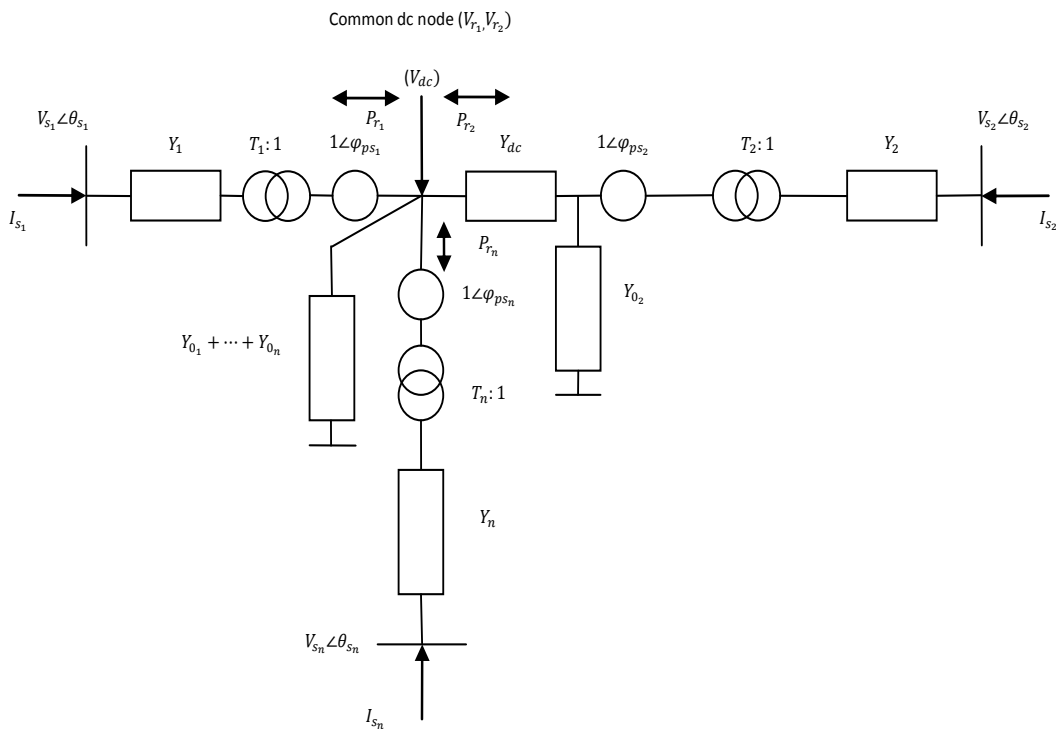


Figure 5.13 - Two-terminal Point-to-Point VSC-HVDC Expanded Compound Transformer Model

It has been observed that the optimum configuration for modelling a point-to-point VSC-HVDC using the compound transformer model is to use at least one expanded compound model to account for DC transmission losses. However depending on the system two expanded models can also be added together to constitute a point-to-point VSC-HVDC system. The modelling approach essentially follows the same principles as in the back-to-back VSC-HVDC systems.

The above model contains the effects of the DC transmission line losses as an internal resistive branch within the expanded compound transformer model admittance matrix as shown in previous section. Similarly, the multi-terminal VSC-HVDC transmission link is depicted in figure (5.14).



**Figure 5.14 - Multi-terminal VSC-HVDC Expanded Compound Transformer Model**

The expanded compound transformer modes of operation follow the same principles of the compound transformer heeding the plausible modes of operation given in table (5.2) to establish a DC power flow.

Furthermore, The additional reactive power equality at the DC bus is added to the system Lagrangian by activating its associated Lagrangian function introduced in equation (5.17) as shown in table (5.13).

Converter Type Model	Reactive Power Equality
Compound Transformer	Activate Lagrangian Function
Expanded Compound Transformer	Activate Lagrangian Function

**Table 5.13 - Reactive Power Equality Constraint for Point-to-Point VSC-HVDC Model**

The complex nodal powers in a multi-terminal VSC-HVDC model are calculated similar to the back-to-back models noting the different admittance elements associated with normal and expanded compound transformers.

For the two-terminal point-to-point VSC-HVDC model in figure (5.13), which comprises of one compound transformer and one expanded model, the admittance matrix is defined as such:

$$Y'_{T_2} = \begin{bmatrix} Y_1 & & -T_1 Y_1 e^{j\varphi_{p1}} & \\ & Y_2(K^{-1})(Y_{0_2} + Y_{dc}) & & -K^{-1}T_2 Y_{dc} Y_2 e^{j\varphi_{p2}} \\ -T_1 Y_1 e^{-j\varphi_{p1}} & & T_1^2 Y_1 + Y_{0_1} & \\ & -K^{-1}T_2 Y_{dc} Y_2 e^{-j\varphi_{p2}} & & K^{-1}Y_{dc}(T_2^2 Y_2 + Y_{0_2}) \end{bmatrix} \quad 5.60$$

From equation (5.60) the complex nodal powers for the two-terminal system in figure (5.13) is calculated by calculating the product of the complex voltages and the complex conjugate currents as such:

$$\begin{bmatrix} S_{s_1} \\ S_{s_2} \\ S_{r_1} \\ S_{r_2} \end{bmatrix} = \begin{bmatrix} V_{s_1} e^{j\theta_{s_1}} & & & \\ & V_{s_2} e^{j\theta_{s_2}} & & \\ & & V_{r_1} e^{j\theta_{r_1}} & \\ & & & V_{r_2} e^{j\theta_{r_2}} \end{bmatrix} \times [Y'_{T_2}]^* \begin{bmatrix} V_{s_1} e^{-j\theta_{s_1}} \\ V_{s_2} e^{-j\theta_{s_2}} \\ V_{r_1} e^{-j\theta_{r_1}} \\ V_{r_2} e^{-j\theta_{r_2}} \end{bmatrix} \quad 5.61$$

Eventually, by conducting matrix multiplication, the complex nodal apparent powers for both voltage source converter models are derived as below:

Sending End:

$$S_{s_1} = V_{s_1}^2 Y_1^* - T_1 V_{s_1} V_{r_1} Y_1^* e^{j(\theta_{s_1} - \theta_{r_1} - \varphi_{ps1})} \quad 5.62$$

And

$$S_{s_2} = V_{s_2}^2 (K^{-1})^* (Y_{0_2}^* + Y_{dc}^*) Y_2^* - T_2 (K^{-1})^* V_{s_2} V_{r_2} Y_2^* Y_{dc}^* e^{j(\theta_{s_2} - \theta_{r_2} - \varphi_{ps2})} \quad 5.63$$

Receiving End:

$$S_{r_1} = (T_1^2 Y_1^* + Y_{0_1}^*) V_{r_1}^2 - T_1 V_{r_1} V_{s_1} Y_1^* e^{j(\theta_{r_1} - \theta_{s_1} + \varphi_{ps1})} \quad 5.64$$

And

$$S_{r_2} = (K^{-1})^* (T_2^2 Y_2^* + Y_{0_2}^*) Y_{dc}^* V_{r_2}^2 - T_2 (K^{-1})^* V_{r_2} V_{s_2} Y_2^* Y_{dc}^* e^{j(\theta_{r_2} - \theta_{s_2} + \varphi_{ps_2})} \quad 5.65$$

The nodal active and reactive powers for the two-terminal point-to-point VSC-HVDC compound transformer model are eventually derived from equations (5.62-5.65). The same procedure can be applied to any number of converters in a multi-terminal VSC-HVDC compound transformer model to derive the nodal active and reactive power flows.

Eventually, for a multi-terminal VSC-HVDC similar to the one in figure (5.14) comprising of  $n_{conv}$  converters comprising of  $n_{comp}$  compound transformers and  $n_{ex}$  expanded compound transformers the admittance matrix is formed similar to the two-terminal point-to-point system.

For simplicity purposes, the admittance matrix in equation (5.11) associated with multi-terminal back-to-back VSC-HVDC compound transformer models has been divided into four sub-matrices as shown below:

$$Y_{T_{n_{comp}}} = \begin{bmatrix} Y_{aa} & Y_{ab} \\ Y_{ba} & Y_{bb} \end{bmatrix} \quad 5.66$$

Equation (5.66) essentially entails a multi-terminal system where  $n_{comp}$  converters are modelled as compound transformers. On the other hand, for a multi-terminal system only comprising of  $n_{ex}$  expanded compound transformers a similar admittance matrix is written:

$$Y'_{T_{n_{ex}}} = \begin{bmatrix} Y'_{aa} & Y'_{ab} \\ Y'_{ba} & Y'_{bb} \end{bmatrix} \quad 5.67$$

Equation (5.67) contains the reduced admittance matrix elements associated with the expanded model given in equation (5.29). Combining the two admittance matrices in equations (5.66) and (5.67) will yield to the admittance matrix for a multi-terminal VSC-HVDC system as shown in equation (5.68).

$$Y_{T_{nconv}} = \begin{bmatrix} Y_{aa} & Y_{ab} \\ Y'_{aa} & Y'_{ab} \\ Y_{ba} & Y_{bb} \\ Y'_{ba} & Y'_{bb} \end{bmatrix} \quad 5.68$$

Eventually the complex nodal powers for a multi-terminal VSC-HVDC compound transformer model comprising of  $ncomp$  compound transformers and  $nex$  expanded compound transformers is calculated as shown in equation (5.69).

$$\begin{bmatrix} S_s \\ S_r \end{bmatrix} = \begin{bmatrix} V_s e^{j\theta_s} \\ V_r e^{j\theta_r} \end{bmatrix} [Y_{T_{nconv}}]^* \begin{bmatrix} V_s e^{-j\theta_s} \\ V_r e^{-j\theta_r} \end{bmatrix} \quad 5.69$$

It should be noted that equation (5.69) presents the most comprehensive representation of the complex nodal powers for a multi-terminal VSC-HVDC system, which has been modelled using compound transformers. The nodal powers can then be calculated for inclusion in the Lagrangian functions associated with each converter in the system. In this way the multi-terminal VSC-HVDC system is essentially modelled in a comprehensive manner within the optimal power flow algorithm.

The functional equality constraints on converters' nodal active and reactive powers as well as control constraints on converters active power are added to the OPF formulation by creating the Lagrangian for point-to-point and multi-terminal VSC-HVDC models. It should be noted that the Lagrangian should contain the additional reactive power constraint for the expanded compound transformers as well:

Two-terminal Point-to-Point:

$$L_{PS} = \sum_{j=1}^2 \sum_{i=s}^r \lambda_{p_i} (P_{i_j}^{calc} - P_{g_{i_j}} + P_{d_{i_j}}) + \sum_{m=1}^2 \sum_{k=s}^r \lambda_{q_{k_m}} (Q_{k_m}^{calc} - Q_{g_{k_m}} + Q_{d_{k_m}}) + \sum_{n=1}^2 \lambda_{\psi_{ps_n}} (P_{ps_n}^{(l)} - P_{spe_n}) + \sum_{\alpha=1}^2 \lambda_{B_{r_\alpha}} (Q_{r_\alpha} - 0.0) \quad 5.70$$

Multi-terminal:

$$L_{PS} = \sum_{j=1}^{nconv} \sum_{i=s}^r \lambda_{p_i} (P_{i_j}^{calc} - P_{g_{i_j}} + P_{d_{i_j}}) + \sum_{m=1}^{nconv} \sum_{k=s}^r \lambda_{q_{k_m}} (Q_{k_m}^{calc} - Q_{g_{k_m}} + Q_{d_{k_m}}) + \sum_{n=1}^{nconv} \lambda_{\psi_{ps_n}} (P_{ps_n}^{(l)} - P_{spe_n}) + \sum_{\alpha=1}^{nconv} \lambda_{B_{r_\alpha}} (Q_{r_\alpha} - 0.0) \quad 5.71$$

The linear system of equations is essentially similar in form to equation (5.59) for both two-terminal point-to-point and multi-terminal VSC-HVDC compound transformer models. Ultimately, the system is solved within the OPF algorithm by iteratively solving equation (5.59) taking into account the limits on both variable and functional constraints as well. In the following sections, the new point-to-point VSC-HVDC model has been tested within the OPF algorithm.

## 5.5 The Inequality Constraints

As for any other OPF formulation, the state variables vector for both compound transformer and the expanded compound transformer has upper and lower limits, which are determined based on their operational requirements. The inequalities exclusive to the compound transformer model are on its variable complex tap phasor stated in equation (4.22). Furthermore, in VSC-HVDC models, there is the additional inequality constraint, which is on the (expanded) compound transformer's variable shunt susceptance as shown in equation (5.72), which properly corresponds to the VSC's capacitive ratings.

$$B_0^{lower} \leq B_0 \leq B_0^{upper} \quad 5.72$$

The variable inequality constraints are activated only if there is a violation in their associated values, in which case they are to be bounded to the system Lagrangian using the quadratic exact penalty function, which was introduced in chapter two. It should be noted that the priority of activation is on the system's nodal voltages as well as phase angles and then the compound transformers' exclusive variables. The direct voltage regulation of the VSC compound transformer model therefore depends on whether there is a violation in the shunt susceptance values or not. The functional inequality constraints are bounded to the system using appropriate Lagrangians. As mentioned in chapter four, the compound transformers' variable complex tap phasor have priority over the nodal active and reactive powers. As always, the limits are checked on variables and functions only after Newton's internal iterations loop (solving the linear system of equations).

## 5.6 Optimal Power Flow Control in Point-to-Point VSC-HVDC System Configurations

In order to better depict the robust operability as well as control capabilities of the compound transformers in modelling voltage source converters, a variety of case scenarios pertaining to point-to-point VSC-HVDC applications have been presented in this section. In the following examples the objective functions remain similar to that of the 8-node benchmark example in chapter two, namely equation (2.53), with the rest of the system data being presented in Appendix II.

### 5.6.1 Two-terminal Point-to-Point VSC-HVDC

The OPF solution for a two-terminal point-to-point VSC-HVDC system has been shown in figure (5.15).

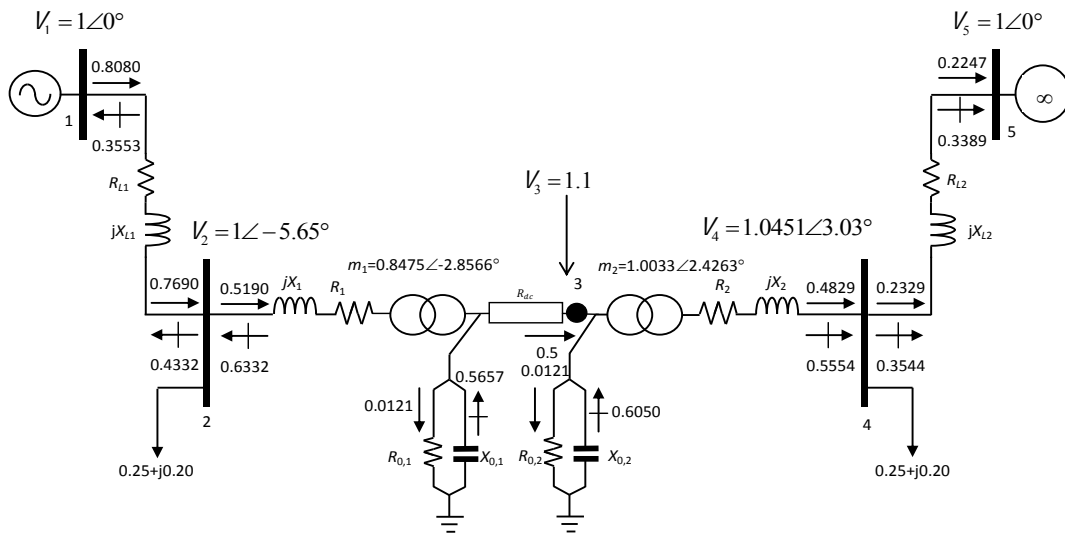


Figure 5.15 - Two-terminal Point-to-Point VSC-HVDC Compound Transformer Model OPF Solution (node “5” is the infinite bus)

As seen in figure (5.15), the VSC-HVDC link is used to connect two autonomous AC grids to each other via a DC transmission link. Thus the power generated in node 1 is now being transferred through the DC link towards node 5, hence the infinite bus. Due to the presence of the DC transmission link (in form of an ohmic resistance), the DC transmission losses are accounted for, and thus, the expanded compound transformer introduced in figure (5.11) is used to take into account these losses. The expanded model is added to the OPF formulation by creating its

exclusive admittance matrix as shown in equation (5.29), which once connected to a normal compound transformer yields to the admittance matrix with the general expression of equation (5.68) representing the whole point-to-point VSC-HVDC system.

Furthermore, the exclusive Lagrangian function for the two-terminal point-to-point VSC-HVDC system is formed as shown in equation (5.70) and by taking into account the power balance equations as well as all the necessary functional equalities including the reactive power equality at the DC bus. The Lagrangian function is then added to the system Lagrangian in the OPF formulation. The converters' modes of operation with which they control the system parameters are selected according to table (5.14).

Converter	Mode of Operation	Power Equality	Voltage Equality	Power/Voltage Control
Rectifier Station	4.1.2.	Activate Lagrangian Function	Add Penalty Function	AC Node (node 2)
Inverter Station	4.2.2.	Activate Lagrangian Function	Add Penalty Function	DC Node

**Table 5.14 - Two-terminal Point-to-Point VSC-HVDC Compound Transformer Model Modes of Operation**

Similar to back-to-back test cases, solving the OPF for point-to-point VSC-HVDC models also call for selecting multiple slack buses, which in this case are buses 1 and 5.

Ultimately, once all the conditions are set, the OPF is run for the above system and is converged in four iterations, without any violations.

The following cost function values for each machine as well as the optimum cost value for the whole system are obtained by the OPF and are shown in table (5.15).

Slack Bus	Generator	Infinite Bus	Overall Cost Function
1	360.825 \$/hr	N/A	346.457 \$/hr
5	N/A	14.370 \$/hr	

**Table 5.15 - System Optimum Cost (Point-to-Point) (in \$/hr)**

Comparing these results with the ones obtained for the two-terminal back-to-back system shown in table (5.4) clearly shows a slight increase in the amount of the objective function value. It has been observed that the overall cost function for

transferring 0.5 per unit of active power through the two-terminal point-to-point VSC-HVDC is slightly costlier (346.5 \$/hr) than transferring the same amount of power through the back-to-back VSC-HVDC link (344.5 \$/hr). The cost surcharge occurs in the system due to the presence of the DC transmission link, which predictably incurs a very small amount of losses. As mentioned earlier, the DC transmission losses are inherently accounted for in the expanded model. The active power is therefore regulated in such a way that it includes the DC transmission losses as shown in figure (5.12). The OPF, however, still sees the point-to-point VSC-HVDC as a back-to-back system with the DC transmission link modelled as an internal ohmic resistance within the expanded model. Consequently, in modelling point-to-point applications using expanded compound transformer, the active power is regulated until after the DC transmission losses are incurred in the system, therefore one does not need to worry about their presence, since they are already accounted for.

### 5.6.2 Multi-terminal VSC-HVDC

A multi-terminal VSC-HVDC transmission link has been used to connect three independent AC grids to each other forming the power system presented in figure (5.16).

The converters modes of operation are shown in table (5.16) accordingly.

Converter	Mode of Operation	Power Equality	Voltage Equality	Voltage Control	Power Control
VSC1 (nodes 2-3)	4.1.2.	Activate Lagrangian Function	Add Penalty Function	AC Node (node 2)	DC Node
VSC2 (nodes 4-3)	4.2.2.	Activate Lagrangian Function	Add Penalty Function	DC Node	DC Node
VSC3 (nodes 6-3)	4.2.2.	Activate Lagrangian Function	Add Penalty Function	DC Node	DC Node

**Table 5.16 - Multi-terminal VSC-HVDC Compound Transformer Model Modes of Operation**

As seen from figure (5.16) to model the point-to-point system, two expanded modes with equal DC resistances are connected to a normal compound transformer model. The power is transferred through nodes 1 and 5 towards node 7 via the multi-terminal VSC-HVDC system.

In order to add the multi-terminal system to the OPF formulation it is only necessary to form its Lagrangian function as shown in equation (5.71), taking into account the exclusive nodal powers associated with the expanded model, namely equations (5.33-5.36) as well as all the control constraints as dictated by table (5.16).

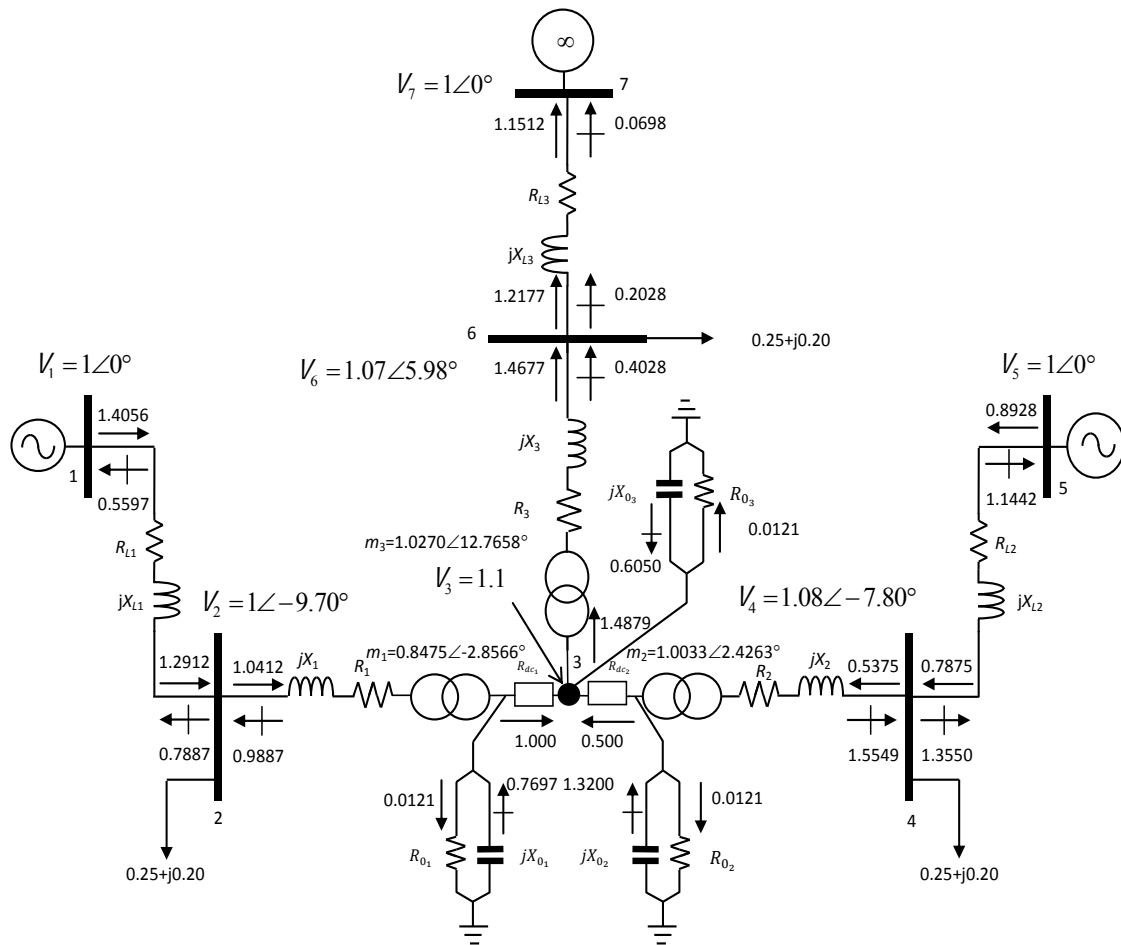


Figure 5.16 - Multi-terminal VSC-HVDC Compound Transformer Model OPF Solution

The OPF is carried out for the above system with the results below.

Slack Bus	Generator	Infinite Bus	Overall Cost Function
1	616.952 \$/hr	N/A	733.998 \$/hr
5	395.440 \$/hr	N/A	
7	N/A	278.391 \$/hr	

Table 5.17 – Multi-terminal VSC-HVDC System Optimum Cost (in \$/hr)

Given the control criteria presented in table (5.16), the results obtained here are comparable to those shown in figure (5.7), namely case two of the back-to-back multi-terminal system. Again, by a simple comparison a slight increase in the amount of final objective function is observable, which is due to the presence of the incurred transmission losses in the DC link.

As always the DC link reactive power remains zero by activating its associated functional equality shown in equation (5.16).

### 5.7 Multi-terminal VSC-HVDC Interconnection System for a realistic AC Network

In the following case scenario, a 46-node system comprising of 15 generators illustrated in figure (5.17), has been introduced.

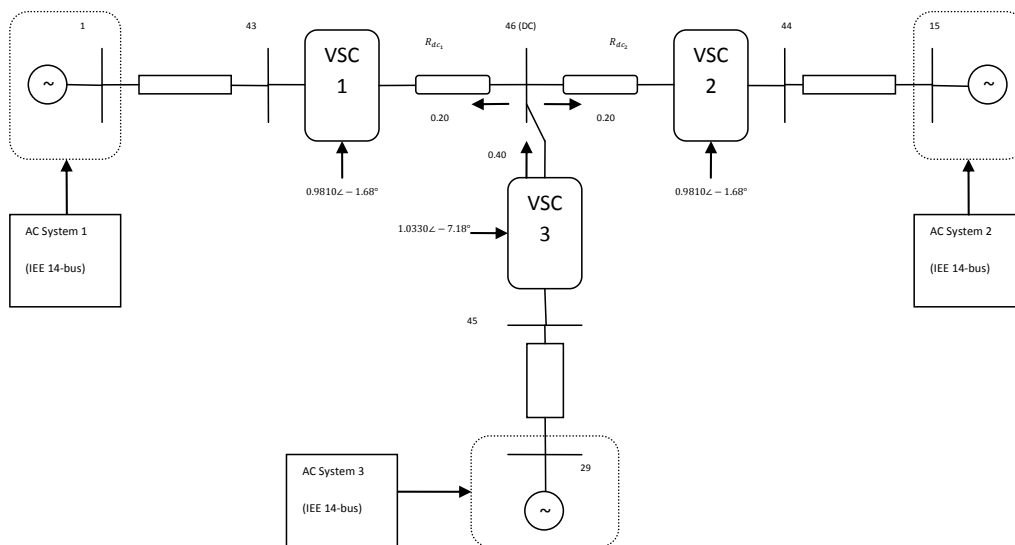


Figure 5.17 – 46-node Test System (only the connecting bus in each 14-bus segment has been shown)

The 46-node system consists of three similar segments each based on the IEEE 14-bus test system, which is in turn a realistic distribution system, interlinked through a multi-terminal VSC-HVDC interconnection system similar to the one illustrated in the previous case scenario (figure 5.16). As mentioned earlier, one of the major purposes of utilising a multi-terminal VSC-HVDC system is to create reliable links for such segmented power systems. The converters are then tasked to control system

active power flow within the DC interconnection system in such a way that conforms well with system operating restrictions.

In order to accommodate the point-to-point multi-terminal system, two expanded compound transformer models are coupled with one normal model. As shown in figure (5.17), the multi-terminal point-to-point VSC-HVDC is used to connect AC System 1 to 2 and 3. Accordingly, the amount of 0.4 per unit of active power is to be delivered from AC System 3 to AC Systems 1 and 2 using the proper control modes as illustrated in table (5.18) below. In this way the operational symmetry of the entire system is properly preserved.

Converter	Mode of Operation	Power Equality	Voltage Equality	Voltage Control	Power Control
VSC1 (nodes 43-46)	4.1.2.	Activate Lagrangian Function	Add Penalty Function	AC Node (node 43)	DC Node
VSC2 (nodes 44-46)	4.1.2.	Activate Lagrangian Function	Add Penalty Function	AC Node (node 44)	DC Node
VSC3 (nodes 45-46)	4.2.2.	Activate Lagrangian Function	Add Penalty Function	DC Node	DC Node

**Table 5.18 – Multi-terminal VSC-HVDC Compound Transformer Model Modes of Operation for the 46-node System**

As it is shown in table (5.18), VSC1 and VSC2 are tasked with regulating the voltage at their AC side whereas the task of maintaining the DC bus voltage has been given to VSC3. As always, since the three AC segments are connected through the VSC-HVDC link, solving the OPF requires solving three decoupled AC power flows for each segment. Buses 1, 15 and 29 have been chosen to act as slack buses for their close proximity to the VSC-HVDC system.

By solving the system Lagrangian similar to the one in equation (5.71), which includes all the necessary functional equalities (including the additional reactive power constraint for the DC link) the OPF, after 5 iterations, converged and generated the results presented in tables (5.19-5.20).

Notice the symmetry between the results for generators in segments 1 and 2, which indicates that an equal amount of active power is distributed between these two segments. The same symmetry is appropriately reflected on the final amounts for

each generator's individual cost function as obtained by the OPF. The final value of the objective function, which essentially is the summation of all the optimum values for the individual cost functions, is arrived at 766.73 \$/hr.

Generator No.	Generator Bus	Active Power Dispatch (in per unit)	Optimum Cost (in \$/hr)
1	1	0.5202	42.8660
2	2	0.5273	43.8299
3	3	0.5492	46.8353
4	6	0.5299	44.1754
5	8	0.5433	46.0133
6	15	0.5202	42.8660
7	16	0.5273	43.8299
8	17	0.5492	46.8353
9	20	0.5299	44.1754
10	22	0.5433	46.0133
11	29	0.7478	78.5479
12	30	0.7455	78.1468
13	31	0.6000	54.1999
14	34	0.6000	54.1999
15	36	0.6000	54.1999

**Table 5.19 – 46-node System Final OPF Results**

As for the previous multi-terminal test cases, the reactive power in the DC link has to be zero. Therefore the additional reactive power control constraint at the DC bus, namely equation (5.16) is activated and added to the system Lagrangian using its associated multiplier. Subsequently, the following results are obtained upon convergence of the OPF algorithm for each VSC in accordance with their control modes depicted in table (5.18) as well as the activated reactive power constraint.

VSC No.	$T\angle\varphi_{ps}$	Active Power (p.u.)		Reactive Power (p.u.)	
		AC Side	DC Side	AC Side	DC Side
VSC1 (Inverter)	$0.9810\angle -1.6794$	-0.1887	+0.2000	-0.2309	Zero
VSC2 (Inverter)	$0.9810\angle -1.6794$	-0.1887	+0.2000	-0.2309	Zero
VSC3 (Rectifier)	$1.0330\angle -7.1832$	+0.4139	-0.4000	-0.4608	Zero

**Table 5.20 – 46-node System Final VSC Results**

Meanwhile, since the converters have identical data their internal switching losses have also been equal to 0.01 per unit. The results presented here clearly illustrates the fact that the new compound transformer model is suitable for analysing medium scale segmented power networks that are most likely to be part of future modern system design scenarios.

## 5.8 Conclusion

The optimal power flow models suitable for realistic representation of VSC-HVDC transmission systems for back-to-back, point-to-point and eventually multi-terminal system configurations have been extensively and thoroughly presented throughout this chapter.

The OPF models introduced in this chapter are based on the compound transformer concept presented in previous chapter. The normal compound transformer is appropriate for modelling back-to-back VSC-HVDC systems where due to presence of no transmission line between the converters, the DC losses are negligible. Similar model is applied for modelling the multi-terminal back-to-back systems. However, the compound transformer model poses a predicament in modelling point-to-point and multi-terminal systems in which DC power flows through DC links and therefore incurs losses. Due to the incurred losses, it is virtually impossible to control the active power remotely between two points separated by a transmission line since setting the appropriate functional equality constraints calls for knowing the losses in advance.

To circumvent this problem, the compound transformer model has been expanded to virtually incorporate the DC transmission losses in its admittance matrix and subsequently its derived nodal active and reactive power flows. Therefore, when modelling point-to-point applications, the OPF still sees the expanded compound transformer models connected to each other as simply back-to-back models. In

order to realise power regulation at the DC node, hence maintain DC power transmission, it is then only necessary to activate the now expanded model's nodal active power at the receiving end, which inherently includes the DC transmission losses as well. The VSC-HVDC compound transformer model has been tested for back-to-back, multi-terminal back-to-back, point-to-point and multi-terminal. It has been realised from the simulations that the compound transformer is capable to satisfy the required control constraints by using the appropriate Lagrangian/penalty functions.

The compound transformer's variable complex tap ratio is responsible for representing the PWM-control characteristics of the converters. The incurred phase angle difference between the sending and receiving ends of the compound transformer for a specific amount of active power regulation at the DC node is essentially obtained by the variations in the phase shifter angle in the compound transformer. The tap changer ratio in the compound transformer is on the other hand responsible for achieving voltage magnitude regulation in either AC or DC ends of the converter. The Lagrangian function associated with active power functional equality is activated throughout the solution process for all HVDC applications and cannot be deactivated. However, as mentioned in chapter four, if the voltage source converter is used as a single compensator and not in an HVDC configuration, this function can be deactivated, should the need arises, by simply penalising its associated multiplier.

Furthermore, the reactive power equality constraint at the DC node is activated by adding an additional term to the VSC-HVDC compound transformer model Lagrangian for back-to-back and point-to-point systems as well as multi-terminal configurations where no reactive power flows are desired in the DC bus.

## 5.9 References

- [1] Arrillaga, J., *High Voltage Direct Current Transmission*. London: The Institute of Electrical Engineers, 1998.
- [2] Song, H. Y., Johns, T. A., *Flexible ac transmission systems (FACTS)*. London: The Institute for Electrical Engineers, 1999.
- [3] Hingorani, G. N., Gyungyi, L., *Understanding FACTS: Concepts and Technologies of Flexible AC Transmission Systems*: IEEE, 2000.

- [4] Acha, E., Agelidis, V. G., Anaya-Lara, O., Miller, T. J. E., *Power Electronic Control in Electrical Systems*: Newnes, 2002.
- [5] Agelidis, V. G., Demetriades, G. D., Flourentzou N., "Recent Advances in High-Voltage Direct-Current Power Transmission Systems," presented at the Industrial Technology, 2006. ICIT 2006. IEEE International Conference on,, 2006.
- [6] Bahrman, M. P., Johnson, B. K. (2007) The ABCs of HVDC transmission technologies. *Power and Energy Magazine, IEEE*. 32-44.
- [7] Davidson, C. C., de Preville, G., "The future of high power electronics in Transmission and Distribution power systems," presented at the Power Electronics and Applications, 2009. EPE '09. 13th European Conference on,, 2009.
- [8] Pan, J., Nuqui, R., Stivastava, K., Jonsson, T., Holmberg, P., Hafner, Y. -J., "AC Grid with Embedded VSC-HVDC for Secure and Efficient Power Delivery " presented at the Energy 2030 Conference, 2008. ENERGY 2008. IEEE, 2008.
- [9] Azimoh, L. C., Folly, K. A., Chowdhury, S. P., "Mitigations of voltage instability in power systems," presented at the Electrical Power & Energy Conference (EPEC), 2009 IEEE, 2009.
- [10] Bersesti, P., Kling, W. L., Hendriks, R. L., Vailati, R., "HVDC Connection of Offshore Wind Farms to the Transmission System," *Energy Conversion, IEEE Transactions on,,* vol. 22, pp. 37-43, 2007.
- [11] de Alegria, I. M., Martin, J. L., Kortabarria, I., Andreu, J., Ereno, P. I., "Transmission alternatives for offshore electrical power," *Renewable and Sustainable Energy Reviews*, vol. 13, pp. 1027-1038, 2009.
- [12] Robinson, J., Jovicic, D., Joos, G., "Analysis and Design of an Offshore Wind Farm Using a MVDC Grid," *Power Delivery, IEEE Transactions on*, vol. 25, pp. 2164-2173, Oct. 2010.
- [13] Gomis-Bellmunt, O., Liang, J., Ekanayake, J., King, R., Jenkins, N.,, "Topologies of multiterminal HVDC-VSC transmission for large offshore wind farms," *Electric Power Systems Research*, vol. 81, pp. 271-281, 2011.
- [14] Stevenson, W. D., Grainger, J. , *Power System Analysis*: McGraw-Hill 1994.
- [15] Clark, H., Edris, A. -A., El-Gasseir, M., Epp, K., Isaacs, A., Woodford, D. (2008) Softening the Blow of Disturbances. *Power and Energy Magazine, IEEE*. 30-41.
- [16] Guoqing, L., Jian, Z. , "Available Transfer Capability Calculation for AC/DC Systems with VSC-HVDC," presented at the Electrical and Control Engineering (ICECE), 2010 International Conference on,, 2010.
- [17] Pizano-Martinez, A., Fuerte-Esquivel, C. R., Ambriz-Perez, H., Acha, E., "Modeling of VSC-Based HVDC Systems for a Newton-Raphson OPF Algorithm," *Power Systems, IEEE Transactions on*, vol. 22, pp. 1794-1803, Nov. 2007.
- [18] Gengyin, L., Ming, Z., Jie, H., Guangkai, L., Haifeng, L., "Power Flow Calculation of Power Systems Incorporating VSC-HVDC," presented at the Power System Technology, International Conference on, 2004.
- [19] Angeles-Camacho, C., Tortelli, O. L., Acha, E., Fuerte-Esquivel, C. R., "Inclusion of a High Voltage DC-Voltage Source Converter Model in a

- Newton-Raphson Power Flow Algorithm," *Generation, Transmission and Distribution, IEE Proceedings*, vol. 150, pp. 691-696, Nov. 2003.
- [20] Fang, J., Gengyin, L., Zhou, M., Liang, X., "Research on the Voltage Source Converter in VSC-HVDC " presented at the Power System Technology (POWERCON), 2010 International Conference on,, 2010.
- [21] Sarkar, S., Vijayan, P., Aliprantis, D. C., Ajarapu, V., "Effect of grid voltage unbalance on operation of a bi-directional converter," presented at the Power Symposium, 2008. NAPS ' 08. 40th North American 2008.
- [22] Smallwood, C. L., "Distributed generation in autonomous and nonautonomous micro grids," presented at the Rural Electric Power Conference, 2002. 2002 IEEE, 2002.
- [23] Westermann, D., Van Hertem, D., Kuster, A., Atmuri, R., Klockm B., Rauhala, T., "Voltage source converter (VSC) HVDC for bulk power transmission - technology and planning method," presented at the AC and DC Power Transmission, 2010. ACDC. 9th IET International Conference on,, 2010.
- [24] Zhang, L., Harnefors, L., Nee, H. -P., "Interconnection of Two Very Weak AC Systems by VSC-HVDC Links Using Power-Synchronization Control," *Power Systems, IEEE Transactions on*, vol. 26, pp. 344-355, 2011.

## 6 Conclusion

### 6.1 General

The main focus of this research project was to develop comprehensive and flexible mathematical models, aimed at out Optimal Power Flow studies, for a variety of power system components specifically, the fully controlled self-commutated Voltage Source Converter (VSC). This model proved to be the basis with which to model a new variant of High Voltage Direct Current transmission systems, namely VSC-HVDC. The work is also concerned with developing models for VSC-FACTS controllers, such as the STATCOM suitable for shunt reactive power compensation. Through a series of carefully devised test cases as well as simulation studies, various models pertaining to different power system components, have all been successfully tested using the OPF algorithm.

The optimal power flow algorithm, decidedly, is the most important analytical toolbox used to ascertain the optimum point of steady state operation of an arbitrary power system under a variety of circumstances, which may be under the influence of different controllers. It can be solved for a variety of objective functions, however, in this research project for consistency purposes, the objective function has remained the generators' quadratic cost function. For this reason, the results generated by the OPF are the optimum operating point of the system in which the generators power dispatch as well as the power flows within the system yield to optimum costs. Since the OPF is a useful tool in determining system's optimum operating point under different circumstances it has been widely used in modern power system analysis and design scenarios.

All of the models presented throughout this research work have been developed within the Augmented Lagrangian Function framework, which has been proven to be a robust analytical framework for constrained optimisation analysis of large-scale non-linear physical systems, electrical systems included. The models therefore have all been formulated within this particular analytical framework, which would then be solved using Newton's iterative method.

The OPF is carried out for systems with or without FACTS controllers. It has then been observed that FACTS controllers exert an influence into the system behaviour characteristics since comparing results for FACTS-OPF simulations with systems with no FACTS controllers yielded different values of the obtained optimum. Therefore, it is concluded that the presence of controllers in an arbitrary system effectively modifies the boundaries of the solution region of the OPF problem, in which an optimum operating point can be obtained. This very fact is discernible from simulation studies carried out in chapters two, three and four for a variety of systems including the benchmark 8-node system, the IEEE 30-node system as well as the benchmark 5-node system. It was observed that the optimum operating point of the system slightly changes when results from compensated and uncompensated systems are compared with each other.

In Chapter Two, the principles of OPF algorithm, as the main analytical toolbox of this research project, have been thoroughly introduced. A variety of solution algorithms have been presented for solving a non-linear constrained optimisation problem such as the OPF, which mostly consider converting the constrained problem into a single or a group of unconstrained problems by penalising the objective function for points outside the feasible solution space. Two inter-related methods have been presented, namely the Penalty Function method and the Augmented Lagrangian Function method. It has been argued that the latter is mathematically more viable than the former since it does not directly penalise the objective function but it is the Lagrangian function that is being penalised. Thus it has been shown that using the augmented Lagrangian function method has considerable numerical advantage and achieves better convergence rates than pure penalty function methods. The augmented Lagrangian function method then has been used in the power systems paradigm in order to develop models for conventional power systems components such as generators, transmission lines as well as transformers and loads. The non-linear OPF problem is then formulated based on the augmented Lagrangian approach, which is solved by Newton's method using a system of linear equations formed from the derivatives of the Lagrangian function. The optimum operating point is reached by a decreasing pace in the gradient through iteratively solving the linear system of equations. It has been explained that by combining the Hessian and Jacobian elements together the solution algorithm can maintain both good level of sparsity in the matrix of

coefficients in the linear system of equations as well as an acceptable convergence rate. The system constraints have been categorised into equality and inequality constraints. In addition, the latter is exclusively handled using a special set of penalty functions dubbed the exact penalty function, which is essentially the augmented Lagrangian function. The system steady state operation as well as any controllability lies within the role of equality constraints. Two types of equality constraints were introduced: Variable and Functional. It has been shown that the most important set of functional equality constraints are the system power balance equations, which effectively denote system's normal steady state conditions and therefore must be satisfied throughout the solution process. The other types of functional constraints are mostly associated with FACTS controllers and are used to model the system controllability. The functional equality constraints pertaining to the system control criteria are activated by adding their additional Lagrangians to the system Lagrangian whereas the variable equality constraints, which are mostly for cases of direct voltage regulation, are activated using appropriate pure quadratic penalty functions in order to nullify their associated state variable increments throughout Newton's iterations. The OPF algorithm has been extensively tested for 8-, 9-, 11-, 14- and 30-node systems to show its robustness in dealing with different operational circumstances.

With regards to Chapter Three, the concept of FACTS-OPF modelling has been introduced as an approach into developing mathematical models for FACTS controllers within the optimal power flow algorithm. The same hierarchical process presented in chapter two has been utilised in this chapter to formulate OPF models for shunt compensators, in particular the variable impedance type Static VAR Compensator (SVC) and the more advanced VSC-type Static Compensator (STATCOM). Since there was no STATCOM-OPF model that is based on augmented Lagrangian function framework it was decided to introduce a good conventional controllable voltage source model for the STATCOM that is compatible with the OPF. As a result, a new Lagrangian function for the STATCOM was developed. The STATCOM model presented is capable of direct voltage regulation as an exclusive variable equality as well as reactive power compensation as an exclusive functional equality. However, it was argued that the two control constraints couldn't be activated simultaneously. It was discussed that since STATCOM's converter reactive power is a function of its nodal voltage

magnitude, in voltage control mode, the reactive power has to remain free so that it could take up any value that agrees with the target voltage magnitude. This phenomenon resembles the voltage regulation in Generator PV buses, in which penalising the associated Lagrange multiplier deactivates the generators' reactive power functional equality constraint. As a result, it was stated that if a STATCOM is directly regulating voltage magnitude in a given node, that node is essentially seen as a PV node. Through a series of simulation scenarios on the 8-node benchmark system the STATCOM-OPF model's controllability has been verified and its robustness against a variety of operational circumstances tested. By comparing results obtained from both SVC-OPF and STATCOM-OPF models, it was inferred that if similar control constraints are activated, for instance if both devices are regulating the voltage magnitude in similar associated compensated buses, then the OPF converges towards the exact same operating point regardless of the type of the shunt compensator. Once again this mathematical phenomenon proves the decisive role of equality constraints in shaping the OPF feasible solution space.

In Chapter Four, the main goal of this project, which was to develop an advanced mathematical model within the OPF algorithm for Voltage Source Converter (VSC), has been successfully realised. Accordingly, an elaborate mathematical model within the OPF algorithm was presented that describes the behaviour characteristics of a fully controlled self-commutated Voltage Source Converter (VSC), which is then used to create multi-terminal HVDC transmission systems. As an improvement to the conventional modelling criterion, which basically treats the VSC as controllable voltage source behind coupling impedance, in this research project, for the first time, a new VSC model for the OPF algorithm was introduced, which was essentially based on what is called a Compound Transformer possessing a variable complex tap phasor. No other mathematical model, associated with VSCs, is known to possess such strong analytical capabilities within the OPF algorithm. The VSC Compound Transformer model details the PWM control characteristic of an actual VSC in form of a controllable variable complex tap phasor. Consequently, the active power flow control is realised by phase angle compensation of the phase shifter in the compound transformer, whereas the nodal voltage magnitude is maintained using the variable tap changer ratio. Based on the compound model's control constraints, which are introduced on its active power flow as well as nodal

voltages, four distinct control modes (modes of operation) have been presented. The same criteria for activating different functional/variable equality constraints govern the selection process of these control modes according to the system operating requirements. The compound transformer model has been successfully tested for all the possible control mode combinations in a simple AC system comprising one generator. In DC system simulations it was observed that by leaving the phase shifter angle to reach the required phase angle difference between ends of the compound transformer, in order to reach a given target value for converter's active power, the phase angle component of the DC node voltage can be properly ignored in the OPF solution process. As a result, the DC node has only voltage magnitude component with no phase angle eliminating the need for introducing additional connection buses in further system simulations such as multi-terminal VSC-HVDC test cases.

The DC tests have been carried out for a single voltage source converter compound transformer model feeding a DC node. It was clearly shown that the VSC compound transformer model is capable of regulating the system parameters, namely the voltage magnitude as well as active power flow, in both system configurations. Furthermore, the new model has successfully isolated the DC node from any changes in the AC side, which in the case of the DC system, was the generators' active power capacities. It was argued that the VSC in DC system simulations presented in chapter four in fact could be configured as a new STATCOM-OPF model. Consequently it was proved that the compound transformer model reliably provides a new mathematical platform for analysing and modelling the behaviour characteristics of the VSC-type FACTS controllers including the STATCOM.

Eventually, in Chapter Five, the model presented in chapter four was used to derive necessary nodal active and reactive powers that are suitable for modelling multi-terminal VSC-HVDC transmission systems for back-to-back, point-to-point and multi-terminal system configurations. The back-to-back models were entirely based on the compound transformer model developed in chapter four. However, it was shown that for modelling point-to-point VSC-HVDC systems, it is necessary to improve the compound transformer model even further. Thus the expanded compound transformer model was introduced, which is exclusively used to model point-to-point VSC-HVDC and their associated multi-terminal systems. Since

maintaining a DC power transmission calls for activating the power equality constraints at the DC node for each converter it was then argued that in a point-to-point system using the normal compound transformer model, it is virtually impossible to maintain a DC power balance, due to the presence of the DC link transmission losses which are virtually unknown at the start of the OPF process. The expanded compound transformer model, on the other hand, circumvented this problem by including the DC transmission losses as an internal resistive branch within the model. Consequently, the expanded model coupled with normal compound transformer models were shown capable of accurately representing the operational characteristics of any VSC-HVDC configuration with any number of terminals. In order to model multi-terminal VSC-HVDC configurations, both back-to-back and point-to-point VSC-HVDC models were developed for ‘ $n$ ’ number of terminals by introducing a special ‘ $2n \times 2n$ ’ admittance matrix from which their associated nodal active and reactive powers are derived. Ultimately, the nodal powers are used to create the Lagrangian comprising the control constraints of the VSC compound models. The VSC compound model Lagrangian is then added to the system Lagrangian in order to carry out the OPF solution process. Since there is no reactive power in the DC side, the compound transformer model when used for describing the operation of VSC-HVDC links required an additional functional equality constraint on the DC bus reactive power effectively rendering it to zero. It was observed that for maintaining the reactive power constraint at the DC node the shunt branch susceptance needed to be variable. Therefore, the shunt susceptance in the compound transformer model (and in the expanded model) was added to the vector of state variables so that a Lagrangian function can be introduced for the DC link reactive power flow as a function of the variable shunt susceptance. Through different simulation scenarios for different back-to-back, point-to-point and multi-terminal configurations the robustness of the VSC-HVDC compound transformer models in a variety of plausible control modes has been tested and verified. Arguably, the OPF model presented in this chapter for the multi-terminal VSC-HVDC links is the most comprehensive description of the multi-terminal VSC-HVDC systems to date.

## **6.2 A Final Note Regarding Embedded HVDC into an AC System**

The system simulations presented in this thesis particularly in chapter five did not include VSC-HVDC systems that are embedded within an AC system. The reason

was that it was mainly assumed that the VSC-HVDC system is used to connect different autonomous AC grids to each other to create a web of asynchronously interconnected AC grids. In order to properly carry out an OPF solution for such systems, it is required to introduce multiple slack nodes as independent reference points for each autonomous AC section. The OPF will then calculate the state variables for each section with respect to their own slack nodes. While this may work satisfactorily when using VSC-HVDC models developed in this thesis to create asynchronous AC grids, the reliability of the solution method is yet to be realised if the situation reverses, namely if the VSC-HVDC system is embedded in an arbitrary AC grid. The argument is that the necessity to select multiple slack nodes in an embedded system may create numerical difficulties especially if there are not enough candidate nodes to be selected as independent reference points. Therefore care needs to be taken if the models are used to simulate embedded VSC-HVDC systems within AC grids. The best and simplest suggestion is to divide the AC grid into multiple sections, each with their own slack nodes. It should however be stressed here that the modelling criterion and the structures of the admittance matrices for multi-terminal VSC-HVDC models presented in chapter five remain the same regardless of the configuration of the system.

### **6.3 Suggestions for Possible Future Work**

The work presented in this research has been extensive and thorough. It presents a new paradigm in VSC-FACTS and HVDC modelling for optimal power flows. It introduces one of the most realistic and flexible mathematical models for the voltage source converter and ensuing VSC-HVDC transmission systems. Nevertheless, the contributions to the field of power system research in this work can be expanded even further. The following are suggested as possible future research items:

- Mathematical models for Doubly-fed Induction Machines can be added to the VSC-HVDC compound models in order to carry out precise optimal power flow analysis on integration systems based for renewable sources of energy, mainly wind farms
- Possible investigation into the compound transformer model so that the shunt branch can be interchanged between secondary and primary sides of

the transformer which ultimately gives better flexibility in adopting various system configurations

- A comprehensive study can be carried out for developing exclusive FACTS-OPF models for VSC-type FACTS controllers including the STATCOM, SSSC and UPFC (a preliminary STATCOM-OPF simulations was presented as DC system simulations in chapter four, which can be used to expand upon)
- Alternative objective functions may be chosen for performing OPF solutions in the systems presented throughout this thesis;

## **Appendix I**

### **I Complex Nodal Power Calculations**

The complex nodal powers are at the heart of any power system-modelling scenario depicting power flows. In order to derive the nodal active and reactive powers in an arbitrary power system it is imperative to first derive its nodal admittance matrix, from which the required elements to properly calculate the nodal active and reactive powers are obtained. In the following sections the nodal powers for elements used in power systems are calculated. The powers used to model the compound transformer in chapter four are also presented in this section.

## I.1 Complex Nodal Power for a given node

Using complex algebra the complex nodal apparent power flow in a given node  $n$  is defined as the product of its nodal voltage and complex conjugate of current, as such:

$$S_n = V_n I_n^*$$

Knowing the following expression is true for admittance matrix of any system, the term above is expanded further and the nodal active and reactive powers are calculated as such.

$$Y = [G + jB]^T$$

$$S_n = V_n \cdot \left[ \sum_k^{Nbus} Y_{nk}^* \cdot V_k^* \right] \rightarrow S_n = V_n \cdot \left[ \sum_k^{Nbus} (G_{nk} - jB_{nk}) \cdot V_k e^{-j\theta_k} \right] e^{j\theta_n} \rightarrow$$

$\rightarrow$

$$S_n = V_n \cdot \left[ \sum_k^{Nbus} (G_{nk} - jB_{nk}) \cdot V_k e^{j(\theta_n - \theta_k)} \right] \rightarrow$$

$\rightarrow$

$$S_n = V_n \cdot \left[ \sum_k^{Nbus} (G_{nk} - jB_{nk}) \cdot V_k \cdot (\cos \theta_{nk} + j \sin \theta_{nk}) \right] \rightarrow$$

$\rightarrow$

$$S_n = V_n \cdot \left[ \sum_k^{Nbus} (V_k G_{nk} \cos \theta_{nk} + j V_k G_{nk} \sin \theta_{nk} - j V_k B_{nk} \cos \theta_{nk} + V_k B_{nk} \sin \theta_{nk}) \right] \rightarrow$$

$\rightarrow$

$$\begin{cases} P_n = \text{Re}(S_n) = V_n \cdot \sum_k^{Nbus} [V_k (G_{nk} \cos \theta_{nk} + B_{nk} \sin \theta_{nk})] \\ Q_n = \text{Im}(S_n) = V_n \cdot \sum_k^{Nbus} [V_k (G_{nk} \sin \theta_{nk} - B_{nk} \cos \theta_{nk})] \end{cases}$$

## I.2 Load Tap Changer Transformer

For a given load tap changer connecting two fictitious nodes,  $k$  and  $m$  together, the admittance matrix is formed as such:

$$Y_{Transformer} = \begin{bmatrix} Y & -TY \\ -TY & T^2Y \end{bmatrix}$$

In which the following expressions apply for the self and mutual admittance elements:

*Self – Elements*

$$\begin{cases} G_{kk} = G \\ B_{kk} = B \\ G_{mm} = T^2G \\ B_{mm} = T^2B \end{cases}$$

*Mutual – Elements*

$$\begin{cases} G_{km} = G_{mk} = -TG \\ B_{km} = B_{mk} = -TB \end{cases}$$

The complex apparent power for the node  $t$  connected to the transformer is defined below:

$$\begin{cases} S_t = V_t \cdot \left[ \sum_{i=k}^m Y_{ti}^* \cdot V_i^* \right] = V_t e^{j\theta_t} \cdot \sum_{i=k}^m (G_{ti} - jB_{ti}) \cdot V_i e^{-j\theta_i} \\ t = [k, m] \end{cases}$$

Similar to the previous section, the active and reactive power for the sending and receiving ends of the transformer are calculated as such:

$$S_t = V_t \left[ \sum_{i=k}^m V_i (G_{ii} - jB_{ii}) e^{j(\theta_t - \theta_i)} \right] = V_t \left[ \sum_{i=k}^m V_i (G_{ii} - jB_{ii}) (\cos \theta_{ti} + j \sin \theta_{ti}) \right] \rightarrow$$

$$S_t = V_t \left[ \sum_{i=k}^m (V_i G_{ii} \cos \theta_{ti} + j V_i G_{ii} \sin \theta_{ti} - j V_i B_{ii} \cos \theta_{ti} + V_i B_{ii} \sin \theta_{ti}) \right] \rightarrow$$

$$P_t = \text{Re}(S_t) = V_t \sum_{i=k}^m V_i (G_{ii} \cos \theta_{ti} + B_{ii} \sin \theta_{ti})$$

$$Q_t = \text{Im}(S_t) = V_t \sum_{i=k}^m V_i (G_{ii} \sin \theta_{ti} - B_{ii} \cos \theta_{ti})$$

Replacing for the self and mutual elements in the calculated active and reactive power equations, the active and reactive powers for sending and receiving ends of the transformer are calculated as follows, knowing that  $\theta_{km} = \theta_k - \theta_m$ :

Sending End:

$$P_k = V_k^2 G - TV_k V_m [G \cos \theta_{km} + B \sin \theta_{km}]$$

$$Q_k = -V_k^2 B - TV_k V_m [G \sin \theta_{km} - B \cos \theta_{km}]$$

Receiving End:

$$P_m = V_m^2 T^2 G - TV_m V_k [G \cos \theta_{mk} + B \sin \theta_{mk}]$$

$$Q_m = -V_m^2 T^2 B - TV_m V_k [G \sin \theta_{mk} - B \cos \theta_{mk}]$$

For consistency purposes the phase angle difference is always calculated with respect to the primary hence,  $\theta_{mk}$  in nodal active and reactive powers for the receiving end of the transformer is replaced by  $-\theta_{km}$ .

Therefore the nodal powers at the receiving end of the transformer are re-written as such:

$$P_m = V_m^2 T^2 G - TV_m V_k [G \cos \theta_{km} - B \sin \theta_{km}]$$

$$Q_m = -V_m^2 T^2 B - TV_m V_k [-G \sin \theta_{km} - B \cos \theta_{km}]$$

The same criteria applies for nodal active and reactive power calculations pertaining to the compound transformer in chapter four, heeding the difference between the admittance matrix elements.

### I.3 Compound Transformer Model Nodal Power Calculations

The admittance matrix pertaining to the compound transformer model developed and presented in chapter four is given below (See figure 4.4a). The effects of the variable complex tap ratio as well as the shunt branch are included in the admittance matrix.

$$Y_{CompT} = \begin{bmatrix} Y & -(T\angle\varphi_{ps})Y \\ -(T\angle-\varphi_{ps})Y & T^2Y + Y_0 \end{bmatrix}$$

The nodal active and reactive powers for the compound transformer are calculated exactly the same as in a normal load tap changing transformer heeding its associated admittance elements as such for a compound transformer connected between fictitious nodes  $k$  and  $m$ :

$$G_{CompT} = \begin{bmatrix} G_{kk} & -TG_{km}e^{+j\varphi_{ps}} \\ -TG_{mk}e^{-j\varphi_{ps}} & T^2G_{mm} + G_0 \end{bmatrix}$$

And

$$B_{CompT} = \begin{bmatrix} B_{kk} & -TB_{km}e^{+j\varphi_{ps}} \\ -TB_{mk}e^{-j\varphi_{ps}} & T^2B_{mm} + B_0 \end{bmatrix}$$

Knowing the expressions for the self- and mutual elements of the admittance matrix components and the equation for complex nodal apparent power, the active and reactive powers are therefore derived as such:

Sending End:

$$P_k = V_k^2 G - TV_k V_m [G \cos(\theta_{km} - \varphi_{ps}) + B \sin(\theta_{km} - \varphi_{ps})]$$

$$Q_k = -V_k^2 B - TV_k V_m [G \sin(\theta_{km} - \varphi_{ps}) - B \cos(\theta_{km} - \varphi_{ps})]$$

Receiving End:

$$P_m = V_m^2(G_0 + T^2G) - TV_mV_k[G\cos(\theta_{mk} - \varphi_{ps}) - B\sin(\theta_{mk} - \varphi_{ps})]$$

$$Q_m = -V_m^2(B_0 + T^2B) - TV_mV_k[-G\sin(\theta_{mk} - \varphi_{ps}) - B\cos(\theta_{mk} - \varphi_{ps})]$$

## II Hessian and Jacobian Elements for the VSC Compound Transformer Model

In this section, the first and second order partial derivatives (Jacobian and Hessian elements) pertaining to the compound transformer model is presented in two sub-sections.

### II.1 The Compound Model

Partial derivatives for the Hessian and Jacobian terms, as well as the Gradient vector, for the compound model are derived from the powers defined below for a compound transformer that is connected between the nodes  $k$  and  $m$ :

$$P_k = V_k^2 G - TV_k V_m [G \cos(\theta_{km} - \varphi_{ps}) + B \sin(\theta_{km} - \varphi_{ps})] \quad [1]$$

$$Q_k = -V_k^2 B - TV_k V_m [G \sin(\theta_{km} - \varphi_{ps}) - B \cos(\theta_{km} - \varphi_{ps})] \quad [2]$$

$$P_m = V_m^2 (G_0 + T^2 G) - TV_m V_k [G \cos(\theta_{km} - \varphi_{ps}) - B \sin(\theta_{km} - \varphi_{ps})] \quad [3]$$

$$Q_m = -V_m^2 (B_0 + T^2 B) - TV_m V_k [-G \sin(\theta_{km} - \varphi_{ps}) - B \cos(\theta_{km} - \varphi_{ps})] \quad [4]$$

The following auxiliary terms are also defined based on the active and reactive powers in sending and receiving ends of the converter:

Sending End:

$$N_{km} = G \cos(\theta_{km} - \varphi) + B \sin(\theta_{km} - \varphi) \quad [5]$$

$$H_{km} = G \sin(\theta_{km} - \varphi) - B \cos(\theta_{km} - \varphi) \quad [6]$$

Receiving End:

$$N_{mk} = G \cos(\theta_{km} - \varphi) - B \sin(\theta_{km} - \varphi) \quad [7]$$

$$H_{mk} = -G \sin(\theta_{km} - \varphi) - B \cos(\theta_{km} - \varphi) \quad [8]$$

### II.1.1 Hessian/Jacobian with respect to vector $z_1 = [\theta, V, \lambda_p, \lambda_q]^T$

#### II.1.1.1 Hessian with respect to phase angle $\theta_k$

$$\nabla_{\theta_k \theta_k}^2 P_k = +TV_k V_m N_{km} \quad [9]$$

$$\nabla_{\theta_k \theta_k}^2 Q_k = +TV_k V_m H_{km} \quad [10]$$

$$\nabla_{\theta_k \theta_k}^2 P_m = +TV_m V_k N_{mk} \quad [11]$$

$$\nabla_{\theta_k \theta_k}^2 Q_m = +TV_m V_k N_{mk} \quad [12]$$

#### II.1.1.2 Hessian with respect to $\theta_k, V_k$

$$\nabla_{\theta_k V_k}^2 P_k = +TV_m H_{km} \quad [13]$$

$$\nabla_{\theta_k V_k}^2 Q_k = -TV_m N_{km} \quad [14]$$

$$\nabla_{\theta_k V_k}^2 P_m = -TV_m H_{mk} \quad [15]$$

$$\nabla_{\theta_k V_k}^2 Q_m = +TV_m N_{mk} \quad [16]$$

For partial derivatives with respect to phase angle and voltage magnitudes of the receiving end ( $\nabla_{\theta_m V_m}^2 X$ ) the indices  $k$  and  $m$  are interchanged.

#### II.1.1.3 Hessian with respect to phase angle $\theta_m$

$$\nabla_{\theta_m \theta_m}^2 P_k = +TV_k V_m N_{km} \quad [17]$$

$$\nabla_{\theta_m \theta_m}^2 Q_k = +TV_k V_m H_{km} \quad [18]$$

$$\nabla_{\theta_m \theta_m}^2 P_m = +TV_m V_k N_{mk} \quad [19]$$

$$\nabla_{\theta_m \theta_m}^2 Q_m = +TV_m V_k H_{mk} \quad [20]$$

#### II.1.1.4 Hessian with respect to $\theta_k, \theta_m$

$$\nabla_{\theta_k \theta_m}^2 P_k = -TV_k V_m N_{km} \quad [21]$$

$$\nabla_{\theta_k \theta_m}^2 Q_k = -TV_k V_m H_{km} \quad [22]$$

$$\nabla_{\theta_k \theta_m}^2 P_m = -TV_m V_k N_{mk} \quad [23]$$

$$\nabla_{\theta_k \theta_m}^2 Q_m = -TV_m V_k H_{mk} \quad [24]$$

#### II.1.1.5 Hessian with respect to $\theta_k, V_m$

$$\nabla_{\theta_k V_m}^2 P_k = +TV_k H_{km} \quad [25]$$

$$\nabla_{\theta_k V_m}^2 Q_k = -TV_k N_{km} \quad [26]$$

$$\nabla_{\theta_k V_m}^2 P_m = -TV_k H_{mk} \quad [27]$$

$$\nabla_{\theta_k V_m}^2 Q_m = +TV_k N_{mk} \quad [28]$$

For partial derivatives with respect to  $\theta_m, V_k$  ( $\nabla_{\theta_m V_k}^2 X$ ), the indices  $k$  and  $m$  are interchanged.

#### II.1.1.6 Hessian with respect to $V_k$

$$\nabla_{V_k V_k}^2 P_k = 2G \quad [29]$$

$$\nabla_{V_k V_k}^2 Q_k = -2B \quad [30]$$

$$\nabla_{V_k V_k}^2 P_m = 0 \quad [31]$$

$$\nabla_{V_k V_k}^2 Q_m = 0 \quad [32]$$

### II.1.1.7 Hessian with respect to $V_m$

$$\nabla_{V_m V_m}^2 P_k = 0 \quad [33]$$

$$\nabla_{V_m V_m}^2 Q_k = 0 \quad [34]$$

$$\nabla_{V_m V_m}^2 P_m = 2(G_0 + T^2 G) \quad [35]$$

$$\nabla_{V_m V_m}^2 Q_m = -2(B_0 + T^2 B) \quad [36]$$

### II.1.1.8 Hessian with respect to $V_k, V_m$

$$\nabla_{V_k V_m}^2 P_k = -TN_{km} \quad [37]$$

$$\nabla_{V_k V_m}^2 Q_k = -TH_{km} \quad [38]$$

$$\nabla_{V_k V_m}^2 P_m = -TN_{mk} \quad [39]$$

$$\nabla_{V_k V_m}^2 Q_m = -TH_{mk} \quad [40]$$

**II.1.1.9 Jacobian with respect to  $\theta_k$**

$$\nabla_{\theta_k} P_k = +TV_k V_m H_{km} \quad [41]$$

$$\nabla_{\theta_k} Q_k = -TV_k V_m N_{km} \quad [42]$$

$$\nabla_{\theta_k} P_m = -TV_m V_k H_{mk} \quad [43]$$

$$\nabla_{\theta_k} Q_m = +TV_m V_k N_{mk} \quad [44]$$

For Jacobian terms of powers with respect to  $\theta_m$  ( $\nabla_{\theta_k} X$ ), the indices  $k$  and  $m$  are interchanged.

**II.1.1.10 Jacobian with respect to  $V_k$**

$$\nabla_{V_k} P_k = 2V_k G - TV_m N_{km} \quad [45]$$

$$\nabla_{V_k} Q_k = -2V_k B - TV_m H_{km} \quad [46]$$

$$\nabla_{V_k} P_m = -TV_m N_{mk} \quad [47]$$

$$\nabla_{V_k} Q_m = -TV_m H_{mk} \quad [48]$$

### II.1.1.11 Jacobian with respect to $V_m$

$$\nabla_{V_m} P_k = -TV_k N_{km} \quad [49]$$

$$\nabla_{V_m} Q_k = -TV_k H_{km} \quad [50]$$

$$\nabla_{V_m} P_m = 2(G_0 + T^2 G)V_m - TV_k N_{mk} \quad [51]$$

$$\nabla_{V_m} Q_m = -2(B_0 + T^2 B)V_m - TV_k H_{mk} \quad [52]$$

### II.1.2 Exclusive Hessian/Jacobian with respect to vector $z_{ps} = [\varphi_{ps}, T, \lambda_{\varphi_{ps}}]^T$

#### II.1.2.1 Hessian/Jacobian with respect to $\varphi_{ps}$

The Hessian/Jacobian terms of powers with respect to  $\varphi_{ps}$  follow the two general formats stated below and therefore will not be repeated here:

$$H \Rightarrow \nabla_{\varphi_{ps} z}^2 X = \nabla_{\theta_m z}^2 X \quad [53]$$

$$J \Rightarrow \nabla_{\varphi_{ps}} X = \nabla_{\theta_m} X \quad [54]$$

#### II.1.2.2 Hessian/Jacobian with respect to $T$

$$\bullet \quad dTd\theta_k$$

$$\nabla_{T\theta_k}^2 P_k = +V_k V_m H_{km} \quad [55]$$

$$\nabla_{T\theta_k}^2 Q_k = -V_k V_m N_{km} \quad [56]$$

$$\nabla_{T\theta_k}^2 P_m = -V_m V_k H_{mk} \quad [57]$$

$$\nabla_{T\theta_k}^2 Q_m = +V_m V_k N_{mk} \quad [58]$$

For Hessian terms with respect to  $T\theta_m$  ( $\nabla_{T\theta_m}^2 X$ ) the indices are interchanged.

•  $dTdV_k$

$$\nabla_{TV_k}^2 P_k = -V_m N_{km} \quad [59]$$

$$\nabla_{TV_k}^2 Q_k = -V_m H_{km} \quad [60]$$

$$\nabla_{TV_k}^2 P_m = -V_m N_{mk} \quad [61]$$

$$\nabla_{TV_k}^2 Q_m = -V_m H_{mk} \quad [62]$$

•  $dTd\lambda_{p_k}$

$$\nabla_T P_k = -V_k V_m N_{km} \quad [63]$$

•  $dTd\lambda_{q_k}$

$$\nabla_T Q_k = -V_k V_m H_{km} \quad [64]$$

- $dTd\lambda_{p_m}$   

$$\nabla_T P_m = 2TV_m^2 G - V_m V_k N_{mk} \quad [65]$$

- $dTd\lambda_{q_m}$   

$$\nabla_T Q_m = -2TV_m^2 B - V_m V_k H_{mk} \quad [66]$$

- $dTdV_m$   

$$\nabla_{TV_m}^2 P_k = -V_k N_{km} \quad [67]$$

$$\nabla_{TV_m}^2 Q_k = -V_k H_{km} \quad [68]$$

$$\nabla_{TV_m}^2 P_m = 4TGV_m - V_k N_{mk} \quad [69]$$

$$\nabla_{TV_m}^2 Q_m = -4TBV_m - V_k H_{mk} \quad [70]$$

- $dTd\varphi_{ps}$   

$$\nabla_{T\varphi_{ps}}^2 X = \nabla_{T\varphi_{ps}}^2 X \quad [71]$$

- $dT^2$   

$$\nabla_{T^2}^2 P_m = 2GV_m^2 \quad [72]$$

$$\nabla_{T^2}^2 Q_m = -2BV_m^2 \quad [73]$$

### II.1.2.3 Gradient terms with respect to $\lambda_{\varphi_{ps}}$

$$\nabla_{\lambda_{\varphi_{ps}}} L = \begin{cases} \Delta P_{km}^{(1)} = P_k - P_{specified} \\ \Delta P_{km}^{(2)} = P_m - P_{specified} \end{cases} \quad [74]$$

## II.2 The Expanded Compound Transformer Model

This section contains the Hessian and Jacobian elements for the expanded compound transformer model explained in chapter five. Notice that the partial derivatives (exclusive terms) are based on active and reactive powers associated with the expanded compound transformer model. It should be noted that the expanded compound transformer is used to model point-to-point and multi-terminal VSC-HVDC links. The vector of state variables for modelling point-to-point VSC-HVDC link has the additional elements pertaining to the converter's shunt variable susceptance to bind the reactive power at the DC node to zero, which takes the shape of  $z_{ps} = [\varphi_{ps}, T, \lambda_{\varphi_{ps}}, B_0, \lambda_B]^T$ .

Note: the partial derivatives for the expanded model are exactly the same with respect to sub-vector  $[z_1, \varphi_{ps}, \lambda_{\varphi_{ps}}]^T$ , the only difference is in partial derivatives with respect to  $T$  and  $B_0$ , because the admittance matrix elements of the expanded model are themselves functions of transformer's tap changer magnitude and variable shunt susceptance. In order to calculate their corresponding Hessian and Jacobian elements the following auxiliary equations are introduced:

### II.2.1 Auxiliary Equations – Tap Changer

Based on the VSC expanded model calculations and its reduced admittance matrix (See chapter five), the following applies to the partial derivatives with respect to converter tap changer magnitude:

$$(K^*)^{-1} = \Delta_R + j\Delta_I \rightarrow \nabla_T (K^*)^{-1} = \nabla_T (\Delta_R) + j\nabla_T (\Delta_I) \quad [75]$$

Solving for  $\nabla_T(K^*)^{-1}$  we will have the following partial derivatives:

$$\nabla_T \Delta_R = \frac{\nabla_T \Delta'(|K|^2) - \Delta'(\nabla_T |K|^2)}{(|K|^2)^2} = \frac{n_1}{d} \quad [76]$$

$$\nabla_T \Delta_I = \frac{\nabla_T \Delta''(|K|^2) - \Delta''(\nabla_T |K|^2)}{(|K|^2)^2} = \frac{n_2}{d} \quad [77]$$

$$\nabla_T^2 \Delta_R = \frac{d(\nabla_T n_1) - n_1(\nabla_T d)}{d^2} \quad [78]$$

$$\nabla_T^2 \Delta_I = \frac{d(\nabla_T n_2) - n_2(\nabla_T d)}{d^2} \quad [79]$$

In which the following terms are defined:

$$|K|^2 = \Delta'^2 + \Delta''^2 \rightarrow \begin{cases} \nabla_T |K|^2 = \nabla_T(\Delta'^2) + \nabla_T(\Delta''^2) \\ \nabla_T^2 |K|^2 = \nabla_T^2(\Delta'^2) + \nabla_T^2(\Delta''^2) \end{cases} \quad [80]$$

Followed by these auxiliary equations:

$$\nabla_T \Delta' = 2TG_1 \quad [81]$$

$$\nabla_T^2 \Delta' = 2G_1 \quad [82]$$

$$\nabla_T \Delta'' = 2TB_1 \quad [83]$$

$$\nabla_{T^2}^2 \Delta'' = 2B_1 \quad [84]$$

$$\nabla_T(\Delta'^2) = 4T^3 G_1^2 + 4TG_1 G_0 + 4TG_1 G_{dc} \quad [85]$$

$$\nabla_{T^2}^2(\Delta'^2) = 12T^2 G_1^2 + 4G_1 G_0 + 4G_1 G_{dc} \quad [86]$$

$$\nabla_T(\Delta''^2) = 4T^3 B_1^2 + 4TB_1 B_0 + 4TB_1 B_{dc} \quad [87]$$

$$\nabla_{T^2}^2(\Delta''^2) = 12T^2 B_1^2 + 4B_1 B_0 + 4B_1 B_{dc} \quad [88]$$

$$\nabla_T(n_1) = (\nabla_{T^2}^2(\Delta'))|K|^2 - (\nabla_{T^2}^2(|K|^2))\Delta' \quad [89]$$

$$\nabla_T(n_2) = (\nabla_{T^2}^2(\Delta''))|K|^2 - (\nabla_{T^2}^2(|K|^2))\Delta'' \quad [90]$$

$$\nabla_T(d) = 2|K|^2 \nabla_T |K|^2 \quad [91]$$

The impedance elements are also themselves functions of the converter's tap changer and therefore they are needed for nodal powers partial derivatives:

Self-Elements: Sending End

$$\nabla_T(G_{eq1}) = (\nabla_T \Delta_R)G_{11} - (\nabla_T \Delta_I)B_{11} \quad [92]$$

$$\nabla_{T^2}^2(G_{eq1}) = (\nabla_{T^2}^2 \Delta_R)G_{11} - (\nabla_{T^2}^2 \Delta_I)B_{11} \quad [93]$$

$$\nabla_T(B_{eq1}) = (\nabla_T \Delta_R)B_{11} + (\nabla_T \Delta_I)G_{11} \quad [94]$$

$$\nabla_{T^2}^2(B_{eq1}) = (\nabla_{T^2}^2 \Delta_R)B_{11} + (\nabla_{T^2}^2 \Delta_I)G_{11} \quad [95]$$

Self-Elements: Receiving End

Auxiliary Equations:

$$\nabla_T G_{22} = (\nabla_T \Delta')G_{dc} - (\nabla_T \Delta'')B_{dc} \quad [96]$$

$$\nabla_{T^2}^2 G_{22} = (\nabla_{T^2}^2 \Delta')G_{dc} - (\nabla_{T^2}^2 \Delta'')B_{dc} \quad [97]$$

$$\nabla_T B_{22} = -\{(\nabla_T \Delta')B_{dc} + (\nabla_T \Delta'')G_{dc}\} \quad [98]$$

$$\nabla_{T^2}^2 B_{22} = -\{(\nabla_{T^2}^2 \Delta')B_{dc} + (\nabla_{T^2}^2 \Delta'')G_{dc}\} \quad [99]$$

Main Equations:

$$\nabla_T(G_{eq2}) = (\nabla_T \Delta_R)G_{22} + (\nabla_T G_{22})\Delta_R - \{(\nabla_T \Delta_I)B_{22} + (\nabla_T B_{22})\Delta_I\} \quad [100]$$

$$\begin{aligned} \nabla_{T^2}^2(G_{eq2}) &= (\nabla_{T^2}^2 \Delta_R)G_{22} + 2(\nabla_T \Delta_R)(\nabla_T G_{22}) + (\nabla_{T^2}^2 G_{22})\Delta_R \\ &\quad - \{(\nabla_{T^2}^2 \Delta_I)B_{22} + 2(\nabla_T B_{22})(\nabla_T \Delta_I) + (\nabla_{T^2}^2 B_{22})\Delta_I\} \end{aligned} \quad [101]$$

$$\nabla_T(B_{eq2}) = (\nabla_T \Delta_R)B_{22} + (\nabla_T B_{22})\Delta_R + (\nabla_T \Delta_I)G_{22} + (\nabla_T G_{22})\Delta_I \quad [102]$$

$$\begin{aligned} \nabla_{T^2}^2(B_{eq2}) &= (\nabla_{T^2}^2 \Delta_R)B_{22} + 2(\nabla_T \Delta_R)(\nabla_T B_{22}) + (\nabla_{T^2}^2 B_{22})\Delta_R \\ &+ (\nabla_{T^2}^2 \Delta_I)G_{22} + 2(\nabla_T G_{22})(\nabla_T \Delta_I) + (\nabla_{T^2}^2 G_{22})\Delta_I \end{aligned} \quad [103]$$

Mutual Elements:

$$\nabla_T G_{eq1dc} = \nabla_T G_{eq2dc} = (\nabla_T \Delta_R)G_{12} - (\nabla_T \Delta_I)B_{12} \quad [104]$$

$$\nabla_{T^2}^2 G_{eq1dc} = \nabla_{T^2}^2 G_{eq2dc} = (\nabla_{T^2}^2 \Delta_R)G_{12} - (\nabla_{T^2}^2 \Delta_I)B_{12} \quad [105]$$

$$\nabla_T B_{eq1dc} = \nabla_T B_{eq2dc} = (\nabla_T \Delta_R)B_{12} + (\nabla_T \Delta_I)G_{12} \quad [106]$$

$$\nabla_{T^2}^2 B_{eq1dc} = \nabla_{T^2}^2 B_{eq2dc} = (\nabla_{T^2}^2 \Delta_R)B_{12} + (\nabla_{T^2}^2 \Delta_I)G_{12} \quad [107]$$

Power auxiliary equations (first and second order partial derivatives):

Sending End:

$$\nabla_T^i N_{km} = \nabla_T^i G_{eq1dc} \cos(\theta_{km} - \varphi_{ps}) \pm \nabla_T^i B_{eq1dc} \sin(\theta_{km} - \varphi_{ps}) \quad [108]$$

$$\nabla_T^i H_{km} = \pm \nabla_T^i G_{eq1dc} \sin(\theta_{km} - \varphi_{ps}) - \nabla_T^i B_{eq1dc} \cos(\theta_{km} - \varphi_{ps}) \quad [109]$$

For receiving end auxiliary equations the indices  $k$  and  $m$  are interchanged. The negative signs in  $(\pm)$  apply in auxiliary equations for receiving end nodal powers.

### II.2.2 Hessian/Jacobian terms with respect to $T$

- $dTd\theta_k$ 

$$\nabla_{T\theta_k}^2 P_k = +V_k V_m (T\nabla_T H_{km} + H_{km}) \quad [110]$$

$$\nabla_{T\theta_k}^2 Q_k = -V_k V_m (T\nabla_T N_{km} + N_{km}) \quad [111]$$

$$\nabla_{T\theta_k}^2 P_m = -V_k V_m (T\nabla_T H_{mk} + H_{mk}) \quad [112]$$

$$\nabla_{T\theta_k}^2 Q_m = +V_k V_m (T\nabla_T N_{mk} + N_{mk}) \quad [113]$$

For Hessian terms with respect to  $T\theta_m$  ( $\nabla_{T\theta_m}^2 X$ ) the indices are interchanged.

- $dTdV_k$ 

$$\nabla_{TV_k}^2 P_k = 2(\nabla_T G_{eq1})V_k - V_m (T\nabla_T N_{km} + N_{km}) \quad [114]$$

$$\nabla_{TV_k}^2 Q_k = -2(\nabla_T B_{eq1})V_k - V_m (T\nabla_T H_{km} + H_{km}) \quad [115]$$

$$\nabla_{TV_k}^2 P_m = -V_m (T\nabla_T N_{mk} + N_{mk}) \quad [116]$$

$$\nabla_{TV_k}^2 Q_m = -V_m (T\nabla_T H_{mk} + H_{mk}) \quad [117]$$

- $dTd\lambda_p / dTd\lambda_q$

$$\nabla_T P_k = (\nabla_T G_{eq1}) V_k^2 - V_k V_m (T \nabla_T N_{km} + N_{km}) \quad [118]$$

$$\nabla_T Q_k = (-\nabla_T B_{eq1}) V_k^2 - V_k V_m (T \nabla_T H_{km} + H_{km}) \quad [119]$$

$$\nabla_T P_m = (\nabla_T G_{eq2}) V_m^2 - V_k V_m (T \nabla_T N_{mk} + N_{mk}) \quad [120]$$

$$\nabla_T Q_m = (-\nabla_T B_{eq2}) V_m^2 - V_k V_m (T \nabla_T H_{mk} + H_{mk}) \quad [121]$$

- $dTdV_m$

$$\nabla_{TV_m}^2 P_k = -V_k (T \nabla_T N_{km} + N_{km}) \quad [122]$$

$$\nabla_{TV_m}^2 Q_k = -V_k (T \nabla_T H_{km} + H_{km}) \quad [123]$$

$$\nabla_{TV_m}^2 P_m = 2(\nabla_T G_{eq2}) V_m - V_k (T \nabla_T N_{mk} + N_{mk}) \quad [124]$$

$$\nabla_{TV_m}^2 Q_m = -2(\nabla_T B_{eq2}) V_m - V_k (T \nabla_T H_{mk} + H_{mk}) \quad [125]$$

- $dTd\varphi_{ps}$

$$\nabla_{T\varphi_{ps}}^2 X = \nabla_{T\varphi_{ps}}^2 X \quad [126]$$

- $dT^2$

$$\nabla_{T^2}^2 P_k = (\nabla_{T^2}^2 G_{eq1}) V_k^2 - (T \nabla_{T^2}^2 N_{km} + 2 \nabla_T N_{km}) V_k V_m \quad [127]$$

$$\nabla_{T^2}^2 Q_k = (-\nabla_{T^2}^2 B_{eq1})V_k^2 - (T\nabla_{T^2}^2 H_{km} + 2\nabla_T H_{km})V_k V_m \quad [128]$$

$$\nabla_{T^2}^2 P_m = (\nabla_{T^2}^2 G_{eq2})V_m^2 - (T\nabla_{T^2}^2 N_{mk} + 2\nabla_T N_{mk})V_k V_m \quad [129]$$

$$\nabla_{T^2}^2 Q_m = (-\nabla_{T^2}^2 B_{eq2})V_m^2 - (T\nabla_{T^2}^2 H_{mk} + 2\nabla_T H_{mk})V_k V_m \quad [130]$$

### II.2.3 Auxiliary Equations – Variable Shunt Susceptance

The variable shunt susceptance is defined in order to simulate the conditions of a DC link in which reactive power flow is zero. Consequently the variable shunt susceptance puts a new constraint on converter's receiving end reactive power forcing it into zero. Since the expanded model admittance matrix elements are themselves functions of its shunt susceptance, therefore new partial derivatives with respect to the expanded model's variable shunt susceptance need to be defined.

The auxiliary equations for Hessian and Jacobian terms with respect to  $B_0$  are defined as such:

$$(K^*)^{-1} = \Delta_R + j\Delta_I \rightarrow \nabla_{B_0} (K^*)^{-1} = \nabla_{B_0} (\Delta_R) + j\nabla_T (\Delta_I) \quad [131]$$

$$\nabla_{B_0} \Delta_R = \frac{-(\nabla_{B_0} (\Delta^2))\Delta'}{(lK l^2)^2} = \frac{a_1}{d} \quad [132]$$

$$\nabla_{B_0} \Delta_I = \frac{(lK l^2) - (\nabla_T (\Delta^2))\Delta''}{(lK l^2)^2} = \frac{a_2}{d} \quad [133]$$

$$\nabla_{B_0^2}^2 \Delta_R = \frac{d(\nabla_{B_0} a_1) - a_1(\nabla_{B_0} d)}{d^2} \quad [134]$$

$$\nabla_{B_0^2}^2 \Delta_I = \frac{d(\nabla_{B_0} a_2) - a_2(\nabla_{B_0} d)}{d^2} \quad [135]$$

In which the following non-zero terms are defined with respect to compound model's variable shunt susceptance:

$$\nabla_{B_0} \Delta'' = 1 \quad [136]$$

$$\nabla_{B_0} (\Delta'^2) = 2B_0 + 2T^2 B_1 + 2B_{dc} \quad [137]$$

$$\nabla_{B_0^2}^2 (\Delta'^2) = 2 \quad [138]$$

$$\nabla_{B_0} (a_1) = -\nabla_{B_0^2}^2 (\Delta'^2) \Delta' = -2\Delta' \quad [139]$$

$$\nabla_{B_0} (a_2) = -\nabla_{B_0^2}^2 (\Delta'^2) \Delta'' = -2\Delta'' \quad [140]$$

$$\nabla_{B_0} (d) = 2 |K|^2 \nabla_{B_0} (\Delta'^2) \quad [141]$$

Notice the difference between auxiliary partial derivatives with respect to the shunt branch variable susceptance and the ones developed in the previous section which were all based on compound model's controllable tap changer magnitude.

The impedance elements are as well defined as functions of the variable shunt susceptance, and therefore their partial derivatives are as such:

Self-Elements: Sending End

Auxiliary Equations:

$$\nabla_{B_0} G_{11} = -B_1 \quad [142]$$

$$\nabla_{B_0^2}^2 G_{11} = 0 \quad [143]$$

$$\nabla_{B_0} B_{11} = -G_1 \quad [144]$$

$$\nabla_{B_0^2}^2 B_{11} = 0 \quad [145]$$

Main Equations:

$$\nabla_{B_0} (G_{eq1}) = (\nabla_{B_0} \Delta_R) G_{11} - \Delta_R (\nabla_{B_0} G_{11}) - \{(\nabla_{B_0} \Delta_I) B_{11} + (\nabla_{B_0} B_{11}) \Delta_I\} \quad [146]$$

$$\nabla_{B_0^2}^2 (G_{eq1}) = (\nabla_{B_0^2}^2 \Delta_R) G_{11} + 2(\nabla_{B_0} \Delta_R) (\nabla_{B_0} G_{11}) - (\nabla_{B_0^2}^2 \Delta_I) B_{11} - (2\nabla_{B_0} \Delta_I) (\nabla_{B_0} B_{11}) \quad [147]$$

$$\nabla_{B_0} (B_{eq1}) = (\nabla_{B_0} \Delta_R) B_{11} + \Delta_R (\nabla_{B_0} B_{11}) + (\nabla_{B_0} \Delta_I) G_{11} + (\nabla_{B_0} G_{11}) \Delta_I \quad [148]$$

$$\nabla_{B_0^2}^2 (B_{eq1}) = (\nabla_{B_0^2}^2 \Delta_R) B_{11} + 2(\nabla_{B_0} \Delta_R) (\nabla_{B_0} B_{11}) + (\nabla_{B_0^2}^2 \Delta_I) G_{11} + (2\nabla_{B_0} \Delta_I) (\nabla_{B_0} G_{11}) \quad [149]$$

Self-Elements: Receiving End

$$\nabla_{B_0} G_{22} = 0 \quad [150]$$

$$\nabla_{B_0^2}^2 G_{22} = 0 \quad [151]$$

$$\nabla_{B_0} B_{22} = -G_{dc} \quad [152]$$

$$\nabla_{B_0^2}^2 B_{22} = 0 \quad [153]$$

Main Equations:

$$\nabla_{B_0} (G_{eq2}) = (\nabla_{B_0} \Delta_R) G_{22} - \{(\nabla_{B_0} \Delta_I) B_{22} + (\nabla_{B_0} B_{22}) \Delta_I\} \quad [154]$$

$$\nabla_{B_0^2}^2 (G_{eq2}) = (\nabla_{B_0^2}^2 \Delta_R) G_{22} - (\nabla_{B_0^2}^2 \Delta_I) B_{22} - (2\nabla_{B_0} \Delta_I) (\nabla_{B_0} B_{22}) \quad [155]$$

$$\nabla_{B_0} (B_{eq2}) = (\nabla_{B_0} \Delta_R) B_{22} + \Delta_R (\nabla_{B_0} B_{22}) + (\nabla_{B_0} \Delta_I) G_{22} \quad [156]$$

$$\nabla_{B_0^2}^2 (B_{eq2}) = (\nabla_{B_0^2}^2 \Delta_R) B_{22} + 2(\nabla_{B_0} \Delta_R) (\nabla_{B_0} B_{22}) + (\nabla_{B_0^2}^2 \Delta_I) G_{22} \quad [157]$$

Mutual Elements:

$$\nabla_{B_0} G_{eq1dc} = \nabla_{B_0} G_{eq2dc} = (\nabla_{B_0} \Delta_R) G_{12} - (\nabla_{B_0} \Delta_I) B_{12} \quad [158]$$

$$\nabla_{B_0^2}^2 G_{eq2dc} = \nabla_{B_0^2} G_{eq2dc} = (\nabla_{B_0^2} \Delta_R) G_{12} - (\nabla_{B_0^2} \Delta_I) B_{12} \quad [159]$$

$$\nabla_{B_0} B_{eq1dc} = \nabla_{B_0} B_{eq2dc} = (\nabla_{B_0} \Delta_R) B_{12} + (\nabla_{B_0} \Delta_I) G_{12} \quad [160]$$

$$\nabla_{B_0^2}^2 B_{eq1dc} = \nabla_{B_0^2}^2 B_{eq2dc} = (\nabla_{B_0^2} \Delta_R) B_{12} + (\nabla_{B_0^2} \Delta_I) G_{12} \quad [161]$$

The power auxiliary equations are formed with respect to the shunt susceptance and their general expressions are the same as in the equations with respect to the variable tap changer. Therefore they will not be mentioned here.

#### II.2.4 Hessian/Jacobian terms with respect to variable shunt susceptance

Most of the general expressions associated with Hessian and Jacobian terms of the expanded model's nodal powers with respect to its shunt susceptance resemble the ones with respect to the variable tap changer ratio, however some terms are different and are presented in this section:

- $dB_0 d\theta_k$ 

$$\nabla_{B_0 \theta_k}^2 P_k = +TV_k V_m \nabla_{B_0} H_{km} \quad [162]$$

$$\nabla_{B_0 \theta_k}^2 Q_k = -TV_k V_m \nabla_T N_{km} \quad [163]$$

$$\nabla_{B_0 \theta_k}^2 P_m = -TV_k V_m \nabla_T H_{mk} \quad [164]$$

$$\nabla_{B_0 \theta_k}^2 Q_m = +TV_k V_m \nabla_T N_{mk} \quad [165]$$

For Hessian terms with respect to  $B_0\theta_m (\nabla_{B_0\theta_m}^2 X)$  the indices are interchanged. The Hessian components with respect to the variable phase shifter and the shunt susceptance are the same as  $\nabla_{B_0\theta_m}^2 X$  terms and will not be re-written here.

$$\begin{aligned} & \bullet \quad dB_0 dV_k \\ & \qquad \nabla_{B_0 V_k}^2 P_m = -TV_m \nabla_{B_0} N_{mk} \end{aligned} \quad [166]$$

$$\nabla_{B_0 V_k}^2 Q_m = -TV_m \nabla_{B_0} H_{mk} \quad [167]$$

For Hessian terms with respect to  $dB_0 dV_m (\nabla_{B_0}^2 X)$ , the indices are interchanged.

$$\begin{aligned} & \bullet \quad dB_0 d\lambda_p / dB_0 d\lambda_q \\ & \qquad \nabla_{B_0} P_k = (\nabla_T G_{eq1}) V_k^2 - TV_k V_m \nabla_{B_0} N_{km} \end{aligned} \quad [168]$$

$$\nabla_{B_0} Q_k = (-\nabla_{B_0} B_{eq1}) V_k^2 - TV_k V_m \nabla_{B_0} H_{km} \quad [169]$$

$$\nabla_{B_0} P_m = (\nabla_{B_0} G_{eq2}) V_m^2 - TV_k V_m \nabla_{B_0} N_{mk} \quad [170]$$

$$\nabla_{B_0} Q_m = (-\nabla_{B_0} B_{eq2}) V_m^2 - TV_k V_m \nabla_{B_0} H_{mk} \quad [171]$$

$$\begin{aligned} & \bullet \quad dB_0^2 \\ & \qquad \nabla_{B_0^2} P_k = (\nabla_{B_0^2} G_{eq1}) V_k^2 - (TV_{B_0^2} N_{km}) V_k V_m \end{aligned} \quad [172]$$

$$\nabla_{B_0^2}^2 Q_k = (-\nabla_{B_0^2}^2 B_{eq1})V_k^2 - (T\nabla_{B_0^2}^2 H_{km})V_k V_m \quad [173]$$

$$\nabla_{B_0^2}^2 P_m = (\nabla_{B_0^2}^2 G_{eq2})V_m^2 - (T\nabla_{B_0^2}^2 N_{mk})V_k V_m \quad [174]$$

$$\nabla_{B_0^2}^2 Q_m = (-\nabla_{B_0^2}^2 B_{eq2})V_m^2 - (T\nabla_{B_0^2}^2 H_{mk})V_k V_m \quad [175]$$

- $dTdB_0$

Since the Jacobian elements with respect to  $T$  have already been calculated in equations (110-113), to calculate the Hessians with respect to both  $T$  and  $B_0$ , it is only necessary to calculate the derivatives of equations (110-113) with respect to  $B_0$ . In other words the expression below applies:

$$\nabla_{TB_0}^2 X = \nabla_{B_0} (\nabla_T X) \quad [176]$$

And  $X$  pertains to the expanded model nodal active and reactive powers.

It should be noted that in all of the above calculations regarding the expanded model, there is no susceptance element in the DC link and therefore by default  $B_{dc}$  has been set to zero. If a non-zero value is chosen for the susceptance element, the current passing through the link admittance no longer represents a DC current.

## Appendix II

### Test System Data (in per unit)

Note: The following system data have been used for all the system simulations that are presented in this thesis. For multi-terminal VSC-HVDC system simulations including the multi-terminal back-to-back test cases, the machines limits region have been expanded to properly reflect on their operating conditions as synchronous motors.

- **8-node System**

Bus No.	Bus Type	$P_G(p.u.)$	$Q_G(p.u.)$	$P_d(p.u.)$	$Q_d(p.u.)$
1	Generator P,V	$0.1 \leq P_{G_1} \leq 2.0$	$-5.00 \leq Q_{G_1} \leq 5.00$	0.00	0.00
2	Generator P,V	$0.1 \leq P_{G_2} \leq 2.0$	$-5.00 \leq Q_{G_2} \leq 5.00$	0.20	0.10
3	Load P,Q	0.00	0.00	0.45	0.15
4	Load P,Q	0.00	0.00	0.40	0.05
5	Load P,Q	0.00	0.00	0.60	0.10
6	Load P,Q	0.00	0.00	0.00	0.00
7	Load P,Q	0.00	0.00	0.00	0.00
8	Load P,Q	0.00	0.00	0.20	0.10

**Table I.1 – Bus Data**

Line No.	Sending End	Receiving End	$R_{line}(p.u.)$	$X_{line}(p.u.)$	$G_{line}(p.u.)$	$B_{line}(p.u.)$
1	1	2	0.02	0.06	0.00	0.06
2	1	3	0.08	0.24	0.00	0.05
3	2	3	0.06	0.18	0.00	0.04
4	2	4	0.06	0.18	0.00	0.04
5	2	5	0.04	0.12	0.00	0.03
6	6	4	0.01	0.03	0.00	0.02
7	4	7	0.04	0.12	0.00	0.025
8	4	8	0.04	0.12	0.00	0.025
9	5	8	0.04	0.10	0.00	0.020

**Table I.2 – Line Data**

<b>Slack</b>	$0.9 \leq V_{slack} \leq 1.5$
<b>Generator Bus</b>	$0.9 \leq V_{gen} \leq 1.1$
<b>Load Bus</b>	$0.9 \leq V_{load} \leq 1.1$

**Table I.3 – Limits Data**

• **9-node System**

Bus No.	Bus Type	$P_G(p.u.)$	$Q_G(p.u.)$	$P_d(p.u.)$	$Q_d(p.u.)$
1	Generator P,V	$0.1 \leq P_{G_1} \leq 2.5$	$-3.00 \leq Q_{G_1} \leq 3.00$	0.00	0.00
2	Generator P,V	$0.1 \leq P_{G_2} \leq 3.0$	$-3.00 \leq Q_{G_2} \leq 3.00$	0.00	0.00
3	Generator P,V	$0.1 \leq P_{G_3} \leq 2.7$	$-3.00 \leq Q_{G_3} \leq 3.00$	0.00	0.00
4	Load P,Q	0.00	0.00	0.00	0.00
5	Load P,Q	0.00	0.00	0.90	0.30
6	Load P,Q	0.00	0.00	0.00	0.00
7	Load P,Q	0.00	0.00	1.00	0.35
8	Load P,Q	0.00	0.00	0.00	0.00
9	Load P,Q	0.00	0.00	1.25	0.50

**Table I.4 – Bus Data**

Line No.	Sending End	Receiving End	$R_{line}(p.u.)$	$X_{line}(p.u.)$	$G_{line}(p.u.)$	$B_{line}(p.u.)$
1	4	5	0.0170	0.0920	0.00	0.1580
2	5	6	0.0390	0.1700	0.00	0.3580
3	6	7	0.0119	0.1008	0.00	0.2090
4	7	8	0.0085	0.0720	0.00	0.1490
5	8	9	0.0320	0.1610	0.00	0.3060
6	9	4	0.01	0.850	0.00	0.1760

**Table I.5 – Line Data**

Transformer No.	Sending Bus	Receiving Bus	$X_t(p.u.)$	Tap (primary)
1	1	4	0.0576	1.0
2	3	6	0.0586	1.0
3	2	8	0.0625	1.0
4 (Test Run Two Only)	4	9	0.0500	1.0

**Table I.6 – Transformer Data**

Slack	$0.9 \leq V_{slack} \leq 1.1$
Generator Bus	$0.9 \leq V_{gen} \leq 1.1$
Load Bus	$0.9 \leq V_{load} \leq 1.1$

**Table I.7 – Limits Data**

• **11-node System**

Bus No.	Bus Type	$P_G(p.u.)$	$Q_G(p.u.)$	$P_d(p.u.)$	$Q_d(p.u.)$
1	Generator P,V	$0.1 \leq P_{G_1} \leq 2.5$	$-5.00 \leq Q_{G_1} \leq 5.00$	0.00	0.00
2	Generator P,V	$0.1 \leq P_{G_2} \leq 2.7$	$-3.00 \leq Q_{G_2} \leq 3.00$	0.20	0.10
3	Load P,Q	0.00	0.00	0.45	0.15
4	Load P,Q	0.00	0.00	0.40	0.05
5	Load P,Q	0.00	0.00	0.60	0.10
6	Load P,Q	0.00	0.00	0.00	0.00
7	Load P,Q	0.00	0.00	0.00	0.00
8	Load P,Q	0.00	0.00	0.20	0.10
9	Load P,Q	0.00	0.00	0.45	0.15
10	Generator P,V	$0.1 \leq P_{G_3} \leq 1.5$	$-3.00 \leq Q_{G_3} \leq 3.00$	0.20	0.05
11	Load P,Q	0.00	0.00	0.10	0.01

**Table I.8 – Bus Data**

Line No.	Sending End	Receiving End	$R_{line}(p.u.)$	$X_{line}(p.u.)$	$G_{line}(p.u.)$	$B_{line}(p.u.)$
1	1	2	0.02	0.06	0.00	0.060
2	1	3	0.08	0.24	0.00	0.050
3	2	3	0.06	0.18	0.00	0.040
4	2	4	0.06	0.18	0.00	0.040
5	2	10	0.04	0.12	0.00	0.030
6	6	4	0.01	0.16	0.00	0.020
7	4	7	0.04	0.12	0.00	0.025
8	4	8	0.04	0.12	0.00	0.025
9	8	5	0.04	0.10	0.00	0.020
10	5	9	0.04	0.12	0.00	0.045
11	9	10	0.04	0.12	0.00	0.045
12	8	11	0.08	0.18	0.00	0.045
13	10	11	0.00	0.14	0.00	0.020

**Table I.9 – Line Data**

Transformer No.	Sending Bus	Receiving Bus	$X_t(p.u.)$	Tap (primary)
1	3	6	0.05	0.987
2	5	7	0.05	0.957

**Table I.10 – Transformer Data**

Shunt Device No.	Shunt Bus	Shunt Susceptance
1	6	0.25
2	7	0.10

**Table I.10 – Shunt Data**

Slack	$0.9 \leq V_{slack} \leq 1.5$
Generator Bus	$0.9 \leq V_{gen} \leq 1.1$
Load Bus	$0.9 \leq V_{load} \leq 1.2$

**Table I.11 – Limits Data**

• **14-node System**

Bus No.	Bus Type	$P_G(p.u.)$	$Q_G(p.u.)$	$P_d(p.u.)$	$Q_d(p.u.)$
1	Generator P,V	$0.1 \leq P_{G_1} \leq 2.5$	$-0.6 \leq Q_{G_1} \leq 0.8$	0.00	0.00
2	Generator P,V	$0.1 \leq P_{G_2} \leq 2.7$	$-0.4 \leq Q_{G_2} \leq 0.6$	0.2170	0.1270
3	Generator P,V	$0.1 \leq P_{G_3} \leq 2.7$	$-0.2 \leq Q_{G_3} \leq 0.4$	0.9420	0.1900
4	Load P,Q	0.00	0.00	0.4780	0.0390
5	Load P,Q	0.00	0.00	0.760	0.160
6	Generator P,V	$0.1 \leq P_{G_4} \leq 2.7$	$-0.2 \leq Q_{G_4} \leq 0.4$	0.1120	0.0750
7	Load P,Q	0.00	0.00	0.00	0.00
8	Generator P,V	$0.1 \leq P_{G_5} \leq 2.7$	$-0.2 \leq Q_{G_5} \leq 0.4$	0.00	0.00
9	Load P,Q	0.00	0.00	0.2950	0.1660
10	Load P,Q	0.00	0.00	0.090	0.0580
11	Load P,Q	0.00	0.00	0.0350	0.0180
12	Load P,Q	0.00	0.00	0.0610	0.0160
13	Load P,Q	0.00	0.00	0.1350	0.0580
14	Load P,Q	0.00	0.00	0.1490	0.0500

**Table I.12 – Bus Data**

Line No.	Sending End	Receiving End	$R_{line}(p.u.)$	$X_{line}(p.u.)$	$G_{line}(p.u.)$	$B_{line}(p.u.)$
1	1	2	0.01938	0.05917	0.00	0.0528
2	1	5	0.05403	0.22304	0.00	0.0492
3	2	3	0.04699	0.19797	0.00	0.0438
4	2	4	0.05811	0.17632	0.00	0.0340
5	2	5	0.05695	0.17388	0.00	0.0346
6	3	4	0.06701	0.17103	0.00	0.0128
7	4	5	0.01335	0.04211	0.00	0.0000

Mathematical Modelling of Multi-terminal VSC-HVDC Links in Power Systems using  
Optimal Power Flows

---

8	6	11	0.09498	0.19890	0.00	0.0000
9	6	12	0.12291	0.25581	0.00	0.0000
10	6	13	0.06615	0.13027	0.00	0.0000
11	9	10	0.03181	0.08450	0.00	0.0000
12	9	14	0.12711	0.27038	0.00	0.0000
13	10	11	0.08205	0.19207	0.00	0.0000
14	12	13	0.22092	0.19988	0.00	0.0000
15	13	14	0.17093	0.34802	0.00	0.0000

**Table I.13 – Line Data**

Transformer No.	Sending Bus	Receiving Bus	$X_l$ (p.u)	Tap (primary)
1	4	7	0.20912	0.987
2	4	9	0.55618	0.969
3	5	6	0.25202	0.932
4	7	8	0.17615	1.0
5	7	9	0.11001	1.0

**Table I.14 – Transformer Data**

Shunt Device No.	Shunt Bus	Shunt Susceptance
1	9	0.19

**Table I.15 – Shunt Data**

Slack	$0.9 \leq V_{slack} \leq 1.15$
Generator Bus	$0.9 \leq V_{gen} \leq 1.15$
Load Bus	$0.9 \leq V_{load} \leq 1.06$

**Table I.16 – Limits Data**

• **30-node System**

Bus No.	Bus Type	$P_G$ (p.u.)	$Q_G$ (p.u.)	$P_d$ (p.u.)	$Q_d$ (p.u.)
1	Generator P,V	$0.0 \leq P_{G_1} \leq 0.8$	$-0.6 \leq Q_{G_1} \leq 0.8$	0.00	0.00
2	Generator P,V	$0.0 \leq P_{G_2} \leq 0.8$	$-0.4 \leq Q_{G_2} \leq 0.5$	0.2170	0.1270
3	Load P,Q	0.00	0.00	0.0240	0.0120
4	Load P,Q	0.00	0.00	0.0760	0.0160
5	Generator P,V	$0.0 \leq P_{G_3} \leq 0.50$	$-0.2 \leq Q_{G_3} \leq 0.4$	0.9420	0.1900
6	Load P,Q	0.00	0.00	0.00	0.00
7	Load P,Q	0.00	0.00	0.2280	0.1090
8	Generator P,V	$0.0 \leq P_{G_4} \leq 0.75$	$-0.2 \leq Q_{G_4} \leq 0.5$	0.3000	0.3000

Mathematical Modelling of Multi-terminal VSC-HVDC Links in Power Systems using  
Optimal Power Flows

---

9	Load P,Q	0.00	0.00	0.00	0.00
10	Load P,Q	0.00	0.00	0.0580	0.0200
11	Generator P,V	$0.0 \leq P_{G_5} \leq 0.30$	$-0.2 \leq Q_{G_5} \leq 0.4$	0.00	0.00
12	Load P,Q	0.00	0.00	0.1120	0.0750
13	Generator P,V	$0.0 \leq P_{G_6} \leq 0.40$	$-0.2 \leq Q_{G_6} \leq 0.4$	0.00	0.00
14	Load P,Q	0.00	0.00	0.0620	0.0160
15	Load P,Q	0.00	0.00	0.0820	0.0250
16	Load P,Q	0.00	0.00	0.0350	0.0180
17	Load P,Q	0.00	0.00	0.0900	0.0580
18	Load P,Q	0.00	0.00	0.0320	0.0090
19	Load P,Q	0.00	0.00	0.0950	0.0340
20	Load P,Q	0.00	0.00	0.0220	0.0070
21	Load P,Q	0.00	0.00	0.1750	0.1120
22	Load P,Q	0.00	0.00	0.00	0.00
23	Load P,Q	0.00	0.00	0.0320	0.0160
24	Load P,Q	0.00	0.00	0.0870	0.0670
25	Load P,Q	0.00	0.00	0.00	0.00
26	Load P,Q	0.00	0.00	0.0350	0.0230
27	Load P,Q	0.00	0.00	0.00	0.00
28	Load P,Q	0.00	0.00	0.00	0.00
29	Load P,Q	0.00	0.00	0.0240	0.0090
30	Load P,Q	0.00	0.00	0.1060	0.0190

**Table I.17 – Bus Data**

Line No.	Sending End	Receiving End	$R_{line} (p.u.)$	$X_{line} (p.u.)$	$G_{line} (p.u.)$	$B_{line} (p.u.)$
1	1	2	0.0192	0.0575	0.00	0.0528
2	1	3	0.0452	0.1652	0.00	0.0408
3	2	4	0.0570	0.1737	0.00	0.0368
4	3	4	0.0132	0.0379	0.00	0.0340
5	2	5	0.0472	0.1983	0.00	0.0418
6	2	6	0.0581	0.1763	0.00	0.0374
7	4	6	0.0119	0.0414	0.00	0.0010
8	5	7	0.0460	0.1160	0.00	0.0204
9	6	7	0.0267	0.0820	0.00	0.0170
10	6	8	0.0120	0.0420	0.00	0.0090
11	12	14	0.1231	0.2559	0.00	0.00
12	12	15	0.0662	0.1304	0.00	0.00
13	12	16	0.0945	0.1987	0.00	0.00

Mathematical Modelling of Multi-terminal VSC-HVDC Links in Power Systems using  
Optimal Power Flows

---

14	14	15	0.2210	0.1997	0.00	0.00
15	16	17	0.0524	0.1923	0.00	0.00
16	15	18	0.1073	0.2185	0.00	0.00
17	18	19	0.0639	0.1292	0.00	0.00
18	19	20	0.0340	0.0680	0.00	0.00
19	10	20	0.0936	0.2090	0.00	0.00
20	10	17	0.0324	0.0845	0.00	0.00
21	10	21	0.0348	0.0749	0.00	0.00
22	10	22	0.0727	0.1499	0.00	0.00
23	21	22	0.0116	0.0236	0.00	0.00
24	15	23	0.1000	0.2020	0.00	0.00
25	22	24	0.1150	0.1790	0.00	0.00
26	23	24	0.1320	0.2700	0.00	0.00
27	24	25	0.1885	0.3292	0.00	0.00
28	25	26	0.2544	0.3800	0.00	0.00
29	25	27	0.1093	0.2087	0.00	0.00
30	27	29	0.2198	0.4153	0.00	0.00
31	27	30	0.3202	0.6027	0.00	0.00
32	29	30	0.2399	0.4533	0.00	0.00
33	8	28	0.0636	0.2000	0.00	0.0428
34	6	28	0.0169	0.0599	0.00	0.0130

**Table I.18 – Line Data**

<b>Transformer No.</b>	<b>Sending Bus</b>	<b>Receiving Bus</b>	<b><math>X_l</math> (p.u)</b>	<b>Tap (primary)</b>
1	6	9	0.2080	0.978
2	6	10	0.5560	0.969
3	9	11	0.2080	1.0
4	9	10	0.1100	1.0
5	4	12	0.2560	0.932
6	12	13	0.1400	1.0
7	28	27	0.3690	0.968

**Table I.19 – Transformer Data**

<b>Shunt Device No.</b>	<b>Shunt Bus</b>	<b>Shunt Susceptance</b>
1	10	0.19
2	24	0.043

**Table I.20 – Shunt Data**

<b>Slack</b>	$0.9 \leq V_{slack} \leq 1.10$
<b>Generator Bus</b>	$0.9 \leq V_{gen} \leq 1.10$
<b>Load Bus</b>	$0.9 \leq V_{load} \leq 1.05$

**Table I.21 – Limits Data**

- **Compound Transformer General Data**

The following parameters apply to the compound transformer introduced in figure (4.4a); the numbers are in per unit.

$R_1$	0.01
$X_1$	0.10
$R_0$	0.04
$X_0$	-1.9992

**Table I.22 – Compound Transformer Model Parameters (per unit)**

- **AC System**

<b>Bus No.</b>	<b>Bus Type</b>	$P_G(p.u.)$	$Q_G(p.u.)$	$P_d(p.u.)$	$Q_d(p.u.)$
1	Generator P,V	$0.1 \leq P_{G_1} \leq 2.0$	$-5.00 \leq Q_{G_1} \leq 5.00$	0.00	0.00
2	Load P,Q	0.00	0.00	0.25	0.20
3	Load P,Q	0.00	0.00	1.00	0.00
4	Load P,Q	0.00	0.00	0.00	0.00

**Table I.23 – Bus Data**

<b>Line No.</b>	<b>Sending End</b>	<b>Receiving End</b>	$R_{line}(p.u.)$	$X_{line}(p.u.)$	$G_{line}(p.u.)$	$B_{line}(p.u.)$
1	1	2	0.05	0.10	0.00	0.00
2	2	4	0.05	0.10	0.00	0.00
3	3	4	0.05	0.10	0.00	0.00

**Table I.24 – Line Data**

<b>Slack</b>	$0.9 \leq V_{slack} \leq 1.2$
<b>Generator Bus</b>	$0.9 \leq V_{gen} \leq 1.2$
<b>Load Bus</b>	$0.9 \leq V_{load} \leq 1.2$

**Table I.25 – Limits Data**

• **DC System – Case One**

Bus No.	Bus Type	$P_G(p.u.)$	$Q_G(p.u.)$	$P_d(p.u.)$	$Q_d(p.u.)$
1	Generator P,V	$0.1 \leq P_{G_1} \leq 2.0$	$-5.00 \leq Q_{G_1} \leq 5.00$	0.00	0.00
2	Load P,Q	0.00	0.00	0.25	0.20
3	Load P,Q	0.00	0.00	1.00	0.00

**Table I.26 – Bus Data**

Line No.	Sending End	Receiving End	$R_{line}(p.u.)$	$X_{line}(p.u.)$	$G_{line}(p.u.)$	$B_{line}(p.u.)$
1	1	2	0.05	0.10	0.00	0.00

**Table I.27 – Line Data**

**Slack**  $0.9 \leq V_{slack} \leq 1.2$

**Generator Bus**  $0.9 \leq V_{gen} \leq 1.2$

**Load Bus**  $0.9 \leq V_{load} \leq 1.1$

**Table I.28 – Limits Data**

• **DC System – Case Two**

Bus No.	Bus Type	$P_G(p.u.)$	$Q_G(p.u.)$	$P_d(p.u.)$	$Q_d(p.u.)$
1	Generator P,V	$0.1 \leq P_{G_1} \leq 2.0$	$-5.00 \leq Q_{G_1} \leq 5.00$	0.00	0.00
2	Load P,Q	0.00	0.00	0.00	0.00
3	Load P,Q	0.00	0.00	1.00	0.00
4	Generator P,V	$0.1 \leq P_{G_2} \leq 2.0$	$-5.00 \leq Q_{G_2} \leq 5.00$	0.00	0.00
5	Load P,Q	0.00	0.00	0.25	0.20

**Table I.29 – Bus Data**

Line No.	Sending End	Receiving End	$R_{line}(p.u.)$	$X_{line}(p.u.)$	$G_{line}(p.u.)$	$B_{line}(p.u.)$
1	1	2	0.05	0.10	0.00	0.00
2	2	4	0.05	0.10	0.00	0.00
3	4	5	0.05	0.10	0.00	0.00

**Table I.30 – Line Data**

**Slack**  $0.9 \leq V_{slack} \leq 1.2$

**Generator Bus**  $0.9 \leq V_{gen} \leq 1.2$

**Load Bus**  $0.9 \leq V_{load} \leq 1.1$

**Table I.30 – Limits Data**

• **Two-terminal back-to-back VSC-HVDC**

Bus No.	Bus Type	$P_G(p.u.)$	$Q_G(p.u.)$	$P_d(p.u.)$	$Q_d(p.u.)$
1	Generator P,V	$-0.3 \leq P_{G_2} \leq 2.0$	$-5.00 \leq Q_{G_1} \leq 5.00$	0.00	0.00
2	Load P,Q	0.00	0.00	0.25	0.20
3	Load P,Q	0.00	0.00	0.00	0.00
4	Load P,Q	0.00	0.00	0.25	0.20
5	Generator P,V	$-0.3 \leq P_{G_2} \leq 2.0$	$-5.00 \leq Q_{G_2} \leq 5.00$	0.00	0.00

**Table I.31 – Bus Data**

Line No.	Sending End	Receiving End	$R_{line}(p.u.)$	$X_{line}(p.u.)$	$G_{line}(p.u.)$	$B_{line}(p.u.)$
1	1	2	0.05	0.10	0.00	0.00
2	2	5	0.05	0.10	0.00	0.00

**Table I.32 – Line Data**

**Slack**  $0.9 \leq V_{slack} \leq 1.2$

**Generator Bus**  $0.9 \leq V_{gen} \leq 1.2$

**Load Bus**  $0.9 \leq V_{load} \leq 1.1$

**Table I.33 – Limits Data**

• **Multi-terminal back-to-back VSC-HVDC**

Bus No.	Bus Type	$P_G(p.u.)$	$Q_G(p.u.)$	$P_d(p.u.)$	$Q_d(p.u.)$
1	Generator P,V	$-0.8 \leq P_{G_2} \leq 2.0$	$-5.00 \leq Q_{G_1} \leq 5.00$	0.00	0.00
2	Load P,Q	0.00	0.00	0.25	0.20
3	Load P,Q	0.00	0.00	0.00	0.00
4	Load P,Q	0.00	0.00	0.25	0.20
5	Generator P,V	$-0.8 \leq P_{G_2} \leq 2.0$	$-5.00 \leq Q_{G_2} \leq 5.00$	0.00	0.00
6	Load P,Q	0.00	0.00	0.25	0.20
7	Generator P,V	$-1.5 \leq P_{G_3} \leq 2.0$	$-5.00 \leq Q_{G_3} \leq 5.00$	0.00	0.00

**Table I.34 – Bus Data**

Line No.	Sending End	Receiving End	$R_{line}(p.u.)$	$X_{line}(p.u.)$	$G_{line}(p.u.)$	$B_{line}(p.u.)$
1	1	2	0.05	0.10	0.00	0.00
2	4	5	0.05	0.10	0.00	0.00
3	6	7	0.05	0.10	0.00	0.00

**Table I.35 – Line Data**

<b>Slack</b>	$0.9 \leq V_{slack} \leq 1.2$
<b>Generator Bus</b>	$0.9 \leq V_{gen} \leq 1.2$
<b>Load Bus</b>	$0.9 \leq V_{load} \leq 1.1$

**Table I.36 – Limits Data**

- **Multi-terminal back-to-back VSC-HVDC: Four-terminal meshed**

This system is essentially an expansion of the previous system (Three-terminal) and thus its associated data are identical. The only difference is the machines' active power operating region, which has been redefined to best reflect the operating conditions of the system:

<b>Machine 1</b>	$-0.7 \leq P_{G_1} \leq 2.0$
<b>Machine 2</b>	$-0.7 \leq P_{G_2} \leq 2.0$
<b>Machine 3</b>	$-0.7 \leq P_{G_3} \leq 2.0$
<b>Machine 4</b>	$-0.7 \leq P_{G_4} \leq 2.0$

**Table I.37 – Machine Limits**

The reactive power operating limits have been similar to those of the previous system.

- **DC Link Data**

The DC link resistance has been chosen to be 0.001 per unit for all the point-to-point and multi-terminal VSC-HVDC system simulations presented throughout this thesis.

- **Point-to-Point and Multi-terminal VSC-HVDC System Data**

The point-to-point system data essentially remains similar to back-to-back and multi-terminal back-to-back system data presented above taking into account the DC link data by using the expanded compound transformer model in the system configuration.

- **46-node System**

The system data for each AC segment is exactly identical to the system data pertaining to IEEE 14-bus system. The VSC-HVDC system data is also the same as in previous test cases.

• **5-node System**

Bus No.	Bus Type	$P_G(p.u.)$	$Q_G(p.u.)$	$P_d(p.u.)$	$Q_d(p.u.)$
1	Generator P,V	$0.1 \leq P_{G_2} \leq 2.0$	$-5.00 \leq Q_{G_1} \leq 5.00$	0.00	0.00
2	Load P,Q	$0.1 \leq P_{G_2} \leq 2.0$	$-3.00 \leq Q_{G_2} \leq 3.00$	0.20	0.10
3	Load P,Q	0.00	0.00	0.45	0.15
4	Load P,Q	0.00	0.00	0.40	0.05
5	Load P,Q	0.00	0.00	0.60	0.10

**Table I.38 – Bus Data**

Line No.	Sending End	Receiving End	$R_{line}(p.u.)$	$X_{line}(p.u.)$	$G_{line}(p.u.)$	$B_{line}(p.u.)$
1	1	2	0.02	0.06	0.00	0.06
2	1	3	0.08	0.24	0.00	0.05
3	2	3	0.06	0.18	0.00	0.04
4	2	4	0.06	0.18	0.00	0.04
5	2	5	0.04	0.12	0.00	0.03
6	3	4	0.01	0.03	0.00	0.02
7	4	5	0.08	0.24	0.00	0.05

**Table I.39 – Line Data**

**Slack**                     $0.9 \leq V_{slack} \leq 1.5$

**Generator Bus**       $0.9 \leq V_{gen} \leq 1.1$

**Load Bus**               $0.9 \leq V_{load} \leq 1.2$

**Table I.40 – Limits Data**